APPENDIX G

FAA BASE STATION ANTENNA MODEL

TABLE OF CONTENTS

TABLE OF CONTENTS 2
LIST OF FIGURES 3
LIST OF TABLES 4
REFERENCES 5
APPENDIX 6
Appendix G. Base Station Transmit Antenna Far-Field Gain Pattern Model 6
G.1 Gain Pattern Model Derivation 6
G.2 Usage of Antenna Gain Pattern Model 8

LIST OF FIGURES

Figure A-1: Far Field Pattern Coordinate System 6
Figure A-2: Base Station Transmit Broad beam Elevation Pattern 7
Figure A-3: Base Station Transmit Broad beam Azimuth Pattern 8

LIST OF TABLES

Table A-1: Base Station Transmit Antenna Parameters 6

REFERENCES

There are no sources in the current document.

APPENDIX

Appendix G. Base Station Transmit Antenna Far-Field Gain Pattern Model

G.1 Gain Pattern Model Derivation

The base station transmit antenna far field pattern model[1] is that associated with a uniformly illuminated rectangular aperture of width "a" and height "b". The aperture is centered on the "xy" coordinate center shown in Figure G-1 with the width "a" being co aligned with the "x" axis and the height "b" with the "y" axis. (Figure G-1 depicts general angular coordinates relative to the indicated axes.)

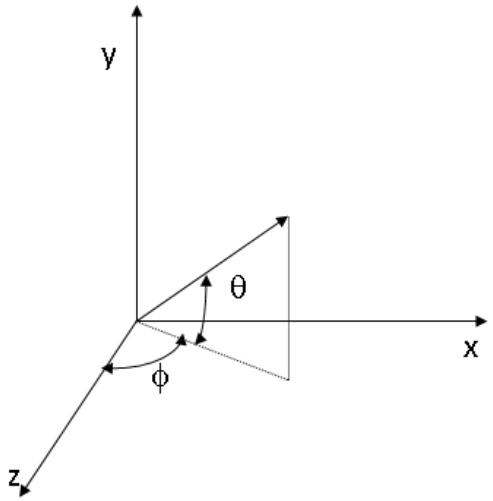

Figure G-1: Far Field Pattern Coordinate System

The beam is centered on the "z" axis with a peak gain, elevation beamwidth and azimuth beamwidth as shown in Table G-1. Table G-1 also lists other important parameters associated with the far field pattern. Table G-1 values are shown for the “narrow beam” (i.e., the study described in 5.3.3.3, Results for Inflight Aircraft Ground Based Base Station Cases) and “broad beam” (i.e., the study described in 5.3.3.6, Results for Inflight Aircraft TAWS/HTAWS and Low Altitude Pos/Nav) cases.

Table G-1: Base Station Transmit Antenna Parameters

Parameter	“Narrow Beam” Value	“Broad Beam” Value
a/λ	0.8278	0.7722535
b/λ	5.7	2.641574
G_o	72.5344	31.8649
η	0.681491	0.686578
Peak Gain	16.94 dB	13.4 dB
Elevation Beamwidth	8.8 deg	18.6 deg

[1] Pattern based on uniformly illuminated rectangular aperture as described in C. A. Balanis, "Antenna Theory: Analysis and Design", John Wiley & Sons, 2005 while accounting for a change in coordinate systems from that used in the book.

Azimuth Beamwidth	64.6 deg	70.0 deg

The equations shown below are used by both the "narrow beam" and "broad beam" models and the dual use is true for all equations in this appendix unless otherwise indicated.

$$g(\theta',\phi') = \begin{Bmatrix} 1, & \theta' = 0 \text{ and } \phi' \in \{\{0\},\{\pi\}\} \\ [\sin^2(\phi') + \cos^4(\theta')\sin^2(\theta')\cos^2(\phi')]/[\sin^2(\phi')\cos^2(\theta') + \sin^2(\theta')], & elsewhere \end{Bmatrix}$$

$$h(\theta',\phi') = \text{sinc}^2[\pi(a/\lambda)\sin(\phi')\cos(\theta')]\text{sinc}^2[\pi(b/\lambda)\sin(\theta')]g(\theta',\phi')\gamma(\phi')$$

A variation between the antenna equations of the "narrow beam" and "broad beam" models for the function, $\gamma(\phi')$, is that an exponential coefficient has a value of either a 3 or 4, as shown below.

Narrow Beam Model: $\gamma(\phi') = \begin{Bmatrix} 1, & |\phi'| \le \pi/2 \\ \exp[-3(|\phi'| - \pi/2)], & \pi/2 < |\phi'| \le \pi \end{Bmatrix}$

Broad Beam Model: $\gamma(\phi') = \begin{Bmatrix} 1, & |\phi'| \le \pi/2 \\ \exp[-3(|\phi'| - \pi/2)], & \pi/2 < |\phi'| \le \pi \end{Bmatrix}$

Then the far field base station antenna gain pattern is given by $G_{xmit}(\theta',\phi') = \eta G_0 h(\theta',\phi')$

Figure G-2 shows an elevation cut of the pattern while Figure G-3 shows the azimuth cut. Note the gain is shown in dB in both figures while the angles are in degrees.

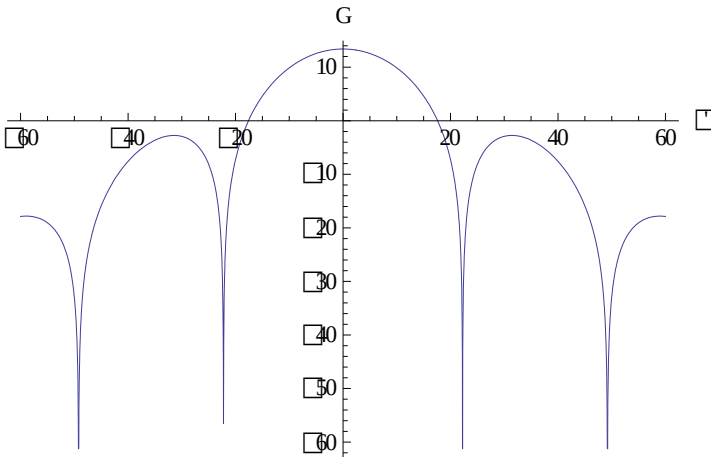

Figure G-2: Base Station Transmit Broad beam Elevation Pattern

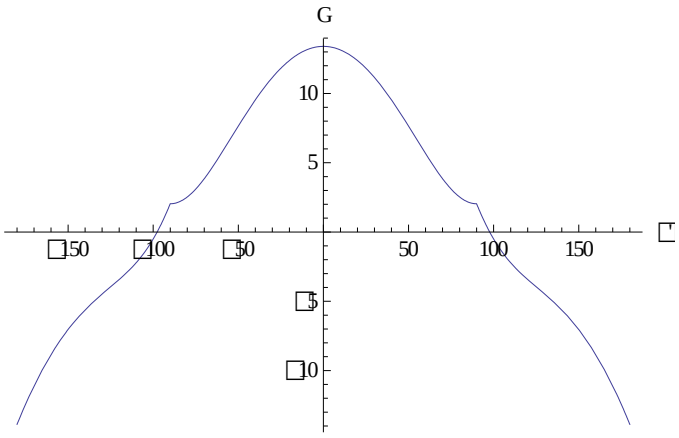

Figure G-3: Base Station Transmit Broad beam Azimuth Pattern

G.2 Usage of Antenna Gain Pattern Model

The coordinate system described above will be tilted down (with respect to the local horizon) ξ degrees (ξ ^{o} rotation about "x" axis) at each base station location in a practical application. Hence to use the above derived gain pattern in a typical "flat earth" untilted coordinate system (θ, ϕ), a transformation of variables must be made. The gain in the untilted coordinate system is given by $G_{xmit}[\theta'(\theta,\phi),\phi'(\theta,\phi)]$; where the elevation and azimuth angle transformation expressions are, respectively

$$\theta'(\theta,\phi) = \sin^{-1}[\cos(\xi\pi/180)\sin(\theta) + \sin(\xi\pi/180)\cos(\theta)\cos(\phi)] \text{ and}$$

$$\phi'(\theta,\phi) = \tan^{-1}[-\sin(\xi\pi/180)\sin(\theta) + \cos(\xi\pi/180)\cos(\theta)\cos(\phi), \cos(\theta)\sin(\phi)]$$

Note that θ, ϕ denote the elevation and azimuth angles respectively in the untilted coordinate system. For EIRP limit computation the relative pattern is normalized to beam center peak gain value: $G_{norm}(\ ) = G_{xmit}(\ )/\eta G_0$.

APPENDIX H

USE CASE DEVELOPMENT

TABLE OF CONTENTS

TABLE OF CONTENTS 2
LIST OF FIGURES 3
LIST OF TABLES 4
REFERENCES 5
APPENDIX 6
Appendix H. Use Case Development 6

LIST OF FIGURES

No table of figures entries found.

LIST OF TABLES

No table of figures entries found.

REFERENCES

There are no sources in the current document.

APPENDIX

Appendix H. Use Case Development

GNSS Receiver Use-Case Development

GPS-ABC Workshop VI

RTCA Washington, DC
March 30, 2017

Stephen Mackey *Hadi Wassaf*

Volpe The National Transportation Systems Center
Advancing transportation innovation for the public good

U.S. Department of Transportation
Office of the Secretary of Transportation
John A. Volpe National Transportation Systems Center

Use Case Outreach

- Worked closely with our federal partners to understand their use case applications
- Conducted outreach with manufacturers who provided use case applications
- Results from these efforts can be located at:
  - Workshop I
  - Workshop II
  - Workshop III
  - Workshop V

Incorporation of Use Cases

- Use cases will be used in conjunction with Interference Tolerance Masks (ITM) and propagation models to provide the power levels that can be tolerated adjacent to GPS/GNSS signals
- Use cases are assembled from DOT's federal partners & industry responses and aggregated by six (6) GPS/GNSS categories:
  - General Aviation [non certified] (GAV)
  - General Location/Navigation (GLN)
  - High Precision & Networks (HPR)
  - Timing (TIM)
  - Cellular (CEL)
  - Space Based (SPB)

Use-Case Summary

Category	Height (feet AGL)		Speed (mph)	Urbanization	Terrain	Antenna Integration	Antenna Orientation
	Min	Max					
GAV	0	40k	920	Urban/Suburban/Rural	Flat/Sloped/Canyon – Open/Impeded - Land/Water	Yes/No	Variable
GLN	0	1,000	600	Urban/Suburban/Rural	Flat/Sloped/Canyon – Open/Impeded - Land/Water	Yes/No	Variable
HPR	0	20,000	180	Urban/Suburban/Rural	Flat/Sloped/Canyon – Open/Impeded - Land/Water	Yes/No	Variable
TIM	0	1000s	100	Urban/Suburban/rural	Flat – Open - Land	No	Fixed
CEL	0	100s	100s	Urban/Suburban/rural	Flat/Sloped/Canyon – Open/Impeded - Land/Water	Yes	Variable
SPB	1,700k	4,300k	16k	n/a	n/a	No	Variable

Selection of Use Case Priorities

PNTAB's View: Minimum Criteria for Testing/Evaluation of Interference Potential of High Power Terrestrial Transmitters in Repurposed Radio Bands

1. **Accept and strictly apply the 1 dB degradation** Interference Protection Criterion (IPC) for worst case conditions (This is the accepted, world-wide standard for PNT and many other radiocommunication applications)
2. Verify interference for **all classes of GPS receivers** is below criteria, especially precision (Real Time Kinematic - requires both user and reference station to be interference-free) and timing receivers (economically these two classes are the highest payoff applications – many $B/year)
3. Test and **verify interference for receivers** in **all operating modes** is less than criteria, particularly **acquisition** and **reacquisition** of GNSS signals under difficult conditions (see attachment of representative interference cases)
4. **Focus analysis on worst cases**: use ***maximum*** **authorized transmitted interference** powers and ***smallest-attenuation*** **propagation models** (antennas and space losses) that do not underrepresent the maximum power of the interfering signal (including multiple transmitters)
5. Ensure **interference to emerging Global Navigation Satellite System (GNSS) signals** (particularly wider bandwidth GPS L1C – Galileo, GLONASS), is less than criteria
6. All **testing must include GNSS expertise** and be **open to public comment** and scrutiny.

Why HPR as an Important Use Case?

- EXCOM Priorities
  - Focus on existing uses ✓
  - Vital Needs:
    - Economic ✓
    - Public Safety ✓
    - Scientific ✓
    - National Security ✓
- PNT Advisory Board Priorities
  - Focus on HPR and TIM ✓
  - Focus analysis on most sensitive case ✓
  - Apply the 1 dB degradation ✓
  - Include GNSS ✓

Category	Existing Uses	Vital Needs				Most Sensitive ITM
		Economic	Public Safety	Scientific	National Security	
GAV	✓	✓	✓	✓	✓	
GLN	✓	✓	✓	✓	✓	
HPR	✓	✓	✓	✓	✓	✓
TIM	✓	✓	✓	✓	✓	
CEL	✓	✓	✓	✓		
SPB	✓	✓	✓	✓	✓	✓

Use Case Scenario Focus

Agriculture/Farming

Construction/Infrastructure

Emergency Response

Agriculture/Farming

- Benefits of GPS:
  - Precise operation/auto-steering for tractors, combines and sprayers
  - Non-restrictive operations (e.g. fog and night)
  - Coordinate movements of multiple tractors or other equipment
  - Optimize seed, fertilizer and pesticides placement based on soil conditions and temperature.
  - Precise planting and watering
  - Yield and crop monitoring
- Makes use of augmentation systems:
  - OmniSTAR , StarFire, Terrestar
  - Real Time Kinematic (RTK)

Agriculture/Farming Scenario – Basic Components

Photo courtesy AbeSnap23/ThinkStock

LTE Cellular Tower

Photo courtesy Valio84sl/ThinkStock

Drone/Crop Monitoring

Photo courtesy of John Deere

GPS Guidance System

Photo courtesy of John Deere

High Precision Farming

Photo courtesy of John Deere

High Precision Farming

Photo courtesy Bennymarty/ThinkStock

Drone/Crop Monitoring

Agriculture/Farming Scenario

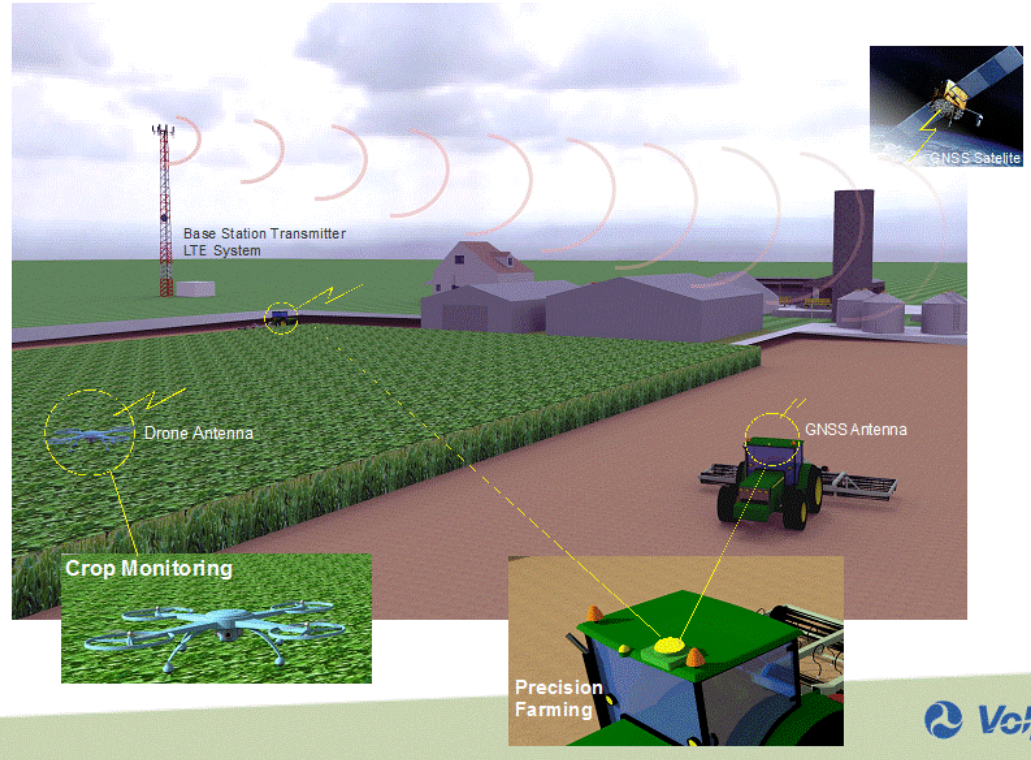

Volpe 12

Agriculture/Farming Summary

- Categories included are HPR and GLN/GAV
- Precision Farming (HPR)
  - Vital Needs: Economic
  - Lateral distances down to 10 feet from the base station
  - Vertical heights within 0-20 of feet above the ground
- Crop Health Monitoring (GLN/GAV)
  - Vital Needs: Economic
  - Lateral distances down to 10 feet from the base station
  - Vertical heights up to (and above) the base station height

Construction/Infrastructure

- Benefits of GPS:
  - Precise machine control for many different type of heavy equipment (e.g. dozers, excavators, pavers, scrapers, compactors)
  - Placement of blades/heavy machinery give precise results (less rework)
  - Improved process control through equipment location monitoring
  - Virtual staking (view points on a screen vs. physical stakes)
  - Time saving from traditional surveying
- Surveyor setup (3d geodetic control area) and monitor machine control operations

Construction/Infrastructure Scenarios - Basic Components

Photo courtesy of WSP Canada Inc

GPS HPR receiver used in construction/surveying

Photo courtesy of WSP Canada Inc

GPS HPR receiver used in construction/surveying

Photo courtesy Medvedkov/ThinkStock

Construction/Surveying

Photo courtesy ThinkStock

GPS HPR receiver used in construction guidance

Photo courtesy AbeSnap23/ThinkStock

LTE Cellular Tower

Photo courtesy Kadmy/ThinkStock

Surveying

Volpe 15

Construction/Infrastructure Scenario

Volpe 16

Construction/Infrastructure (HPR) Summary

- Construction/infrastructure (HPR)
- Vital Needs: Economic
- Lateral distances down to 1 – 2 city blocks from the base station
- Vertical heights up to (and above) the base station height

Emergency Services

- Medical and police personnel are increasingly using GPS to locate patients both during emergencies and regular activities
- Police resource tracking (increased awareness of where their officers are located)
- Drones/UAV/UAS will take on increasing importance in dealing with natural and other disasters/incidents

Emergency Services Scenarios - Basic Components

Photo courtesy Tiero/ThinkStock

Drone/Emergency Response/Disasters

Photo courtesy StockSolutions/ThinkStock

Ankle Bracelet Monitoring

Photo courtesy Mokee81/ThinkStock

Police/Emergency Response/Resource Tracking

Photo courtesy Mrdoomits/ThinkStock

Emergency Response/ Resource Tracking

Photo courtesy AbeSnap23/ThinkStock

LTE Cellular Tower

Photo courtesy ThinkStock

Drone/Emergency Response/Disasters

Emergency Response Scenario

Volpe 20

Emergency Response Summary

- Two categories included GAV and GLN
  - UAS/UAV/Drone (GLN/GAV)
  - Emergency Services/Asset Tracking (GLN)
  - Emergency Response/Asset Tracking (GLN)
- Lateral distances down to 10 feet from the base station
- Vertical heights up to (and above) the base station height
- Vital Needs:
  - Public safety / Safety of life
  - National Security

Other Considerations

GPS/GNSS Receiver Modification

- Receiver modification to reduce susceptibility to out of band emissions?
- Many receivers are sealed and modification are complicated if not impossible
- Even if you can modify the receivers, how do identify "all" users?
- May result in loss of augmentation (e.g., Mobile Satellite Service delivered corrections) capability

Photo courtesy Scanrail/ThinkStock

Photo courtesy Comstock/ThinkStock

* http://www.deere.com/en_US/docs/html/brochures/publication.html?id=004d03e7#14
** http://www.trimble.com/mappingGIS/pro6-Pro-Series-Receivers.aspx?tab=Features_and_Benefits

Summary

- Every possible use case is not covered - as there are thousands of use cases
- Cases illustrated are applications that happen routinely and can bound the results/impact of base station transmitters
- Inverse and propagation modeling will utilize the height and location limits of the these use case application to determine worst case base station transmit power levels

APPENDIX I

FORWARD MODELING RESULTS

TABLE OF CONTENTS

TABLE OF CONTENTS 2
LIST OF FIGURES 4
LIST OF TABLES 9
REFERENCES 10
APPENDIX 11
Appendix I. Forward Modeling Results 11
I.1 Macro Urban Base Station, GPS C/A-code 11
I.1.1 GAV 11
I.1.2 GLN 16
I.1.3 HPR 21
I.1.4 TIM 27
I.1.5 CEL 32
I.2 Small Cell Outdoor/Urban Micro Urban Base Station, GPS C/A-code 36
I.2.1 GAV 36
I.2.2 GLN 41
I.2.3 HPR 46
I.2.4 TIM 50
I.2.5 CEL 56
I.3 Handsets, GPS C/A-code 61
I.3.1 GAV 61
I.3.2 GLN 65
I.3.3 HPR 70
I.3.4 TIM 73
I.3.5 CEL 77
I.4 Sensitivity Analyses 82
I.4.1 Non-bounding DUTs 82
I.4.2 Other GNSS Signal Types 87

I.4.3 Propagation Models 88

LIST OF FIGURES

Figure I-1: Maximum Impacted Lateral Distance for Bounding GAV, Macro Urban Base Station (EIRP = 59 dBm) 12
Figure I-2: Macro Urban Base Station (EIRP = 59 dBm), Bounding GAV, 1475 MHz..... 12
Figure I-3: Macro Urban Base Station (EIRP = 59 dBm), Bounding GAV, 1490 MHz..... 13
Figure I-4: Macro Urban Base Station (EIRP = 59 dBm), Bounding GAV, 1505 MHz..... 13
Figure I-5: Macro Urban Base Station (EIRP = 59 dBm), Bounding GAV, 1520 MHz..... 13
Figure I-6: Macro Urban Base Station (EIRP = 59 dBm), Bounding GAV, 1525 MHz..... 14
Figure I-7: Macro Urban Base Station (EIRP = 59 dBm), Bounding GAV, 1530 MHz..... 14
Figure I-8: Macro Urban Base Station (EIRP = 59 dBm), Bounding GAV, 1535 MHz..... 14
Figure I-9: Macro Urban Base Station (EIRP = 59 dBm), Bounding GAV, 1540 MHz..... 15
Figure I-10: Macro Urban Base Station (EIRP = 59 dBm), Bounding GAV, 1545 MHz..... 15
Figure I-11: Macro Urban Base Station (EIRP = 59 dBm), Bounding GAV, 1550 MHz..... 15
Figure I-12: Macro Urban Base Station (EIRP = 59 dBm), Bounding GAV, 1675 MHz..... 16
Figure I-13: Maximum Impacted Lateral Distance for Bounding GLN, Macro Urban Base Station with EIRP of 59 dBm/sector..... 17
Figure I-14: Macro Urban Base Station (EIRP = 59 dBm), Bounding GLN, 1475 MHz 17
Figure I-15: Macro Urban Base Station (EIRP = 59 dBm), Bounding GLN, 1490 MHz 18
Figure I-16: Macro Urban Base Station (EIRP = 59 dBm), Bounding GLN, 1505 MHz 18
Figure I-17: Macro Urban Base Station (EIRP = 59 dBm), Bounding GLN, 1520 MHz 18
Figure I-18: Macro Urban Base Station (EIRP = 59 dBm), Bounding GLN, 1525 MHz 19
Figure I-19: Macro Urban Base Station (EIRP = 59 dBm), Bounding GLN, 1530 MHz 19
Figure I-20: Macro Urban Base Station (EIRP = 59 dBm), Bounding GLN, 1535 MHz 19
Figure I-21: Macro Urban Base Station (EIRP = 59 dBm), Bounding GLN, 1540 MHz 20
Figure I-22: Macro Urban Base Station (EIRP = 59 dBm), Bounding GLN, 1545 MHz 20
Figure I-23: Macro Urban Base Station (EIRP = 59 dBm), Bounding GLN, 1550 MHz 20
Figure I-24: Macro Urban Base Station (EIRP = 59 dBm), Bounding GLN, 1675 MHz 21
Figure I-25: Maximum Impacted Lateral Distance for Bounding HPR, Macro Urban Base Station with EIRP of 59 dBm/sector..... 22
Figure I-26: Macro Urban Base Station (EIRP = 59 dBm), Bounding HPR, 1475 MHz..... 22
Figure I-27: Macro Urban Base Station (EIRP = 59 dBm), Bounding HPR, 1490 MHz..... 23
Figure I-28: Macro Urban Base Station (EIRP = 59 dBm), Bounding HPR, 1505 MHz..... 23
Figure I-29: Macro Urban Base Station (EIRP = 59 dBm), Bounding HPR, 1520 MHz..... 23
Figure I-30: Macro Urban Base Station (EIRP = 59 dBm), Bounding HPR, 1525 MHz..... 24
Figure I-31: Macro Urban Base Station (EIRP = 59 dBm), Bounding HPR, 1530 MHz..... 24
Figure I-32: Macro Urban Base Station (EIRP = 59 dBm), Bounding HPR, 1535 MHz..... 24
Figure I-33: Macro Urban Base Station (EIRP = 59 dBm), Bounding HPR, 1540 MHz..... 25

Figure I-34: Macro Urban Base Station (EIRP = 59 dBm), Bounding HPR, 1545 MHz..... 25
Figure I-35: Macro Urban Base Station (EIRP = 59 dBm), Bounding HPR, 1550 MHz..... 25
Figure I-36: Macro Urban Base Station (EIRP = 59 dBm), Bounding HPR, 1675 MHz..... 26
Figure I-37: Maximum Impacted Lateral Distance for Bounding TIM, Macro Urban Base Station with EIRP of 59 dBm/sector..... 27
Figure I-38: Macro Urban Base Station (EIRP = 59 dBm), Bounding TIM, 1475 MHz..... 28
Figure I-39: Macro Urban Base Station (EIRP = 59 dBm), Bounding TIM, 1490 MHz..... 28
Figure I-40: Macro Urban Base Station (EIRP = 59 dBm), Bounding TIM, 1505 MHz..... 29
Figure I-41: Macro Urban Base Station (EIRP = 59 dBm), Bounding TIM, 1520 MHz..... 29
Figure I-42: Macro Urban Base Station (EIRP = 59 dBm), Bounding TIM, 1525 MHz..... 29
Figure I-43: Macro Urban Base Station (EIRP = 59 dBm), Bounding TIM, 1530 MHz..... 30
Figure I-44: Macro Urban Base Station (EIRP = 59 dBm), Bounding TIM, 1535 MHz..... 30
Figure I-45: Macro Urban Base Station (EIRP = 59 dBm), Bounding TIM, 1540 MHz..... 30
Figure I-46: Macro Urban Base Station (EIRP = 59 dBm), Bounding TIM, 1545 MHz..... 31
Figure I-47: Macro Urban Base Station (EIRP = 59 dBm), Bounding TIM, 1550 MHz..... 31
Figure I-48: Macro Urban Base Station (EIRP = 59 dBm), Bounding TIM, 1675 MHz..... 31
Figure I-49: Maximum Impacted Lateral Distance for Bounding CEL, Macro Urban Base Station with EIRP of 59 dBm/sector..... 33
Figure I-50: Macro Urban Base Station (EIRP = 59 dBm), Bounding CEL, 1525 MHz..... 34
Figure I-51: Macro Urban Base Station (EIRP = 59 dBm), Bounding CEL, 1530 MHz..... 34
Figure I-52: Macro Urban Base Station (EIRP = 59 dBm), Bounding CEL, 1535 MHz..... 35
Figure I-53: Macro Urban Base Station (EIRP = 59 dBm), Bounding CEL, 1540 MHz..... 35
Figure I-54: Macro Urban Base Station (EIRP = 59 dBm), Bounding CEL, 1545 MHz..... 35
Figure I-55: Macro Urban Base Station (EIRP = 59 dBm), Bounding CEL, 1550 MHz..... 36
Figure I-56: Macro Urban Base Station (EIRP = 59 dBm), Bounding CEL, 1675 MHz..... 36
Figure I-57: Small Cell Outdoor/Micro Urban (EIRP = 40 dBm), Bounding GAV 37
Figure I-58: Small Cell Outdoor/Micro Urban (EIRP = 40 dBm), Bounding GAV, 1475 MHz 37
Figure I-59: Small Cell Outdoor/Micro Urban (EIRP = 40 dBm), Bounding GAV, 1490 MHz 38
Figure I-60: Small Cell Outdoor/Micro Urban (EIRP = 40 dBm), Bounding GAV, 1505 MHz 38
Figure I-61: Small Cell Outdoor/Micro Urban (EIRP = 40 dBm), Bounding GAV, 1520 MHz 38
Figure I-62: Small Cell Outdoor/Micro Urban (EIRP = 40 dBm), Bounding GAV, 1525 MHz 39
Figure I-63: Small Cell Outdoor/Micro Urban (EIRP = 40 dBm), Bounding GAV, 1530 MHz 39
Figure I-64: Small Cell Outdoor/Micro Urban (EIRP = 40 dBm), Bounding GAV, 1535 MHz 39
Figure I-65: Small Cell Outdoor/Micro Urban (EIRP = 40 dBm), Bounding GAV, 1540 MHz 40
Figure I-66: Small Cell Outdoor/Micro Urban (EIRP = 40 dBm), Bounding GAV, 1545 MHz 40
Figure I-67: Small Cell Outdoor/Micro Urban (EIRP = 40 dBm), Bounding GAV, 1550 MHz 40
Figure I-68: Small Cell Outdoor/Micro Urban (EIRP = 40 dBm), Bounding GAV, 1675 MHz 41
Figure I-69: Small Cell Outdoor/Micro Urban (EIRP = 40 dBm), Bounding GLN..... 41
Figure I-70: Small Cell Outdoor/Micro Urban (EIRP = 40 dBm), Bounding GLN, 1475 MHz 42

Figure I-71: Small Cell Outdoor/Micro Urban (EIRP = 40 dBm), Bounding GLN, 1490 MHz 42
Figure I-72: Small Cell Outdoor/Micro Urban (EIRP = 40 dBm), Bounding GLN, 1505 MHz 42
Figure I-73: Small Cell Outdoor/Micro Urban (EIRP = 40 dBm), Bounding GLN, 1520 MHz 43
Figure I-74: Small Cell Outdoor/Micro Urban (EIRP = 40 dBm), Bounding GLN, 1525 MHz 43
Figure I-75: Small Cell Outdoor/Micro Urban (EIRP = 40 dBm), Bounding GLN, 1530 MHz 43
Figure I-76: Small Cell Outdoor/Micro Urban (EIRP = 40 dBm), Bounding GLN, 1535 MHz 44
Figure I-77: Small Cell Outdoor/Micro Urban (EIRP = 40 dBm), Bounding GLN, 1540 MHz 44
Figure I-78: Small Cell Outdoor/Micro Urban (EIRP = 40 dBm), Bounding GLN, 1545 MHz 44
Figure I-79: Small Cell Outdoor/Micro Urban (EIRP = 40 dBm), Bounding GLN, 1550 MHz 45
Figure I-80: Small Cell Outdoor/Micro Urban (EIRP = 40 dBm), Bounding GLN, 1675 MHz 45
Figure I-81: Small Cell Outdoor/Micro Urban, Bounding HPR..... 46
Figure I-82: Small Cell Outdoor/Micro Urban (EIRP = 40 dBm), Bounding HPR, 1475 MHz. 46
Figure I-83: Small Cell Outdoor/Micro Urban (EIRP = 40 dBm), Bounding HPR, 1490 MHz. 47
Figure I-84: Small Cell Outdoor/Micro Urban (EIRP = 40 dBm), Bounding HPR, 1505 MHz. 47
Figure I-85: Small Cell Outdoor/Micro Urban (EIRP = 40 dBm), Bounding HPR, 1520 MHz. 47
Figure I-86: Small Cell Outdoor/Micro Urban (EIRP = 40 dBm), Bounding HPR, 1525 MHz. 48
Figure I-87: Small Cell Outdoor/Micro Urban (EIRP = 40 dBm), Bounding HPR, 1530 MHz. 48
Figure I-88: Small Cell Outdoor/Micro Urban (EIRP = 40 dBm), Bounding HPR, 1535 MHz. 48
Figure I-89: Small Cell Outdoor/Micro Urban (EIRP = 40 dBm), Bounding HPR, 1540 MHz. 49
Figure I-90: Small Cell Outdoor/Micro Urban (EIRP = 40 dBm), Bounding HPR, 1545 MHz. 49
Figure I-91: Small Cell Outdoor/Micro Urban (EIRP = 40 dBm), Bounding HPR, 1550 MHz. 49
Figure I-92: Small Cell Outdoor/Micro Urban (EIRP = 40 dBm), Bounding HPR, 1675 MHz. 50
Figure I-93: Small Cell Outdoor/Micro Urban (EIRP = 40 dBm), Bounding TIM..... 50
Figure I-94: Small Cell Outdoor/Micro Urban (EIRP = 40 dBm), Bounding TIM, 1475 MHz . 51
Figure I-95: Small Cell Outdoor/Micro Urban (EIRP = 40 dBm), Bounding TIM, 1490 MHz . 52
Figure I-96: Small Cell Outdoor/Micro Urban (EIRP = 40 dBm), Bounding TIM, 1505 MHz . 53
Figure I-97: Small Cell Outdoor/Micro Urban (EIRP = 40 dBm), Bounding TIM, 1520 MHz . 53
Figure I-98: Small Cell Outdoor/Micro Urban (EIRP = 40 dBm), Bounding TIM, 1525 MHz . 54
Figure I-99: Small Cell Outdoor/Micro Urban (EIRP = 40 dBm), Bounding TIM, 1530 MHz . 54
Figure I-100: Small Cell Outdoor/Micro Urban (EIRP = 40 dBm), Bounding TIM, 1535 MHz 54
Figure I-101: Small Cell Outdoor/Micro Urban (EIRP = 40 dBm), Bounding TIM, 1540 MHz 55
Figure I-102: Small Cell Outdoor/Micro Urban (EIRP = 40 dBm), Bounding TIM, 1545 MHz 55
Figure I-103: Small Cell Outdoor/Micro Urban (EIRP = 40 dBm), Bounding TIM, 1550 MHz 55
Figure I-104: Small Cell Outdoor/Micro Urban (EIRP = 40 dBm), Bounding TIM, 1675 MHz 56
Figure I-105: Small Cell Outdoor/Micro Urban (EIRP = 40 dBm), Bounding CEL 57
Figure I-106: Small Cell Outdoor/Micro Urban (EIRP = 40 dBm), Bounding CEL, 1525 MHz 58
Figure I-107: Small Cell Outdoor/Micro Urban (EIRP = 40 dBm), Bounding CEL, 1530 MHz 59
Figure I-108: Small Cell Outdoor/Micro Urban (EIRP = 40 dBm), Bounding CEL, 1535 MHz 59
Figure I-109: Small Cell Outdoor/Micro Urban (EIRP = 40 dBm), Bounding CEL, 1540 MHz 60

Figure I-110: Small Cell Outdoor/Micro Urban (EIRP = 40 dBm), Bounding CEL, 1545 MHz 60
Figure I-111: Small Cell Outdoor/Micro Urban (EIRP = 40 dBm), Bounding CEL, 1550 MHz 60
Figure I-112: Small Cell Outdoor/Micro Urban (EIRP = 40 dBm), Bounding CEL, 1675 MHz 61
Figure I-113: Handset (EIRP = 23 dBm), Bounding GAV 62
Figure I-114: Handset (EIRP = 23 dBm), Bounding GAV, 1620 MHz 62
Figure I-115: Handset (EIRP = 23 dBm), Bounding GAV, 1625 MHz 63
Figure I-116: Handset (EIRP = 23 dBm), Bounding GAV, 1630 MHz 63
Figure I-117: Handset (EIRP = 23 dBm), Bounding GAV, 1635 MHz 64
Figure I-118: Handset (EIRP = 23 dBm), Bounding GAV, 1640 MHz 64
Figure I-119: Handset (EIRP = 23 dBm), Bounding GAV, 1645 MHz 65
Figure I-120: Handset (EIRP = 23 dBm), Bounding GAV, 1660 MHz 65
Figure I-121: Handset (EIRP = 23 dBm), Bounding GLN 66
Figure I-122: Handset (EIRP = 23 dBm), Bounding GLN, 1620 MHz 66
Figure I-123: Handset (EIRP = 23 dBm), Bounding GLN, 1625 MHz 67
Figure I-124: Handset (EIRP = 23 dBm), Bounding GLN, 1630 MHz 67
Figure I-125: Handset (EIRP = 23 dBm), Bounding GLN, 1635 MHz 68
Figure I-126: Handset (EIRP = 23 dBm), Bounding GLN, 1640 MHz 68
Figure I-127: Handset (EIRP = 23 dBm), Bounding GLN, 1645 MHz 69
Figure I-128: Handset (EIRP = 23 dBm), Bounding GLN, 1660 MHz 69
Figure I-129: Handset (EIRP = 23 dBm), Bounding HPR 70
Figure I-130: Handset (EIRP = 23 dBm), Bounding HPR, 1620 MHz 70
Figure I-131: Handset (EIRP = 23 dBm), Bounding HPR, 1625 MHz 71
Figure I-132: Handset (EIRP = 23 dBm), Bounding HPR, 1630 MHz 71
Figure I-133: Handset (EIRP = 23 dBm), Bounding HPR, 1635 MHz 71
Figure I-134: Handset (EIRP = 23 dBm), Bounding HPR, 1640 MHz 72
Figure I-135: Handset (EIRP = 23 dBm), Bounding HPR, 1645 MHz 72
Figure I-136: Handset (EIRP = 23 dBm), Bounding HPR, 1660 MHz 72
Figure I-137: Handset (EIRP = 23 dBm), Bounding TIM 73
Figure I-138: Handset (EIRP = 23 dBm), Bounding TIM, 1620 MHz 74
Figure I-139: Handset (EIRP = 23 dBm), Bounding TIM, 1625 MHz 74
Figure I-140: Handset (EIRP = 23 dBm), Bounding TIM, 1630 MHz 75
Figure I-141: Handset (EIRP = 23 dBm), Bounding TIM, 1635 MHz 75
Figure I-142: Handset (EIRP = 23 dBm), Bounding TIM, 1640 MHz 76
Figure I-143: Handset (EIRP = 23 dBm), Bounding TIM, 1645 MHz 76
Figure I-144: Handset (EIRP = 23 dBm), Bounding TIM, 1660 MHz 77
Figure I-145: Handset (EIRP = 23 dBm), Bounding CEL 78
Figure I-146: Handset (EIRP = 23 dBm), Bounding CEL, 1620 MHz 79
Figure I-147: Handset (EIRP = 23 dBm), Bounding CEL, 1625 MHz 79
Figure I-148: Handset (EIRP = 23 dBm), Bounding CEL, 1630 MHz 80

Figure I-149: Handset (EIRP = 23 dBm), Bounding CEL, 1635 MHz 80
Figure I-150: Handset (EIRP = 23 dBm), Bounding CEL, 1640 MHz 81
Figure I-151: Handset (EIRP = 23 dBm), Bounding CEL, 1645 MHz 81
Figure I-152: Handset (EIRP = 23 dBm), Bounding CEL, 1660 MHz 82
Figure I-153: Maximum Impacted Lateral Distance for GAV, Macro Urban Base Station (EIRP = 59 dBm) 83
Figure I-154: Maximum Impacted Lateral Distance for GLN, Macro Urban Base Station (EIRP = 59 dBm) 84
Figure I-155: Maximum Impacted Lateral Distance for HPR, Macro Urban Base Station (EIRP = 59 dBm) 85
Figure I-156: Maximum Impacted Lateral Distance for TIM, Macro Urban Base Station (EIRP = 59 dBm) 86
Figure I-157: Maximum Impacted Lateral Distance for CEL, Macro Urban Base Station (EIRP = 59 dBm) 87
Figure I-158: Small Cell Outdoor/Micro Urban (EIRP = 40 dBm), Bounding GLN, 1530 MHz: (a) GPS C/A-code (b) GLONASS L1C 88
Figure I-159: Impacted Area for Cellular DUT from 23 dBm EIRP Mobile Device at 1550 MHz (a) as predicted using free-space propagation model, (b) as predicted using two-ray propagation model 89

LIST OF TABLES

No table of figures entries found.

REFERENCES

There are no sources in the current document.

APPENDIX

Appendix I. Forward Modeling Results

This appendix presents forward modeling results. Section I.1 provides results for macro urban base stations (EIRP = 59 dBm, antenna height = 25 m). Section I.2 provides results for micro urban/small cell outdoor base stations (EIRP = 40 dBm, antenna height = 6 m). Section I.3 provides results for mobile devices (EIRP = 23 dBm, antenna height = 2 m). These three sections (Sections I.1, I.2, and I.3) only include results for the most sensitive (bounding) GPS C/A-code receiver for each frequency in each receiver category (except certified-aviation and spaceborne).

Section I.4 provides the results of a sensitivity analysis. This section explores the variability in forward modeling results with input assumptions including: (1) percentile of DUTs protected (e.g., protecting the median DUT vs. the bounding DUT for each frequency and each receiver category), (2) consideration of other GNSS signal types besides the GPS C/A-code, and (3) propagation model.

I.1 Macro Urban Base Station, GPS C/A-code

This section presents results for 10-MHz LTE signals broadcast by macro urban base stations (three sectors with 59 dBm EIRP/sector, 16 dBi antennas at 25 m AGL with 10 deg downtilt), free-space propagation, and bounding mask.

I.1.1 GAV

Figure I-1 plots the maximum impacted lateral distance for three types of impact to the most sensitive (bounding) DUT for each frequency: (1) interference results in a 1-dB CNR degradation (blue), (2) interference results in loss of lock on low-elevation angle satellites (red), and (3) interference results in loss of lock for high-elevation angle satellites (orange). Figure I-2 to Figure I-12 show the two-dimensional impacted area regions for tested frequencies from 1475 MHz to 1675 MHz.

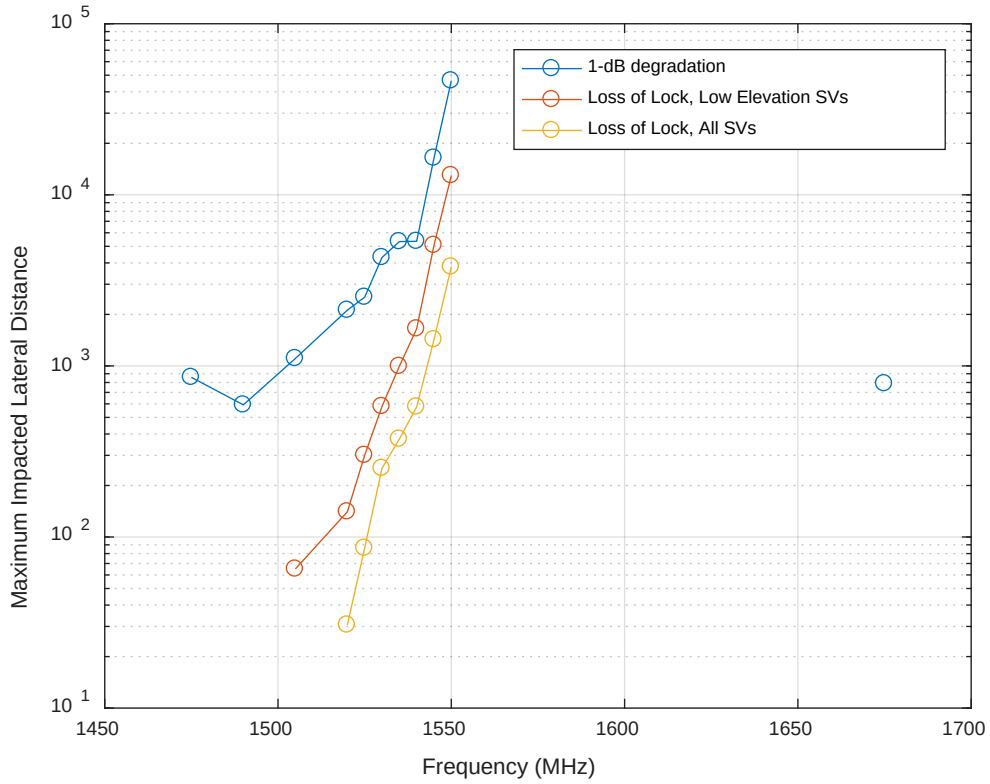

Figure I-1: Maximum Impacted Lateral Distance for Bounding GAV, Macro Urban Base Station (EIRP = 59 dBm)

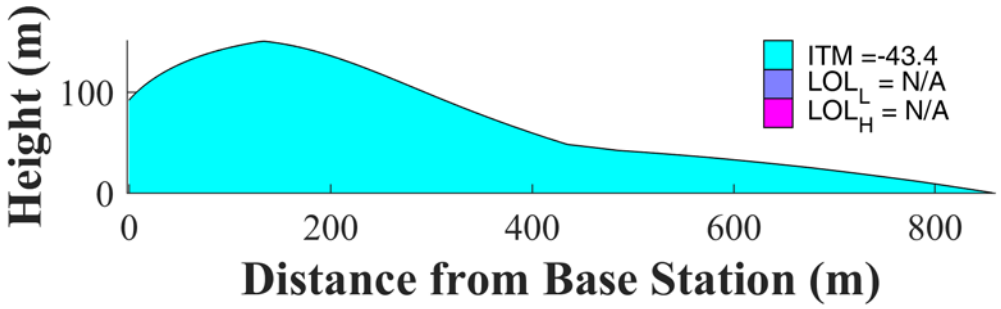

Figure I-2: Macro Urban Base Station (EIRP = 59 dBm), Bounding GAV, 1475 MHz

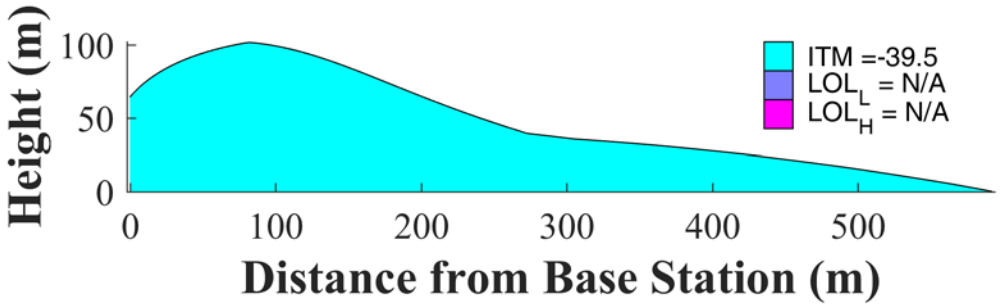

Figure I-3: Macro Urban Base Station (EIRP = 59 dBm), Bounding GAV, 1490 MHz

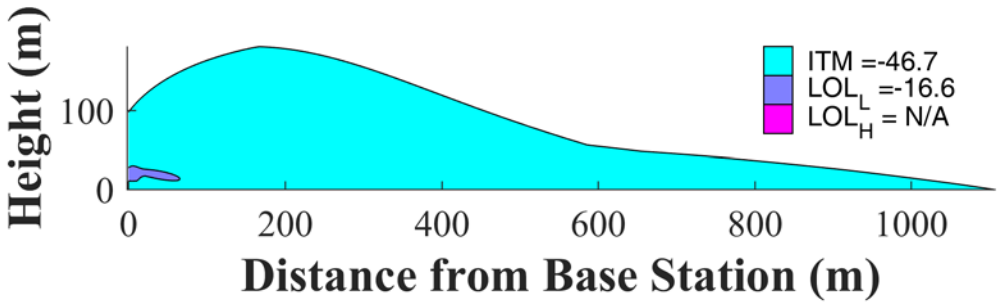

Figure I-4: Macro Urban Base Station (EIRP = 59 dBm), Bounding GAV, 1505 MHz

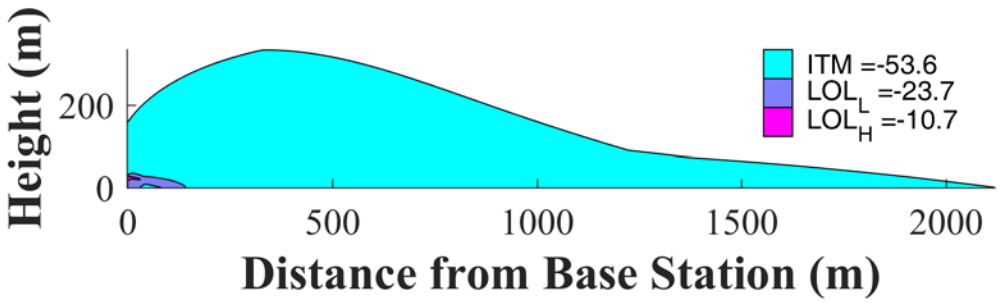

Figure I-5: Macro Urban Base Station (EIRP = 59 dBm), Bounding GAV, 1520 MHz

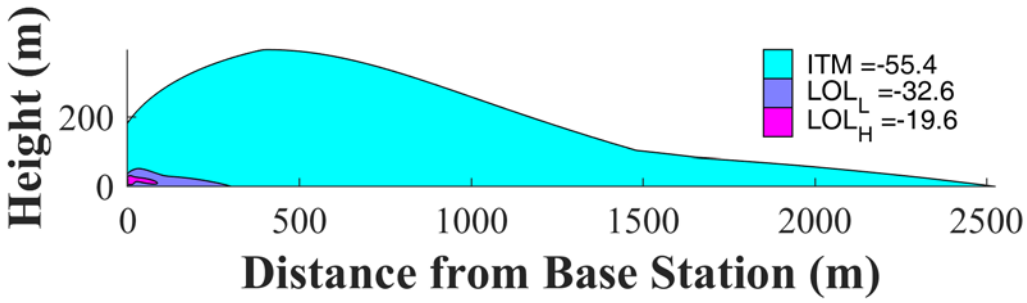

Figure I-6: Macro Urban Base Station (EIRP = 59 dBm), Bounding GAV, 1525 MHz

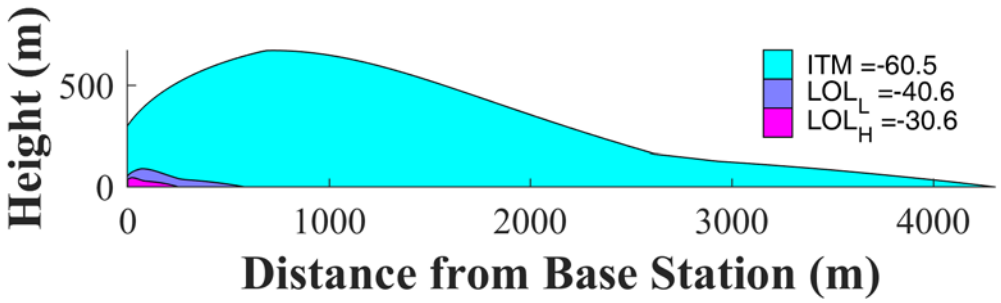

Figure I-7: Macro Urban Base Station (EIRP = 59 dBm), Bounding GAV, 1530 MHz

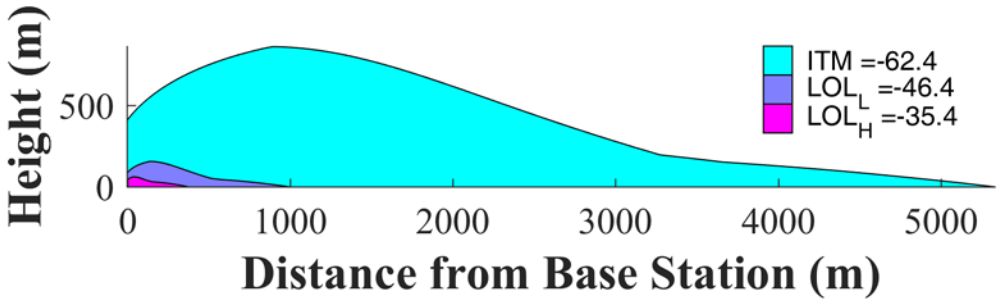

Figure I-8: Macro Urban Base Station (EIRP = 59 dBm), Bounding GAV, 1535 MHz

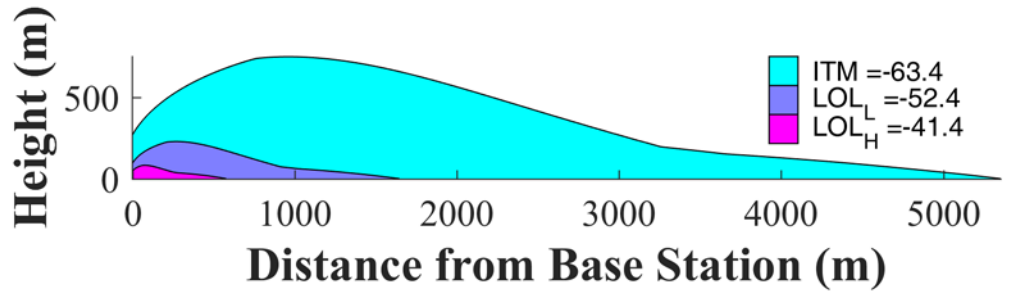

Figure I-9: Macro Urban Base Station (EIRP = 59 dBm), Bounding GAV, 1540 MHz

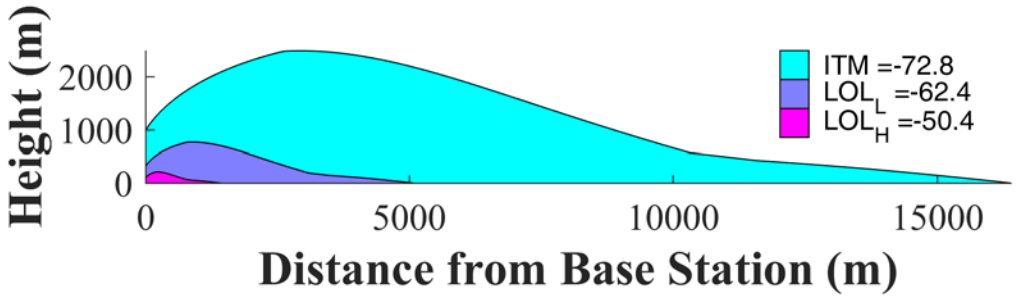

Figure I-10: Macro Urban Base Station (EIRP = 59 dBm), Bounding GAV, 1545 MHz

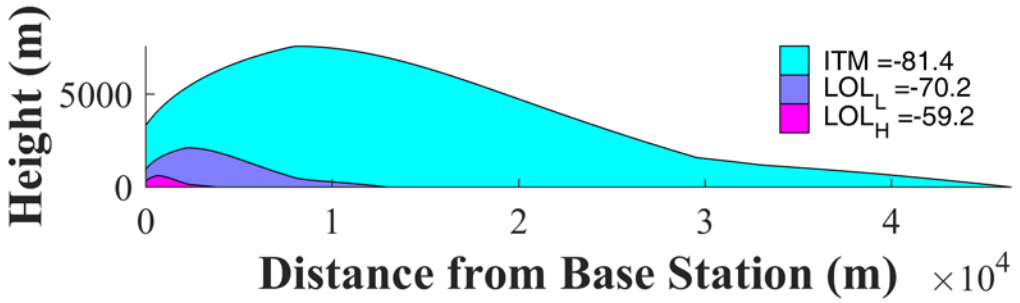

Figure I-11: Macro Urban Base Station (EIRP = 59 dBm), Bounding GAV, 1550 MHz

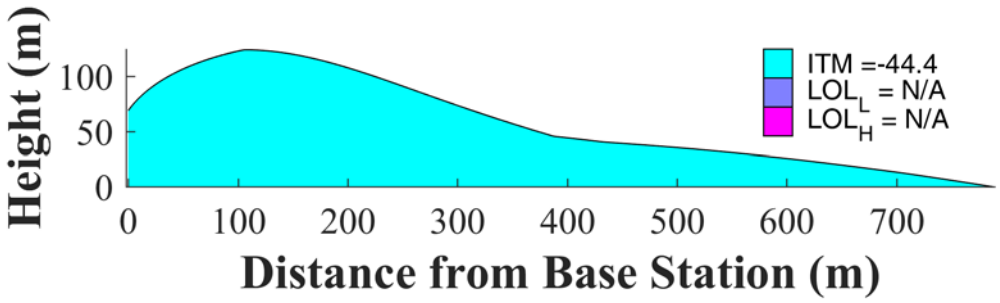

Figure I-12: Macro Urban Base Station (EIRP = 59 dBm), Bounding GAV, 1675 MHz

I.1.2 GLN

Figure I-13 plots the maximum impacted lateral distance for three types of impact to the most sensitive (bounding) DUT for each frequency: (1) interference results in a 1-dB CNR degradation (blue), (2) interference results in loss of lock on low-elevation angle satellites (red), and (3) interference results in loss of lock for high-elevation angle satellites (orange). Figure I-14 to Figure I-24 show the two-dimensional impacted area regions for tested frequencies from 1475 MHz to 1675 MHz.

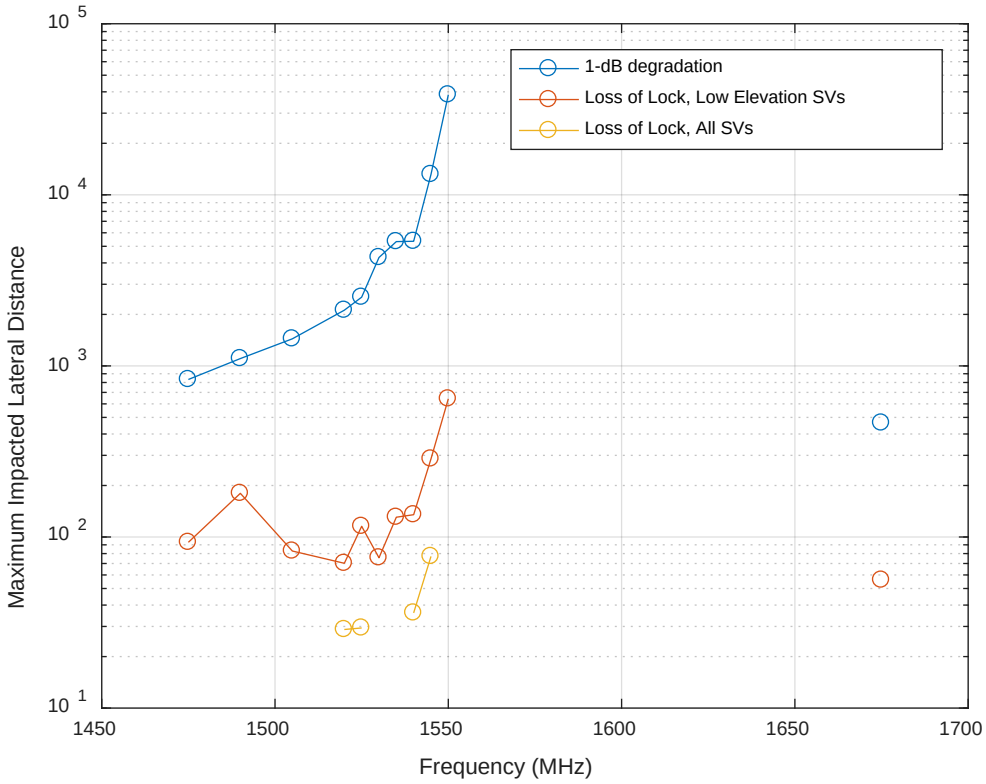

Figure I-13: Maximum Impacted Lateral Distance for Bounding GLN, Macro Urban Base Station with EIRP of 59 dBm/sector

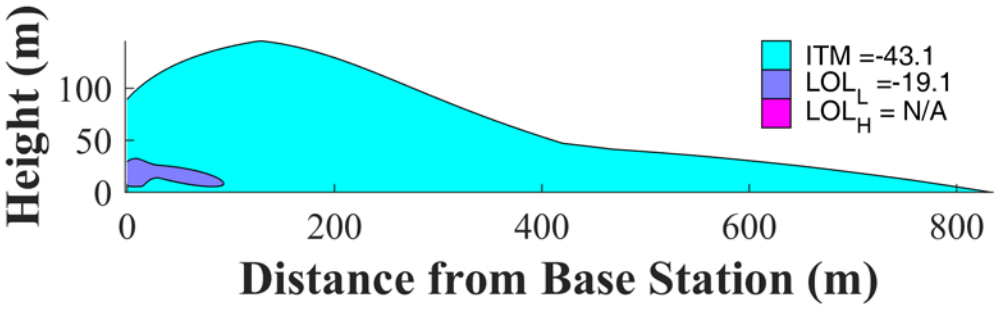

Figure I-14: Macro Urban Base Station (EIRP = 59 dBm), Bounding GLN, 1475 MHz

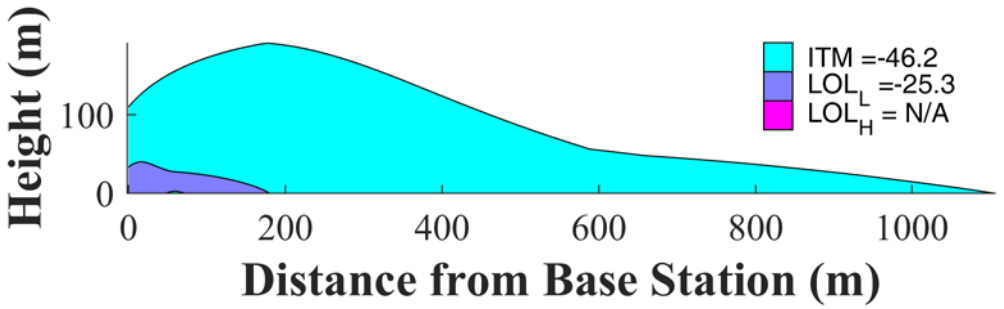

Figure I-15: Macro Urban Base Station (EIRP = 59 dBm), Bounding GLN, 1490 MHz

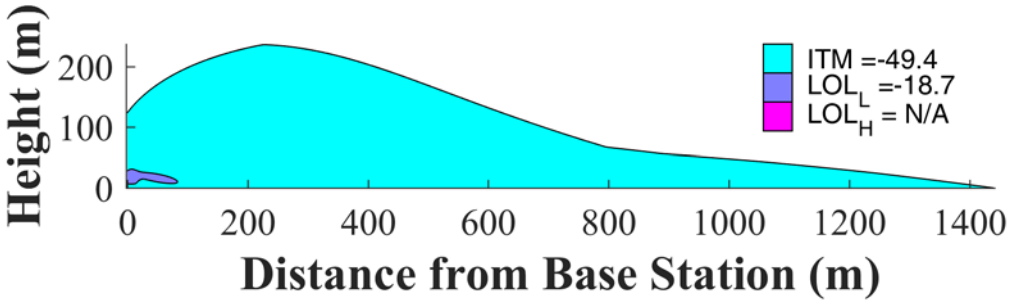

Figure I-16: Macro Urban Base Station (EIRP = 59 dBm), Bounding GLN, 1505 MHz

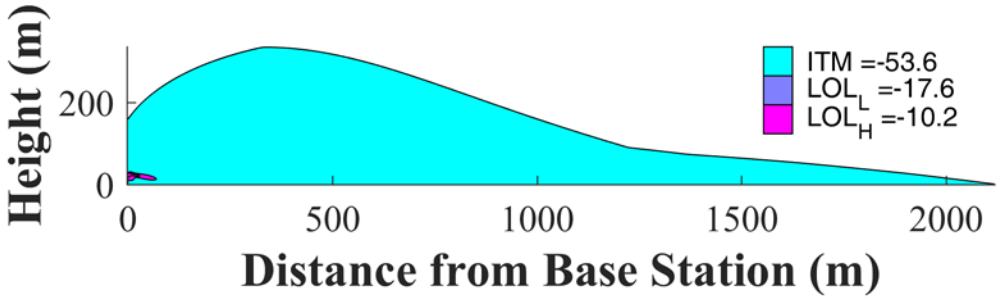

Figure I-17: Macro Urban Base Station (EIRP = 59 dBm), Bounding GLN, 1520 MHz

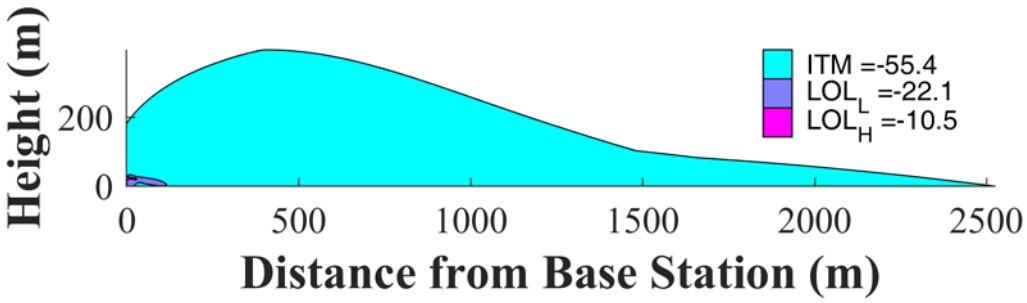

Figure I-18: Macro Urban Base Station (EIRP = 59 dBm), Bounding GLN, 1525 MHz

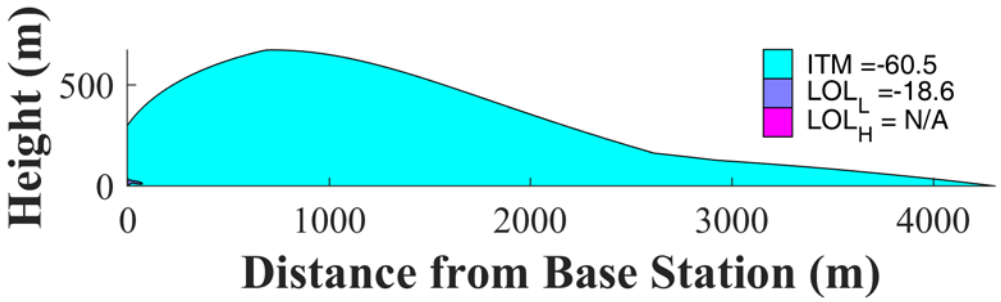

Figure I-19: Macro Urban Base Station (EIRP = 59 dBm), Bounding GLN, 1530 MHz

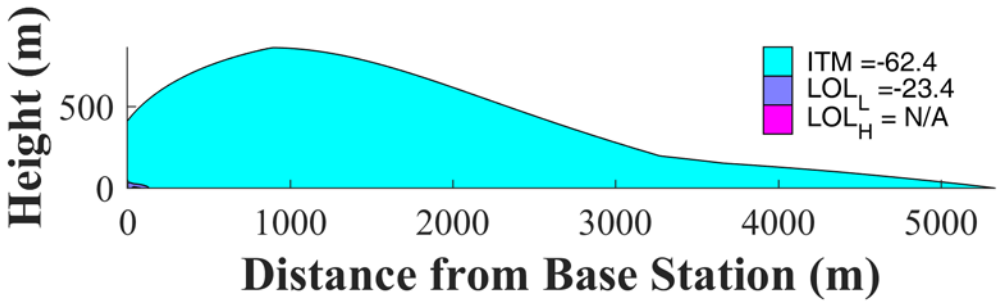

Figure I-20: Macro Urban Base Station (EIRP = 59 dBm), Bounding GLN, 1535 MHz

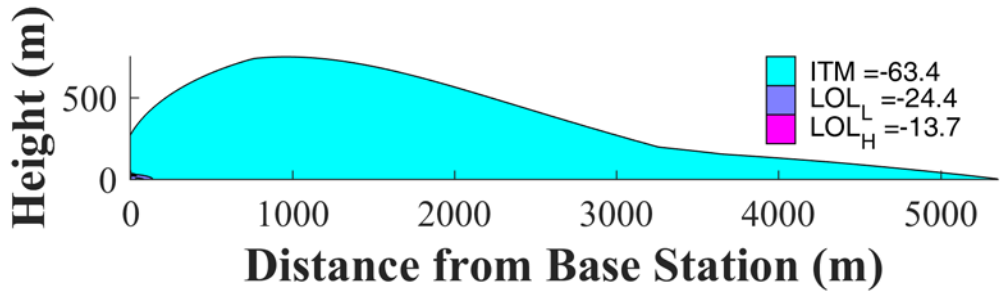

Figure I-21: Macro Urban Base Station (EIRP = 59 dBm), Bounding GLN, 1540 MHz

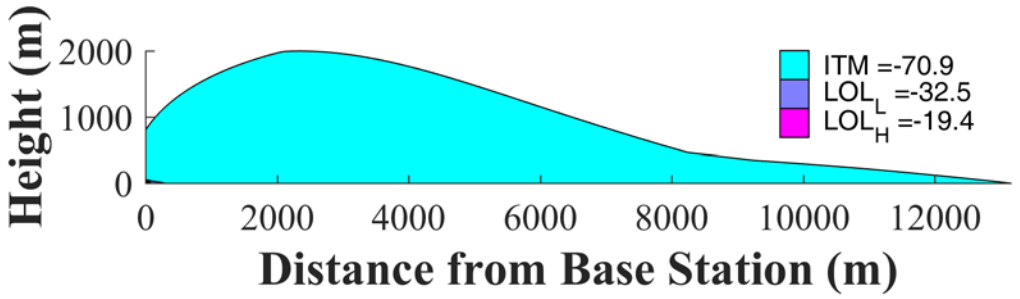

Figure I-22: Macro Urban Base Station (EIRP = 59 dBm), Bounding GLN, 1545 MHz

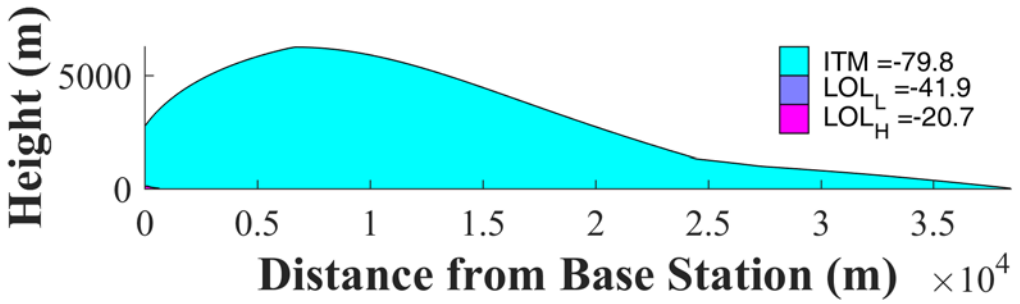

Figure I-23: Macro Urban Base Station (EIRP = 59 dBm), Bounding GLN, 1550 MHz

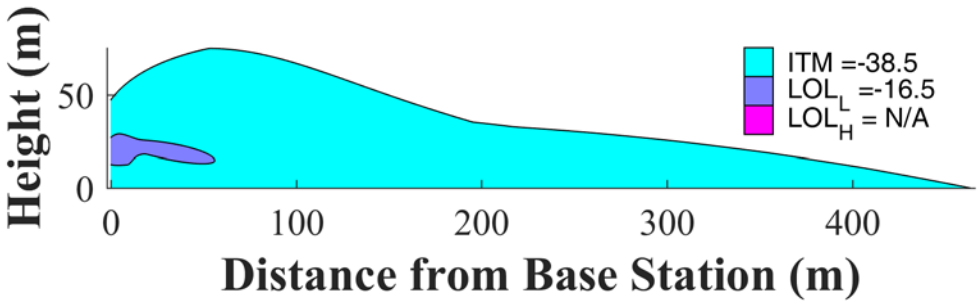

Figure I-24: Macro Urban Base Station (EIRP = 59 dBm), Bounding GLN, 1675 MHz

I.1.3 HPR

Figure I-25 plots the maximum impacted lateral distance for three types of impact to the most sensitive (bounding) DUT for each frequency: (1) interference results in a 1-dB CNR degradation (blue), (2) interference results in loss of lock on low-elevation angle satellites (red), and (3) interference results in loss of lock for high-elevation angle satellites (orange). Figure I-26 to Figure I-36 show the two-dimensional impacted area regions for tested frequencies from 1475 MHz to 1675 MHz.

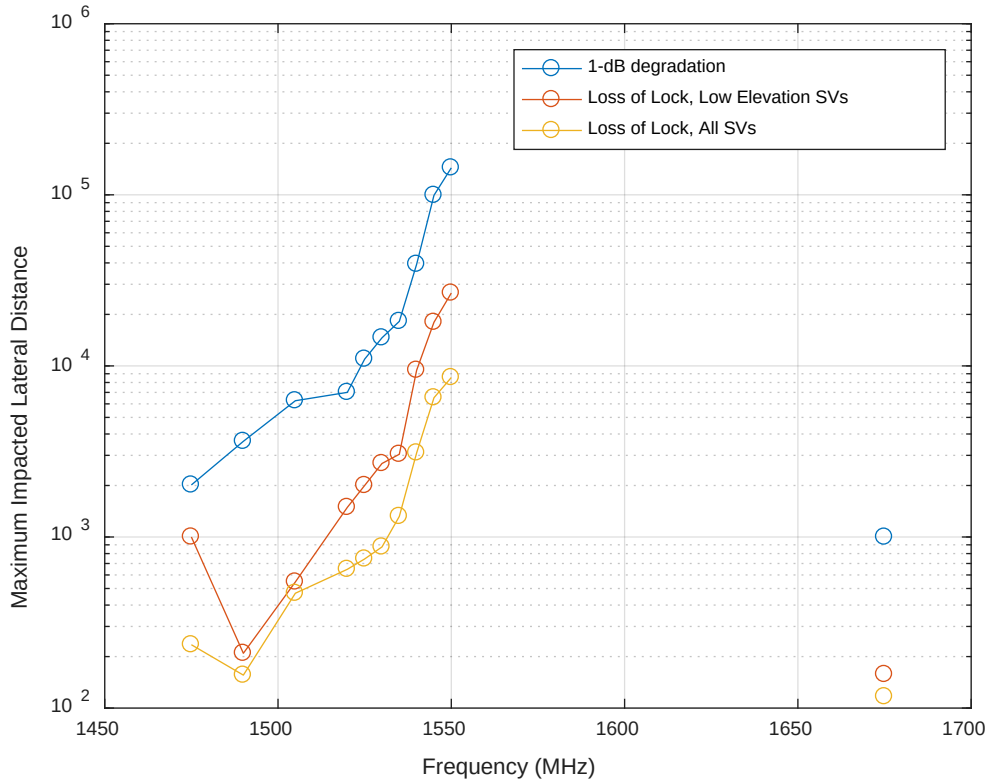

Figure I-25: Maximum Impacted Lateral Distance for Bounding HPR, Macro Urban Base Station with EIRP of 59 dBm/sector

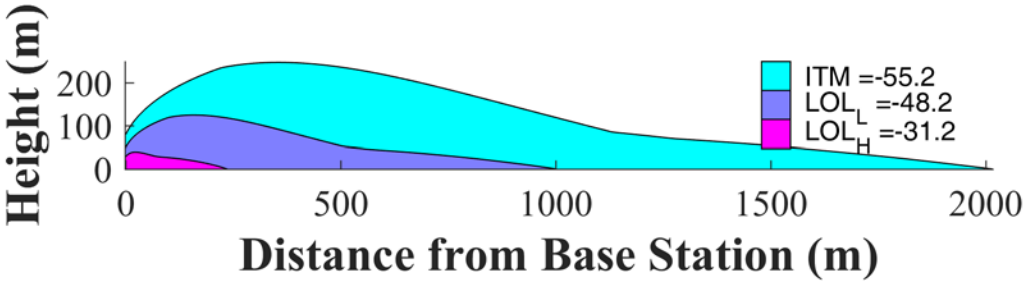

Figure I-26: Macro Urban Base Station (EIRP = 59 dBm), Bounding HPR, 1475 MHz

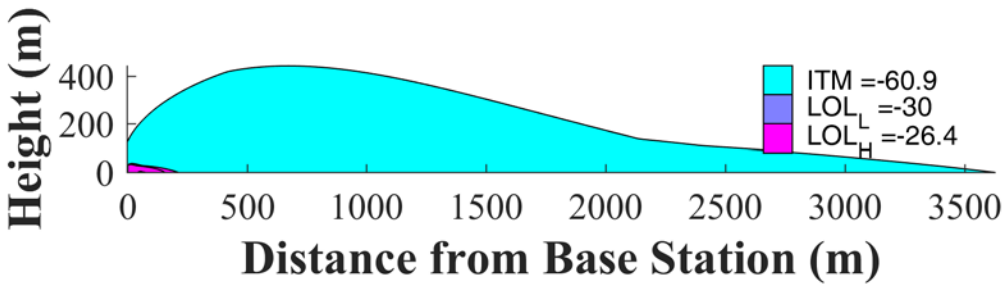

Figure I-27: Macro Urban Base Station (EIRP = 59 dBm), Bounding HPR, 1490 MHz

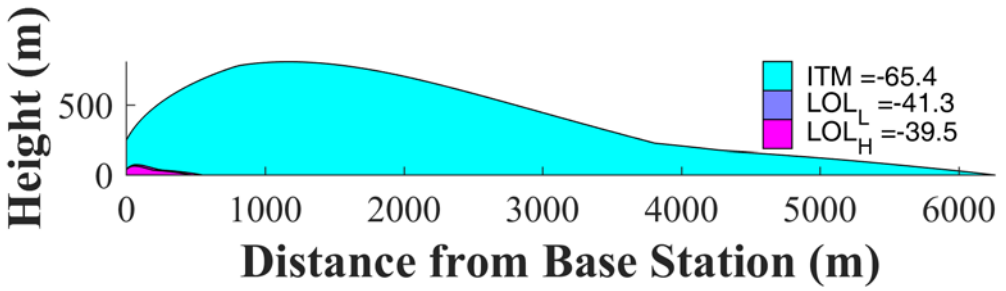

Figure I-28: Macro Urban Base Station (EIRP = 59 dBm), Bounding HPR, 1505 MHz

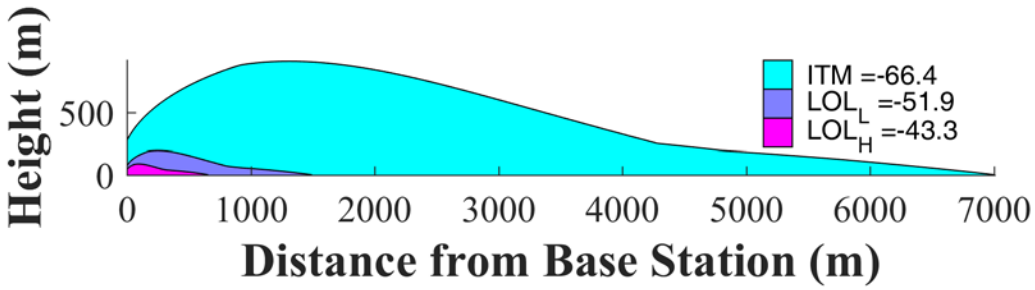

Figure I-29: Macro Urban Base Station (EIRP = 59 dBm), Bounding HPR, 1520 MHz

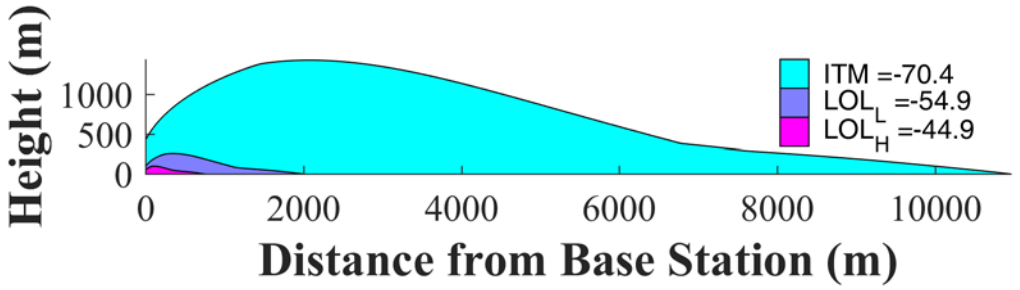

Figure I-30: Macro Urban Base Station (EIRP = 59 dBm), Bounding HPR, 1525 MHz

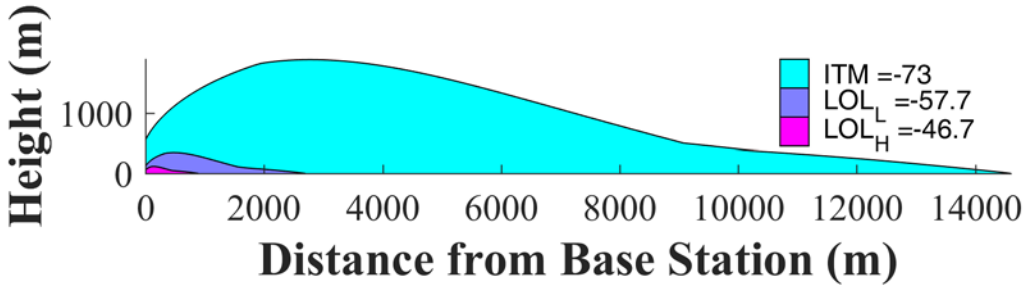

Figure I-31: Macro Urban Base Station (EIRP = 59 dBm), Bounding HPR, 1530 MHz

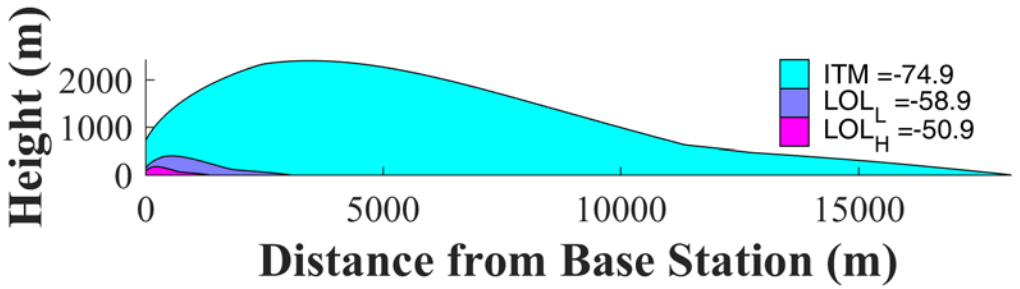

Figure I-32: Macro Urban Base Station (EIRP = 59 dBm), Bounding HPR, 1535 MHz

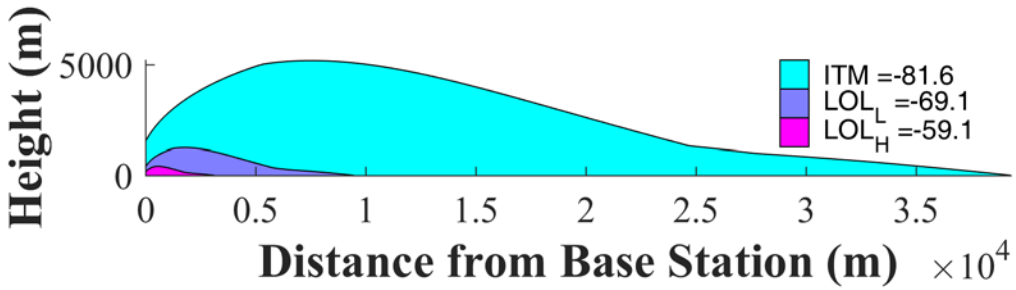

Figure I-33: Macro Urban Base Station (EIRP = 59 dBm), Bounding HPR, 1540 MHz

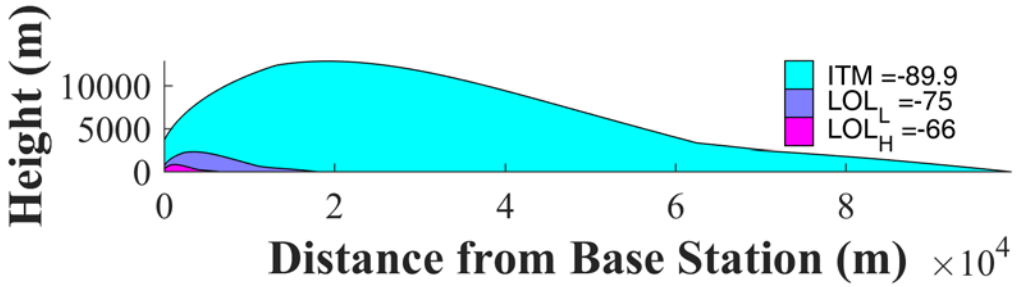

Figure I-34: Macro Urban Base Station (EIRP = 59 dBm), Bounding HPR, 1545 MHz

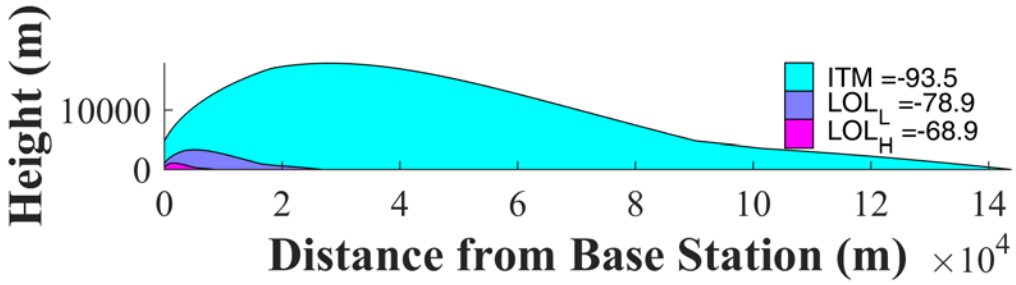

Figure I-35: Macro Urban Base Station (EIRP = 59 dBm), Bounding HPR, 1550 MHz

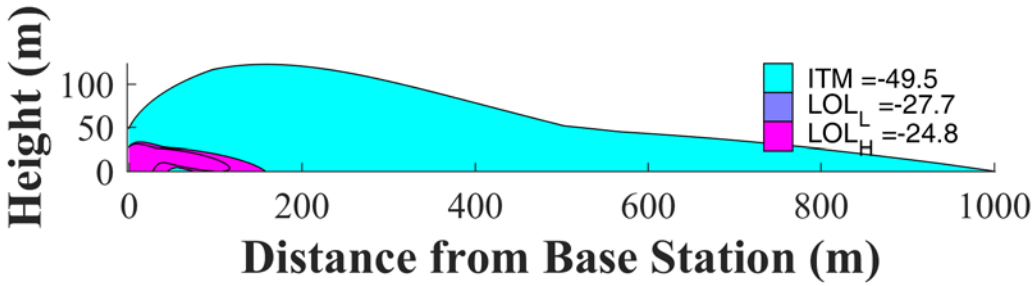

Figure I-36: Macro Urban Base Station (EIRP = 59 dBm), Bounding HPR, 1675 MHz

I.1.4 TIM

Figure I-37 plots the maximum impacted lateral distance for three types of impact to the most sensitive (bounding) DUT for each frequency: (1) interference results in a 1-dB CNR degradation (blue), (2) interference results in loss of lock on low-elevation angle satellites (red), and (3) interference results in loss of lock for high-elevation angle satellites (orange). Figure I-38 to Figure I-48 show the two-dimensional impacted area regions for tested frequencies from 1475 MHz to 1675 MHz.

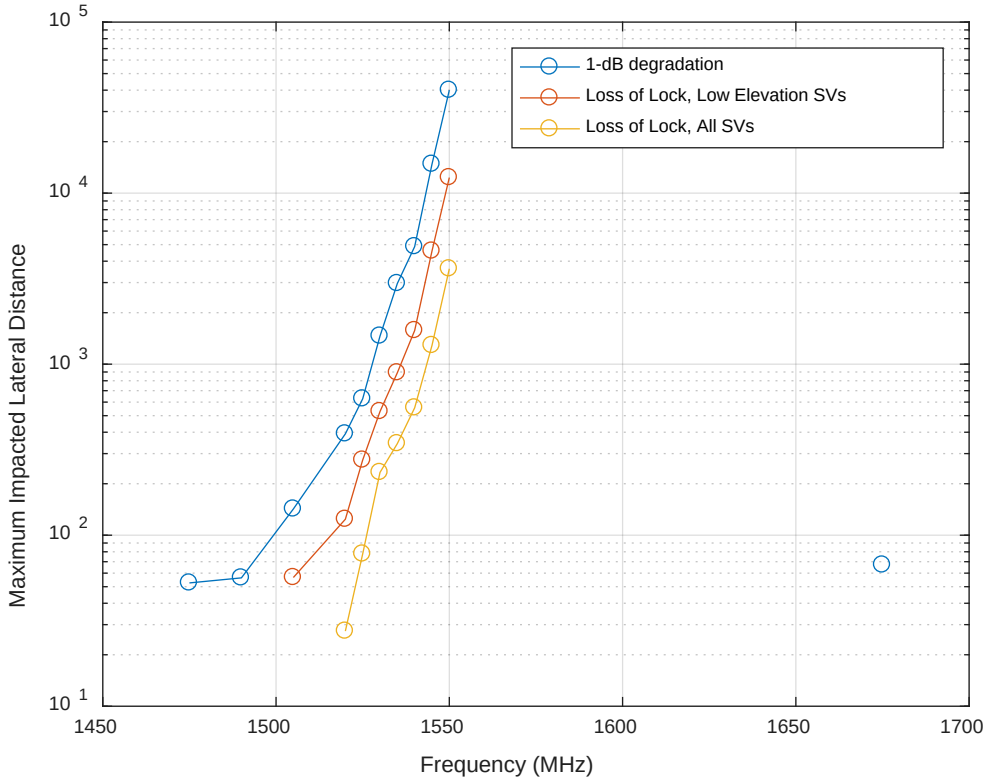

Figure I-37: Maximum Impacted Lateral Distance for Bounding TIM, Macro Urban Base Station with EIRP of 59 dBm/sector

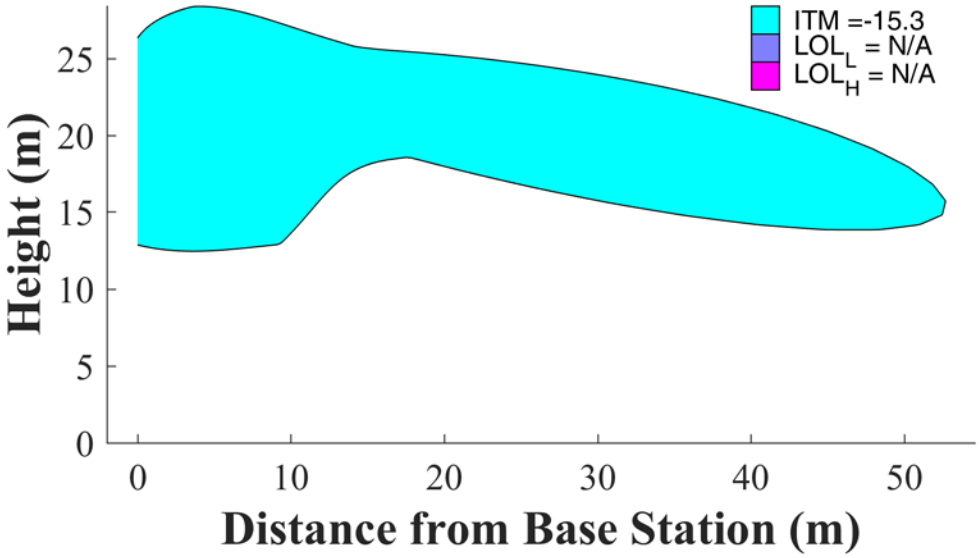

Figure I-38: Macro Urban Base Station (EIRP = 59 dBm), Bounding TIM, 1475 MHz

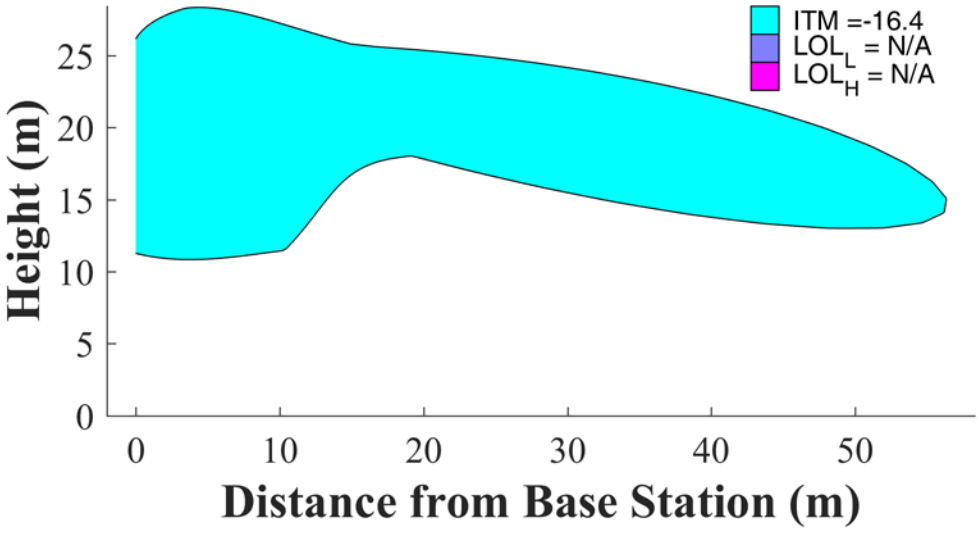

Figure I-39: Macro Urban Base Station (EIRP = 59 dBm), Bounding TIM, 1490 MHz

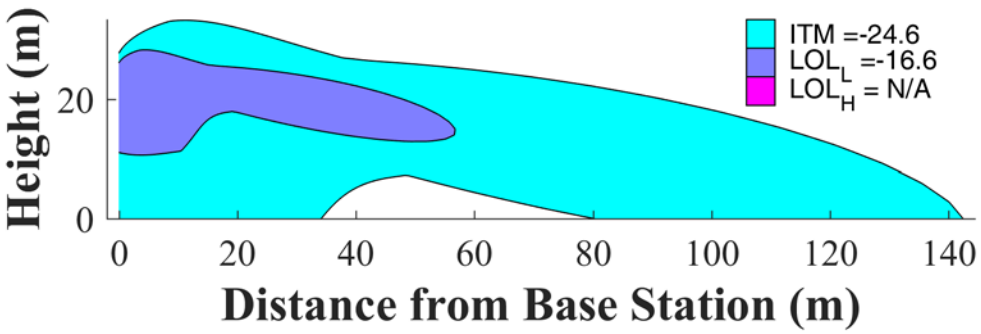

Figure I-40: Macro Urban Base Station (EIRP = 59 dBm), Bounding TIM, 1505 MHz

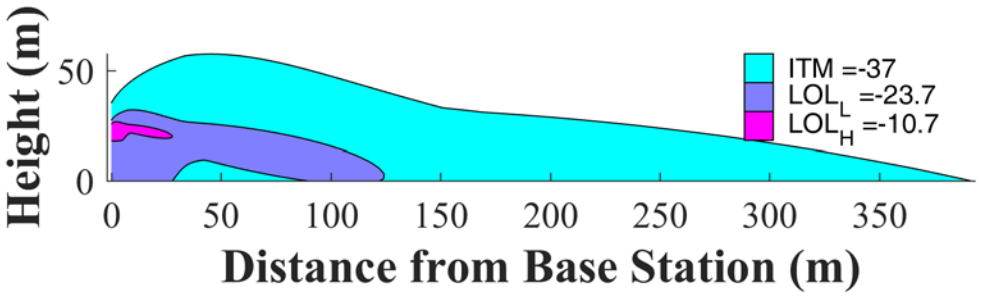

Figure I-41: Macro Urban Base Station (EIRP = 59 dBm), Bounding TIM, 1520 MHz

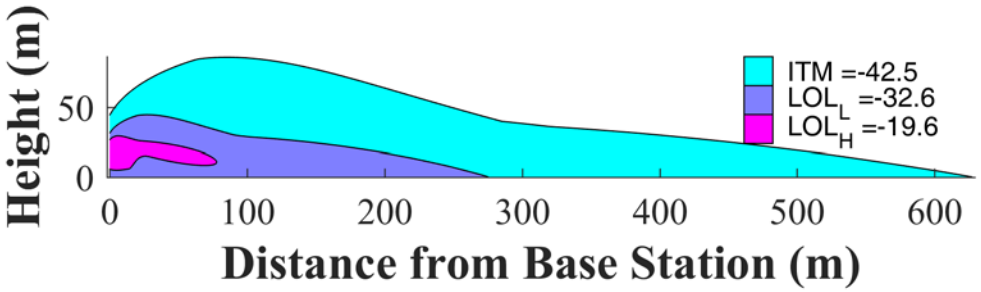

Figure I-42: Macro Urban Base Station (EIRP = 59 dBm), Bounding TIM, 1525 MHz

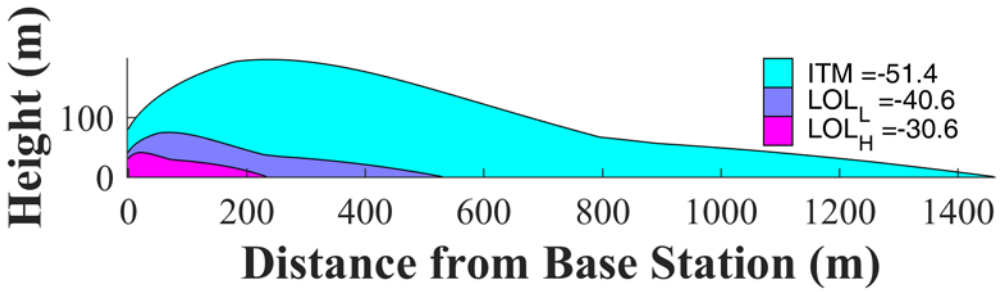

Figure I-43: Macro Urban Base Station (EIRP = 59 dBm), Bounding TIM, 1530 MHz

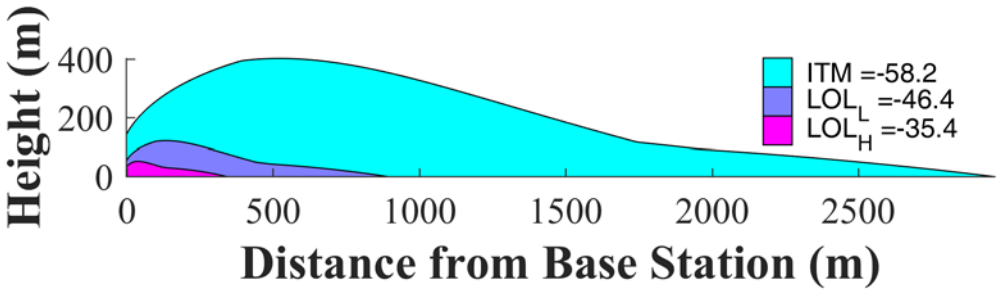

Figure I-44: Macro Urban Base Station (EIRP = 59 dBm), Bounding TIM, 1535 MHz

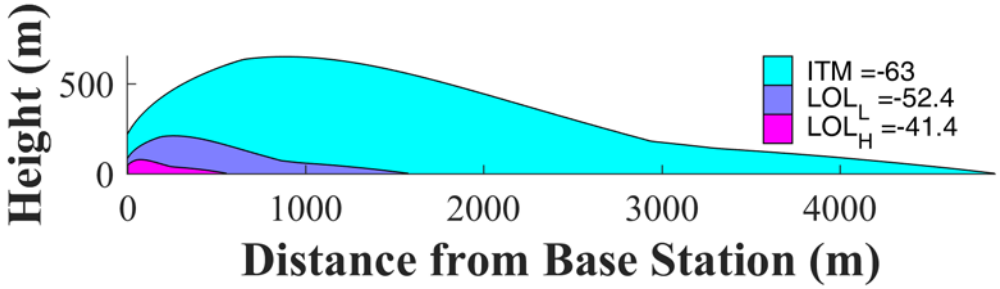

Figure I-45: Macro Urban Base Station (EIRP = 59 dBm), Bounding TIM, 1540 MHz

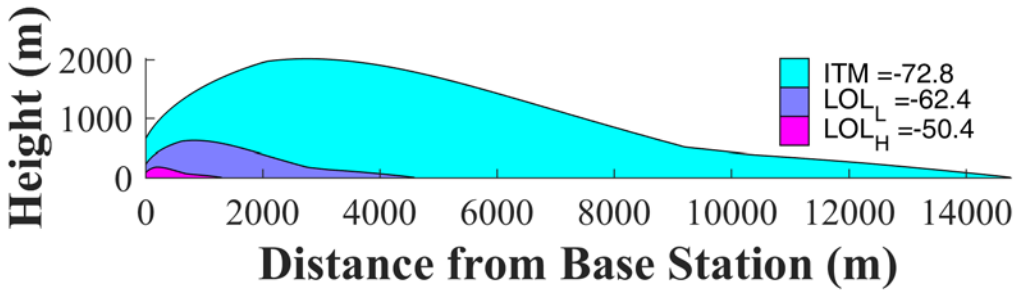

Figure I-46: Macro Urban Base Station (EIRP = 59 dBm), Bounding TIM, 1545 MHz

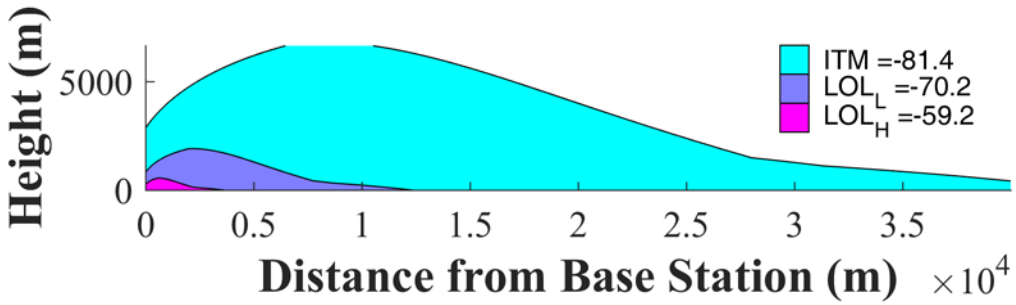

Figure I-47: Macro Urban Base Station (EIRP = 59 dBm), Bounding TIM, 1550 MHz

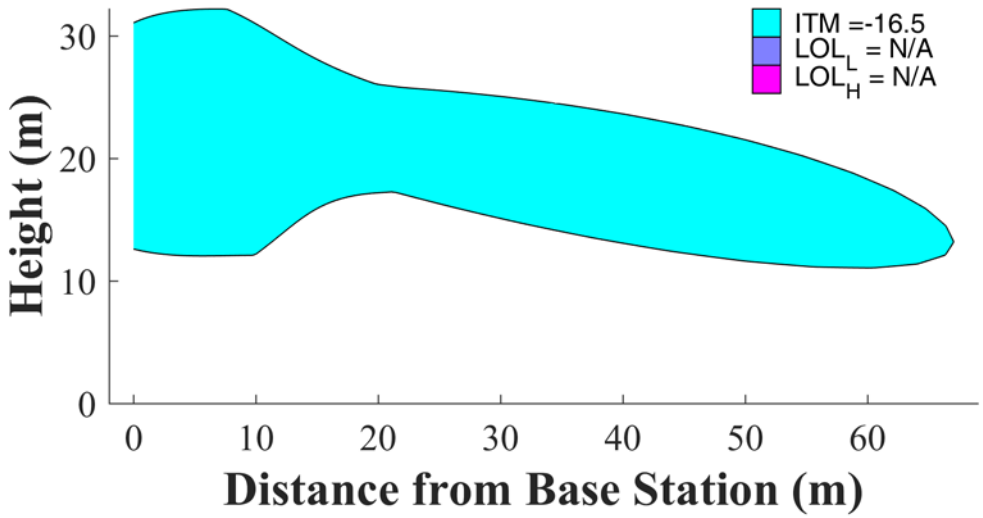

Figure I-48: Macro Urban Base Station (EIRP = 59 dBm), Bounding TIM, 1675 MHz

I.1.5 CEL

Figure I-49 plots the maximum impacted lateral distance for three types of impact to the most sensitive (bounding) DUT for each frequency: (1) interference results in a 1-dB CNR degradation (blue), (2) interference results in loss of lock on -10 dB satellites[1] (red), and (3) interference results in loss of lock for high-elevation angle satellites (orange). Figure I-50 to Figure I-56 show the two-dimensional impacted area regions for tested frequencies from 1525 MHz to 1675 MHz. (Note that for the other LTE frequencies tested, there was no impact).

[1] All of the plots in this Appendix that use the loss-of-lock interference level towards nominally powered satellites are referred to as "all SVs" and towards -10 dB satellites as "low elevation SVs" since a typical DUT antenna exhibited 10 dB less gain towards low elevation angles as compared to its gain at zenith. However, these curves should be interpreted differently for CEL devices since as described in the main body of this report, CEL antennas were modeled as isotropic. The "all SVs" curve can still be interpreted as the interference level that would result in loss of tracking of all satellites, but the "low elevation SVs" curve should be interpreted as the interference level that would result in the device losing lock on satellite signals that are attenuated by 10 dB due, e.g., to line-of-sight blockage.

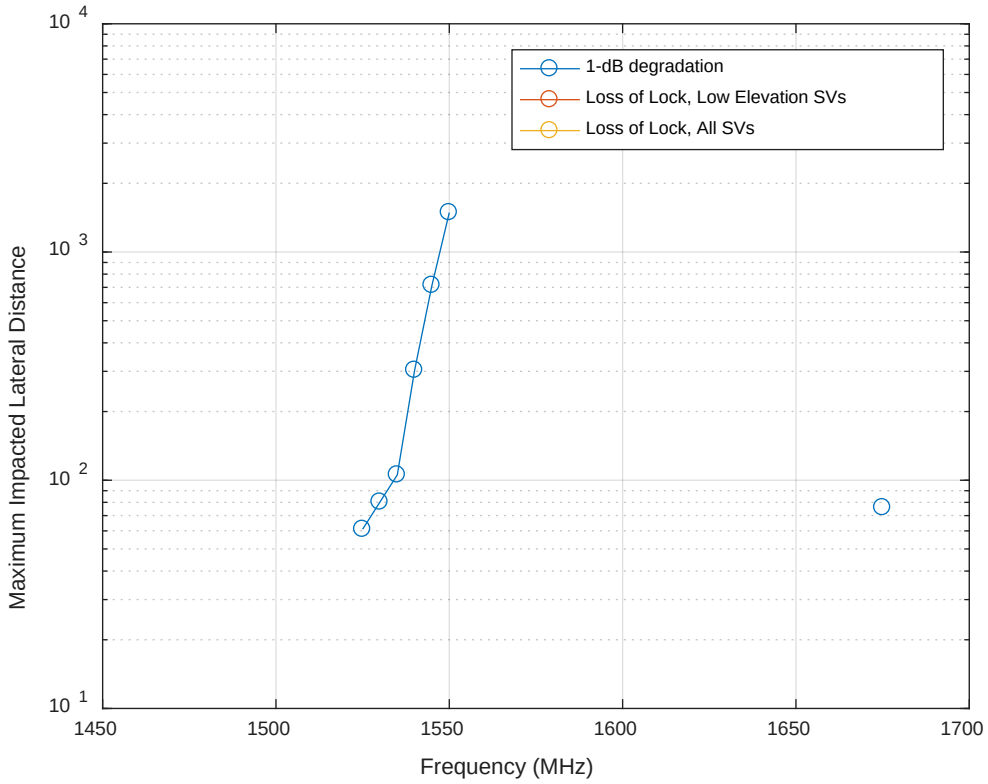

Figure I-49: Maximum Impacted Lateral Distance for Bounding CEL, Macro Urban Base Station with EIRP of 59 dBm/sector

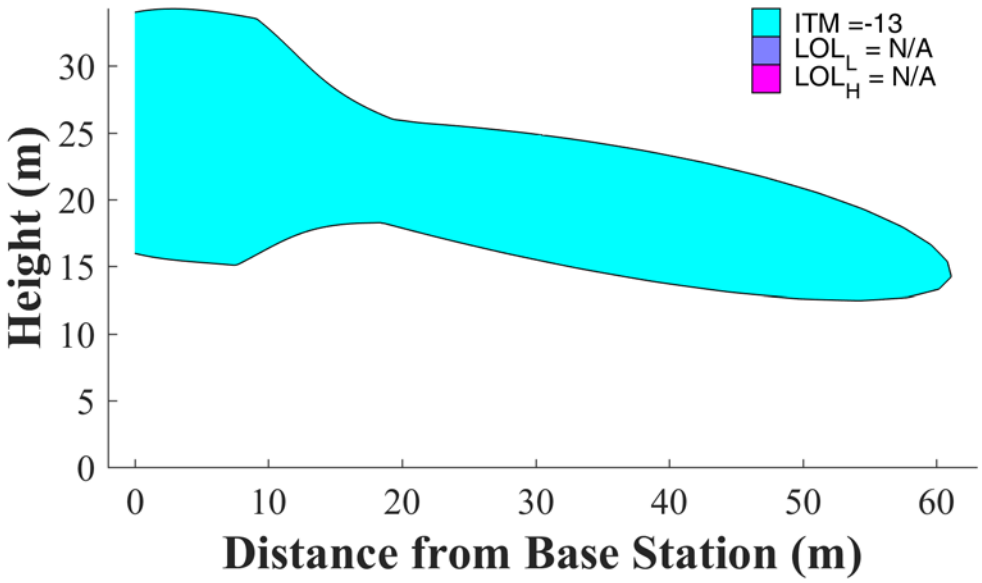

Figure I-50: Macro Urban Base Station (EIRP = 59 dBm), Bounding CEL, 1525 MHz

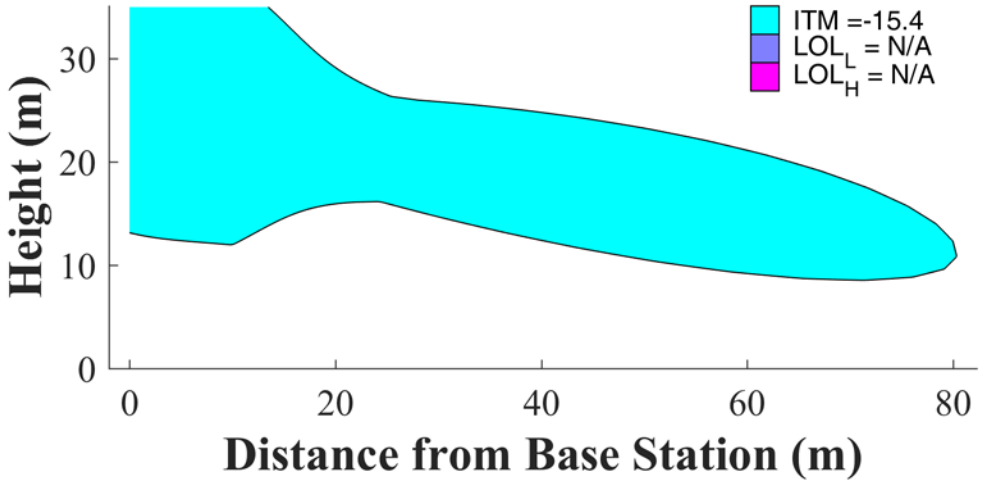

Figure I-51: Macro Urban Base Station (EIRP = 59 dBm), Bounding CEL, 1530 MHz

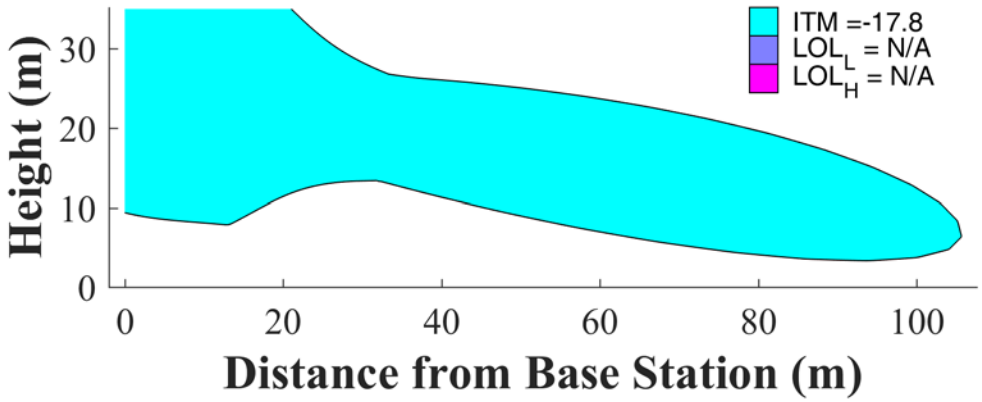

Figure I-52: Macro Urban Base Station (EIRP = 59 dBm), Bounding CEL, 1535 MHz

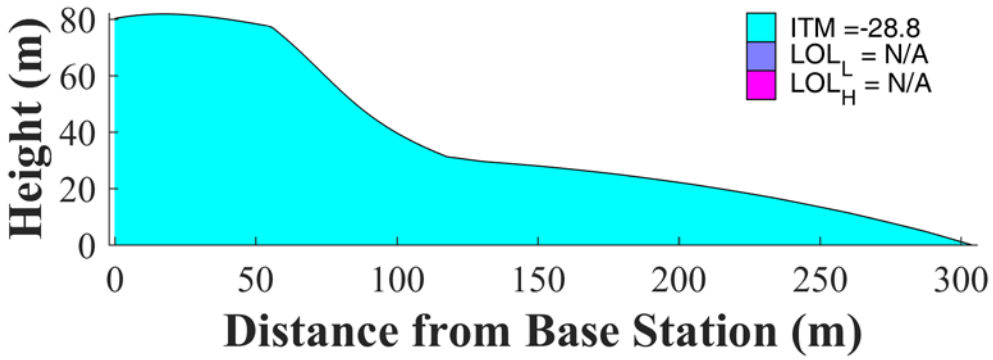

Figure I-53: Macro Urban Base Station (EIRP = 59 dBm), Bounding CEL, 1540 MHz

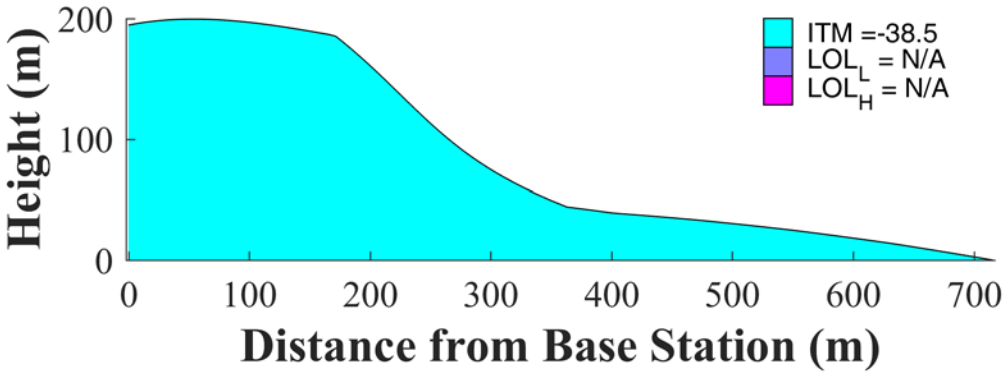

Figure I-54: Macro Urban Base Station (EIRP = 59 dBm), Bounding CEL, 1545 MHz

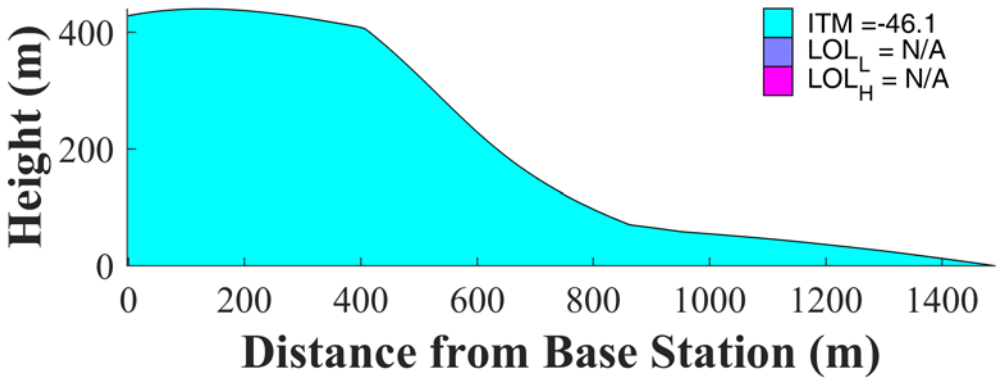

Figure I-55: Macro Urban Base Station (EIRP = 59 dBm), Bounding CEL, 1550 MHz

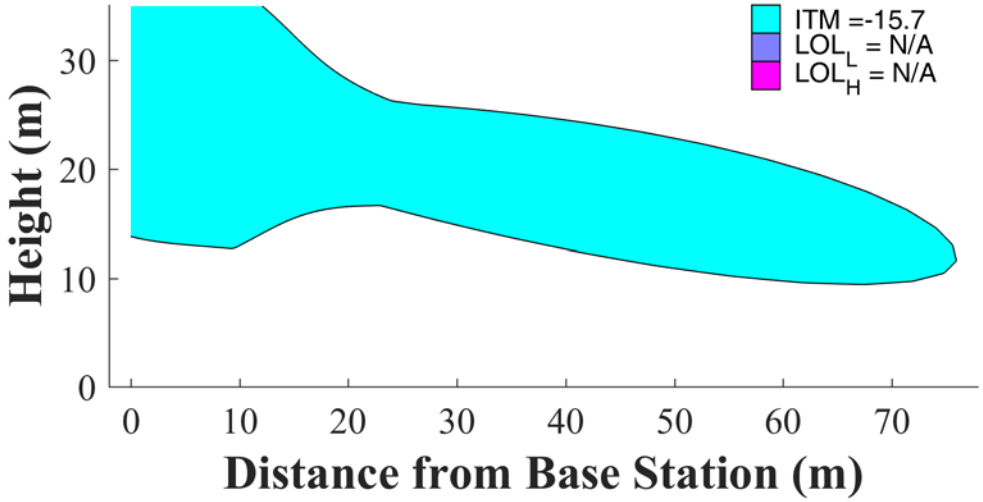

Figure I-56: Macro Urban Base Station (EIRP = 59 dBm), Bounding CEL, 1675 MHz

I.2 Small Cell Outdoor/Urban Micro Urban Base Station, GPS C/A-code

This section presents results for 10-MHz LTE signals broadcast by small cell outdoor/micro urban base stations (one sector with 40 dBm EIRP, 5 dBi antenna at 6 m AGL), free-space propagation, bounding mask.

I.2.1 GAV

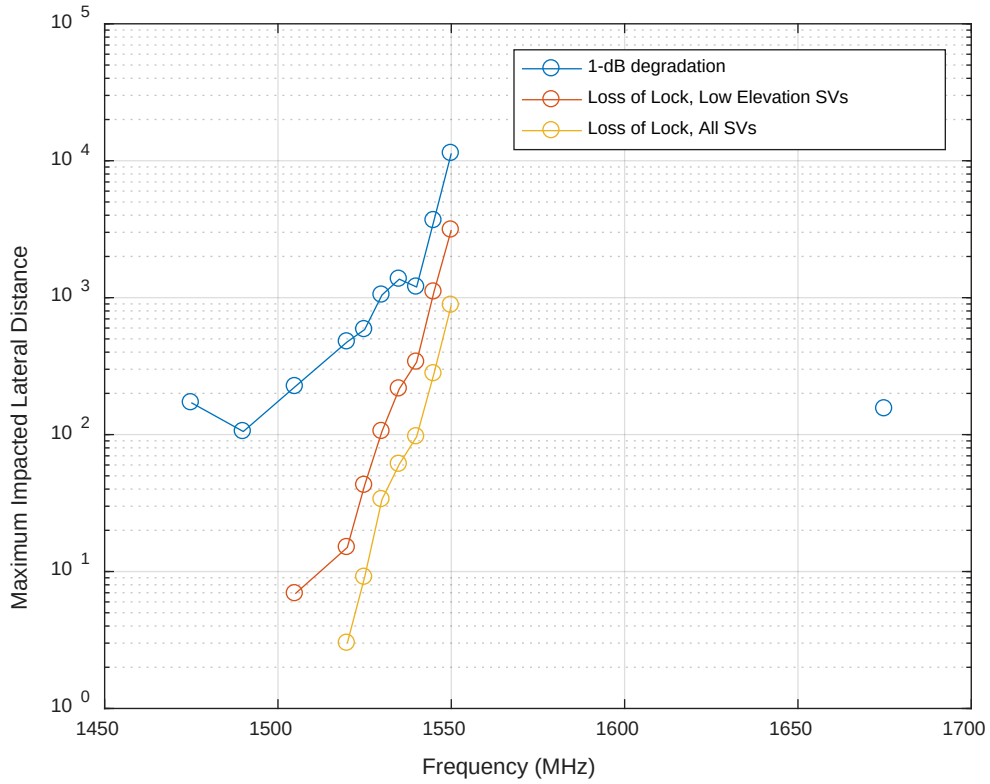

Figure I-57: Small Cell Outdoor/Micro Urban (EIRP = 40 dBm), Bounding GAV

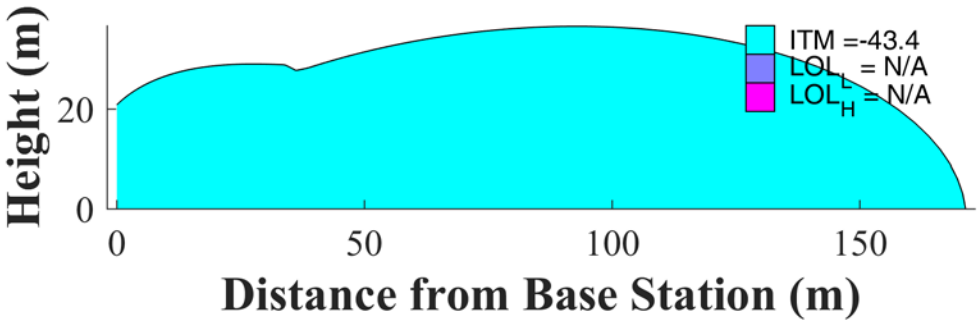

Figure I-58: Small Cell Outdoor/Micro Urban (EIRP = 40 dBm), Bounding GAV, 1475 MHz

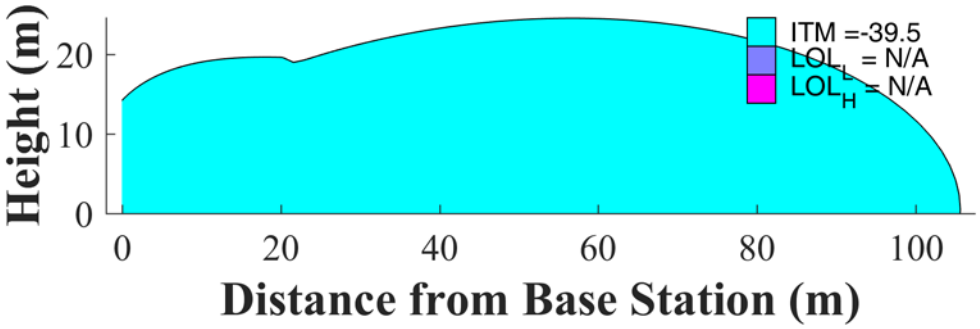

Figure I-59: Small Cell Outdoor/Micro Urban (EIRP = 40 dBm), Bounding GAV, 1490 MHz

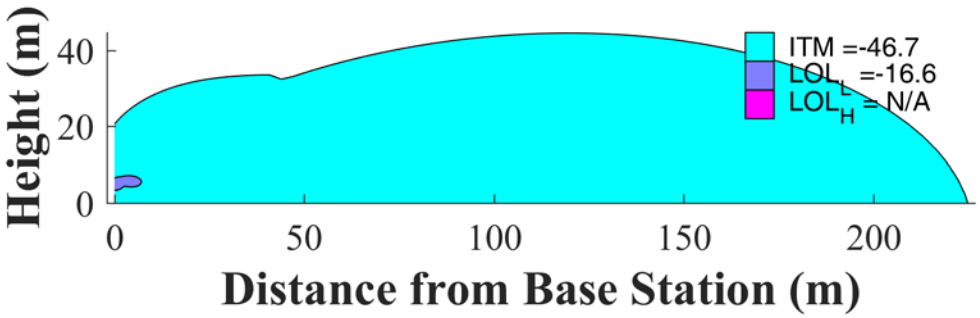

Figure I-60: Small Cell Outdoor/Micro Urban (EIRP = 40 dBm), Bounding GAV, 1505 MHz

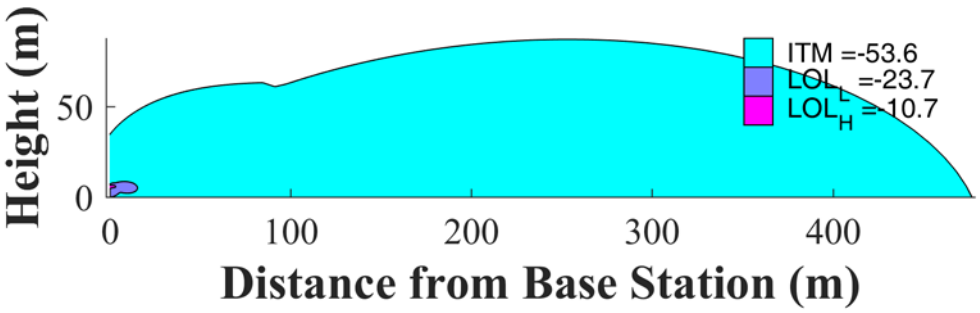

Figure I-61: Small Cell Outdoor/Micro Urban (EIRP = 40 dBm), Bounding GAV, 1520 MHz

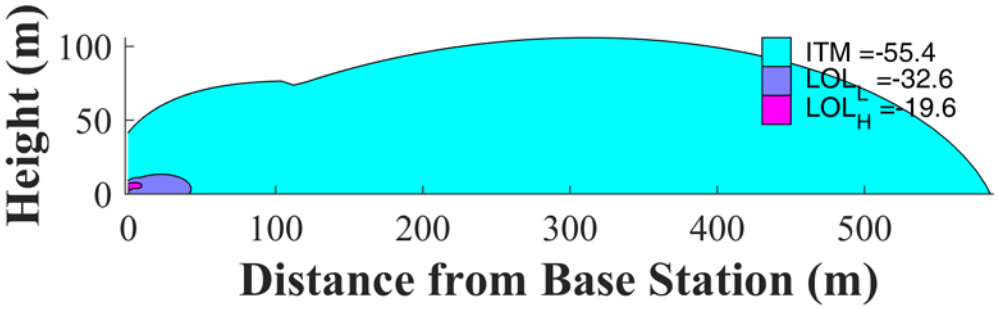

Figure I-62: Small Cell Outdoor/Micro Urban (EIRP = 40 dBm), Bounding GAV, 1525 MHz

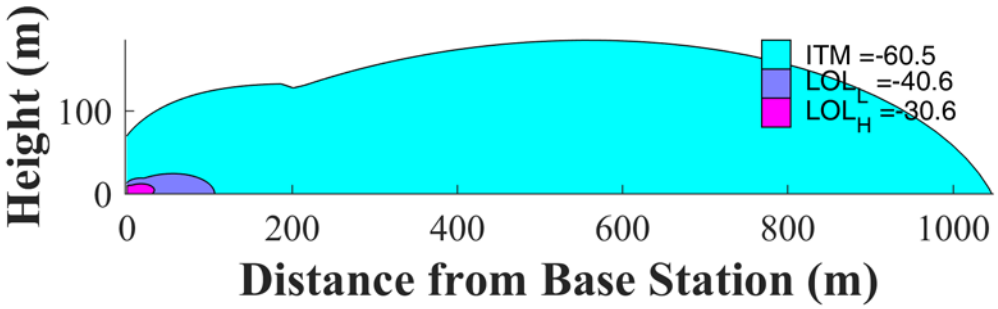

Figure I-63: Small Cell Outdoor/Micro Urban (EIRP = 40 dBm), Bounding GAV, 1530 MHz

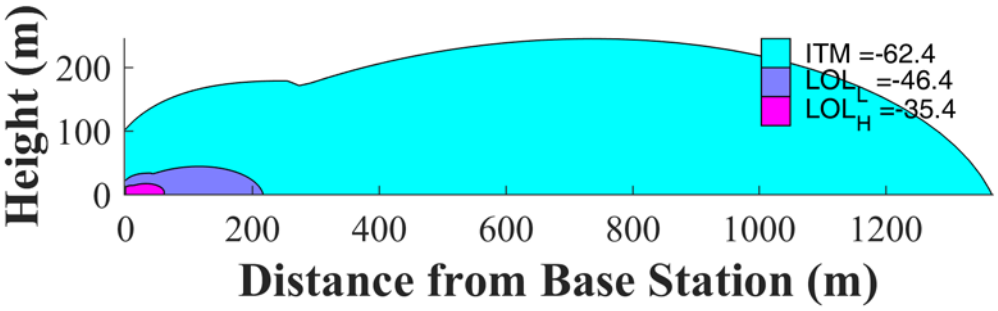

Figure I-64: Small Cell Outdoor/Micro Urban (EIRP = 40 dBm), Bounding GAV, 1535 MHz

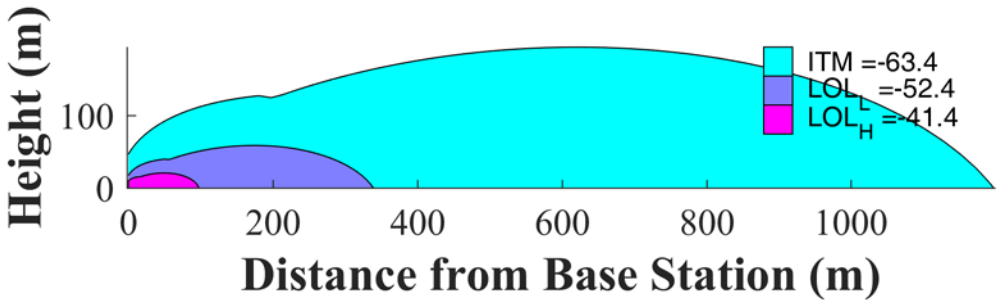

Figure I-65: Small Cell Outdoor/Micro Urban (EIRP = 40 dBm), Bounding GAV, 1540 MHz

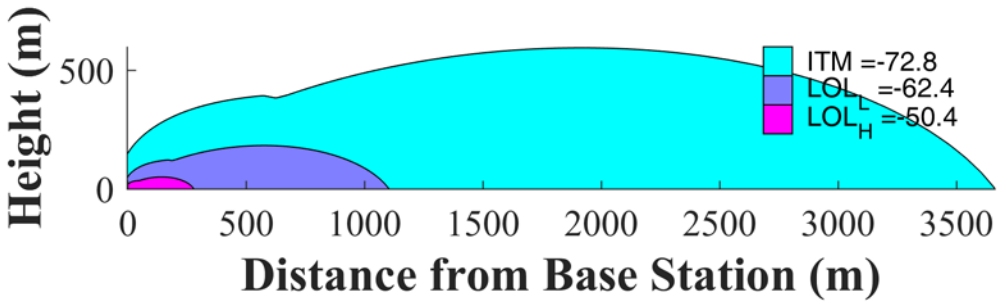

Figure I-66: Small Cell Outdoor/Micro Urban (EIRP = 40 dBm), Bounding GAV, 1545 MHz

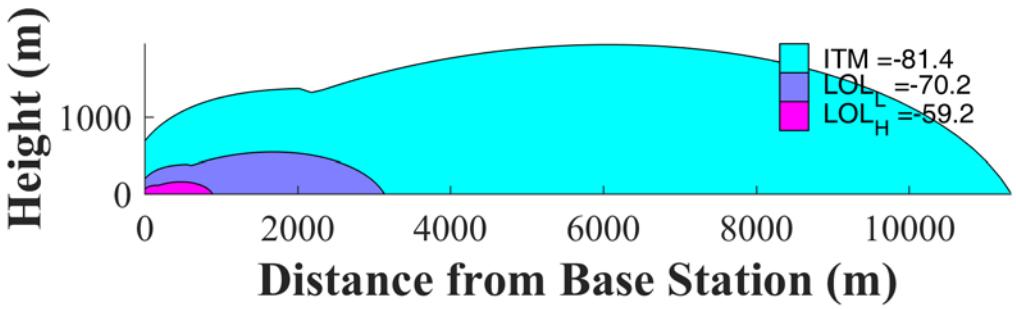

Figure I-67: Small Cell Outdoor/Micro Urban (EIRP = 40 dBm), Bounding GAV, 1550 MHz

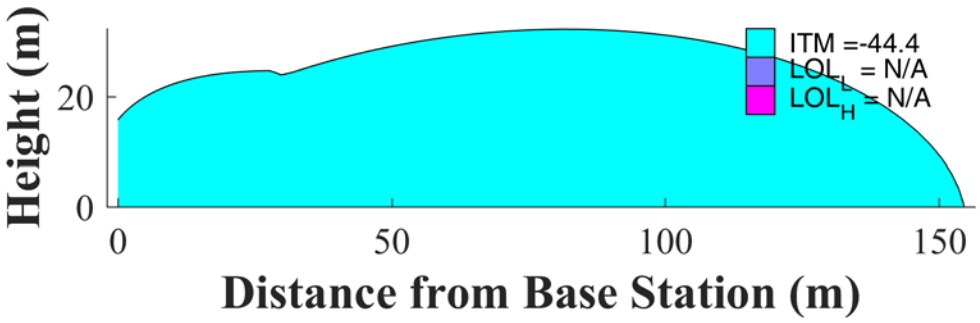

Figure I-68: Small Cell Outdoor/Micro Urban (EIRP = 40 dBm), Bounding GAV, 1675 MHz

I.2.2 GLN

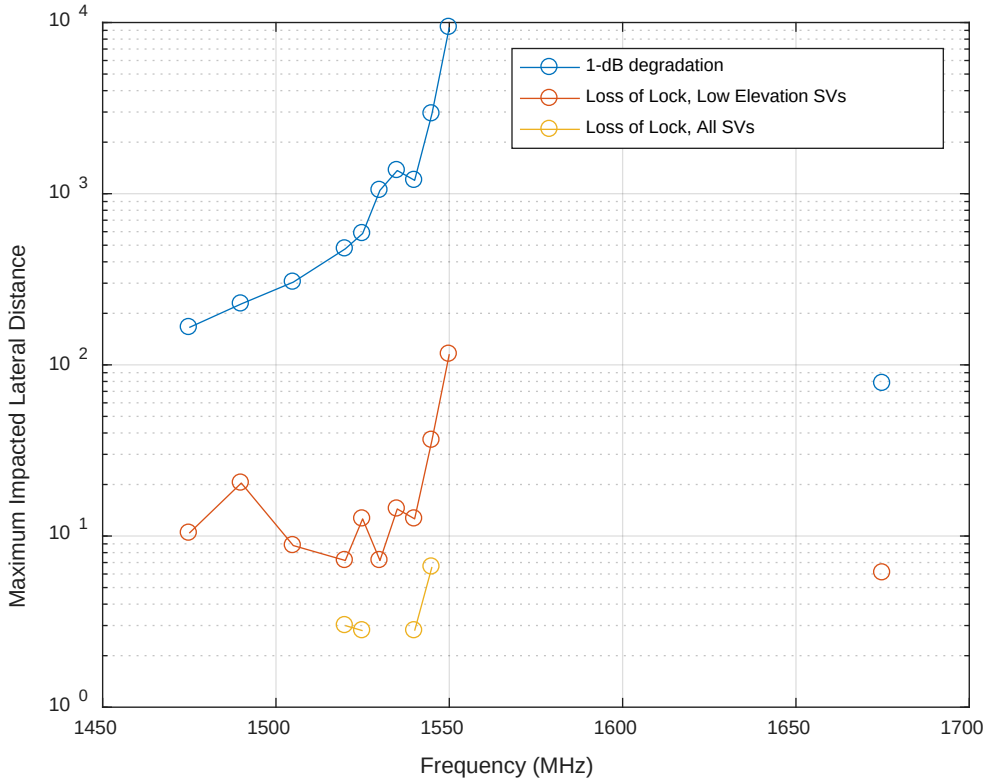

Figure I-69: Small Cell Outdoor/Micro Urban (EIRP = 40 dBm), Bounding GLN

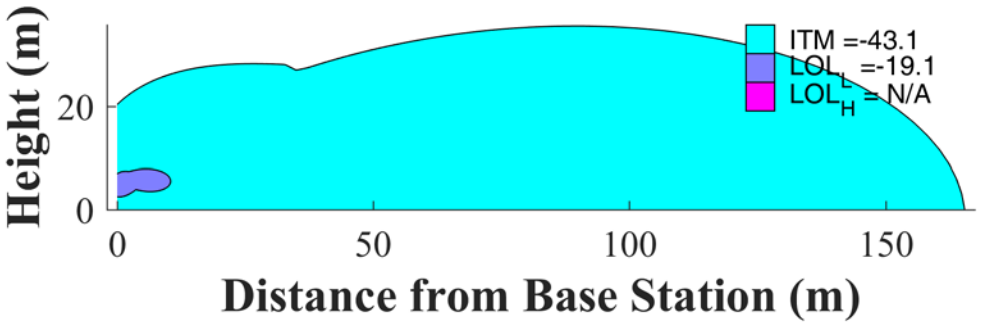

Figure I-70: Small Cell Outdoor/Micro Urban (EIRP = 40 dBm), Bounding GLN, 1475 MHz

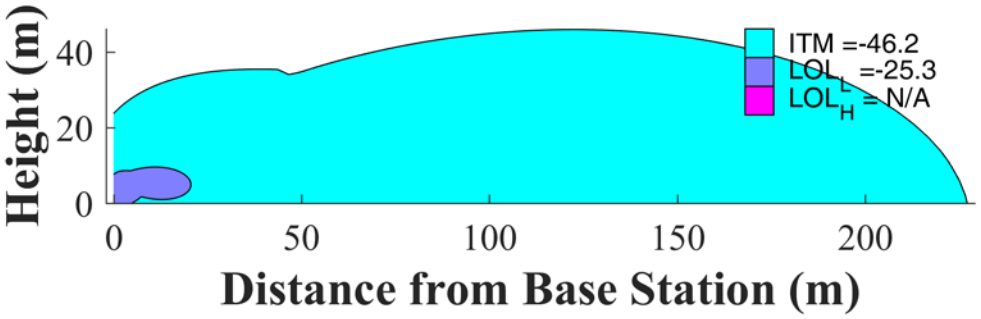

Figure I-71: Small Cell Outdoor/Micro Urban (EIRP = 40 dBm), Bounding GLN, 1490 MHz

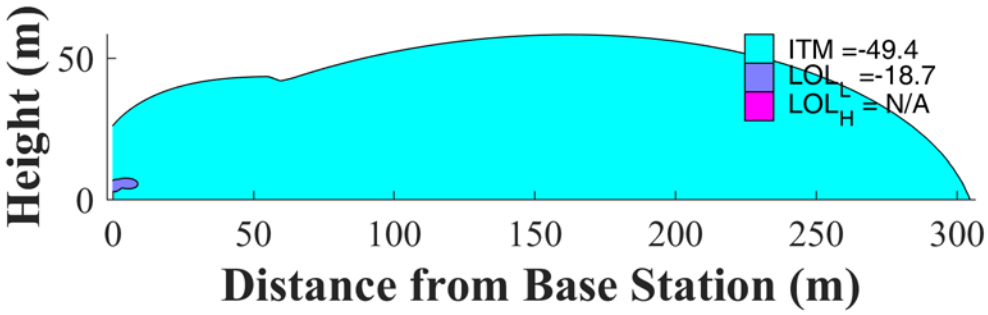

Figure I-72: Small Cell Outdoor/Micro Urban (EIRP = 40 dBm), Bounding GLN, 1505 MHz

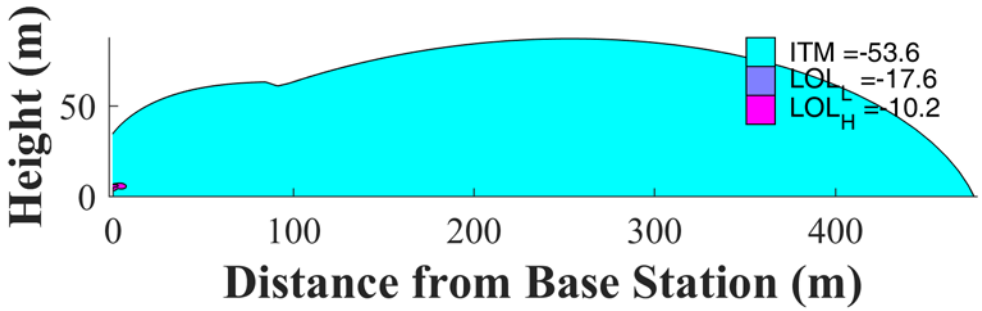

Figure I-73: Small Cell Outdoor/Micro Urban (EIRP = 40 dBm), Bounding GLN, 1520 MHz

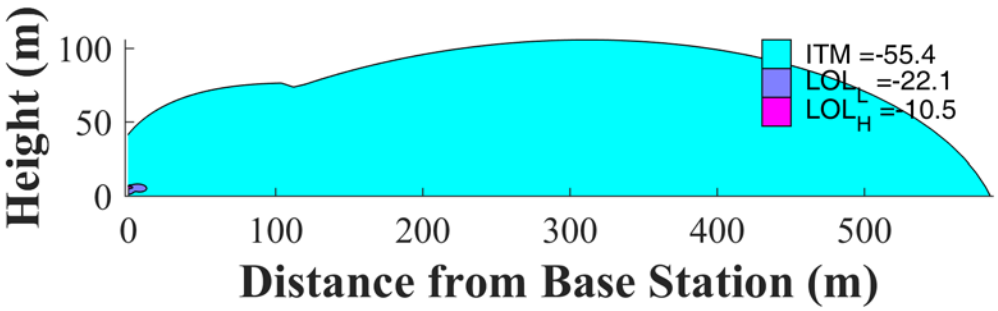

Figure I-74: Small Cell Outdoor/Micro Urban (EIRP = 40 dBm), Bounding GLN, 1525 MHz

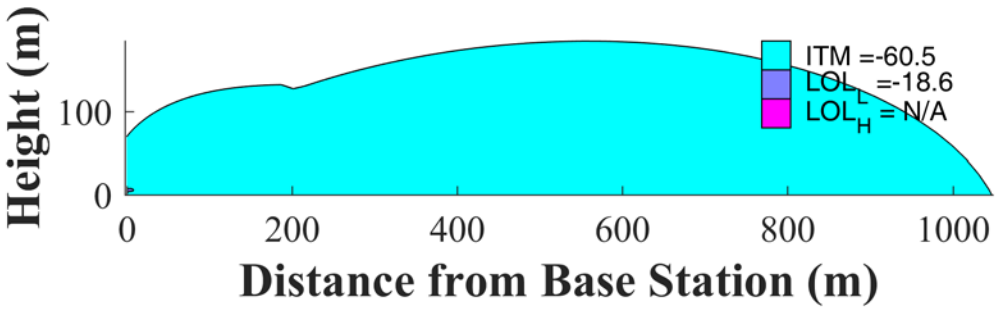

Figure I-75: Small Cell Outdoor/Micro Urban (EIRP = 40 dBm), Bounding GLN, 1530 MHz

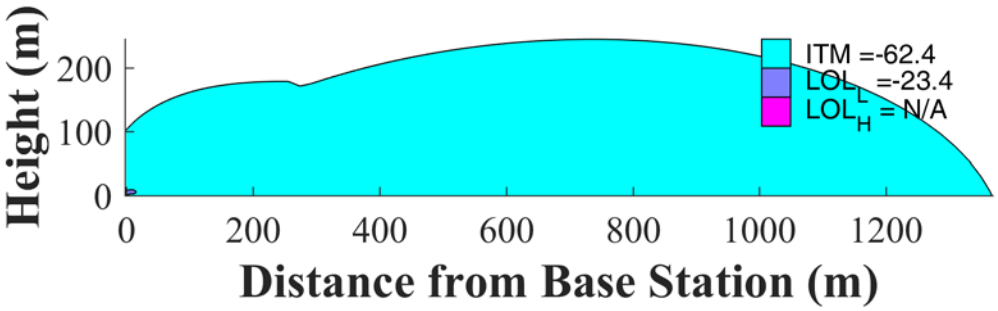

Figure I-76: Small Cell Outdoor/Micro Urban (EIRP = 40 dBm), Bounding GLN, 1535 MHz

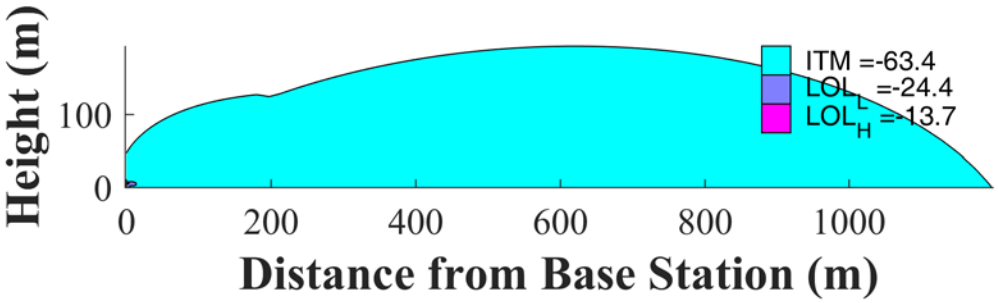

Figure I-77: Small Cell Outdoor/Micro Urban (EIRP = 40 dBm), Bounding GLN, 1540 MHz

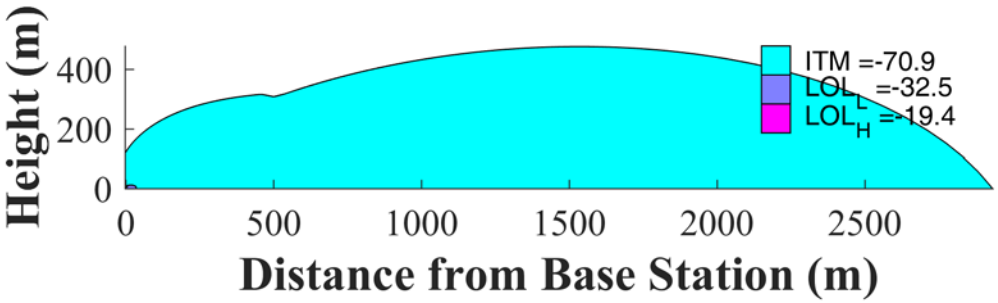

Figure I-78: Small Cell Outdoor/Micro Urban (EIRP = 40 dBm), Bounding GLN, 1545 MHz

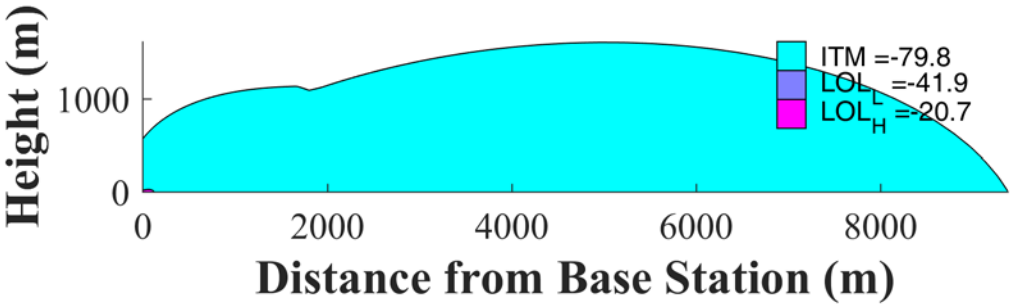

Figure I-79: Small Cell Outdoor/Micro Urban (EIRP = 40 dBm), Bounding GLN, 1550 MHz

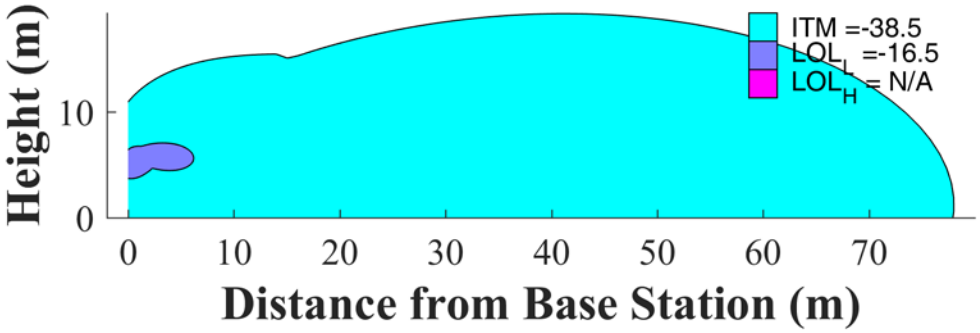

Figure I-80: Small Cell Outdoor/Micro Urban (EIRP = 40 dBm), Bounding GLN, 1675 MHz

I.2.3 HPR

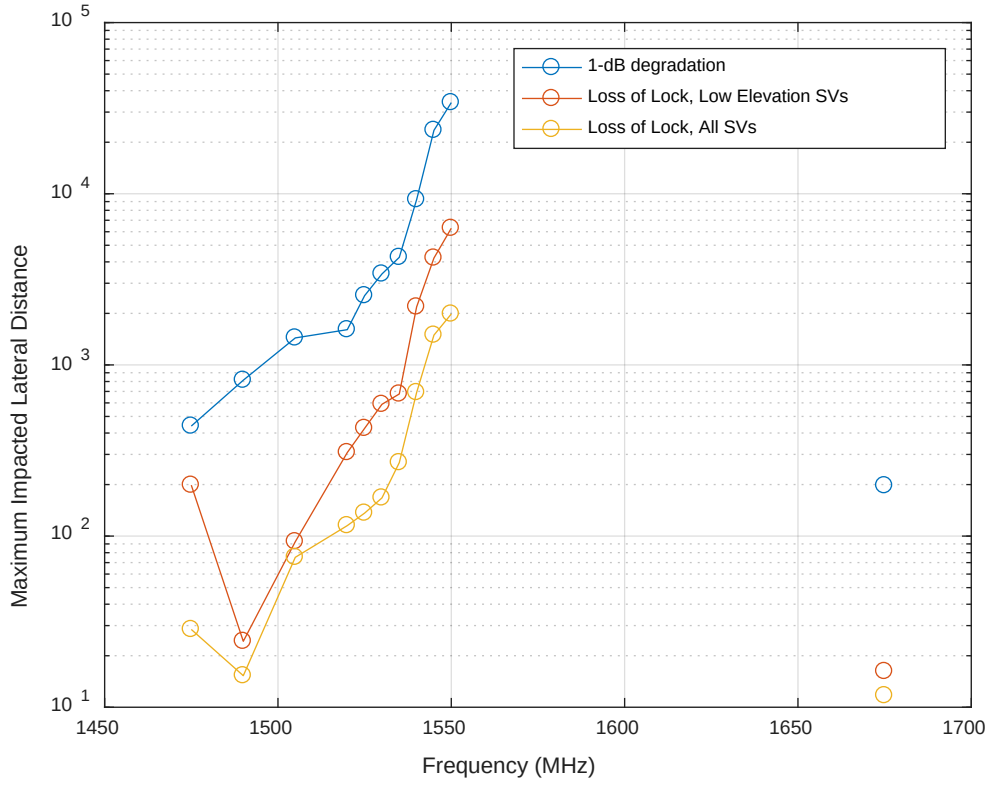

Figure I-81: Small Cell Outdoor/Micro Urban, Bounding HPR

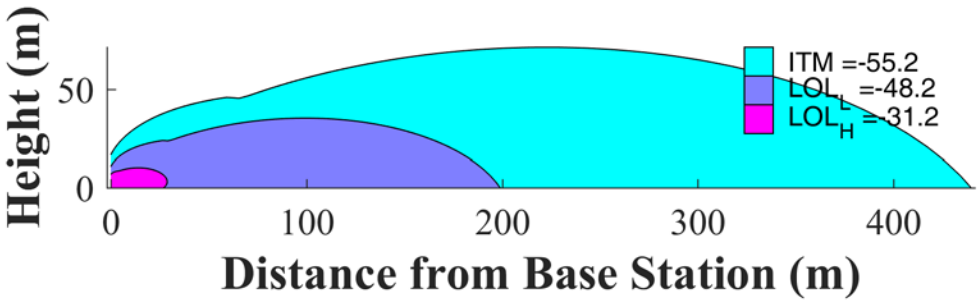

Figure I-82: Small Cell Outdoor/Micro Urban (EIRP = 40 dBm), Bounding HPR, 1475 MHz

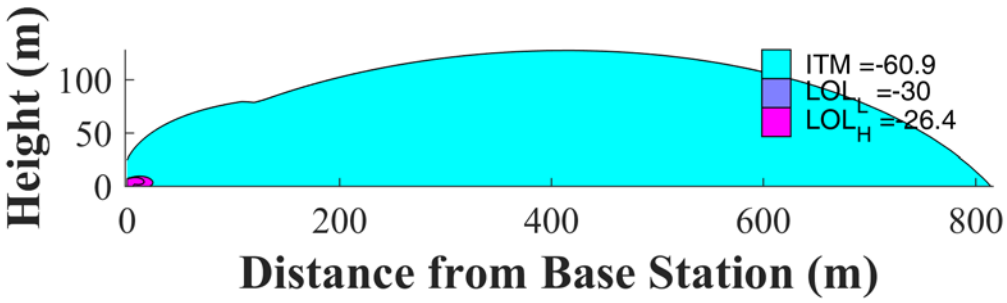

Figure I-83: Small Cell Outdoor/Micro Urban (EIRP = 40 dBm), Bounding HPR, 1490 MHz

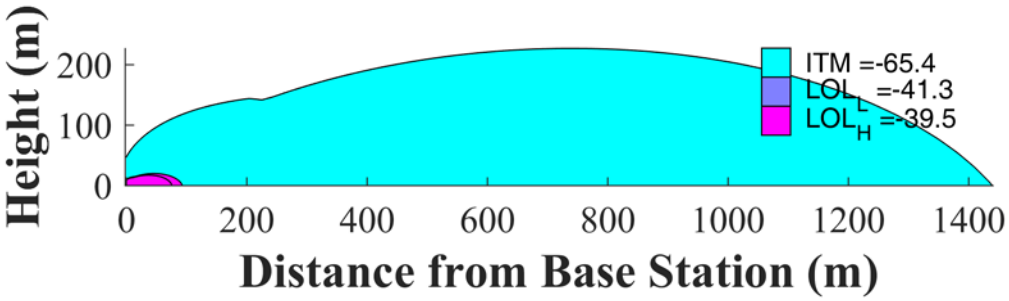

Figure I-84: Small Cell Outdoor/Micro Urban (EIRP = 40 dBm), Bounding HPR, 1505 MHz

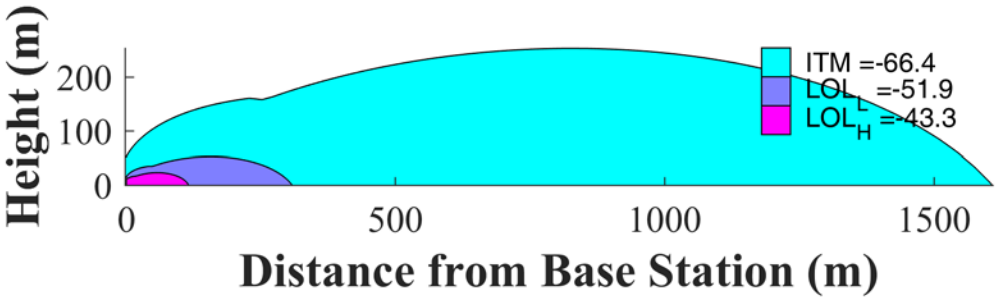

Figure I-85: Small Cell Outdoor/Micro Urban (EIRP = 40 dBm), Bounding HPR, 1520 MHz

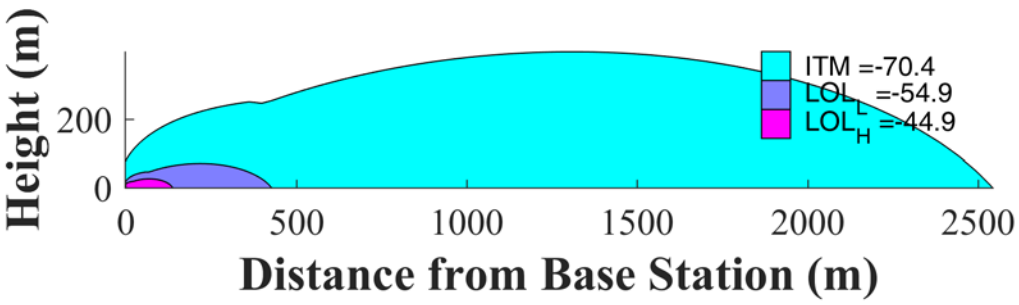

Figure I-86: Small Cell Outdoor/Micro Urban (EIRP = 40 dBm), Bounding HPR, 1525 MHz

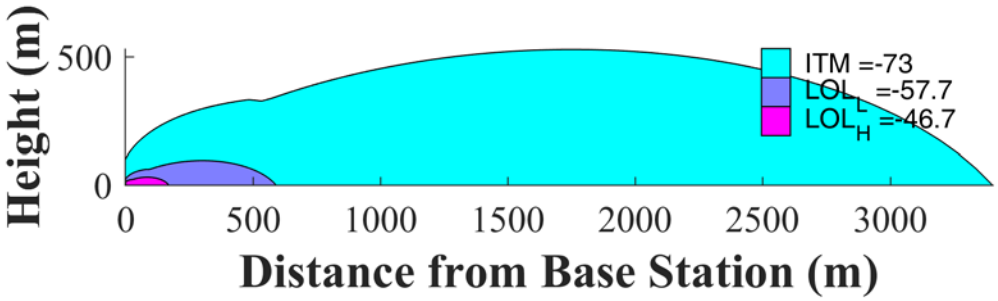

Figure I-87: Small Cell Outdoor/Micro Urban (EIRP = 40 dBm), Bounding HPR, 1530 MHz

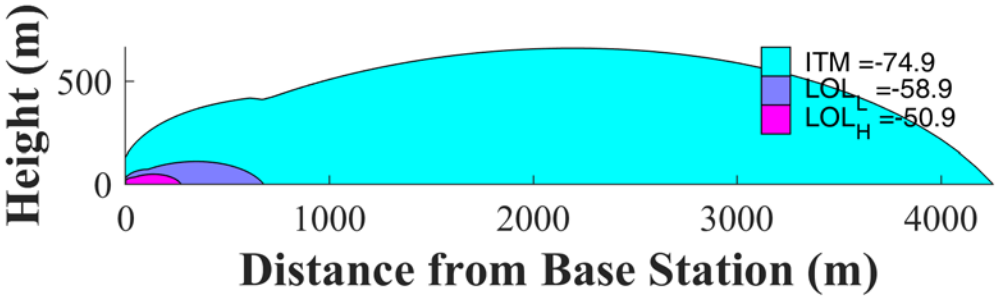

Figure I-88: Small Cell Outdoor/Micro Urban (EIRP = 40 dBm), Bounding HPR, 1535 MHz

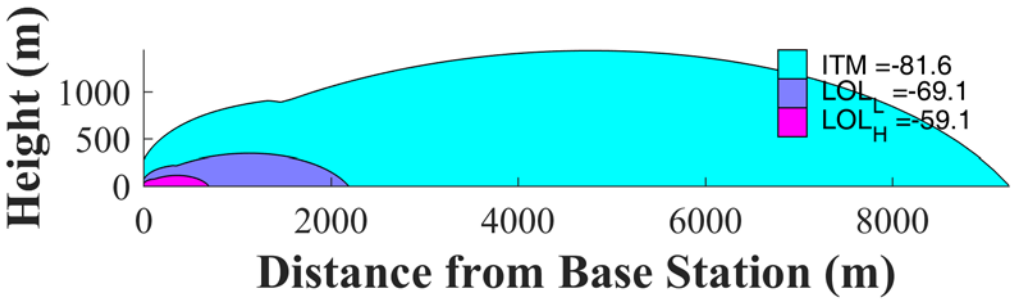

Figure I-89: Small Cell Outdoor/Micro Urban (EIRP = 40 dBm), Bounding HPR, 1540 MHz

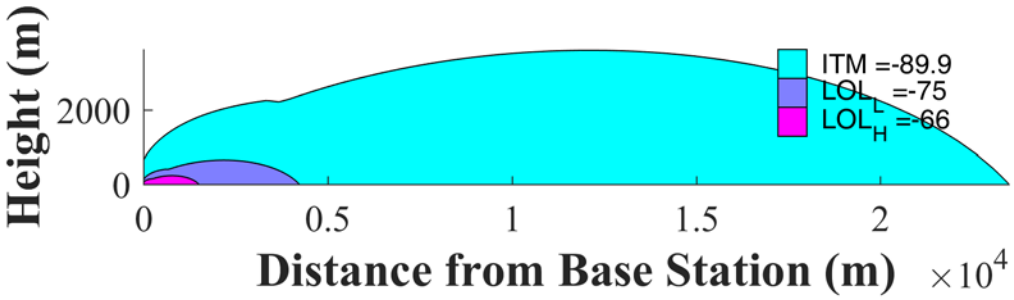

Figure I-90: Small Cell Outdoor/Micro Urban (EIRP = 40 dBm), Bounding HPR, 1545 MHz

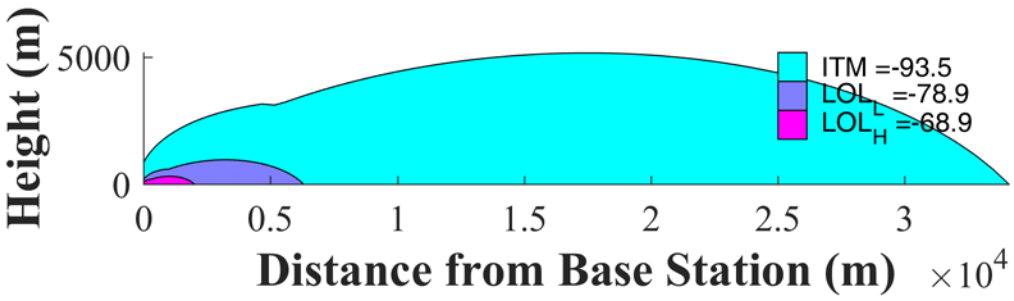

Figure I-91: Small Cell Outdoor/Micro Urban (EIRP = 40 dBm), Bounding HPR, 1550 MHz

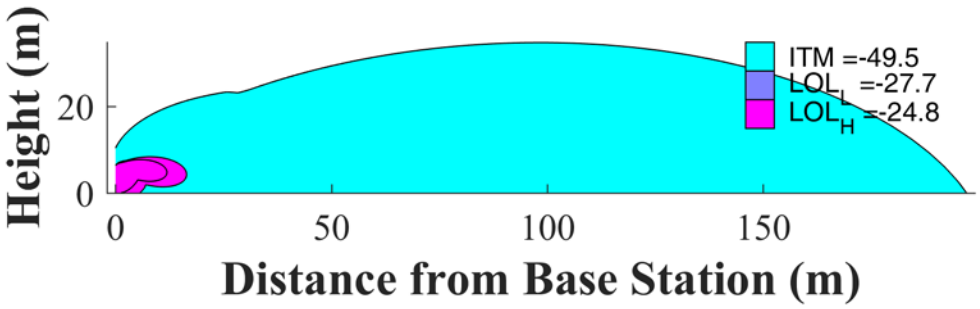

Figure I-92: Small Cell Outdoor/Micro Urban (EIRP = 40 dBm), Bounding HPR, 1675 MHz

I.2.4 TIM

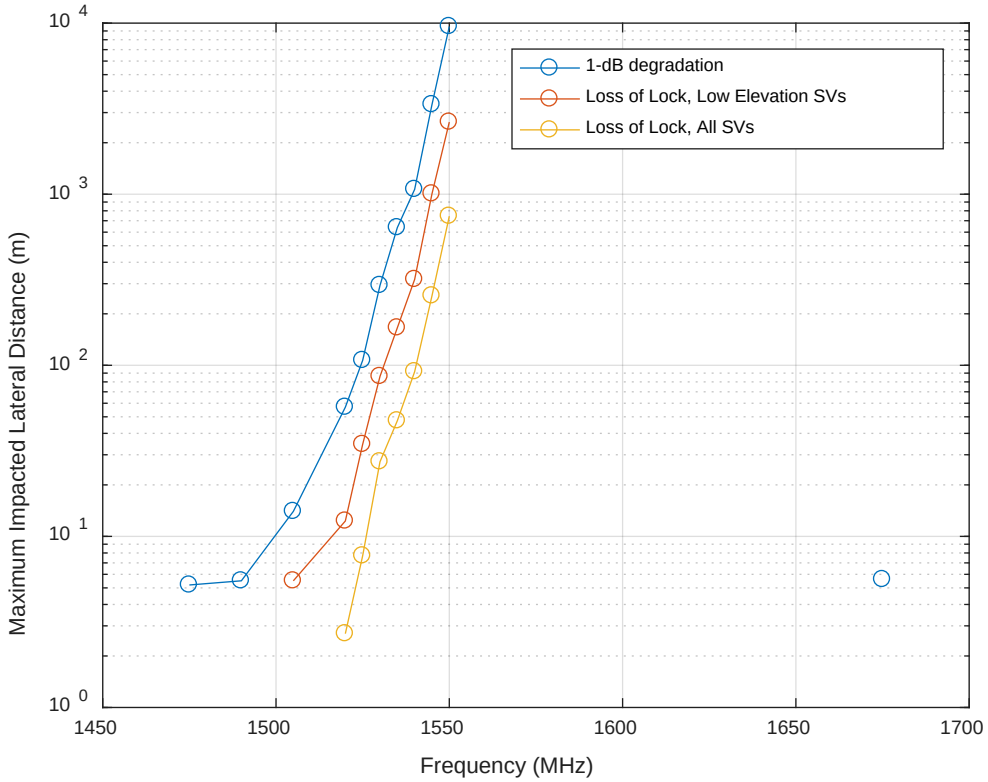

Figure I-93: Small Cell Outdoor/Micro Urban (EIRP = 40 dBm), Bounding TIM

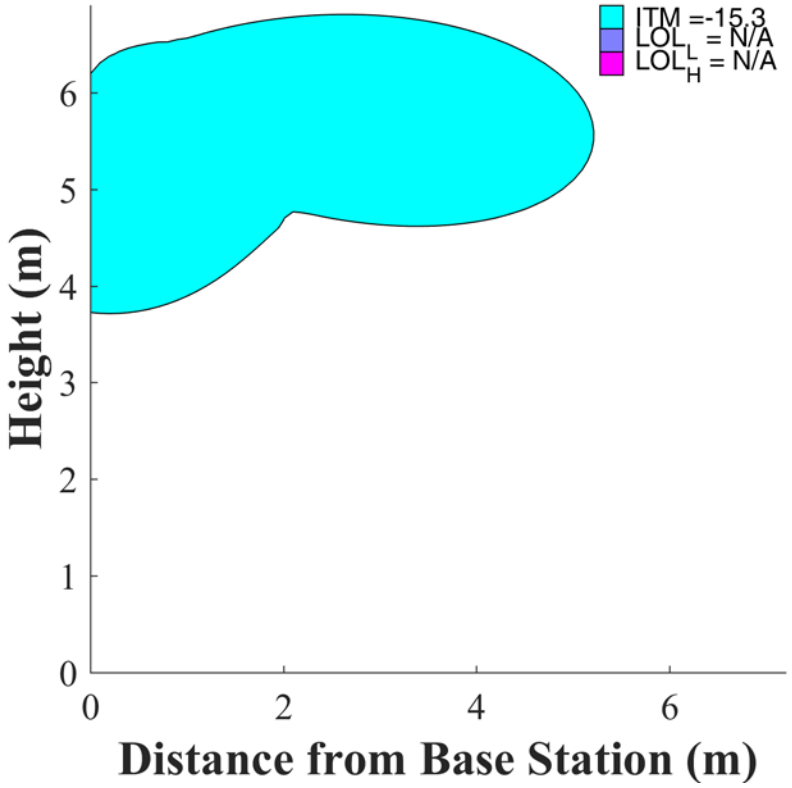

Figure I-94: Small Cell Outdoor/Micro Urban (EIRP = 40 dBm), Bounding TIM, 1475 MHz

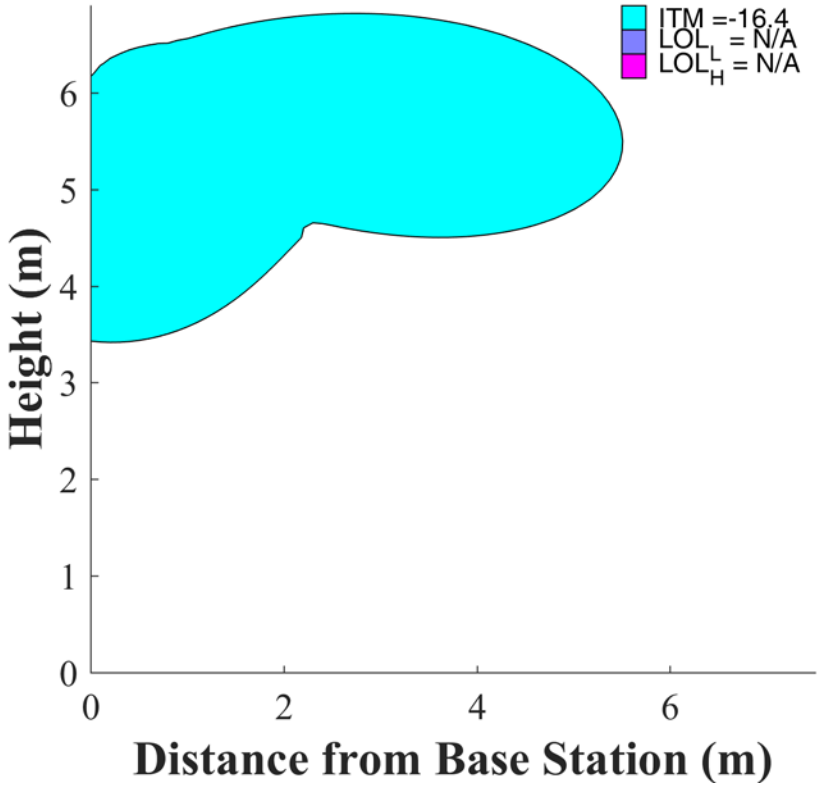

Figure I-95: Small Cell Outdoor/Micro Urban (EIRP = 40 dBm), Bounding TIM, 1490 MHz

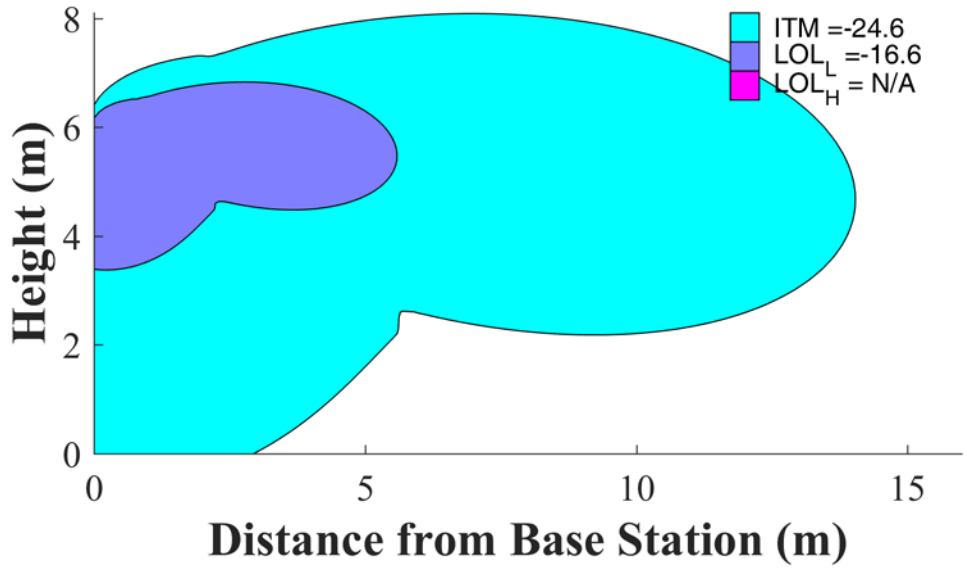

Figure I-96: Small Cell Outdoor/Micro Urban (EIRP = 40 dBm), Bounding TIM, 1505 MHz

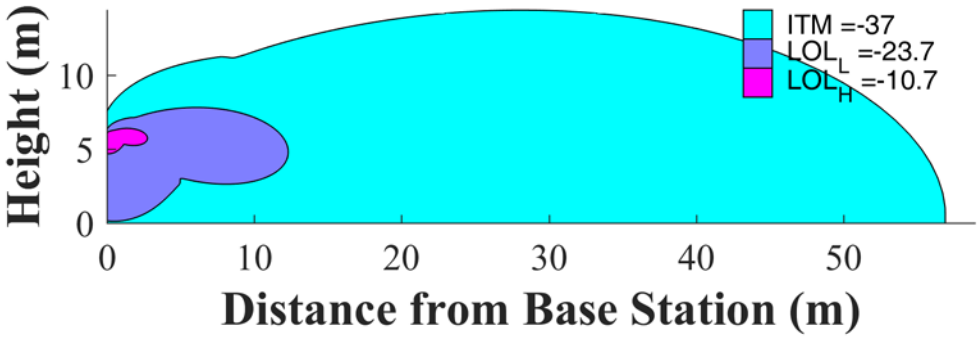

Figure I-97: Small Cell Outdoor/Micro Urban (EIRP = 40 dBm), Bounding TIM, 1520 MHz

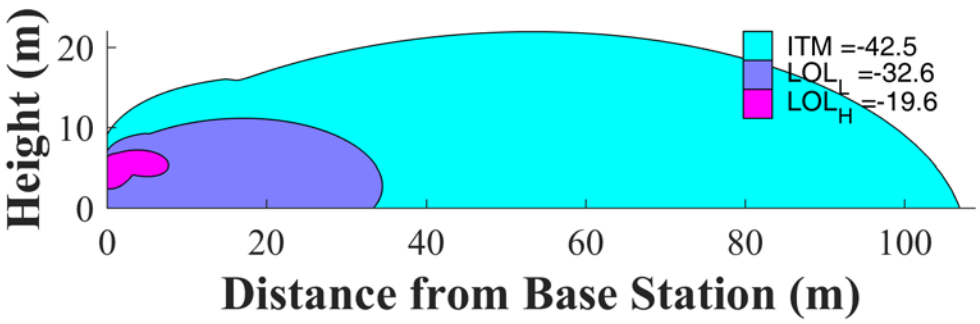

Figure I-98: Small Cell Outdoor/Micro Urban (EIRP = 40 dBm), Bounding TIM, 1525 MHz

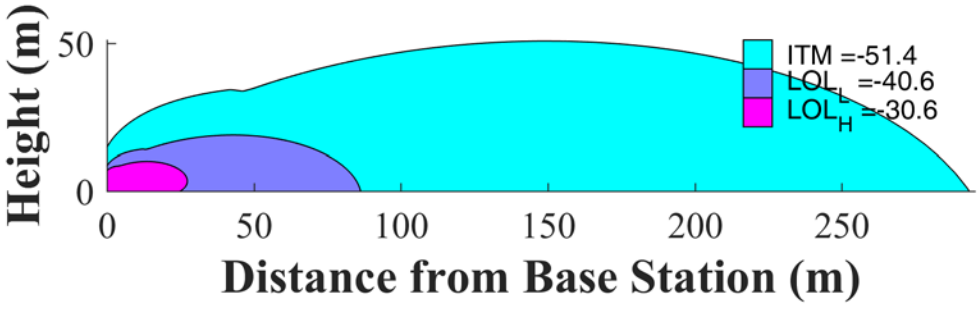

Figure I-99: Small Cell Outdoor/Micro Urban (EIRP = 40 dBm), Bounding TIM, 1530 MHz

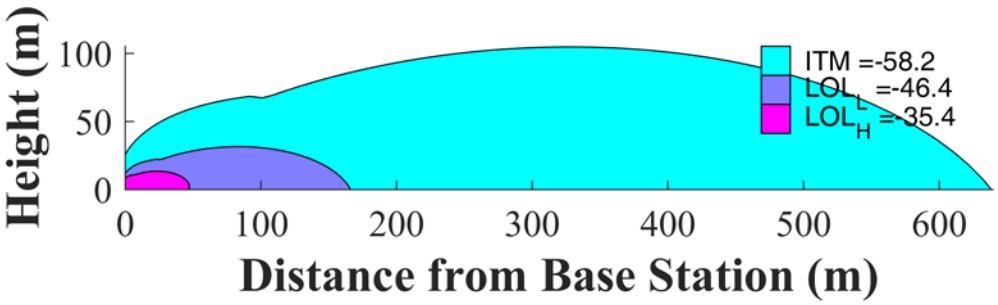

Figure I-100: Small Cell Outdoor/Micro Urban (EIRP = 40 dBm), Bounding TIM, 1535 MHz

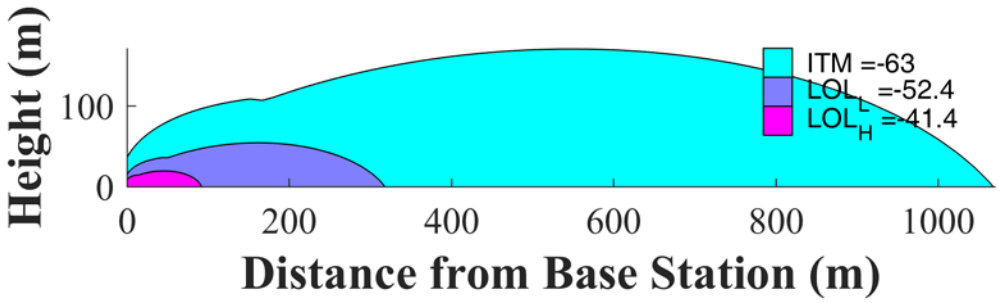

Figure I-101: Small Cell Outdoor/Micro Urban (EIRP = 40 dBm), Bounding TIM, 1540 MHz

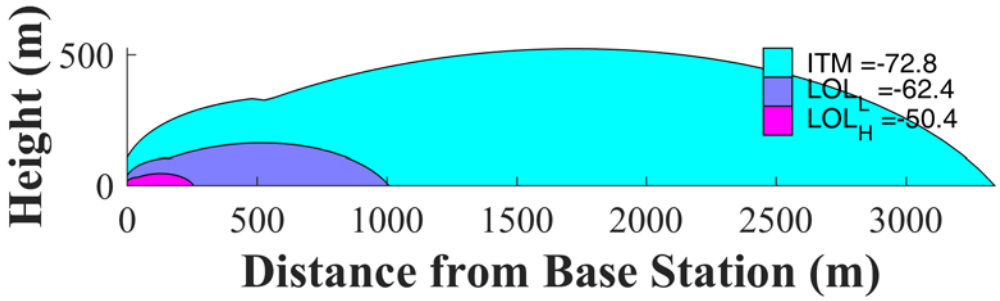

Figure I-102: Small Cell Outdoor/Micro Urban (EIRP = 40 dBm), Bounding TIM, 1545 MHz

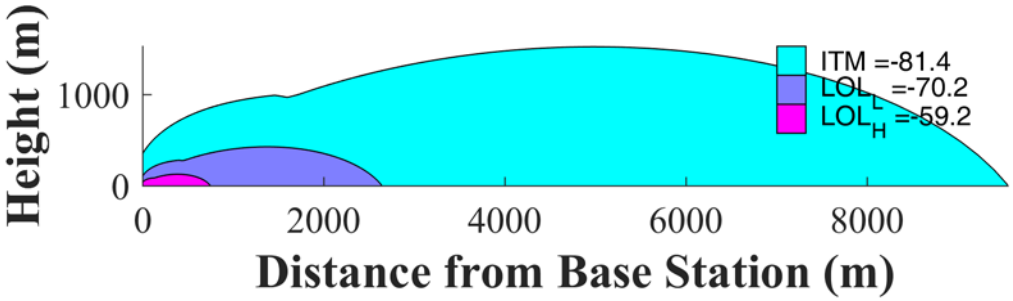

Figure I-103: Small Cell Outdoor/Micro Urban (EIRP = 40 dBm), Bounding TIM, 1550 MHz

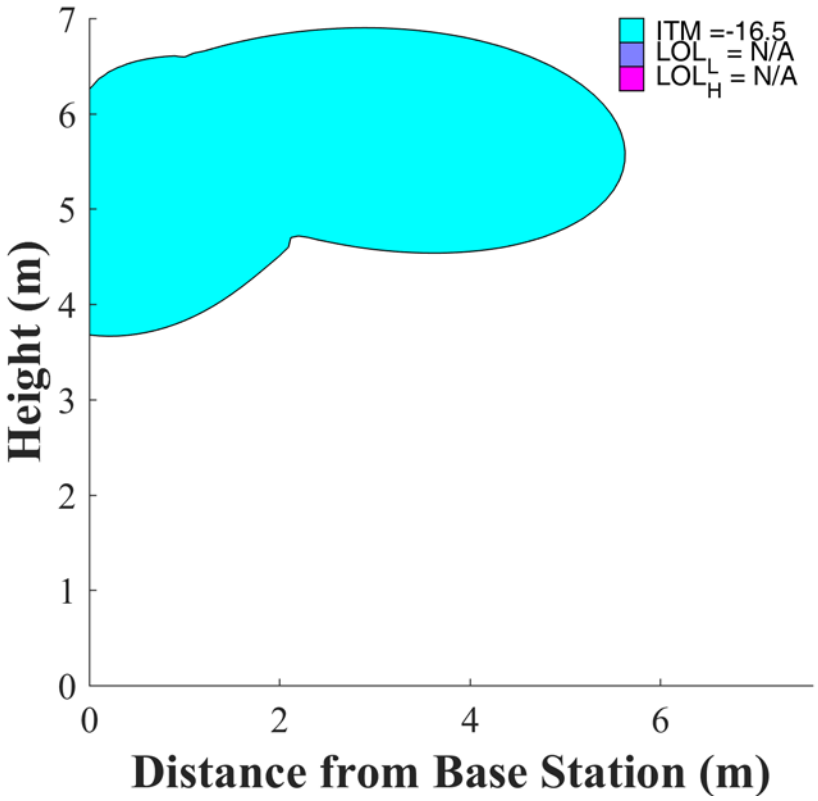

Figure I-104: Small Cell Outdoor/Micro Urban (EIRP = 40 dBm), Bounding TIM, 1675 MHz

I.2.5 CEL

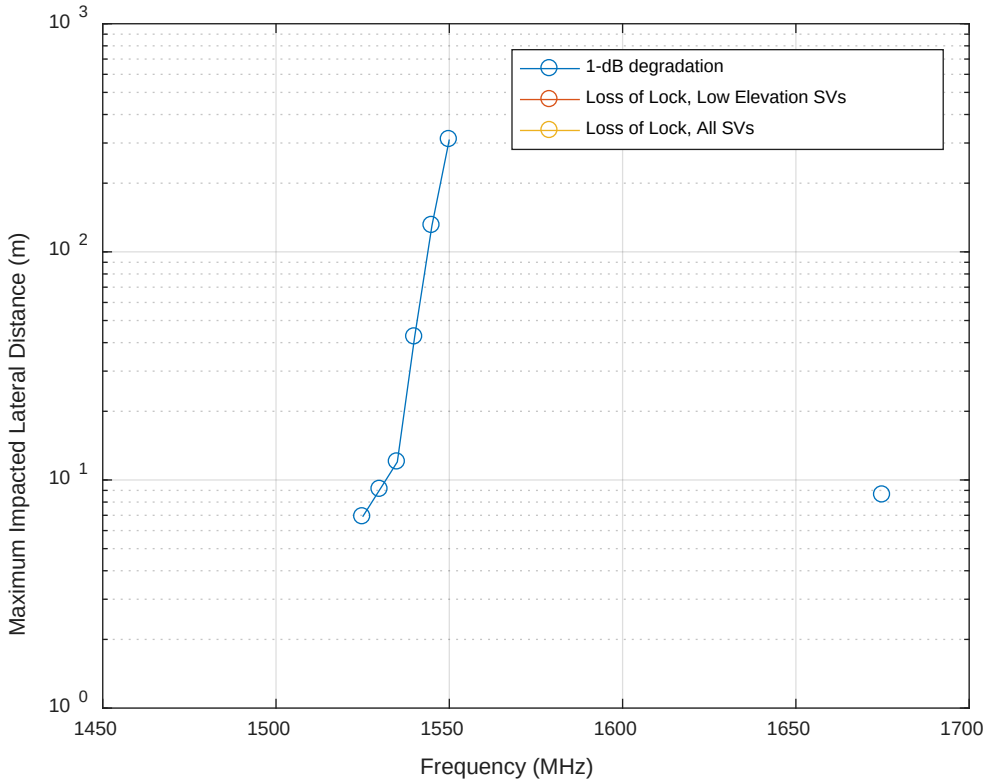

Figure I-105: Small Cell Outdoor/Micro Urban (EIRP = 40 dBm), Bounding CEL

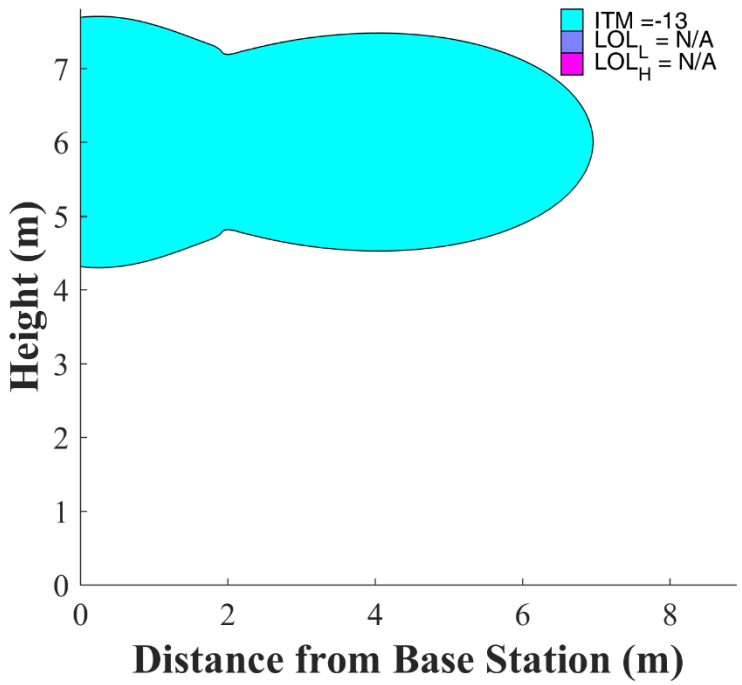

Figure I-106: Small Cell Outdoor/Micro Urban (EIRP = 40 dBm), Bounding CEL, 1525 MHz

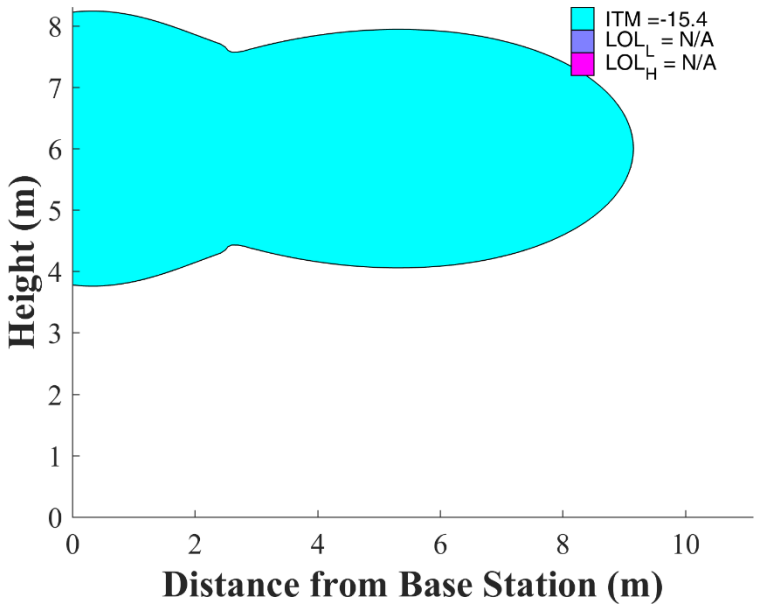

Figure I-107: Small Cell Outdoor/Micro Urban (EIRP = 40 dBm), Bounding CEL, 1530 MHz

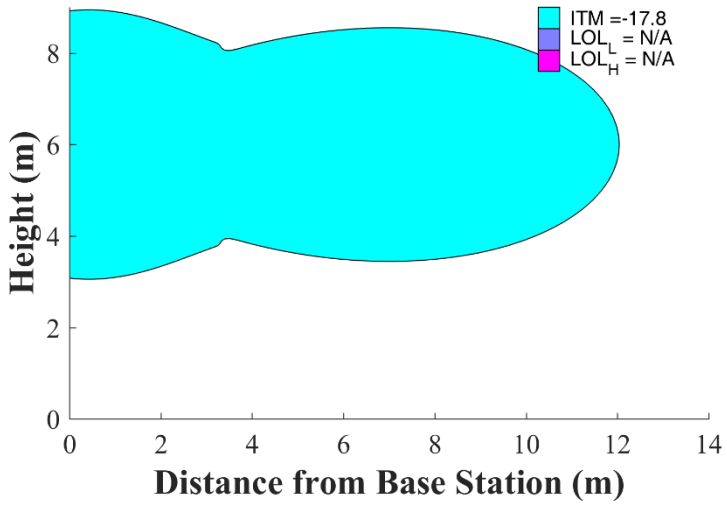

Figure I-108: Small Cell Outdoor/Micro Urban (EIRP = 40 dBm), Bounding CEL, 1535 MHz

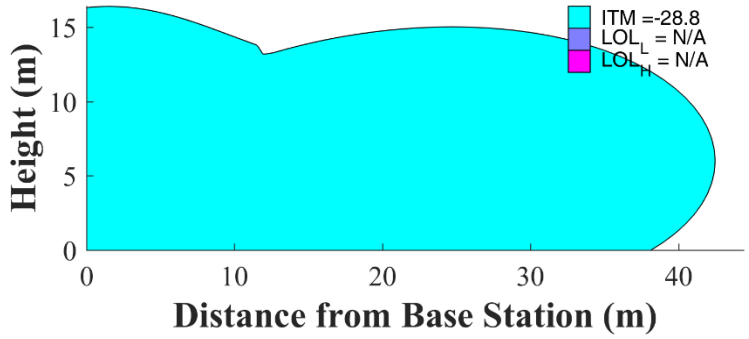

Figure I-109: Small Cell Outdoor/Micro Urban (EIRP = 40 dBm), Bounding CEL, 1540 MHz

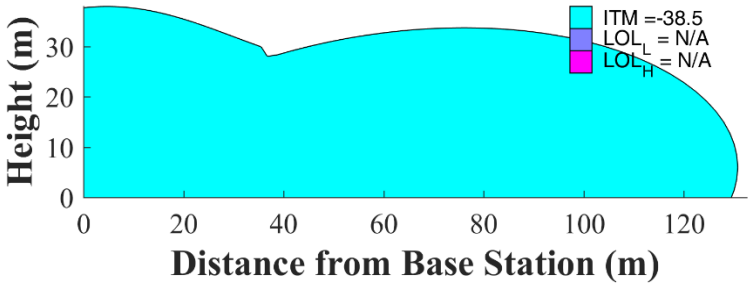

Figure I-110: Small Cell Outdoor/Micro Urban (EIRP = 40 dBm), Bounding CEL, 1545 MHz

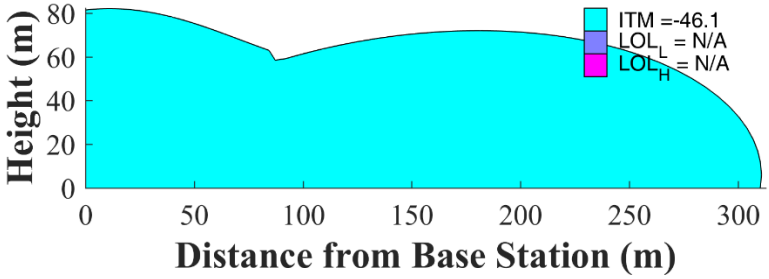

Figure I-111: Small Cell Outdoor/Micro Urban (EIRP = 40 dBm), Bounding CEL, 1550 MHz

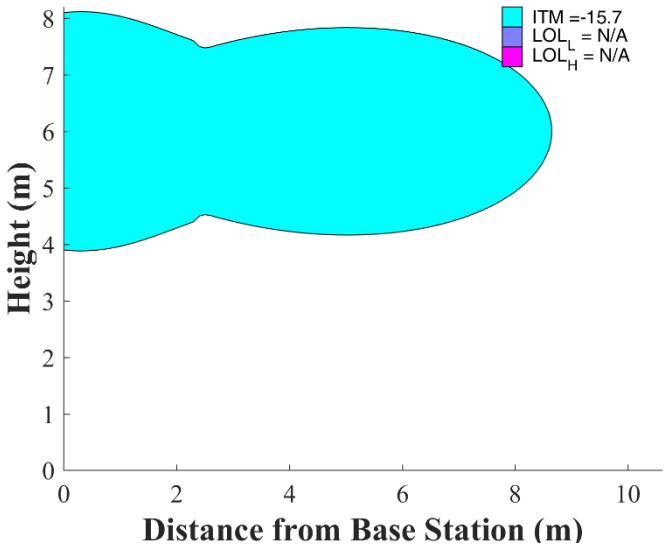

Figure I-112: Small Cell Outdoor/Micro Urban (EIRP = 40 dBm), Bounding CEL, 1675 MHz

Figure X. Small Cell Outdoor/Micro Urban (EIRP = 40 dBm), Bounding CEL

I.3 Handsets, GPS C/A-code

This section presents results for 10-MHz LTE signals broadcast by handsets (EIRP = 23 dBm, isotropic antenna at 2 m AGL), free-space propagation, bounding mask.

I.3.1 GAV

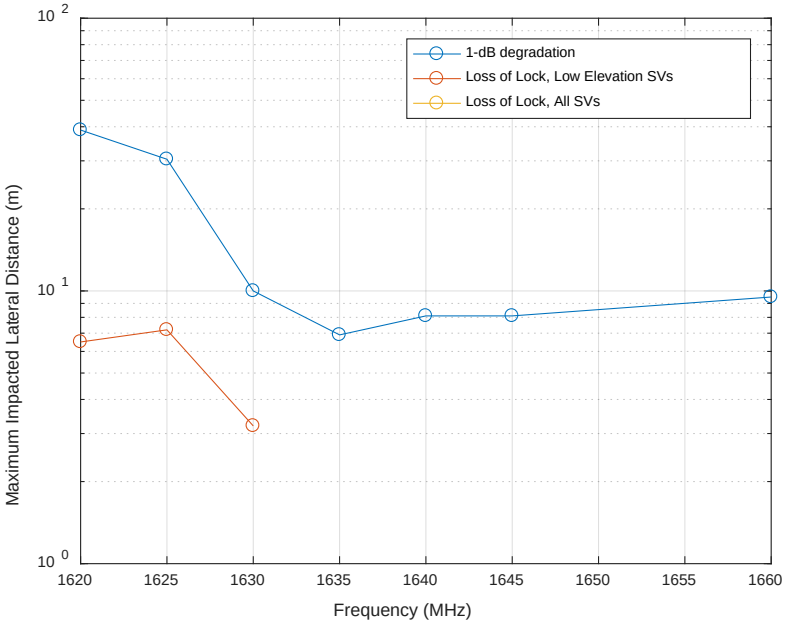

Figure I-113: Handset (EIRP = 23 dBm), Bounding GAV

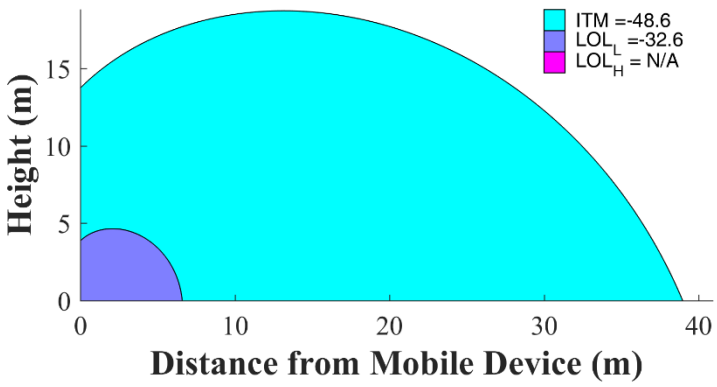

Figure I-114: Handset (EIRP = 23 dBm), Bounding GAV, 1620 MHz

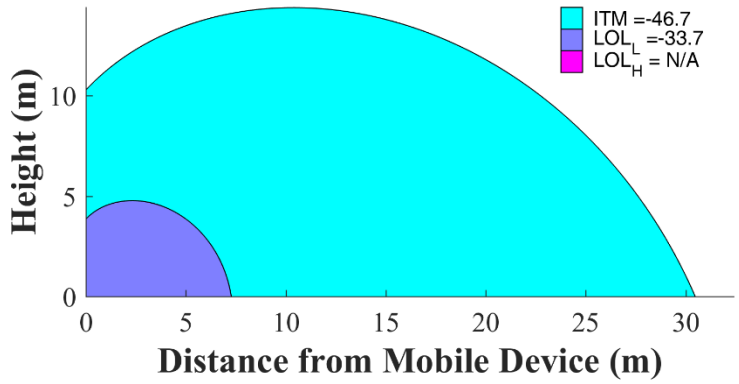

Figure I-115: Handset (EIRP = 23 dBm), Bounding GAV, 1625 MHz

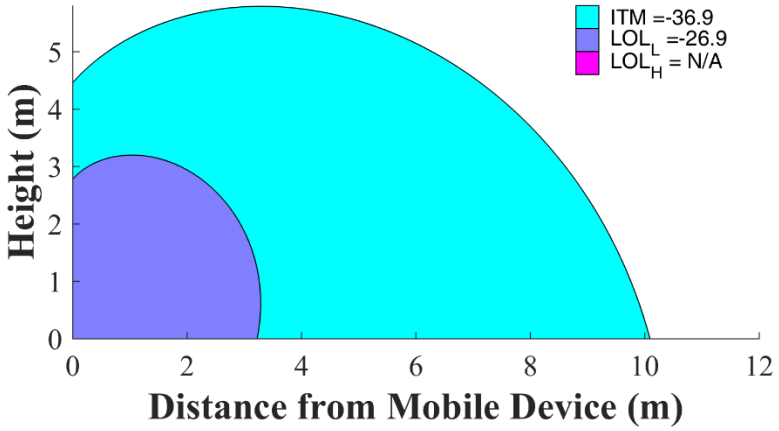

Figure I-116: Handset (EIRP = 23 dBm), Bounding GAV, 1630 MHz

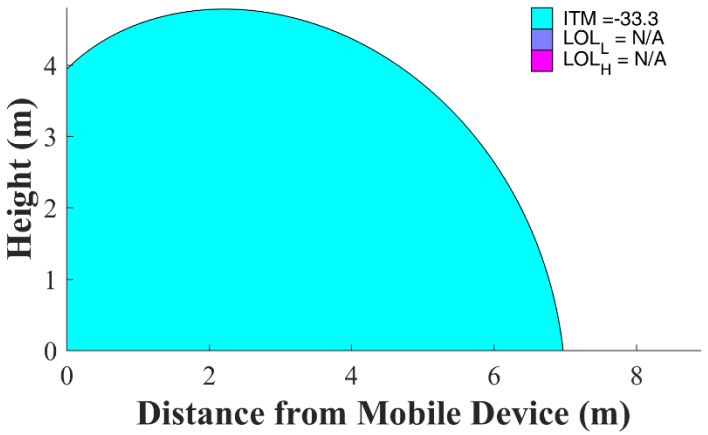

Figure I-117: Handset (EIRP = 23 dBm), Bounding GAV, 1635 MHz

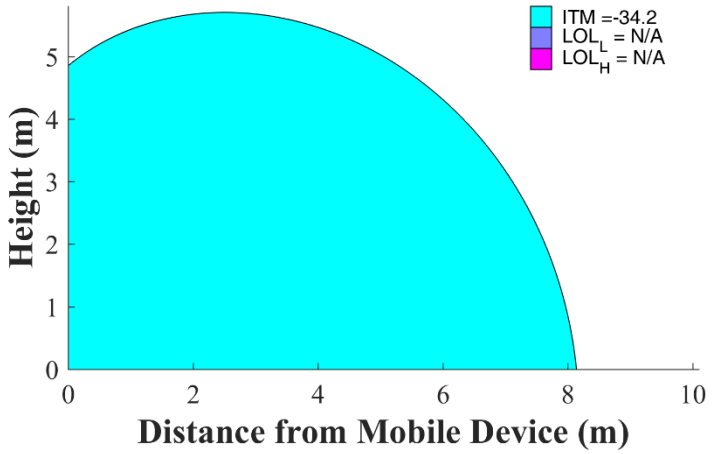

Figure I-118: Handset (EIRP = 23 dBm), Bounding GAV, 1640 MHz

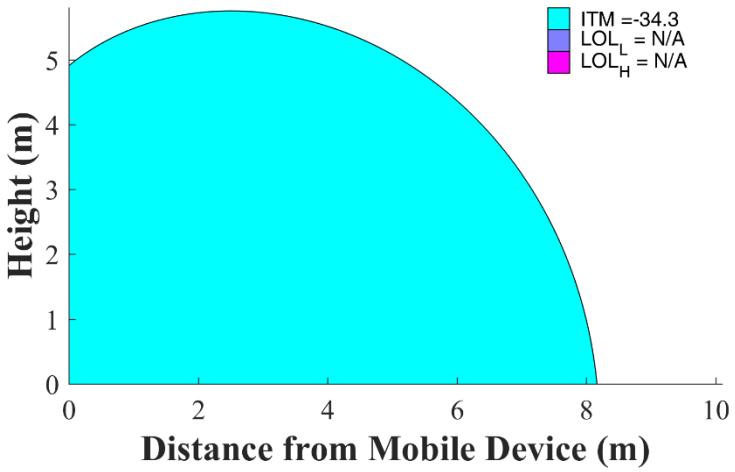

Figure I-119: Handset (EIRP = 23 dBm), Bounding GAV, 1645 MHz

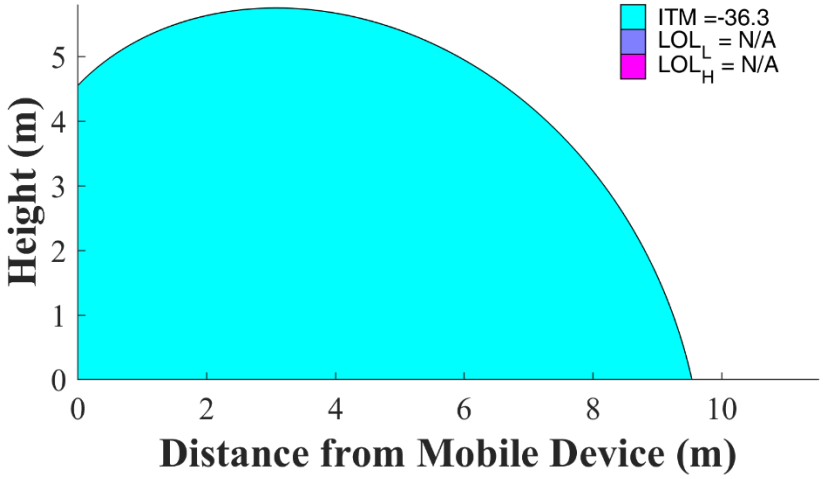

Figure I-120: Handset (EIRP = 23 dBm), Bounding GAV, 1660 MHz

I.3.2 GLN

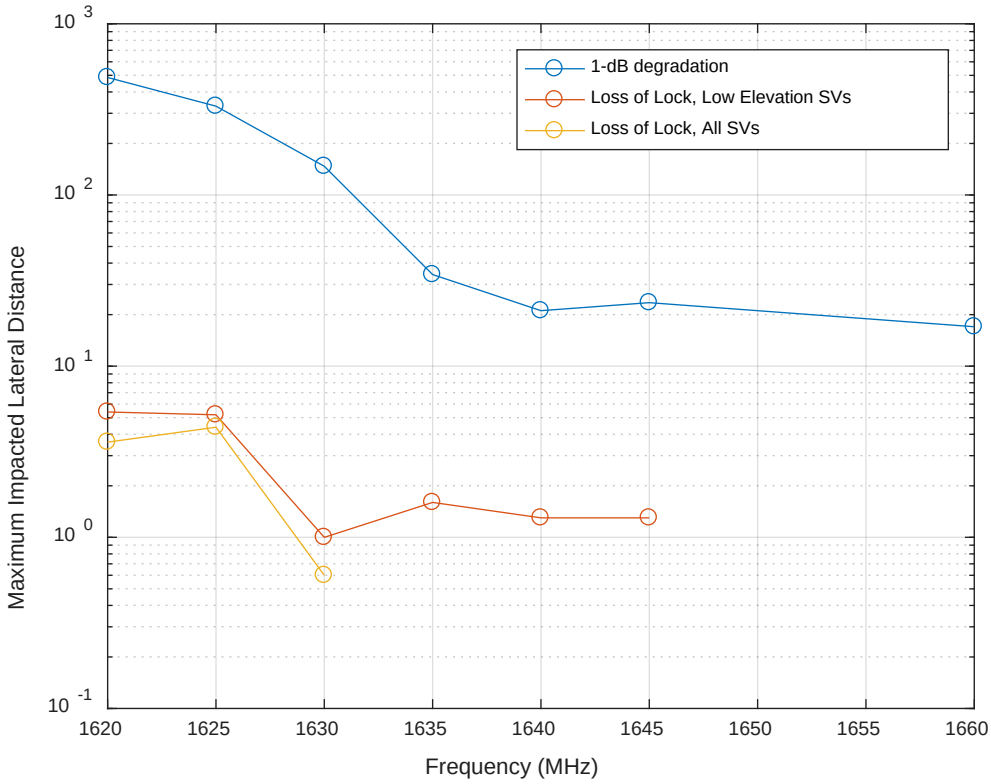

Figure I-121: Handset (EIRP = 23 dBm), Bounding GLN

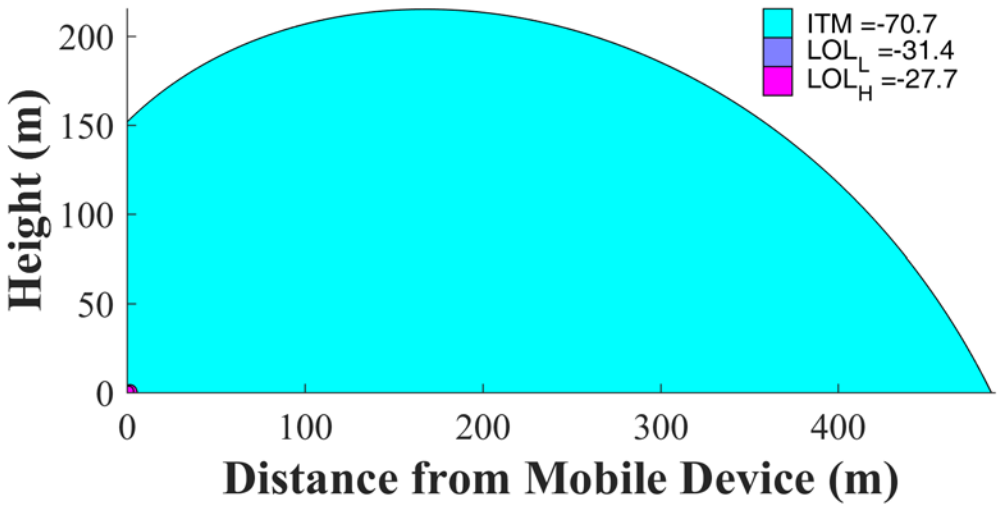

Figure I-122: Handset (EIRP = 23 dBm), Bounding GLN, 1620 MHz

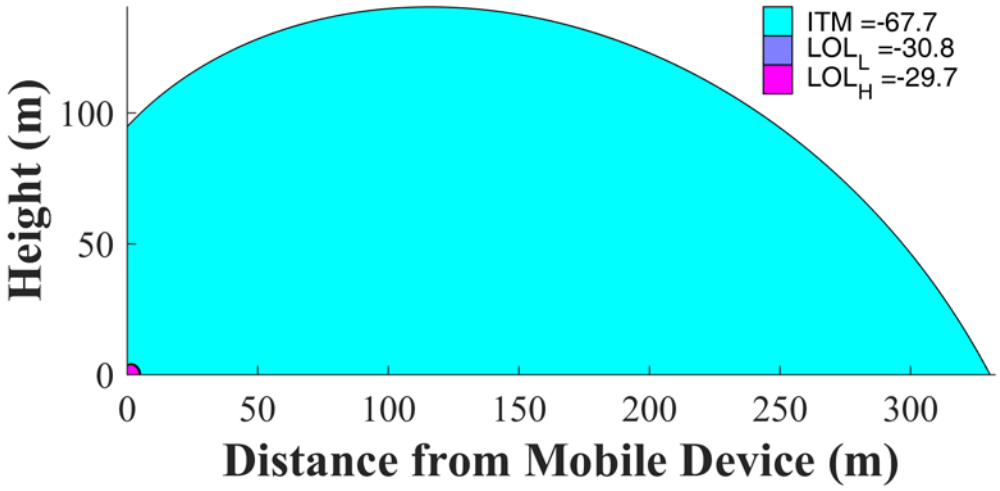

Figure I-123: Handset (EIRP = 23 dBm), Bounding GLN, 1625 MHz

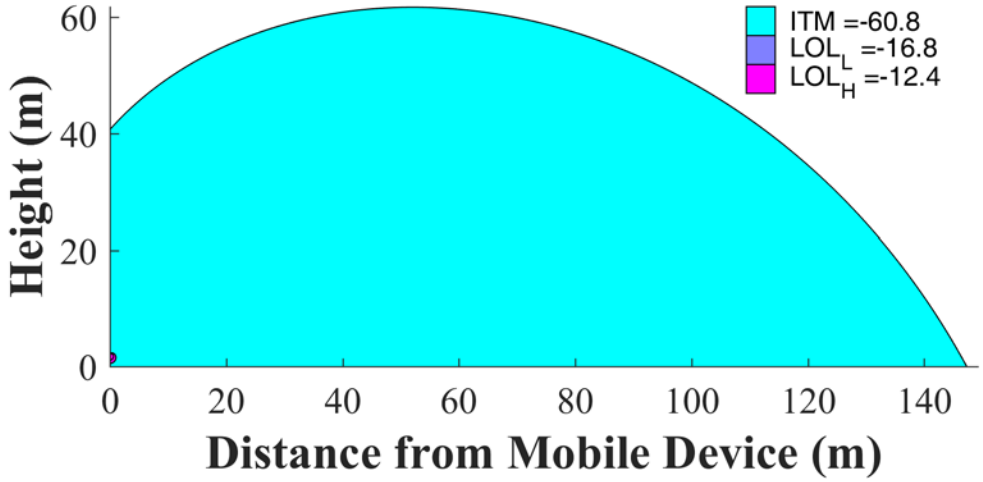

Figure I-124: Handset (EIRP = 23 dBm), Bounding GLN, 1630 MHz

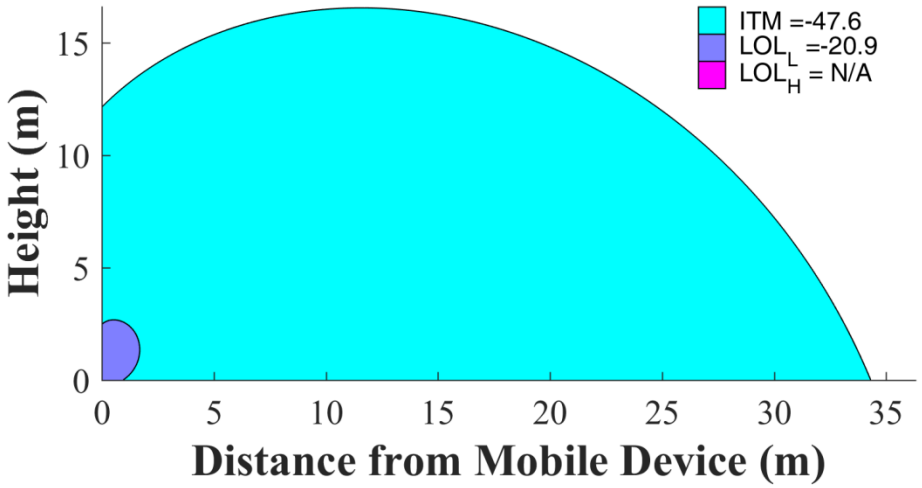

Figure I-125: Handset (EIRP = 23 dBm), Bounding GLN, 1635 MHz

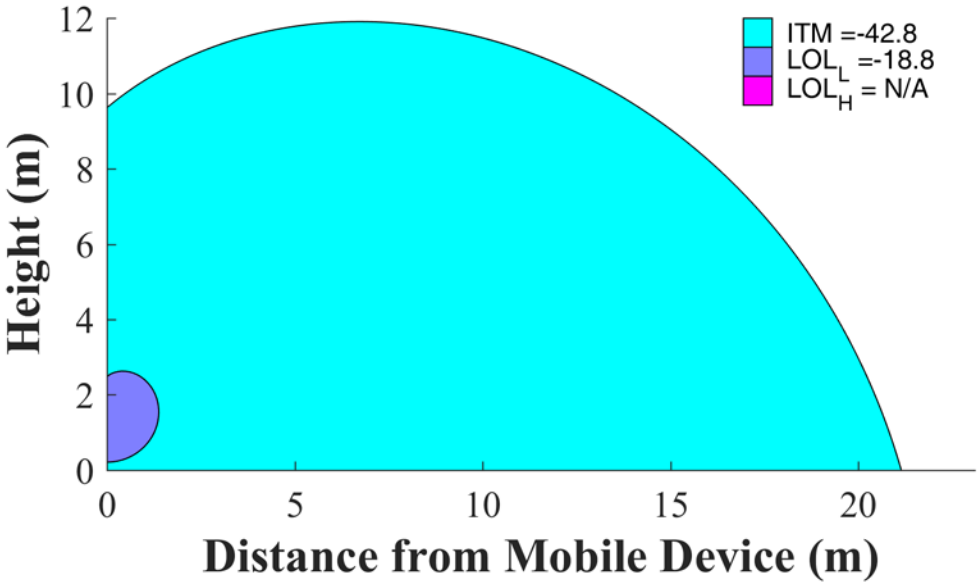

Figure I-126: Handset (EIRP = 23 dBm), Bounding GLN, 1640 MHz

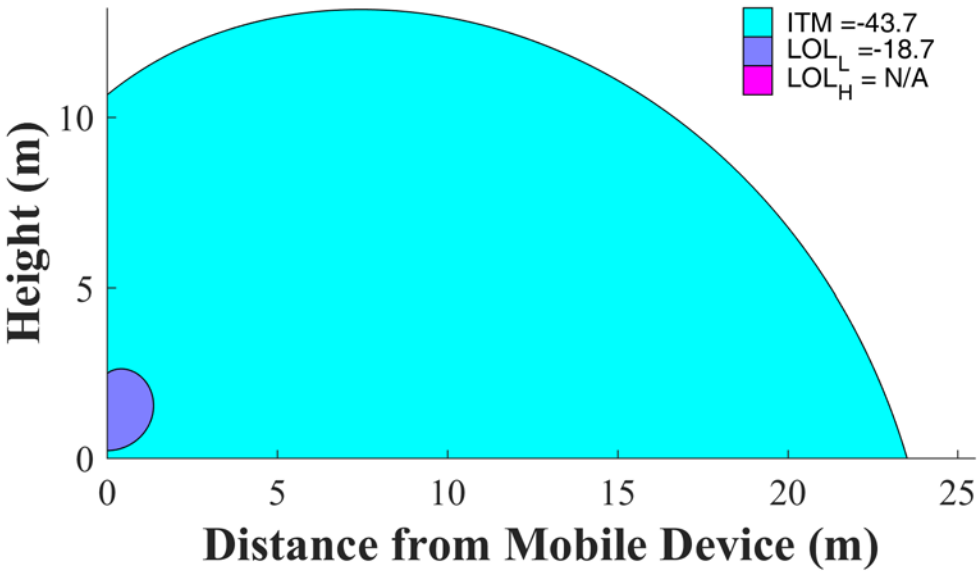

Figure I-127: Handset (EIRP = 23 dBm), Bounding GLN, 1645 MHz

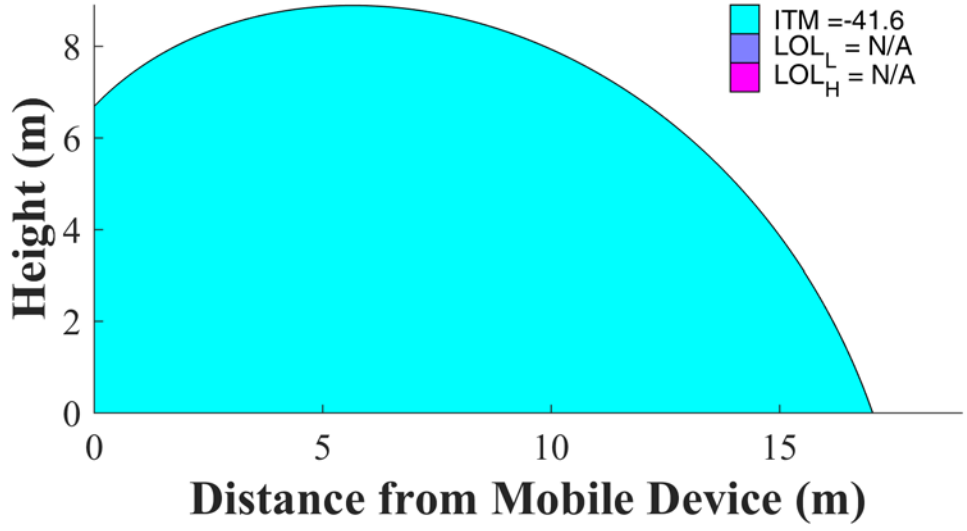

Figure I-128: Handset (EIRP = 23 dBm), Bounding GLN, 1660 MHz

I.3.3 HPR

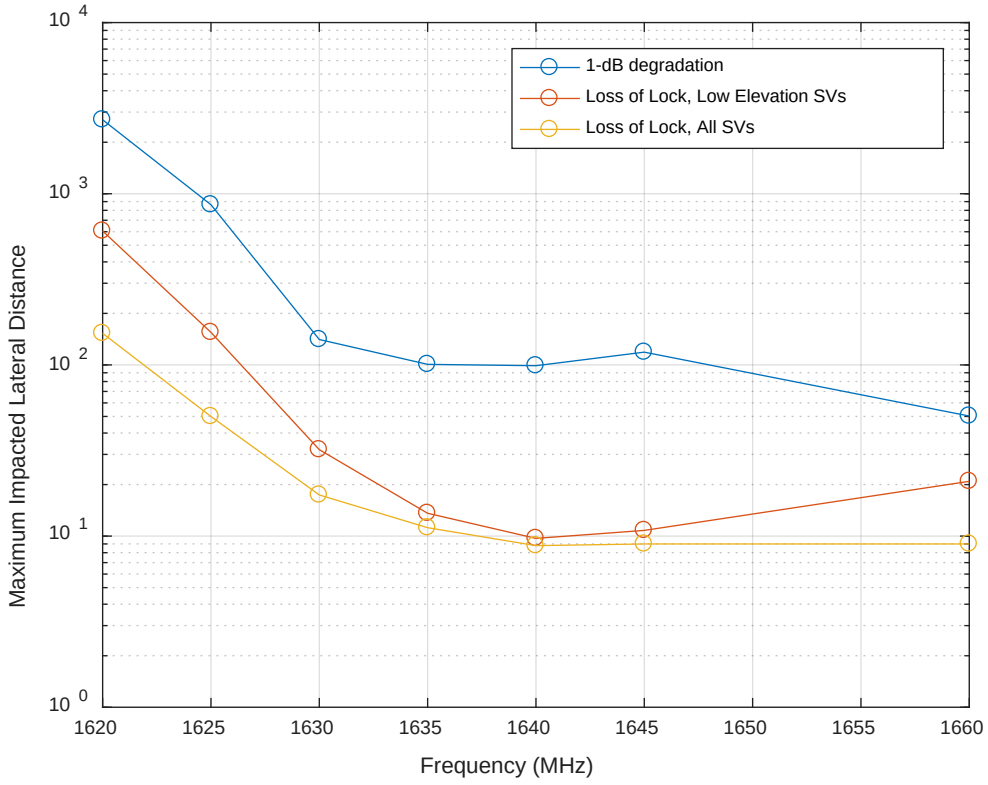

Figure I-129: Handset (EIRP = 23 dBm), Bounding HPR

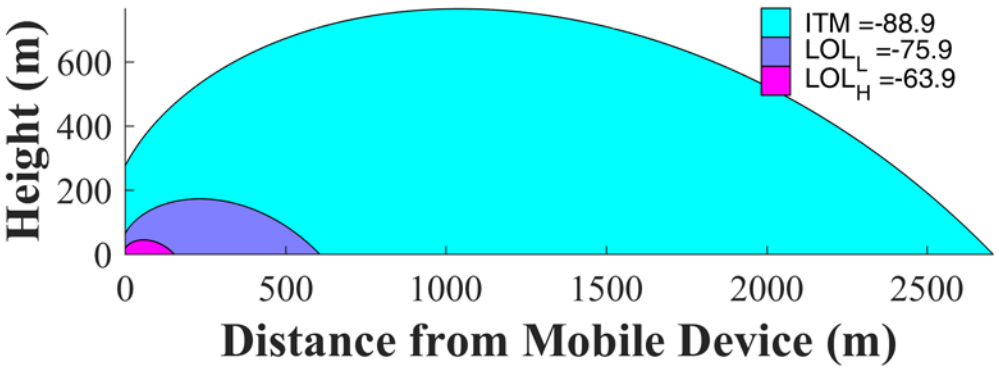

Figure I-130: Handset (EIRP = 23 dBm), Bounding HPR, 1620 MHz

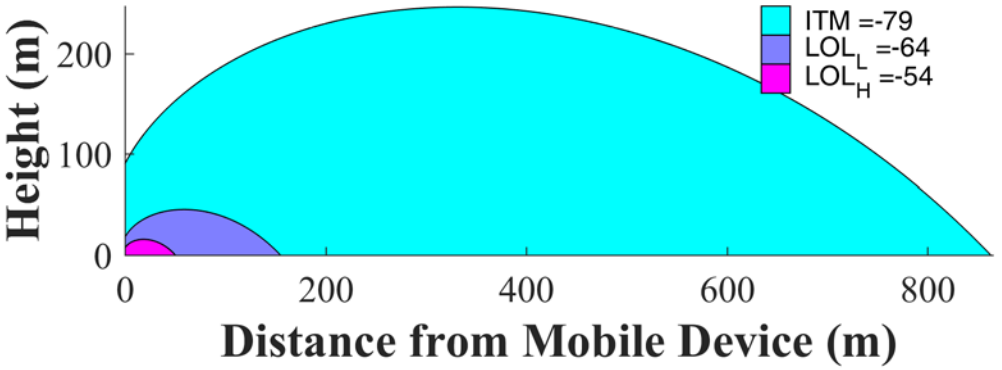

Figure I-131: Handset (EIRP = 23 dBm), Bounding HPR, 1625 MHz

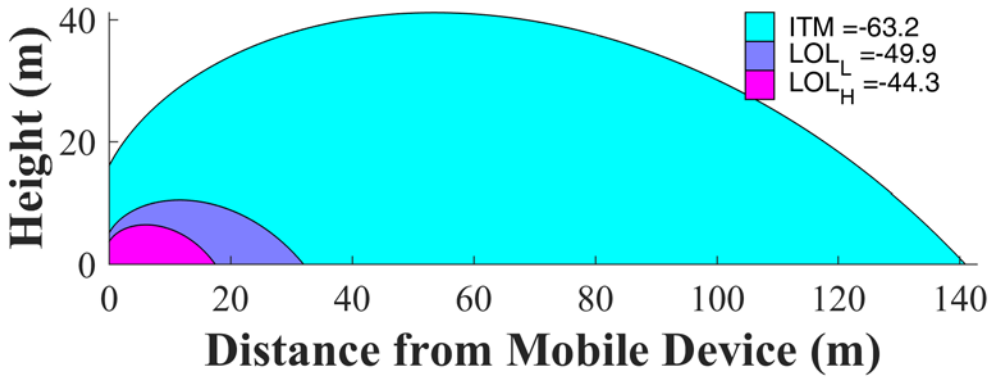

Figure I-132: Handset (EIRP = 23 dBm), Bounding HPR, 1630 MHz

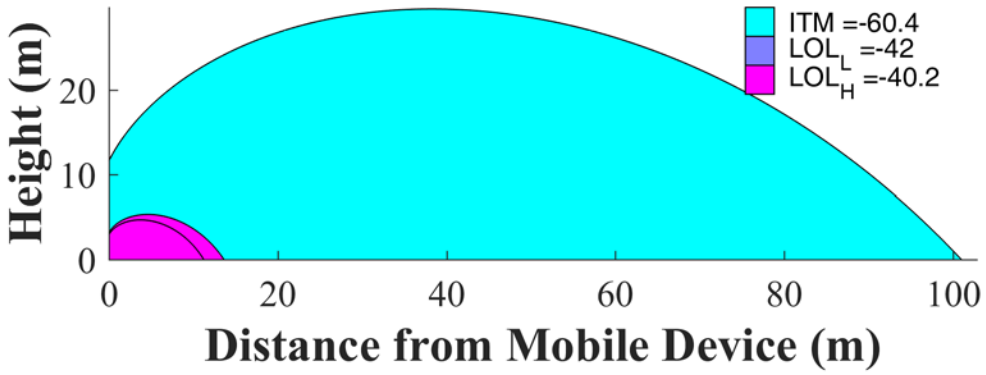

Figure I-133: Handset (EIRP = 23 dBm), Bounding HPR, 1635 MHz

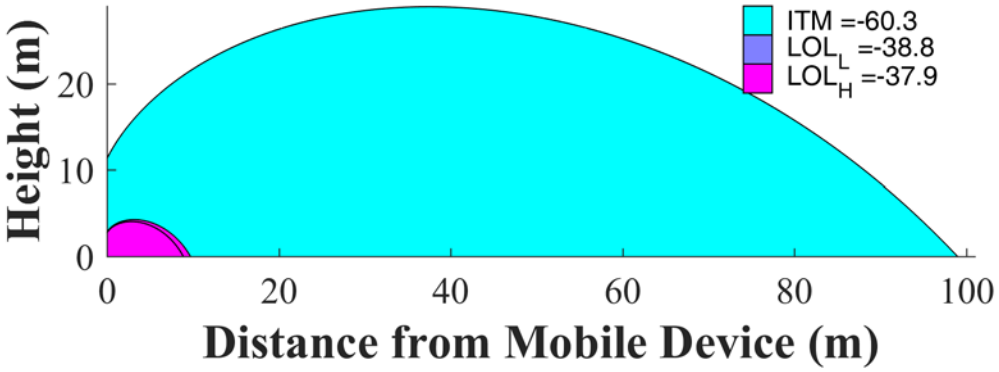

Figure I-134: Handset (EIRP = 23 dBm), Bounding HPR, 1640 MHz

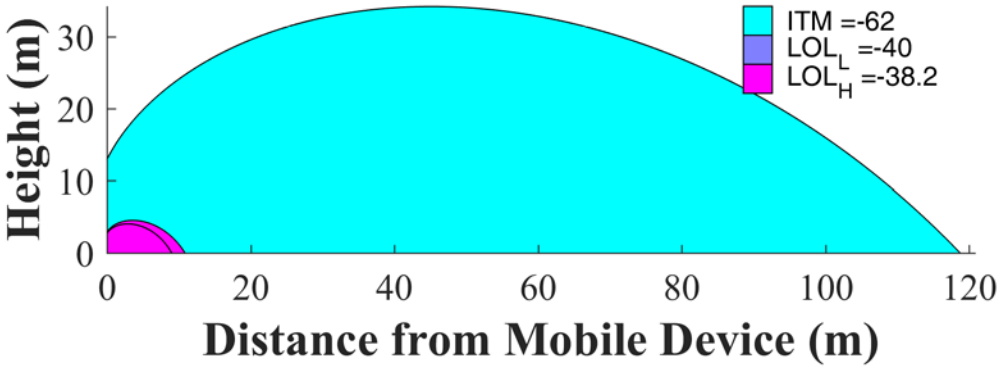

Figure I-135: Handset (EIRP = 23 dBm), Bounding HPR, 1645 MHz

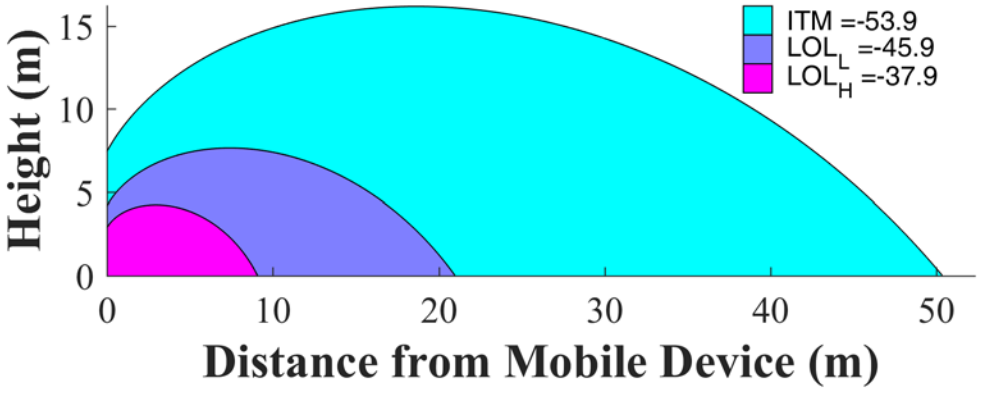

Figure I-136: Handset (EIRP = 23 dBm), Bounding HPR, 1660 MHz

I.3.4 TIM

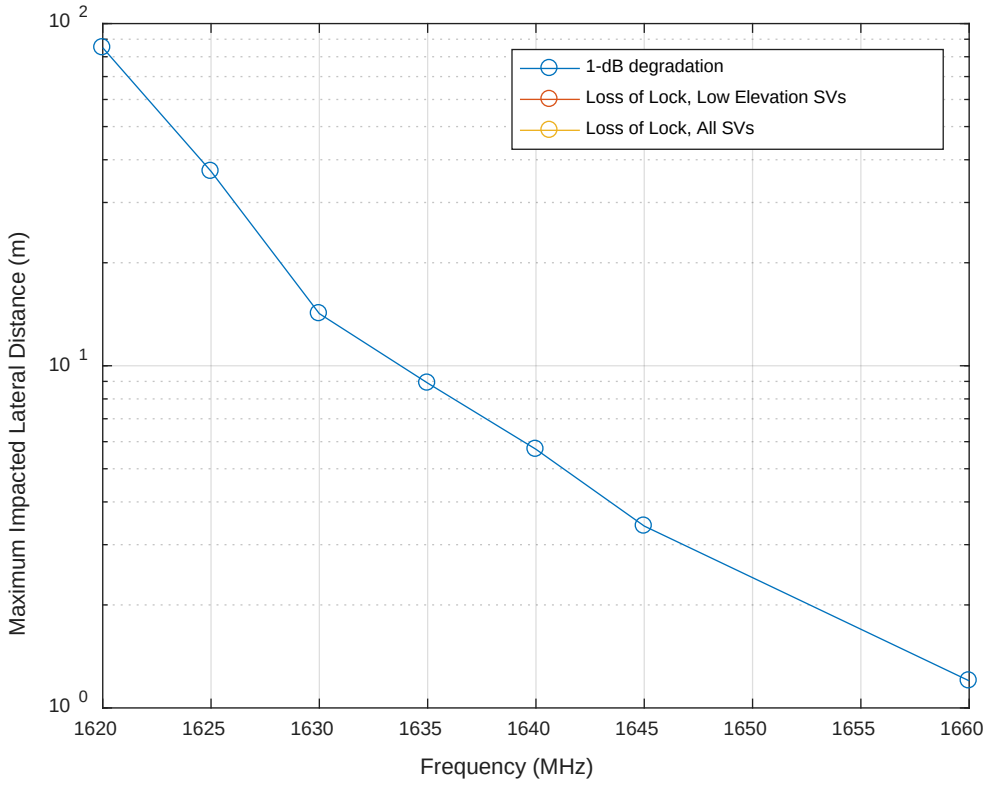

Figure I-137: Handset (EIRP = 23 dBm), Bounding TIM

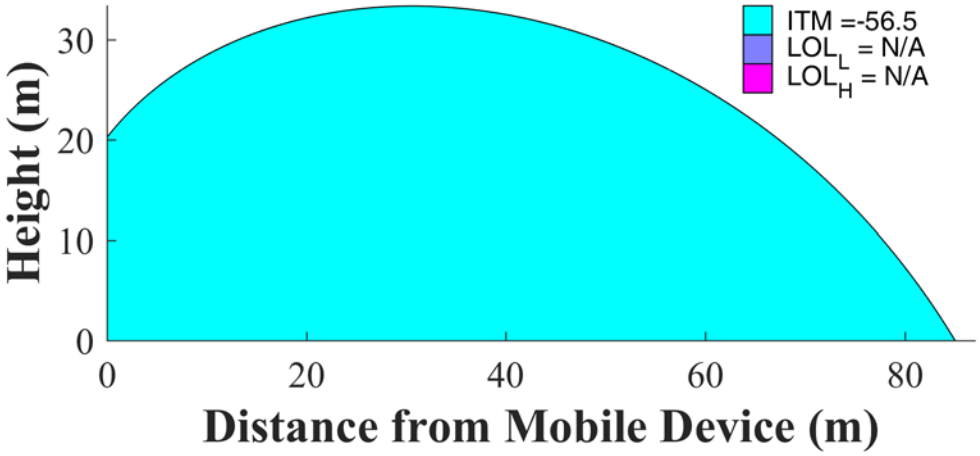

Figure I-138: Handset (EIRP = 23 dBm), Bounding TIM, 1620 MHz

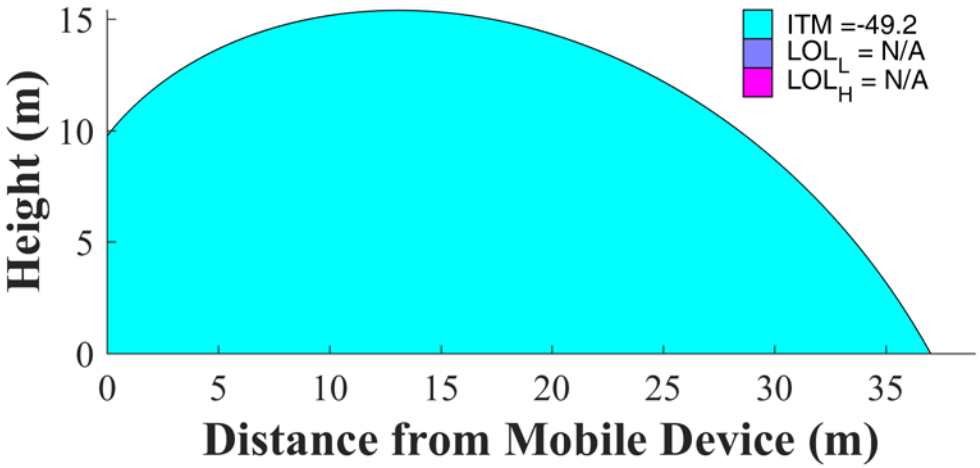

Figure I-139: Handset (EIRP = 23 dBm), Bounding TIM, 1625 MHz

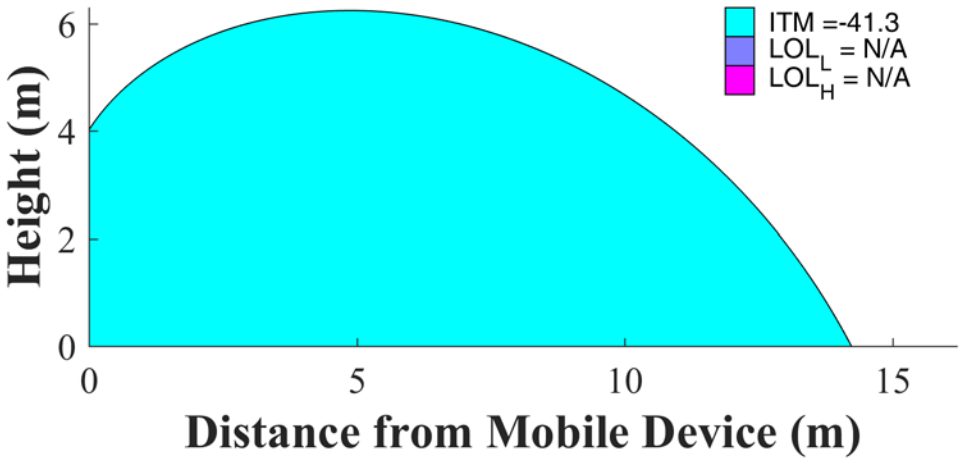

Figure I-140: Handset (EIRP = 23 dBm), Bounding TIM, 1630 MHz

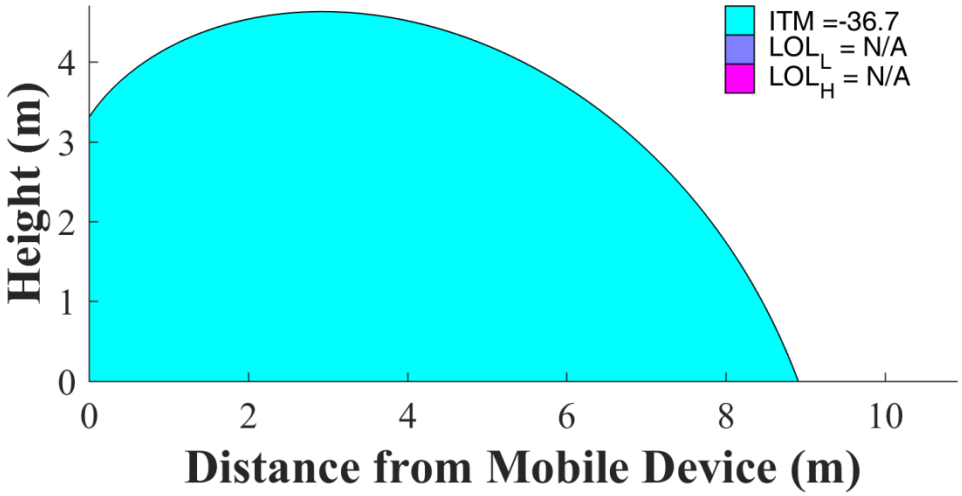

Figure I-141: Handset (EIRP = 23 dBm), Bounding TIM, 1635 MHz

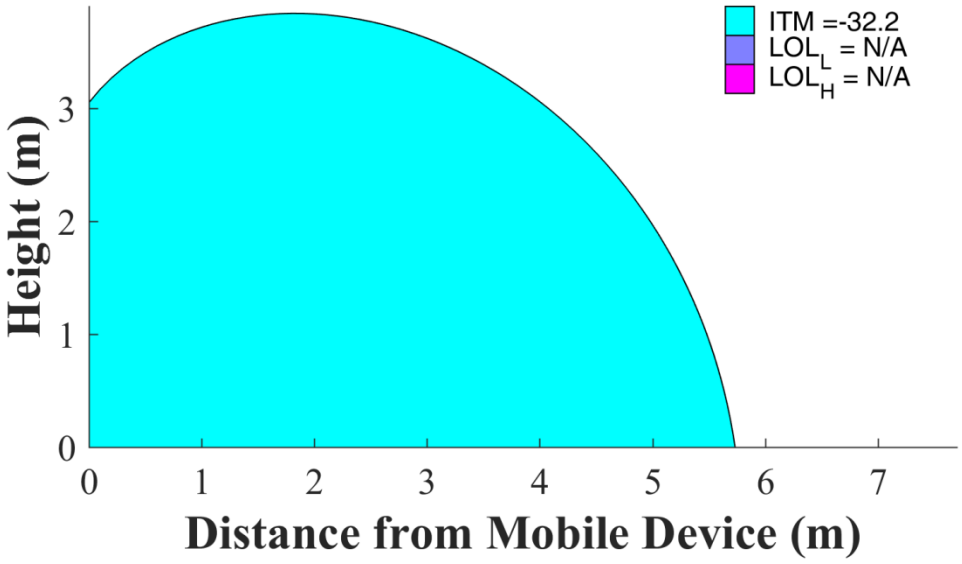

Figure I-142: Handset (EIRP = 23 dBm), Bounding TIM, 1640 MHz

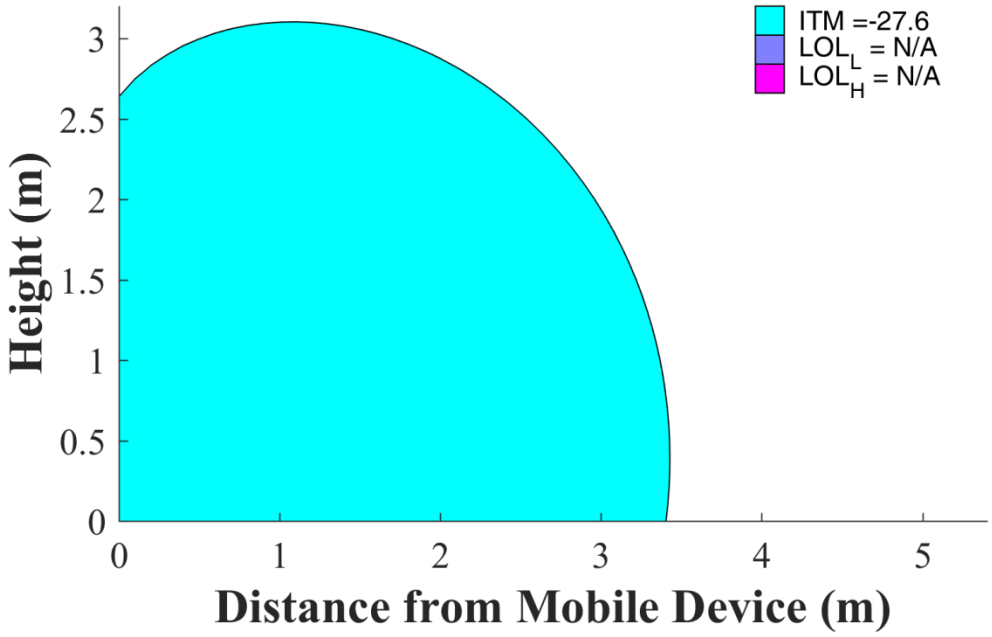

Figure I-143: Handset (EIRP = 23 dBm), Bounding TIM, 1645 MHz

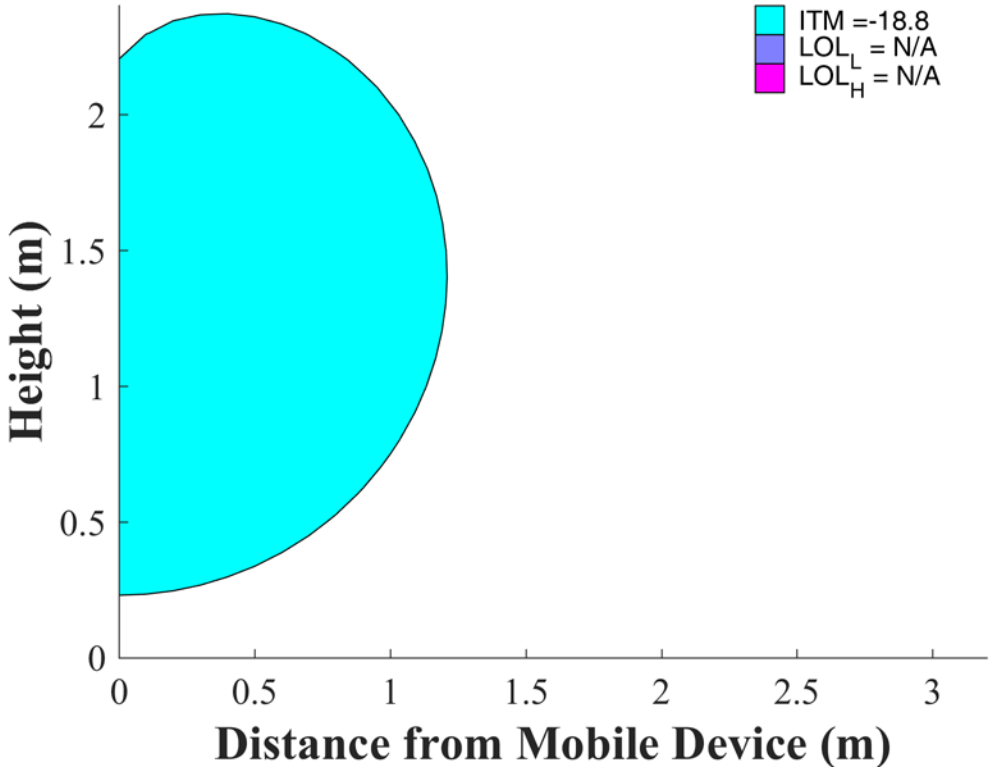

Figure I-144: Handset (EIRP = 23 dBm), Bounding TIM, 1660 MHz

I.3.5 CEL

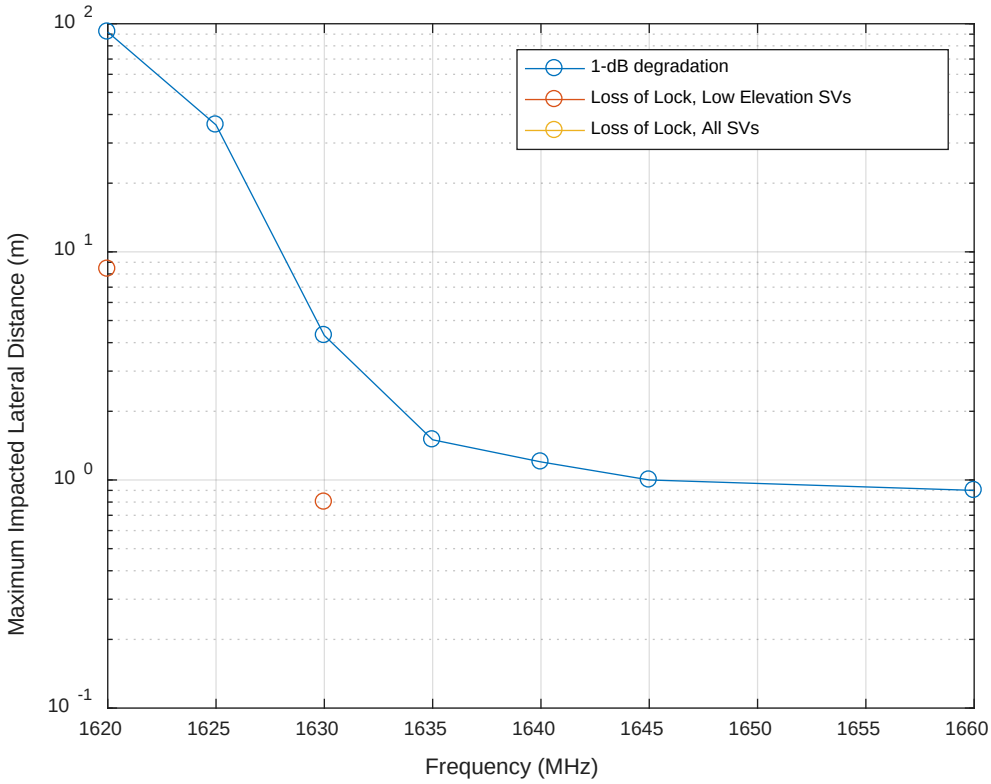

Figure I-145: Handset (EIRP = 23 dBm), Bounding CEL

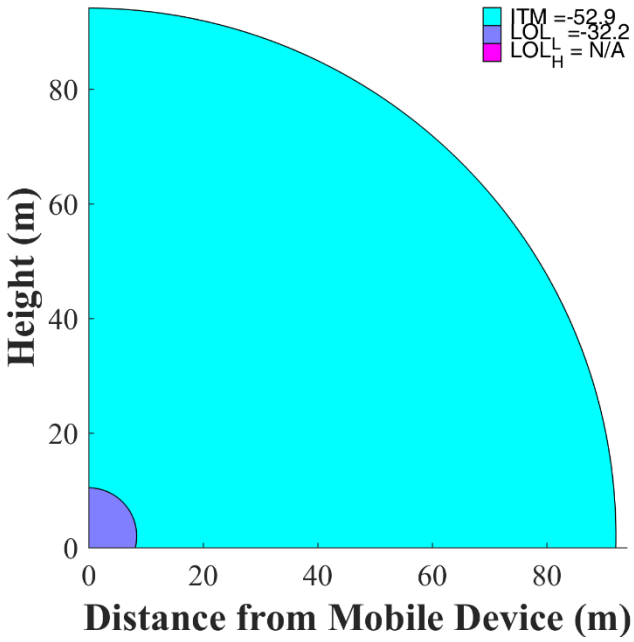

Figure I-146: Handset (EIRP = 23 dBm), Bounding CEL, 1620 MHz

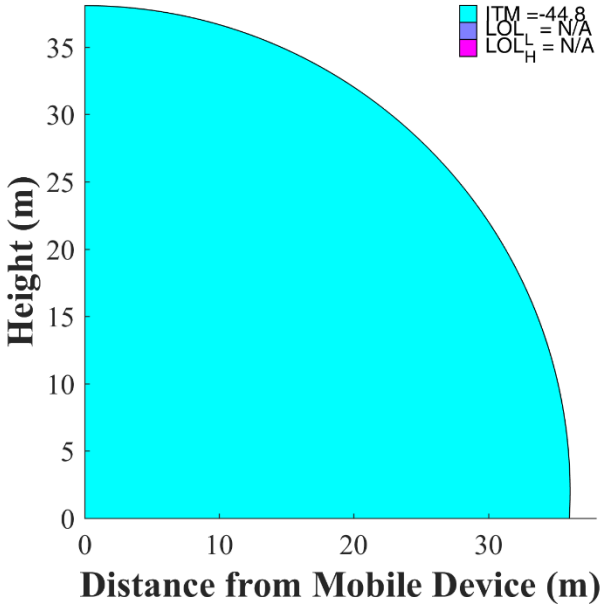

Figure I-147: Handset (EIRP = 23 dBm), Bounding CEL, 1625 MHz

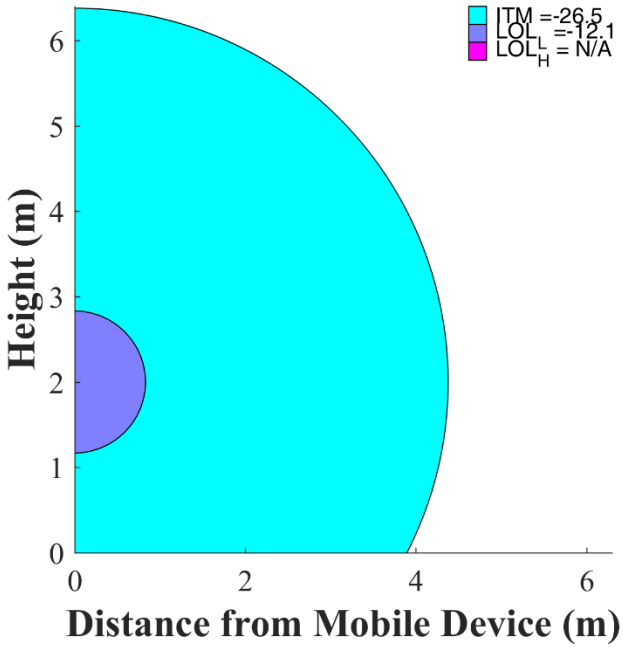

Figure I-148: Handset (EIRP = 23 dBm), Bounding CEL, 1630 MHz

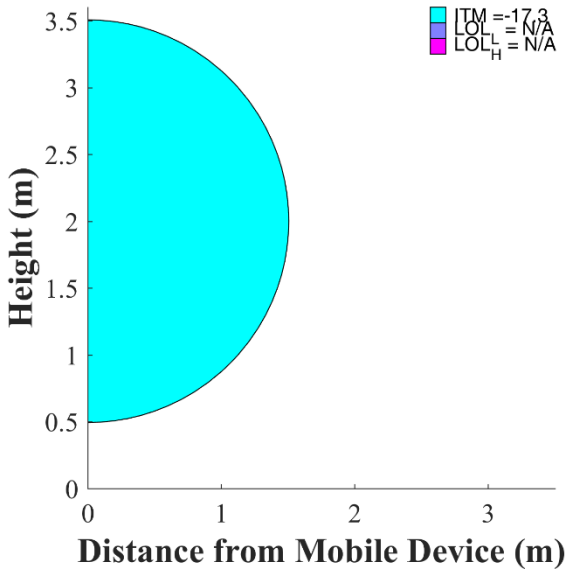

Figure I-149: Handset (EIRP = 23 dBm), Bounding CEL, 1635 MHz

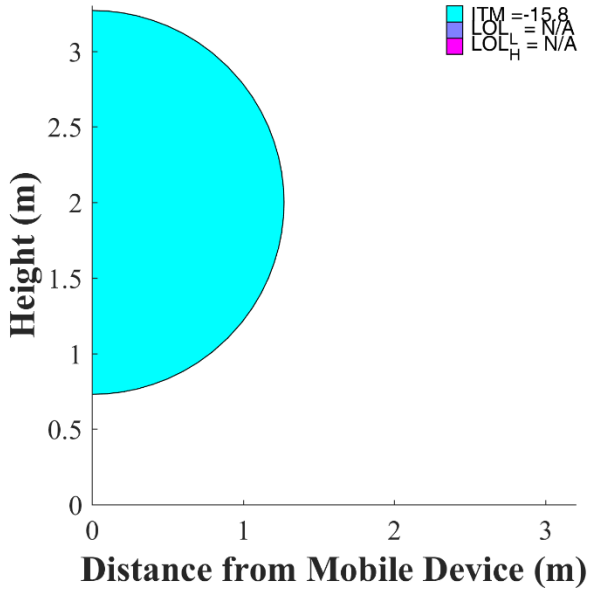

Figure I-150: Handset (EIRP = 23 dBm), Bounding CEL, 1640 MHz

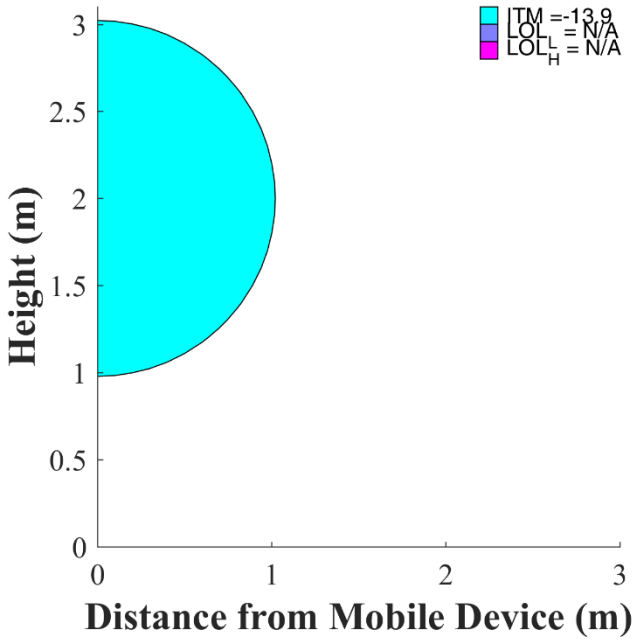

Figure I-151: Handset (EIRP = 23 dBm), Bounding CEL, 1645 MHz

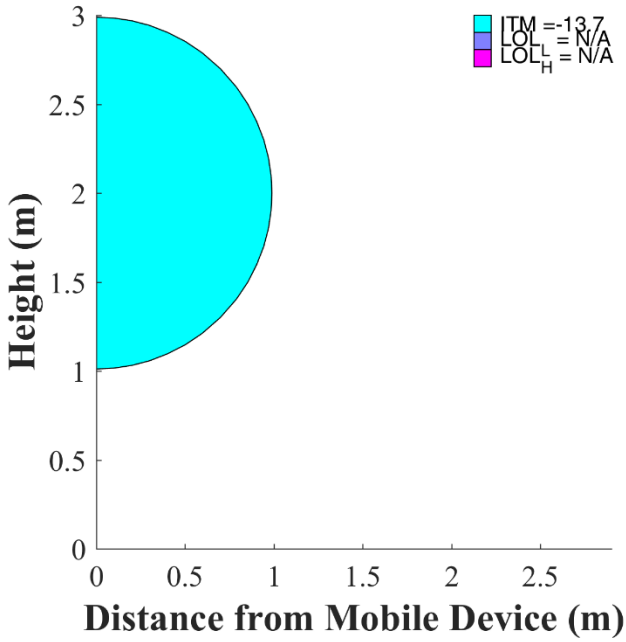

Figure I-152: Handset (EIRP = 23 dBm), Bounding CEL, 1660 MHz

I.4 Sensitivity Analyses

Sections I.1 to I.3 presented results that were applicable for:

- The most sensitive (bounding) DUT of each receiver category for each frequency.
- GPS C/A-code tracking.
- Environments where the free-space path loss model is appropriate.

This section examines sensitivity of the results to these assumptions.

I.4.1 Non-bounding DUTs

Figure I-153 to Figure I-157 provide results for the maximum impacted lateral distance for both the bounding and median DUTs for each receiver category and frequency. The results in these plots are applicable for a single macro urban base station (EIRP = 59 dBm) and for reception of the GPS C/A-code. It is important to note that “median” pertains only to the set of devices tested

at WSMR for each category, and these results should not be interpreted as being applicable to the "median" of fielded GPS/GNSS receivers. As expected, the impacted distances are significantly smaller for the median vs bounding DUTs. Loss-of-lock curves are only included in the HPR plot (Figure I-155) since the median DUTs for all of the other receiver categories did not lose lock on either the nominal or -10 dB satellite signals at any tested frequency.

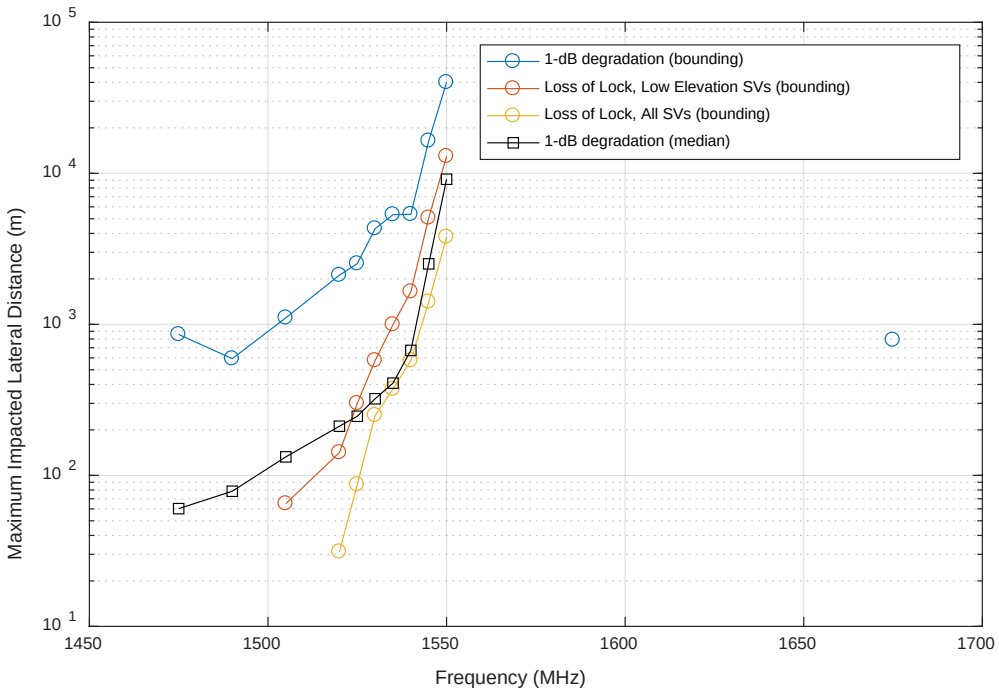

Figure I-153: Maximum Impacted Lateral Distance for GAV, Macro Urban Base Station (EIRP = 59 dBm)

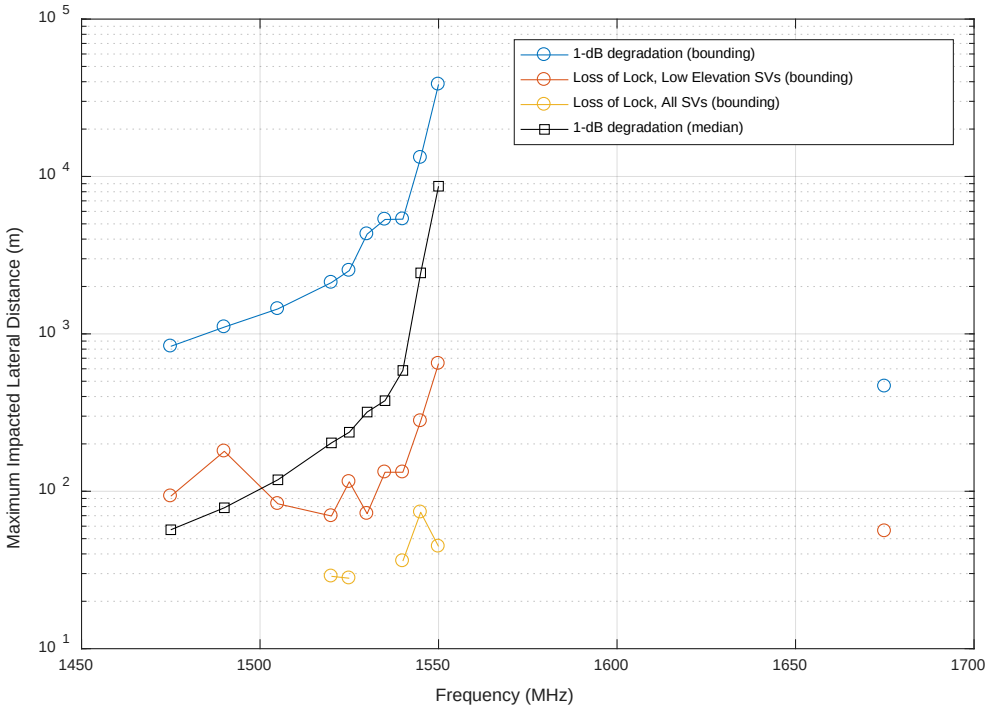

Figure I-154: Maximum Impacted Lateral Distance for GLN, Macro Urban Base Station (EIRP = 59 dBm)

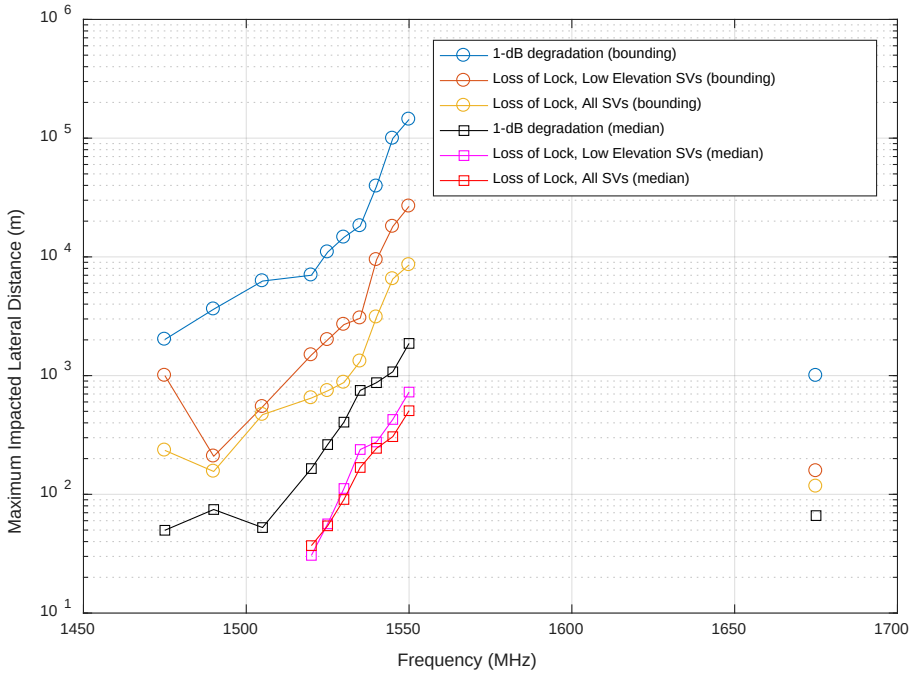

Figure I-155: Maximum Impacted Lateral Distance for HPR, Macro Urban Base Station (EIRP = 59 dBm)

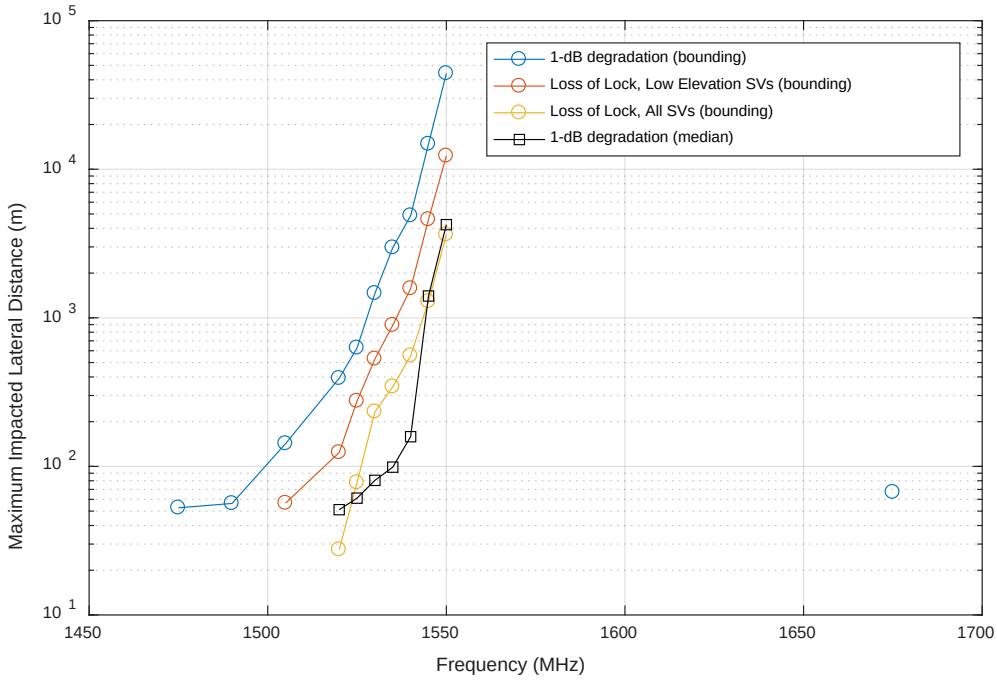

Figure I-156: Maximum Impacted Lateral Distance for TIM, Macro Urban Base Station (EIRP = 59 dBm)

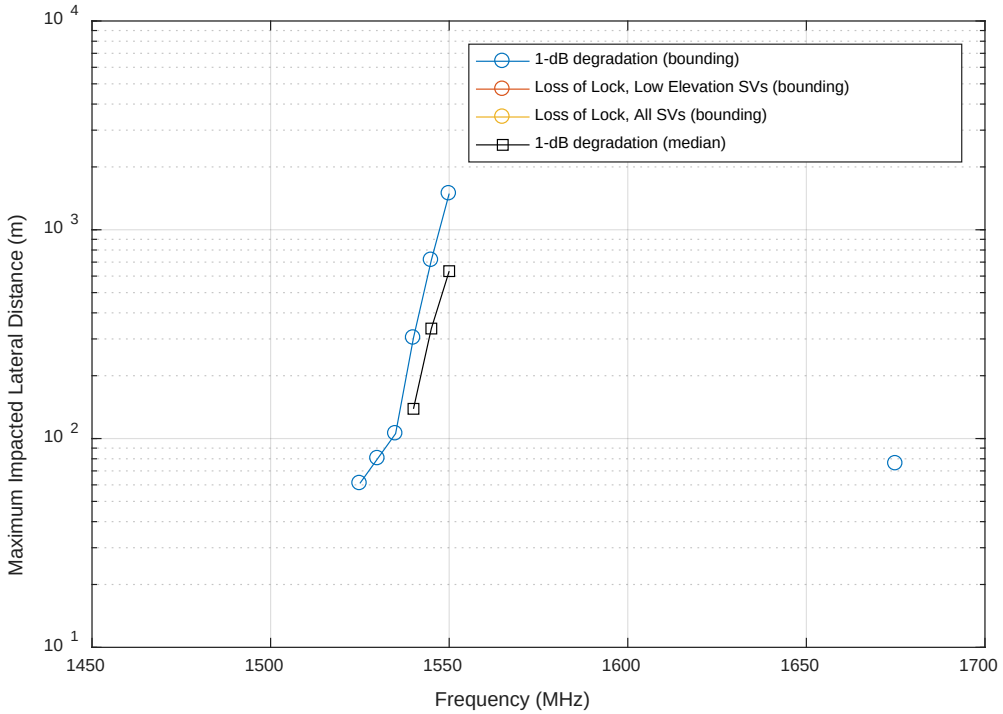

Figure I-157: Maximum Impacted Lateral Distance for CEL, Macro Urban Base Station (EIRP = 59 dBm)

I.4.2 Other GNSS Signal Types

Sections I.1 through I.3 presented results only for GPS C/A-code reception. Oftentimes, DUTs that were capable of tracking other GNSS signal types were more sensitive to interference for the processing of the other signals. As an example, Figure I-158 shows the impacted areas for a small cell outdoor base station operating at 1530 MHz for the most-sensitive GLN DUT. The top figure (a) is for GPS C/A-code, and the bottom figure (b) for GLONASS L1C.

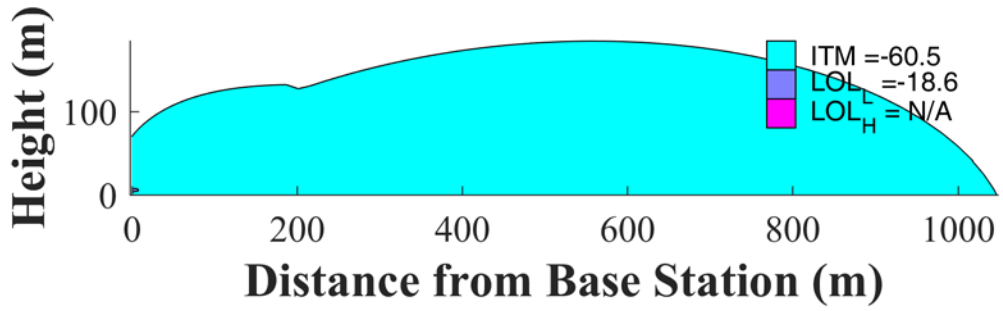

(a)

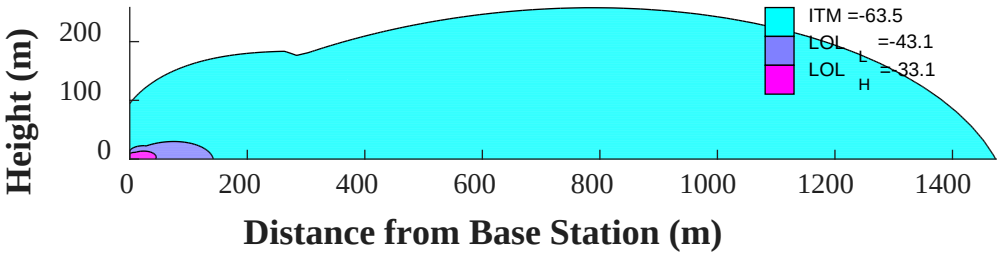

(b)

Figure I-158: Small Cell Outdoor/Micro Urban (EIRP = 40 dBm), Bounding GLN, 1530 MHz: (a) GPS C/A-code (b) GLONASS L1C

I.4.3 Propagation Models

Sections I.1 through I.3 presented forward modeling results that presumed free-space propagation. Depending on the operational environment, these results can be excessively optimistic or pessimistic.

When there is a clear line-of-sight path between the transmitting and receiving antennas and additionally a strong ground reflection, the free-space propagation model can yield optimistic results (i.e., the maximum impacted distance may be greater than predicted). In such environments, a two-ray path model may provide greater accuracy in predicting received power levels. Figure I-159 provides an example of the difference in impacted areas between free-space propagation and two-ray propagation. The two-ray result presumes that the reflecting ground surface is smooth concrete. As a second example, received power levels from an LTE base station in a rural area near Las Vegas were observed at power levels significantly greater than

predicted using the free-space path loss model at lateral distances of up to 9 km.[2] The base station antenna height was 18 m and the received power was measured at a height of around 2 m.

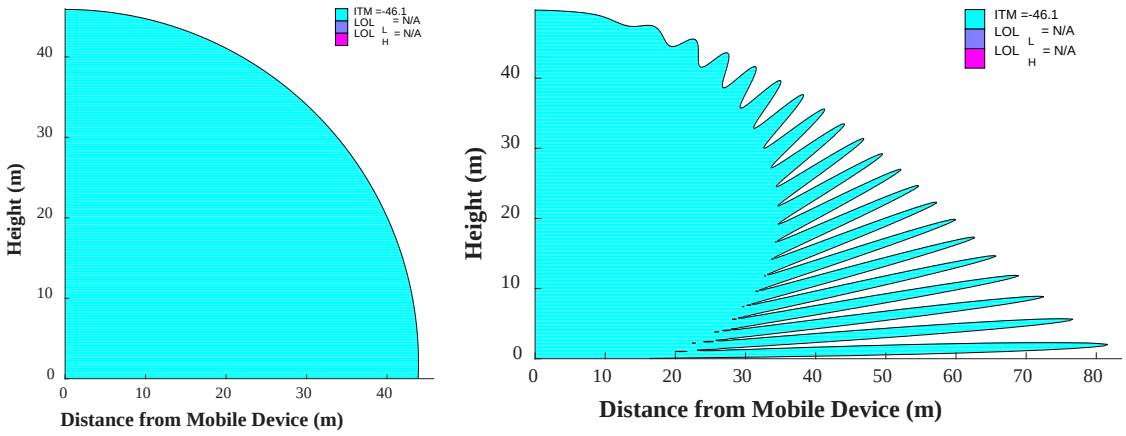

Figure I-159: Impacted Area for Cellular DUT from 23 dBm EIRP Mobile Device at 1550 MHz (a) as predicted using free-space propagation model, (b) as predicted using two-ray propagation model

When there is significant blockage between the transmitting and receiving antennas, the free-space propagation model can at times yield pessimistic results (i.e., the maximum impacted distance may be far smaller than predicted). For example, received power measurements from an LTE base station in a dense urban area within Las Vegas were typically observed to be 10 – 20 dB below those levels predicted using free-space propagation for lateral distances of up to 2 km.[3] The base station antenna height was 72 m and the received power was measured at a height of around 2 m. It should be noted that, even though the received power was most frequently less than predicted using free-space, in some locations far from the base station (> 1 km) power levels were observed to be as high as or exceeding the free-space propagation model predictions. Such observations were much more frequent within 500 km of the base station.

Given the prevalence of line-of-sight blockages in urban and dense suburban areas, the free-space results in Sections I.1 through I.3 are likely to be significantly pessimistic for distances

[2] See p. 110 of https://ecfsapi.fcc.gov/file/7021690471.pdf.
[3] See p. 107 of https://ecfsapi.fcc.gov/file/7021690471.pdf.

exceeding a few hundred meters for all azimuths and significantly pessimistic for some azimuths at shorter distances. Importantly, however, LTE macro base stations may be separated by distances as small as 250 m and small cell outdoor base stations even shorter distances (see Table 3-13). Over several hundred meters in all environments including dense urban, the free-space propagation and two-ray propagation models are appropriately conservative models to protect GPS/GNSS receivers from interference from adjacent band mobile broadband systems.

APPENDIX J

INVERSE MODELING RESULTS

TABLE OF CONTENTS

TABLE OF CONTENTS 2
LIST OF FIGURES 4
LIST OF TABLES 6
REFERENCES 7
APPENDIX 8
Appendix J. Bounding and Median EIRP Tolerance Masks (ETM) for Single Transmitter 8
J.1 GPS L1 C/A ETMs 8
J.1.1 Micro Urban Deployment 8
J.1.1.1 Bounding ETMs 8
J.1.1.1.1 FSPL Propagation Model 8
J.1.1.1.2 2-Ray Path loss model 10
J.1.1.2 Median ETMs 11
J.1.1.2.1 FSPL Propagation Model 12
J.1.1.2.2 2-Ray Path loss model 13
J.1.2 Macro Urban Deployment 14
J.1.2.1 Bounding ETMs 15
J.1.2.1.1 FSPL Propagation Model 15
J.1.2.1.2 2-Ray Path loss model 16
J.1.2.2 Median ETMs 18
J.1.2.2.1 FSPL Propagation Model 18
J.1.2.2.2 2-Ray Path loss model 20
J.2 All GNSS services 22
J.2.1 Micro Urban Deployment 22
J.2.1.1 Bounding ETMs 22
J.2.1.1.1 FSPL Propagation Model 22
J.2.1.1.2 2-Ray Path loss model 24
J.2.1.2 Median ETMs 26

J.2.1.2.1 FSPL Propagation Model 26
J.2.1.2.2 2-Ray Path loss model 28
J.2.2 Macro Urban Deployment 29
J.2.2.1 Bounding ETMs 30
J.2.2.1.1 FSPL Propagation Model 30
J.2.2.1.2 2-Ray Path loss model 31
J.2.2.2 Median ETMs 33
J.2.2.2.1 FSPL Propagation Model 33
J.2.2.2.2 2-Ray Path loss model 35

LIST OF FIGURES

Figure J-1: GPS L1 C/A, Micro Urban, Bounding EIRP Mask: FSPL, $d_{Standoff}$ = 500 m 8
Figure J-2: GPS L1 C/A, Micro Urban, Bounding EIRP Mask: FSPL, $d_{Standoff}$ = 100 m 9
Figure J-3: GPS L1 C/A, Micro Urban, Bounding EIRP Mask: FSPL, $d_{Standoff}$ = 10 m 9
Figure J-4: GPS L1 C/A, Micro Urban, Bounding EIRP Mask: 2-Ray, $d_{Standoff}$ = 500 m 10
Figure J-5: GPS L1 C/A, Micro Urban, Bounding EIRP Mask: 2-Ray, $d_{Standoff}$ = 100 m 10
Figure J-6: GPS L1 C/A, Micro Urban, Bounding EIRP Mask: 2-Ray, $d_{Standoff}$ = 10 m 11
Figure J-7: GPS L1 C/A, Micro Urban, Median EIRP Mask: FSPL, $d_{Standoff}$ = 500 m 12
Figure J-8: GPS L1 C/A, Micro Urban, Median EIRP Mask: FSPL, $d_{Standoff}$ = 100 m 12
Figure J-9: GPS L1 C/A, Micro Urban, Median EIRP Mask: FSPL, $d_{Standoff}$ = 10 m 13
Figure J-10: GPS L1 C/A, Micro Urban, Median EIRP Mask: 2-Ray, $d_{Standoff}$ = 500 m 13
Figure J-11: GPS L1 C/A, Micro Urban, Median EIRP Mask: 2-Ray, $d_{Standoff}$ = 100 m 14
Figure J-12: GPS L1 C/A, Micro Urban, Median EIRP Mask: 2-Ray, $d_{Standoff}$ = 10 m 14
Figure J-13: GPS L1 C/A, Macro Urban, Bounding EIRP Mask: FSPL, $d_{Standoff}$ = 1000 m 15
Figure J-14: GPS L1 C/A, Macro Urban, Bounding EIRP Mask: FSPL, $d_{Standoff}$ = 100 m 16
Figure J-15: GPS L1 C/A, Macro Urban, Bounding EIRP Mask: FSPL, $d_{Standoff}$ = 10 m 16
Figure J-16: GPS L1 C/A, Macro Urban, Bounding EIRP Mask: 2-Ray, $d_{Standoff}$ = 1000 m 17
Figure J-17: GPS L1 C/A, Macro Urban, Bounding EIRP Mask: 2-Ray, $d_{Standoff}$ = 100 m 17
Figure J-18: GPS L1 C/A, Macro Urban, Bounding EIRP Mask: 2-Ray, $d_{Standoff}$ = 10 m 18
Figure J-19: GPS L1 C/A, Macro Urban, Median EIRP Mask: FSPL, $d_{Standoff}$ = 1000 m 19
Figure J-20: GPS L1 C/A, Macro Urban, Median EIRP Mask: FSPL, $d_{Standoff}$ = 100 m 19
Figure J-21: GPS L1 C/A, Macro Urban, Median EIRP Mask: FSPL, $d_{Standoff}$ = 10 m 20
Figure J-22: GPS L1 C/A, Macro Urban, Median EIRP Mask: 2-Ray, $d_{Standoff}$ = 1000 m 21
Figure J-23: GPS L1 C/A, Macro Urban, Median EIRP Mask: 2-Ray, $d_{Standoff}$ = 100 m 21
Figure J-24: GPS L1 C/A, Macro Urban, Median EIRP Mask: 2-Ray, $d_{Standoff}$ = 10 m 22
Figure J-25: All GNSS, Micro Urban, Bounding EIRP Mask: FSPL, $d_{Standoff}$ = 500 m 23
Figure J-26: All GNSS, Micro Urban, Bounding EIRP Mask: FSPL, $d_{Standoff}$ = 100 m 23
Figure J-27: All GNSS, Micro Urban, Bounding EIRP Mask: FSPL, $d_{Standoff}$ = 10 m 24
Figure J-28: All GNSS, Micro Urban, Bounding EIRP Mask: 2-Ray, $d_{Standoff}$ = 500 m 25
Figure J-29: All GNSS, Micro Urban, Bounding EIRP Mask: 2-Ray, $d_{Standoff}$ = 100 m 25
Figure J-30: All GNSS, Micro Urban, Bounding EIRP Mask: 2-Ray, $d_{Standoff}$ = 10 m 26
Figure J-31: All GNSS, Micro Urban, Median EIRP Mask: FSPL, $d_{Standoff}$ = 500 m 27
Figure J-32: All GNSS, Micro Urban, Median EIRP Mask: FSPL, $d_{Standoff}$ = 100 m 27
Figure J-33: All GNSS, Micro Urban, Median EIRP Mask: FSPL, $d_{Standoff}$ = 10 m 28
Figure J-34: All GNSS, Micro Urban, Median EIRP Mask: 2-Ray, $d_{Standoff}$ = 500 m 28
Figure J-35: All GNSS, Micro Urban, Median EIRP Mask: 2-Ray, $d_{Standoff}$ = 100 m 29
Figure J-36: All GNSS, Micro Urban, Median EIRP Mask: 2-Ray, $d_{Standoff}$ = 10 m 29

Figure J-37: All GNSS, Macro Urban, Bounding EIRP Mask: FSPL, $d_{Standoff}$ = 1000 m 30
Figure J-38: All GNSS, Macro Urban, Bounding EIRP Mask: FSPL, $d_{Standoff}$ = 100 m 31
Figure J-39: All GNSS, Macro Urban, Bounding EIRP Mask: FSPL, $d_{Standoff}$ = 10 m 31
Figure J-40: All GNSS, Macro Urban, Bounding EIRP Mask: 2-Ray, $d_{Standoff}$ = 1000 m..... 32
Figure J-41: All GNSS, Macro Urban, Bounding EIRP Mask: 2-Ray, $d_{Standoff}$ = 100 m..... 32
Figure J-42: All GNSS, Macro Urban, Bounding EIRP Mask: 2-Ray, $d_{Standoff}$ = 10 m..... 33
Figure J-43: All GNSS, Macro Urban, Median EIRP Mask: FSPL, $d_{Standoff}$ = 1000 m..... 34
Figure J-44: All GNSS, Macro Urban, Median EIRP Mask: FSPL, $d_{Standoff}$ = 100 m..... 34
Figure J-45: All GNSS, Macro Urban, Median EIRP Mask: FSPL, $d_{Standoff}$ = 10 m..... 35
Figure J-46: All GNSS, Macro Urban, Median EIRP Mask: 2-Ray, $d_{Standoff}$ = 1000 m 36
Figure J-47: All GNSS, Macro Urban, Median EIRP Mask: 2-Ray, $d_{Standoff}$ = 100 m 36
Figure J-48: All GNSS, Macro Urban, Median EIRP Mask: 2-Ray, $d_{Standoff}$ = 10 m 37

LIST OF TABLES

No table of figures entries found.

REFERENCES

There are no sources in the current document.

APPENDIX

Appendix J. Bounding and Median EIRP Tolerance Masks (ETM) for Single Transmitter

J.1 GPS L1 C/A ETMs

J.1.1 Micro Urban Deployment

J.1.1.1 Bounding ETMs

J.1.1.1.1 FSPL Propagation Model

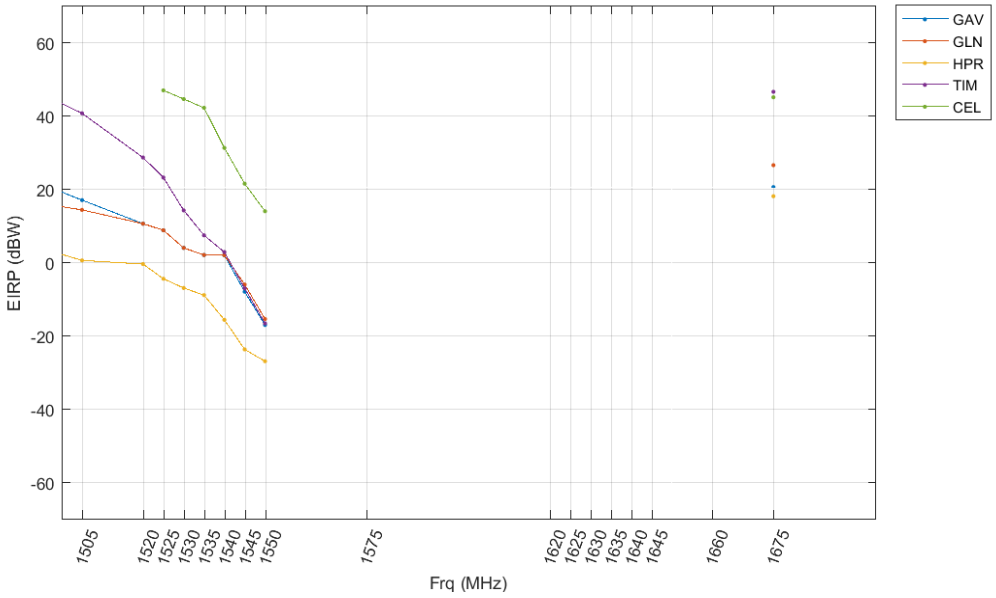

Figure J-1: GPS L1 C/A, Micro Urban, Bounding EIRP Mask: FSPL, $d_{Standoff}$ = 500 m

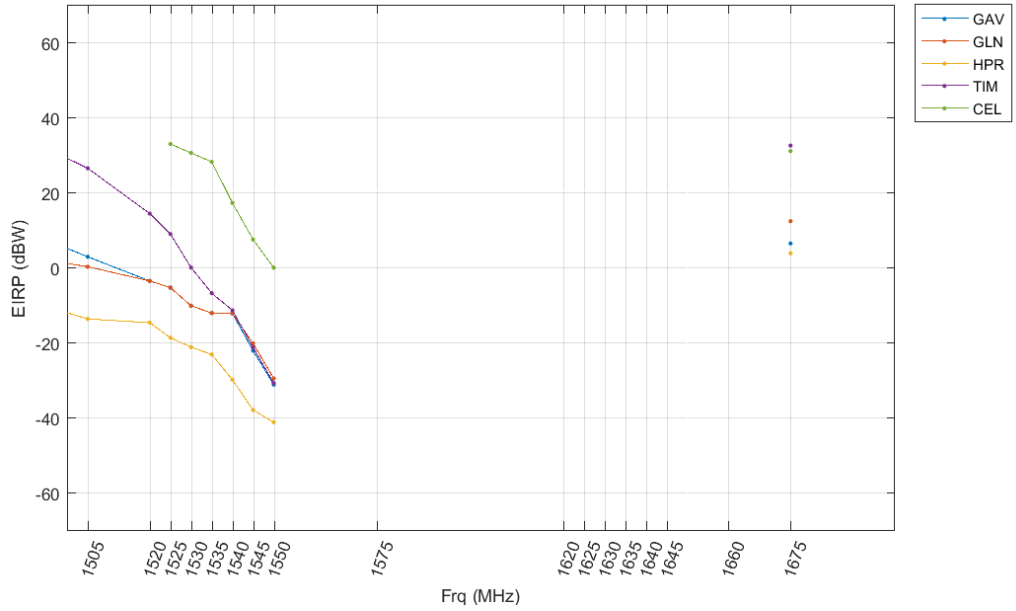

Figure J-2: GPS L1 C/A, Micro Urban, Bounding EIRP Mask: FSPL, $d_{Standoff}$ = 100 m

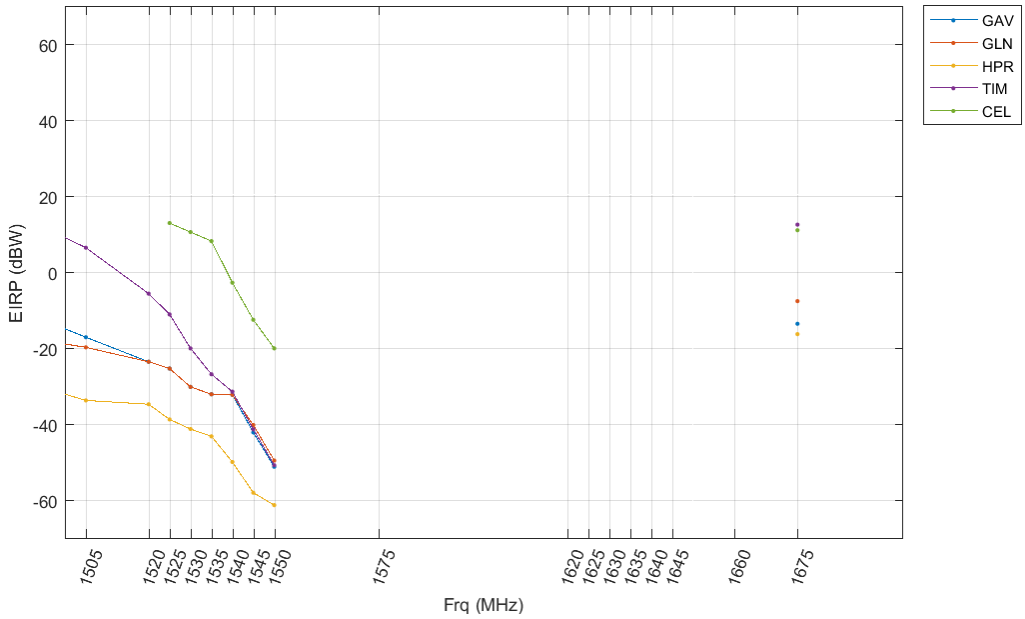

Figure J-3: GPS L1 C/A, Micro Urban, Bounding EIRP Mask: FSPL, $d_{Standoff}$ = 10 m

J.1.1.1.2 2-Ray Path loss model

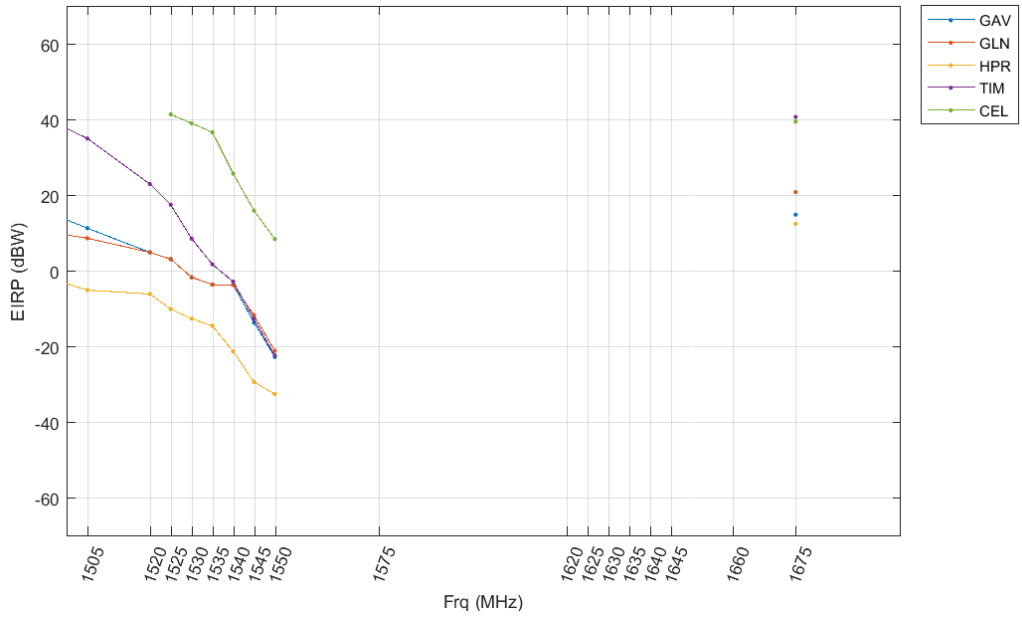

Figure J-4: GPS L1 C/A, Micro Urban, Bounding EIRP Mask: 2-Ray, $d_{Standoff}$ = 500 m

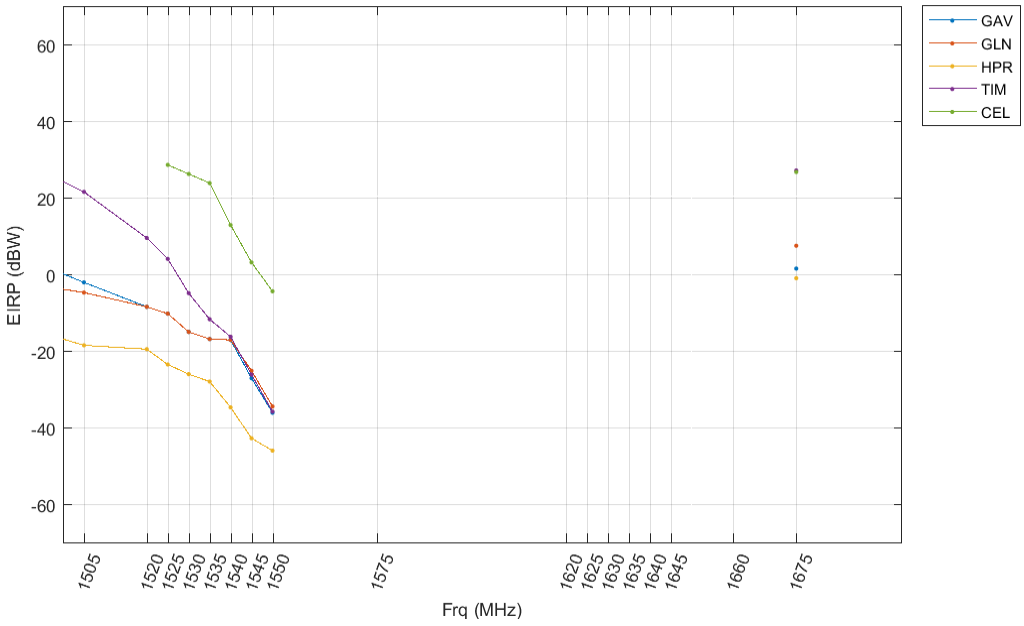

Figure J-5: GPS L1 C/A, Micro Urban, Bounding EIRP Mask: 2-Ray, $d_{Standoff}$ = 100 m

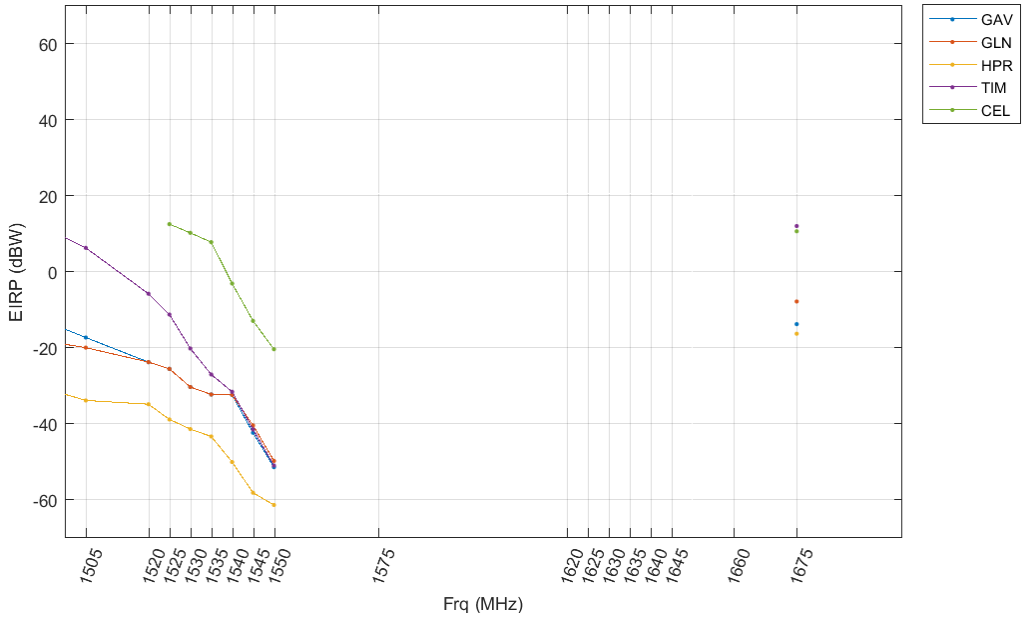

Figure J-6: GPS L1 C/A, Micro Urban, Bounding EIRP Mask: 2-Ray, $d_{Standoff}$ = 10 m

J.1.1.2 Median ETMs

J.1.1.2.1 FSPL Propagation Model

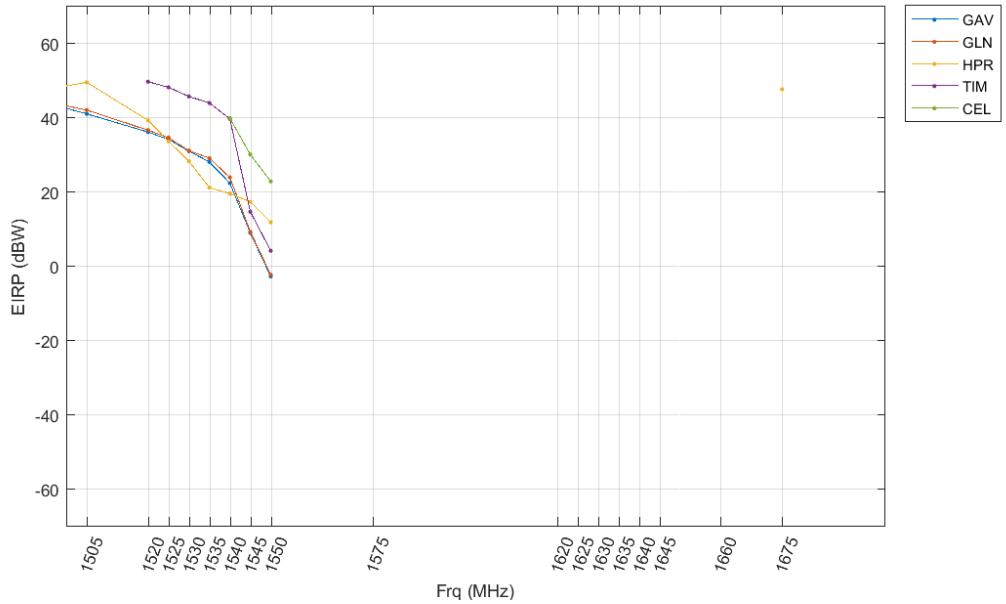

Figure J-7: GPS L1 C/A, Micro Urban, Median EIRP Mask: FSPL, $d_{Standoff}$ = 500 m

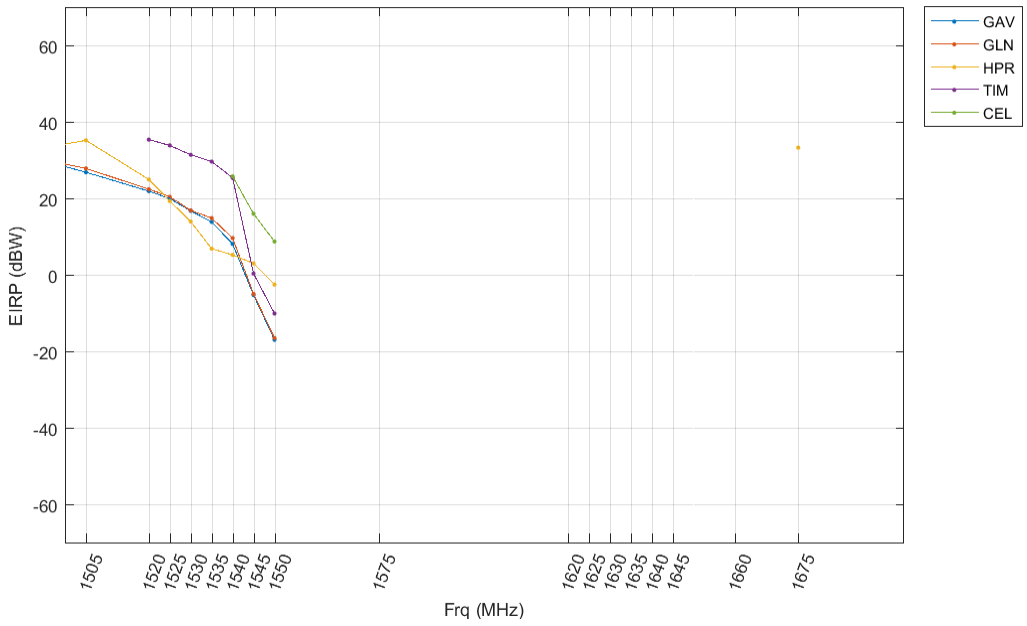

Figure J-8: GPS L1 C/A, Micro Urban, Median EIRP Mask: FSPL, $d_{Standoff}$ = 100 m

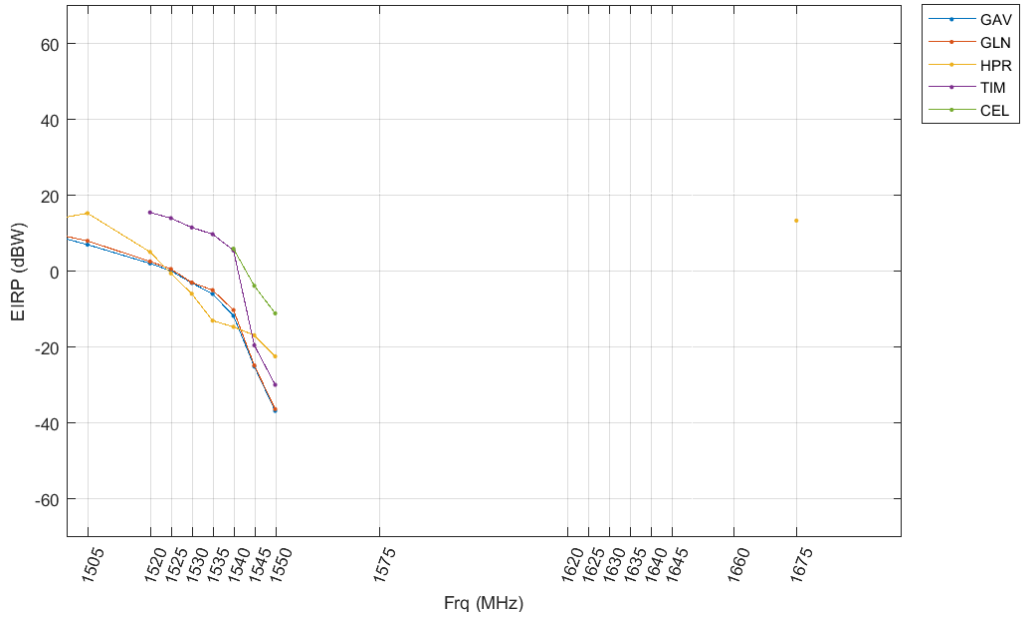

Figure J-9: GPS L1 C/A, Micro Urban, Median EIRP Mask: FSPL, $d_{Standoff}$ = 10 m

J.1.1.2.2 2-Ray Path loss model

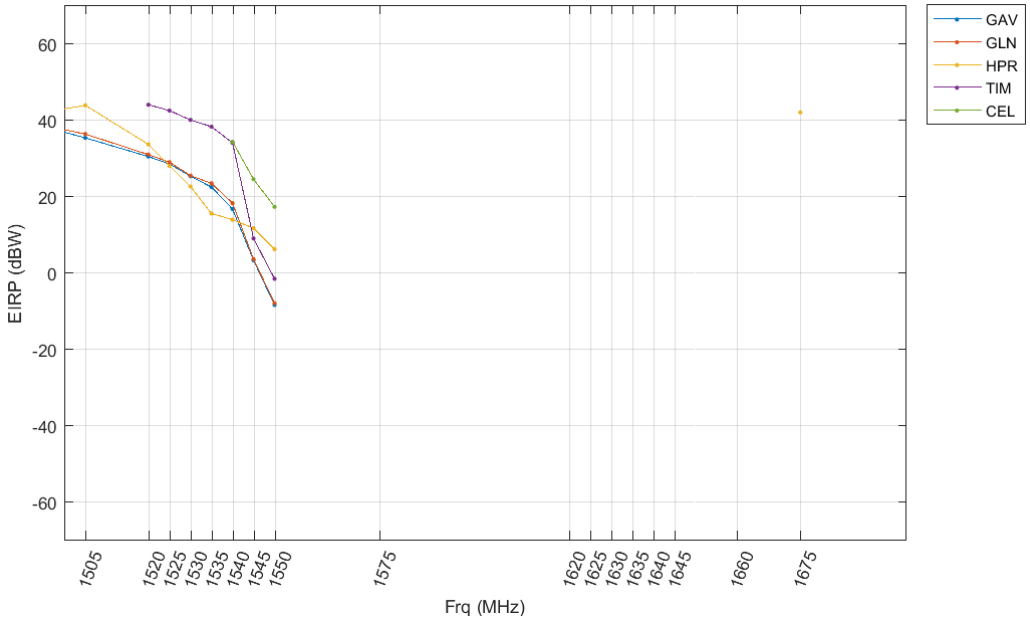

Figure J-10: GPS L1 C/A, Micro Urban, Median EIRP Mask: 2-Ray, $d_{Standoff}$ = 500 m

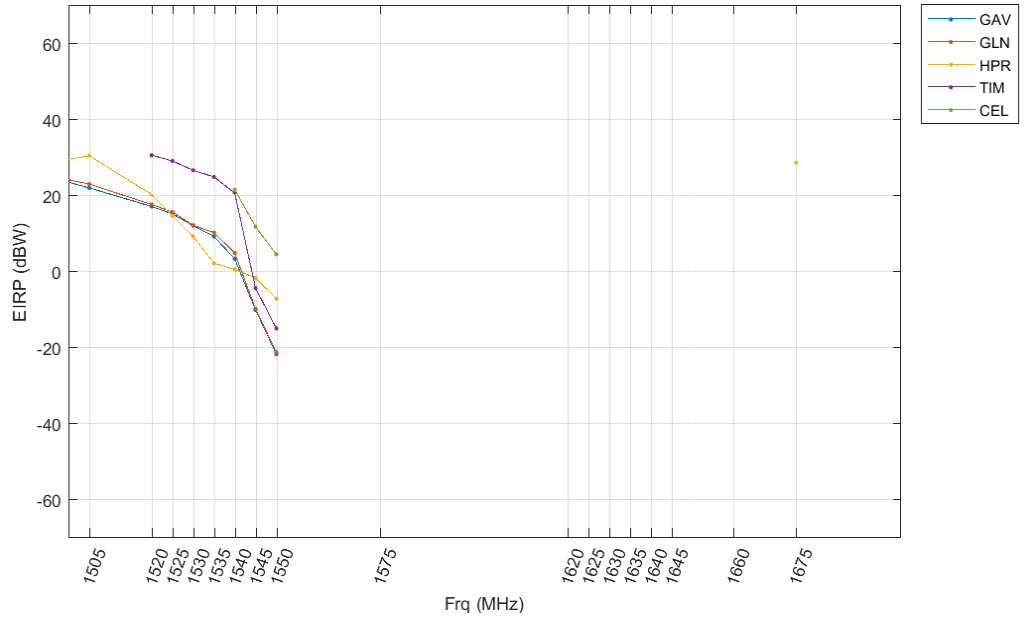

Figure J-11: GPS L1 C/A, Micro Urban, Median EIRP Mask: 2-Ray, $d_{Standoff}$ = 100 m

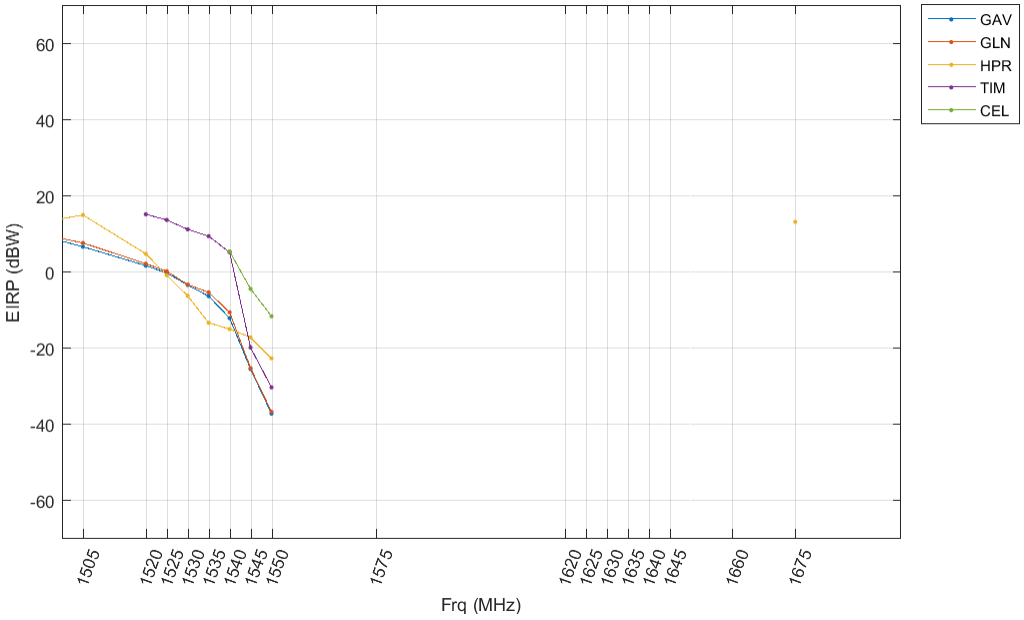

Figure J-12: GPS L1 C/A, Micro Urban, Median EIRP Mask: 2-Ray, $d_{Standoff}$ = 10 m

J.1.2 Macro Urban Deployment

J.1.2.1 Bounding ETMs

J.1.2.1.1 FSPL Propagation Model

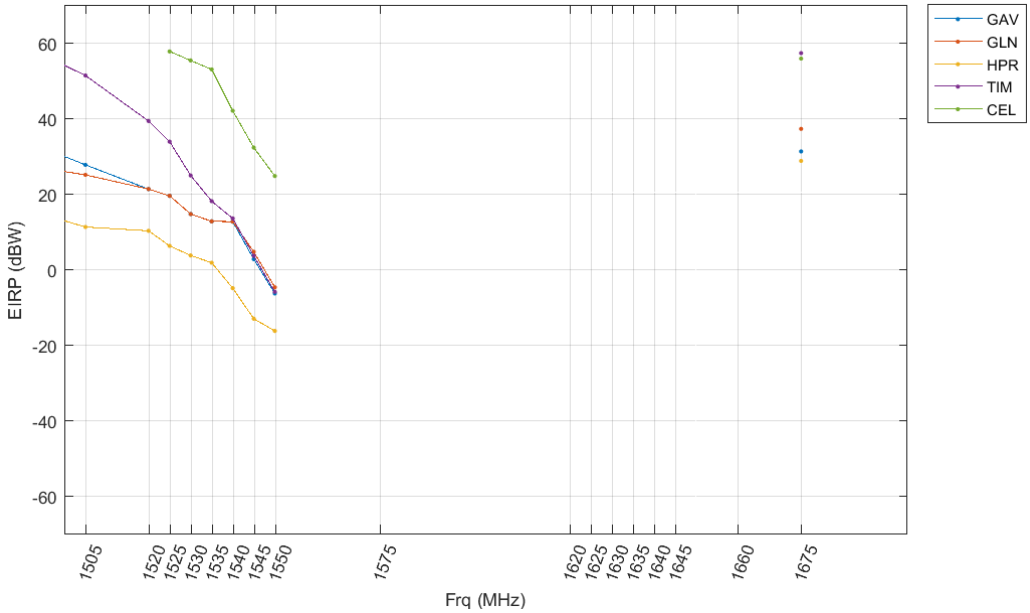

Figure J-13: GPS L1 C/A, Macro Urban, Bounding EIRP Mask: FSPL, $d_{Standoff}$ = 1000 m

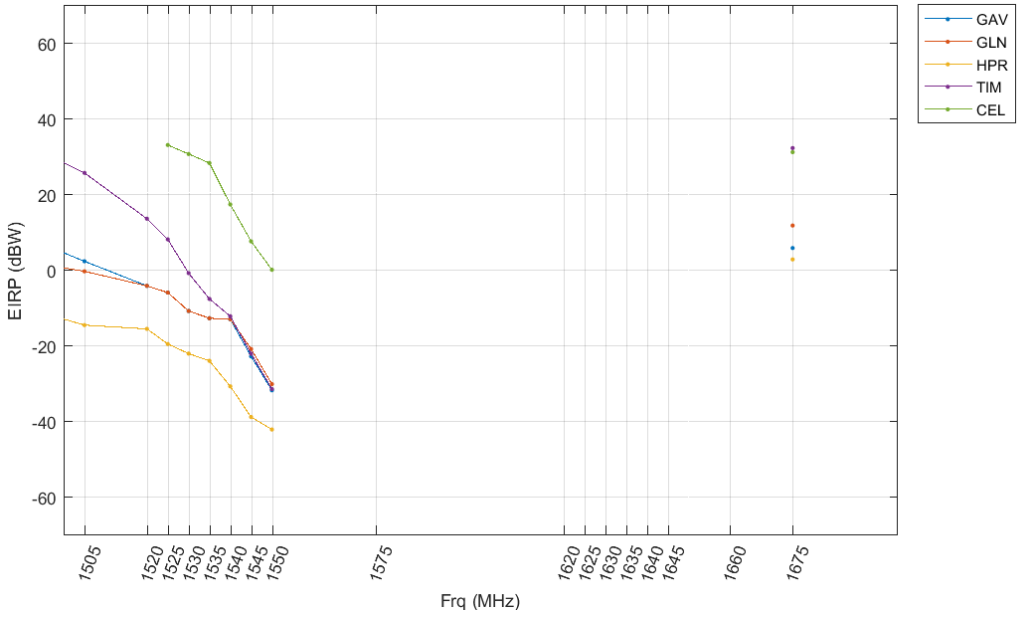

Figure J-14: GPS L1 C/A, Macro Urban, Bounding EIRP Mask: FSPL, $d_{Standoff}$ = 100 m

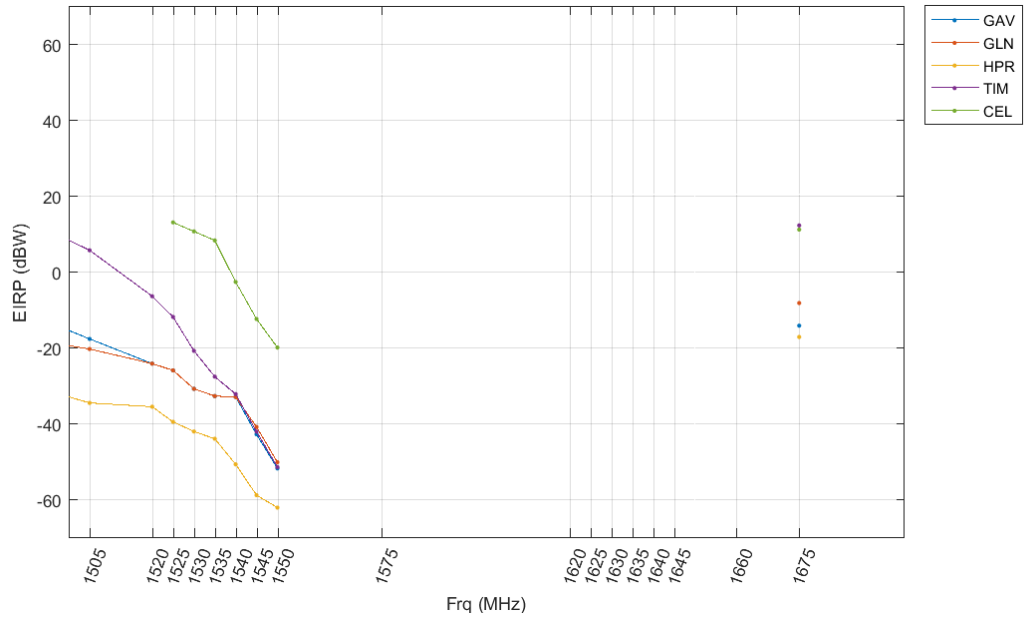

Figure J-15: GPS L1 C/A, Macro Urban, Bounding EIRP Mask: FSPL, $d_{Standoff}$ = 10 m

J.1.2.1.2 2-Ray Path loss model

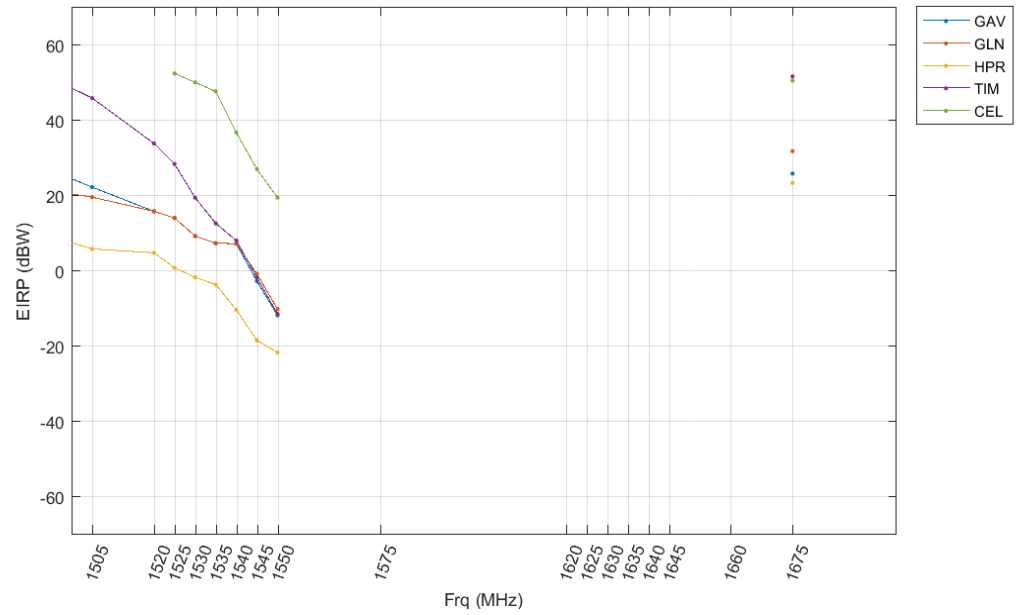

Figure J-16: GPS L1 C/A, Macro Urban, Bounding EIRP Mask: 2-Ray, $d_{Standoff}$ = 1000 m

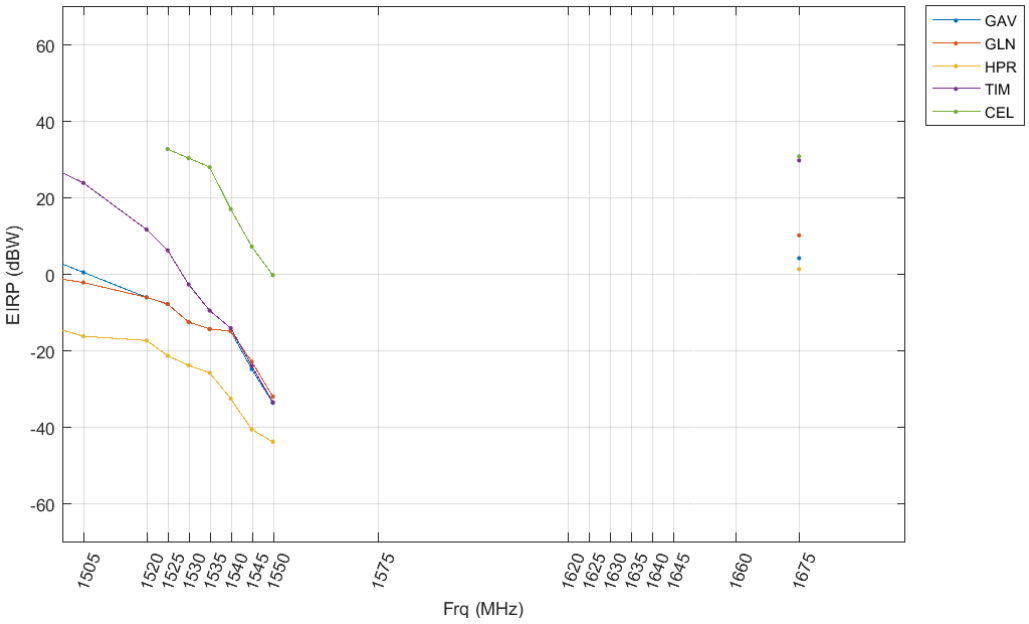

Figure J-17: GPS L1 C/A, Macro Urban, Bounding EIRP Mask: 2-Ray, $d_{Standoff}$ = 100 m

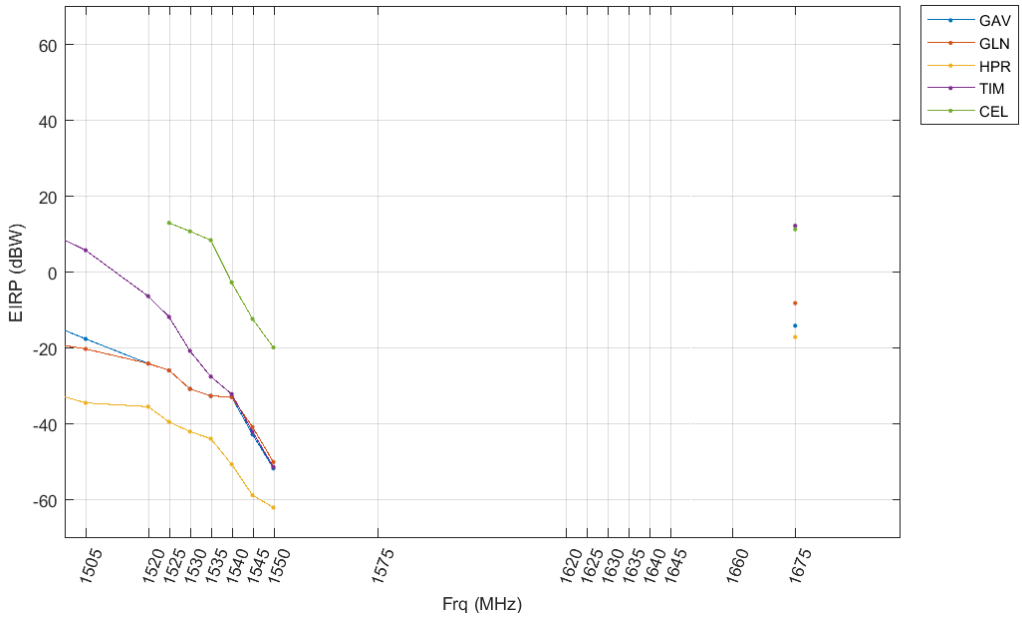

Figure J-18: GPS L1 C/A, Macro Urban, Bounding EIRP Mask: 2-Ray, $d_{Standoff}$ = 10 m

J.1.2.2 Median ETMs

J.1.2.2.1 FSPL Propagation Model

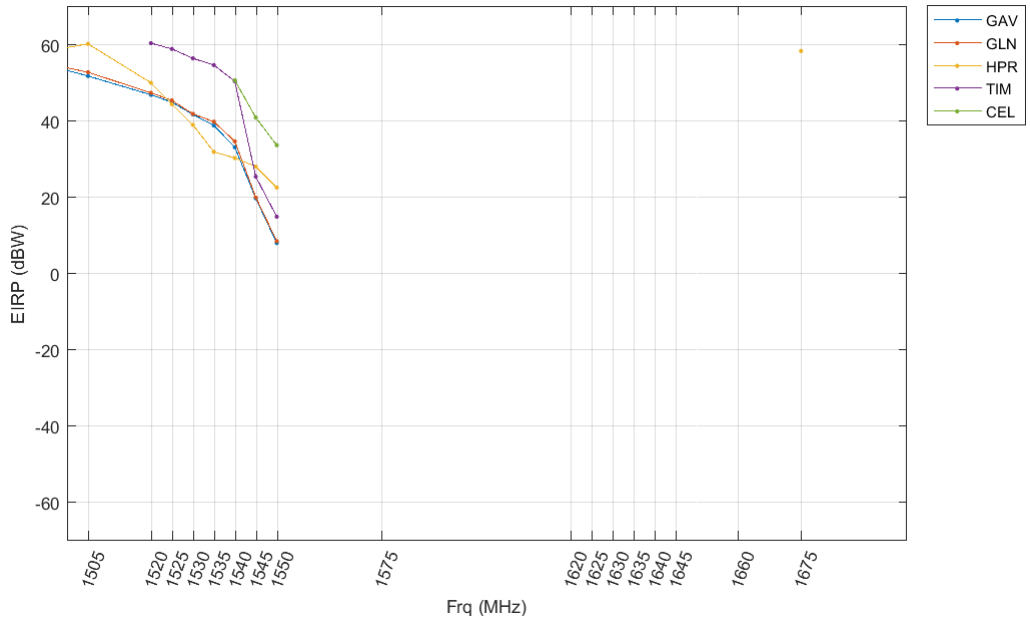

Figure J-19: GPS L1 C/A, Macro Urban, Median EIRP Mask: FSPL, $d_{Standoff}$ = 1000 m

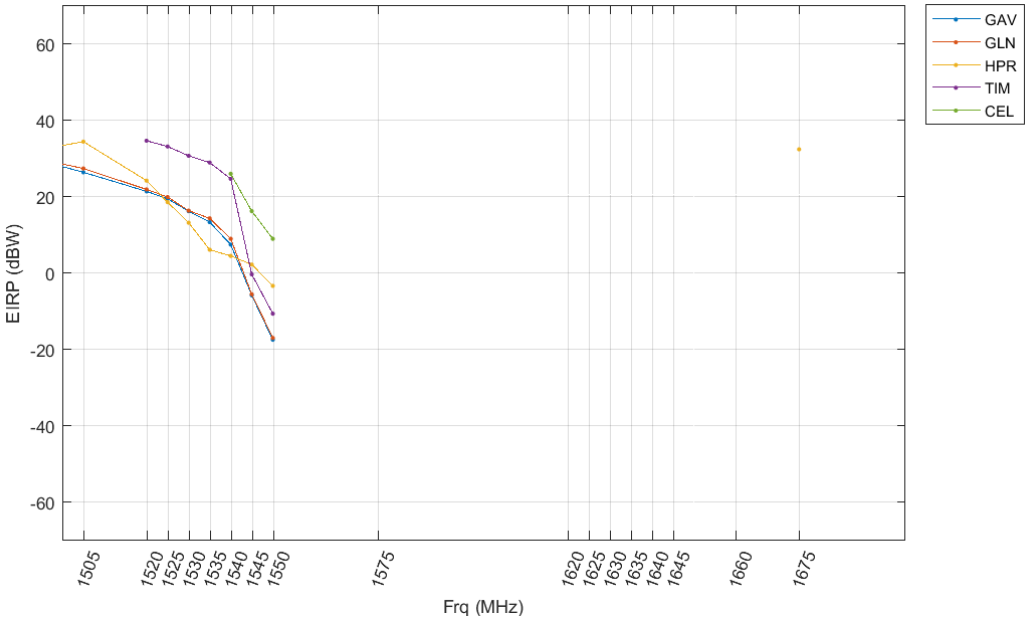

Figure J-20: GPS L1 C/A, Macro Urban, Median EIRP Mask: FSPL, $d_{Standoff}$ = 100 m

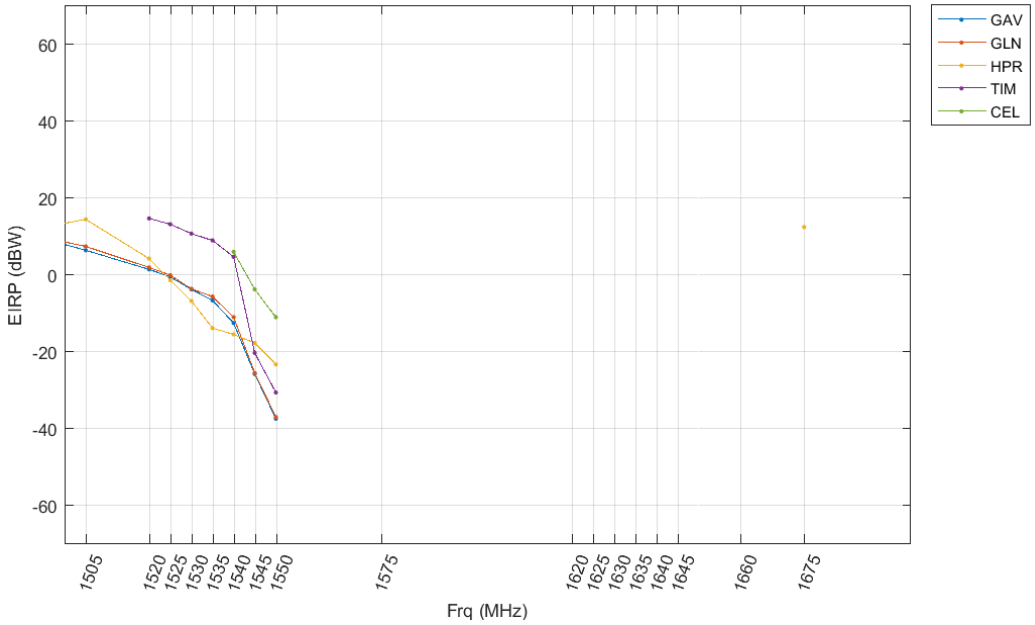

Figure J-21: GPS L1 C/A, Macro Urban, Median EIRP Mask: FSPL, $d_{Standoff}$ = 10 m

J.1.2.2.2 2-Ray Path loss model

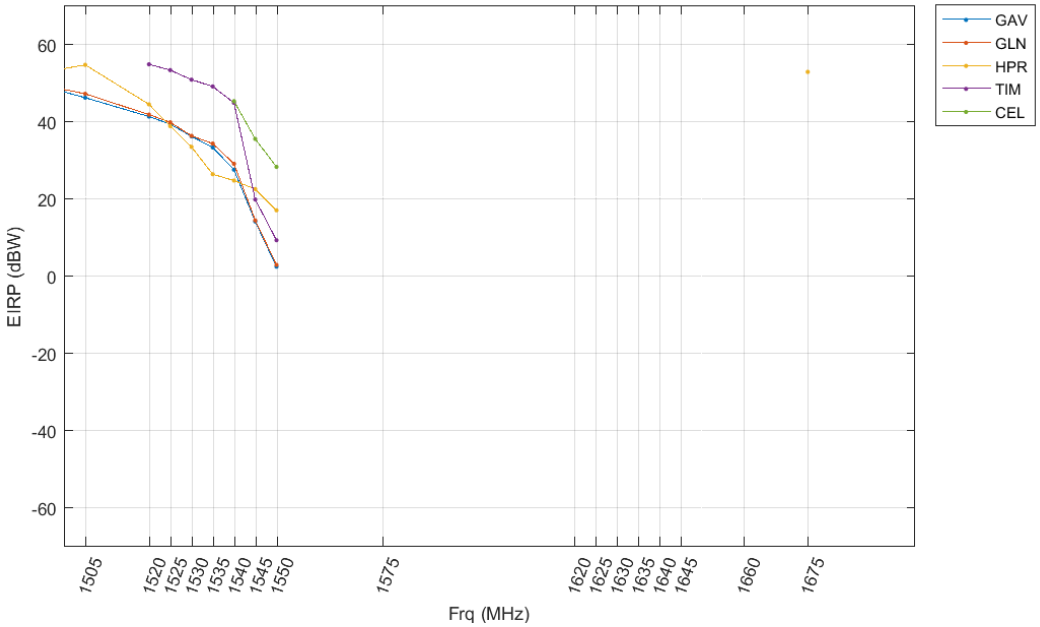

Figure J-22: GPS L1 C/A, Macro Urban, Median EIRP Mask: 2-Ray, $d_{Standoff}$ = 1000 m

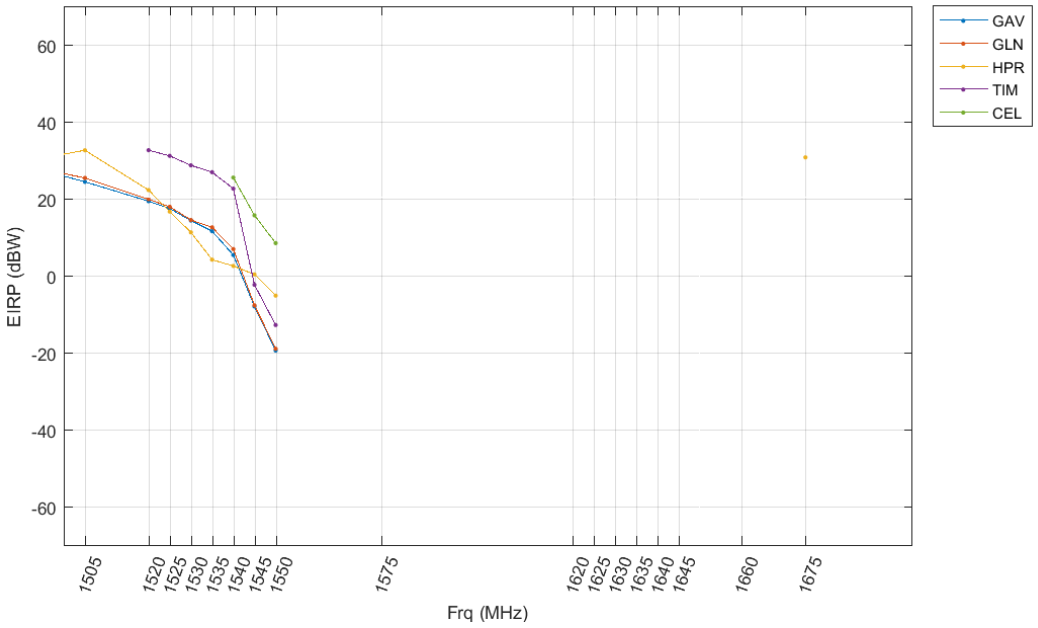

Figure J-23: GPS L1 C/A, Macro Urban, Median EIRP Mask: 2-Ray, $d_{Standoff}$ = 100 m

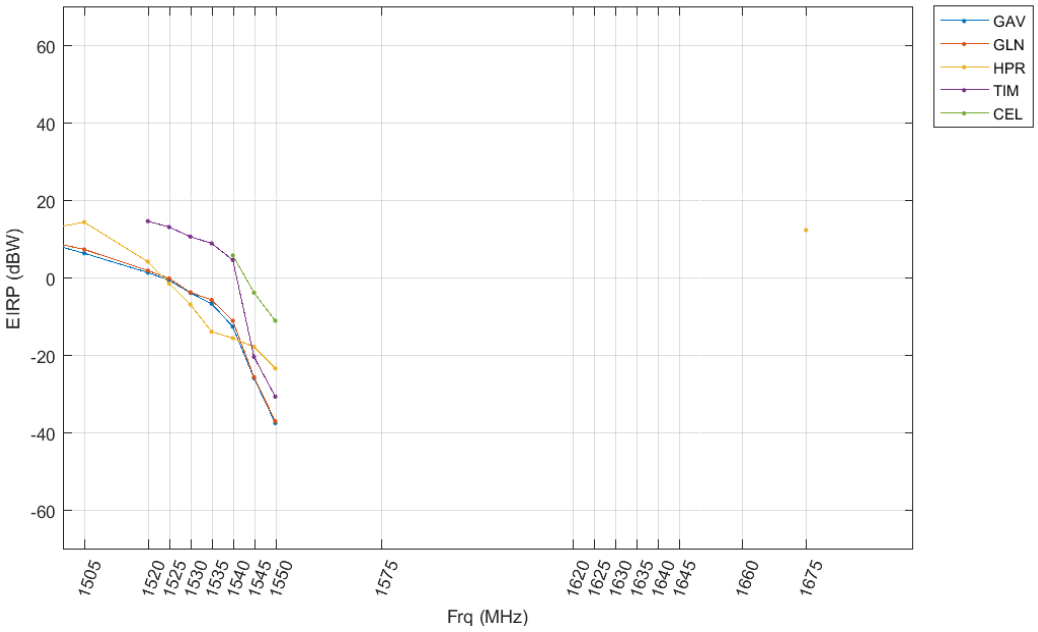

Figure J-24: GPS L1 C/A, Macro Urban, Median EIRP Mask: 2-Ray, $d_{Standoff}$ = 10 m

J.2 All GNSS services

J.2.1 Micro Urban Deployment

J.2.1.1 Bounding ETMs

J.2.1.1.1 FSPL Propagation Model

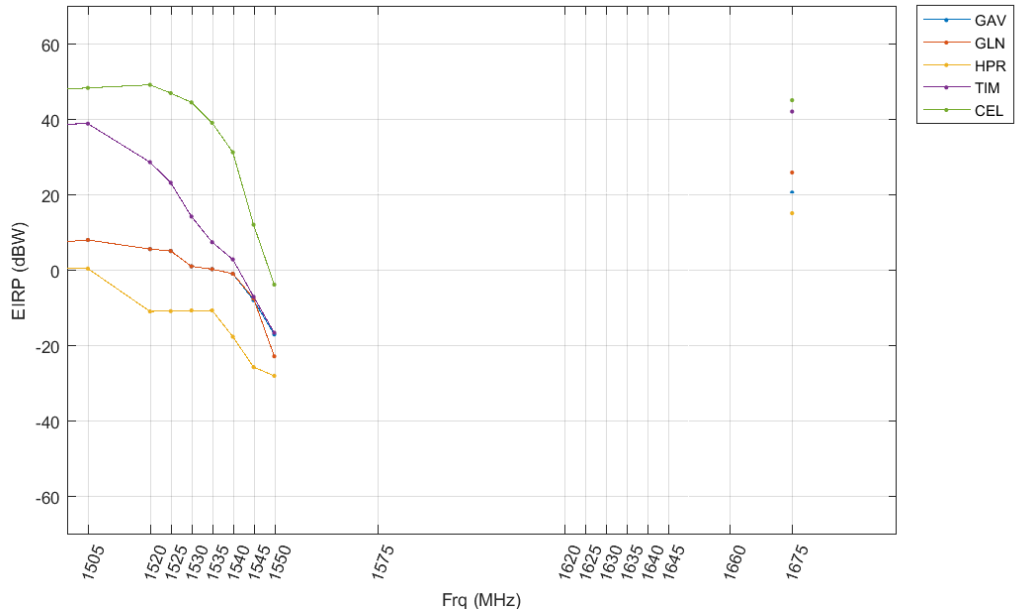

Figure J-25: All GNSS, Micro Urban, Bounding EIRP Mask: FSPL, $d_{Standoff}$ = 500 m

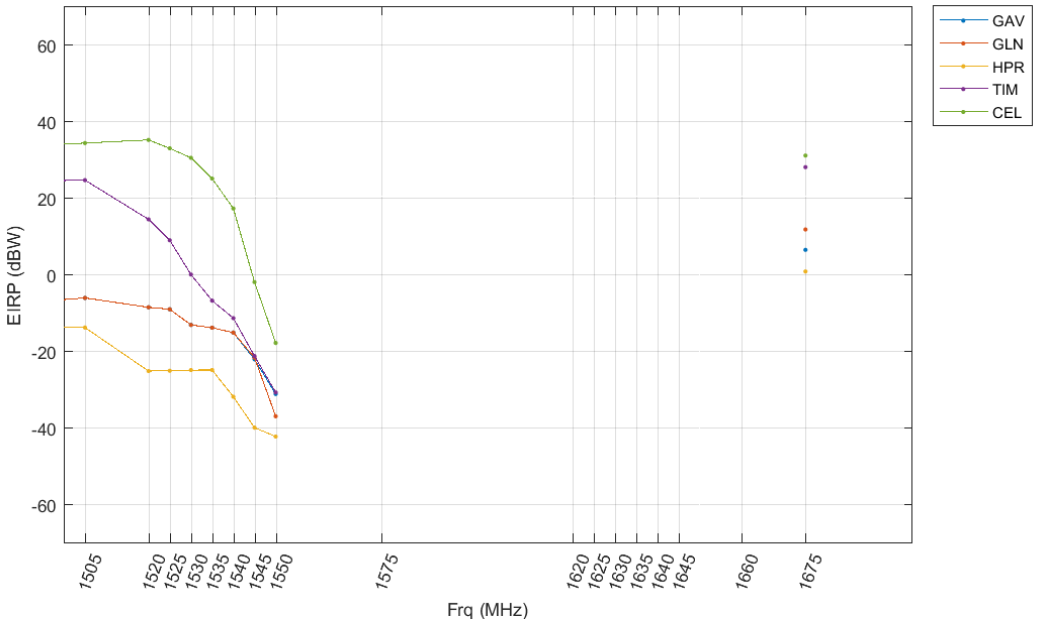

Figure J-26: All GNSS, Micro Urban, Bounding EIRP Mask: FSPL, $d_{Standoff}$ = 100 m

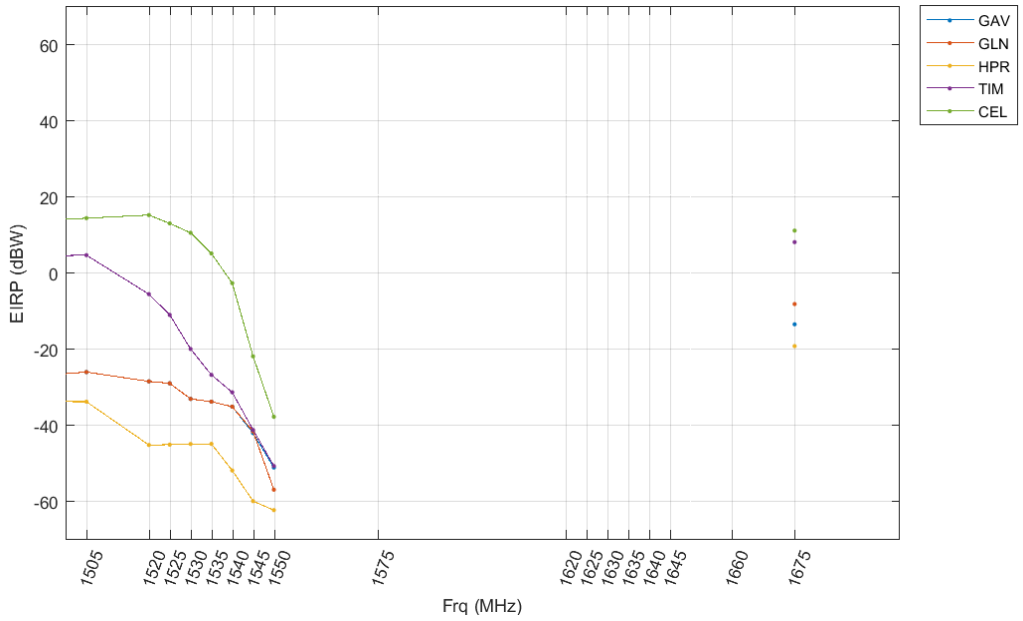

Figure J-27: All GNSS, Micro Urban, Bounding EIRP Mask: FSPL, $d_{Standoff}$ = 10 m

J.2.1.1.2 2-Ray Path loss model

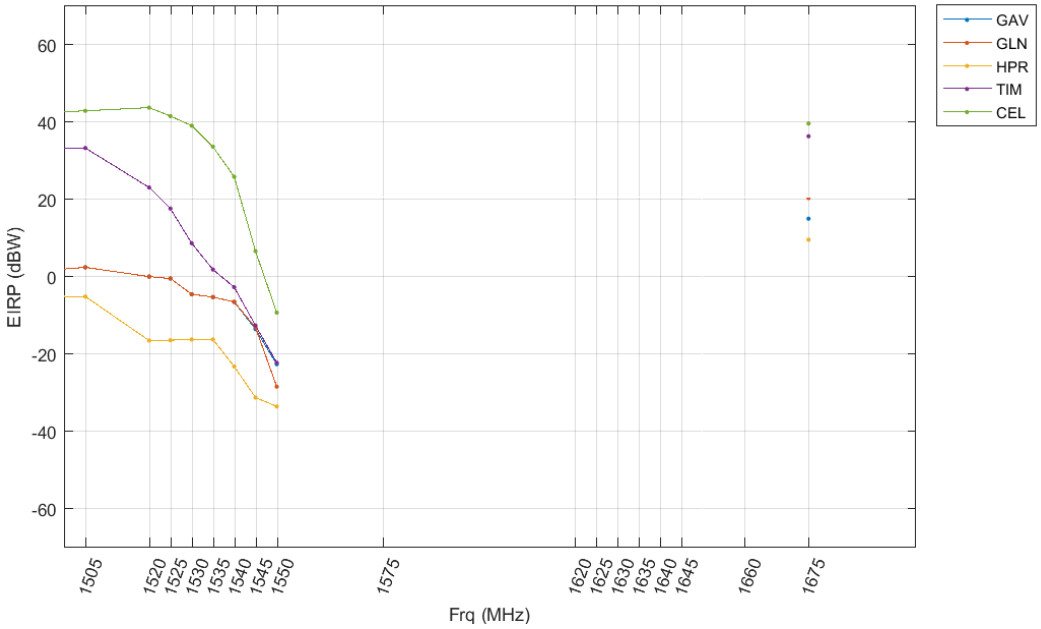

Figure J-28: All GNSS, Micro Urban, Bounding EIRP Mask: 2-Ray, $d_{Standoff}$ = 500 m

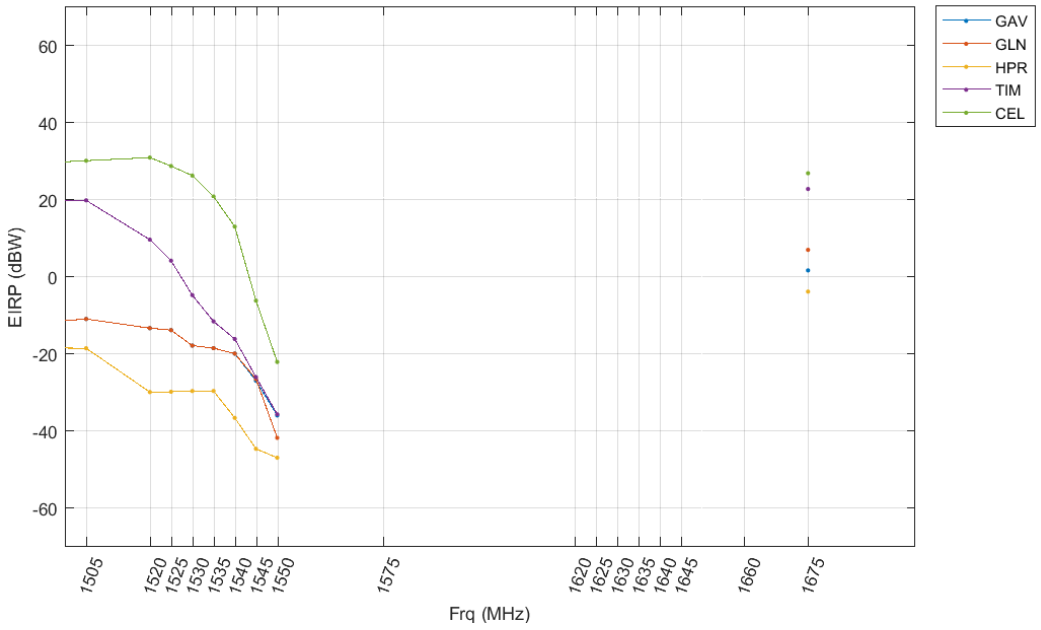

Figure J-29: All GNSS, Micro Urban, Bounding EIRP Mask: 2-Ray, $d_{Standoff}$ = 100 m

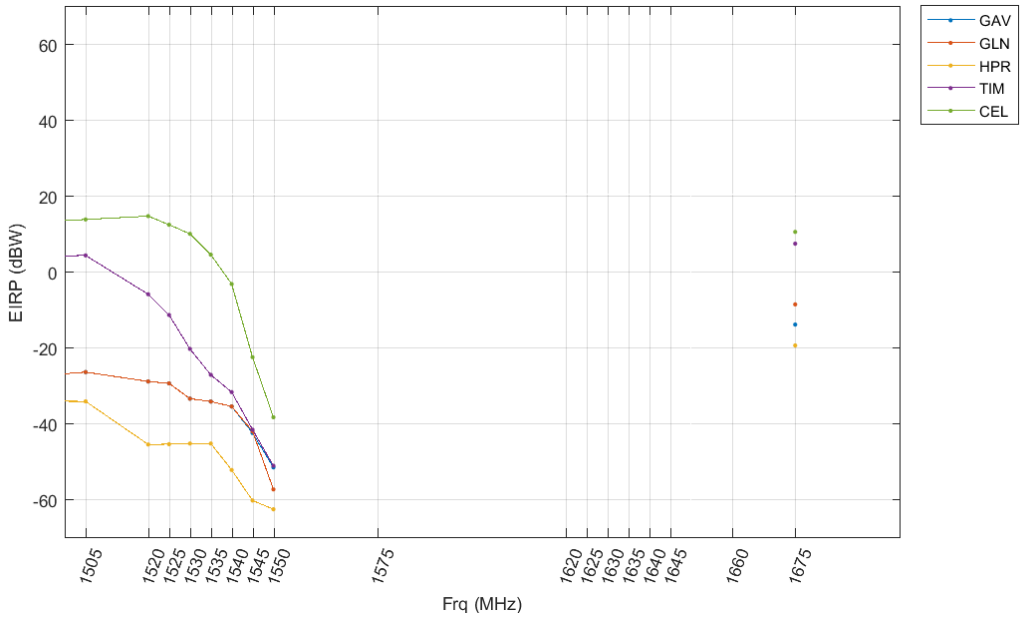

Figure J-30: All GNSS, Micro Urban, Bounding EIRP Mask: 2-Ray, $d_{Standoff}$ = 10 m

J.2.1.2 Median ETMs

J.2.1.2.1 FSPL Propagation Model

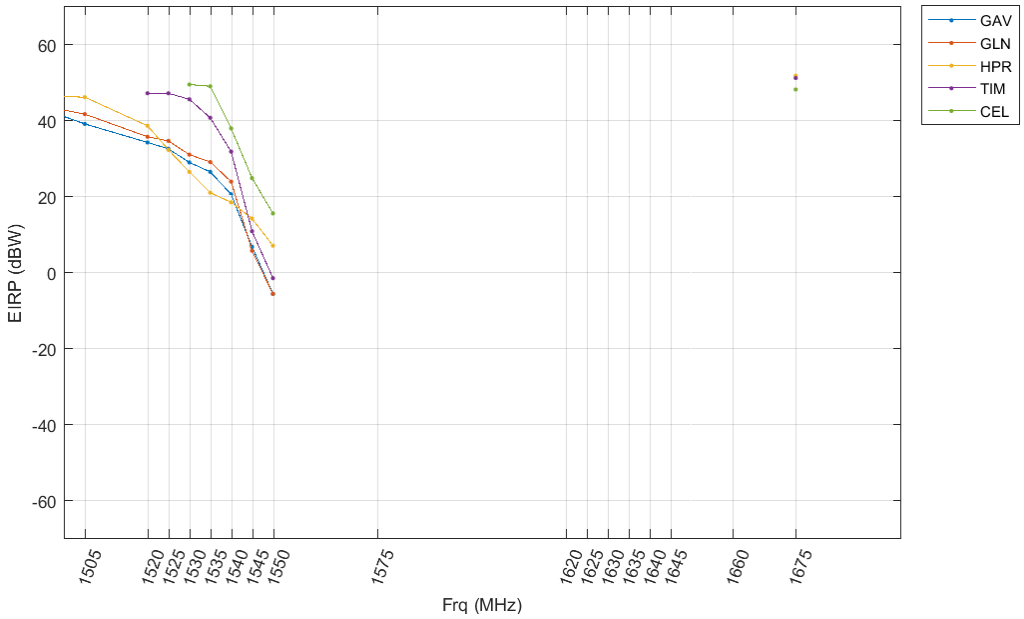

Figure J-31: All GNSS, Micro Urban, Median EIRP Mask: FSPL, $d_{Standoff}$ = 500 m

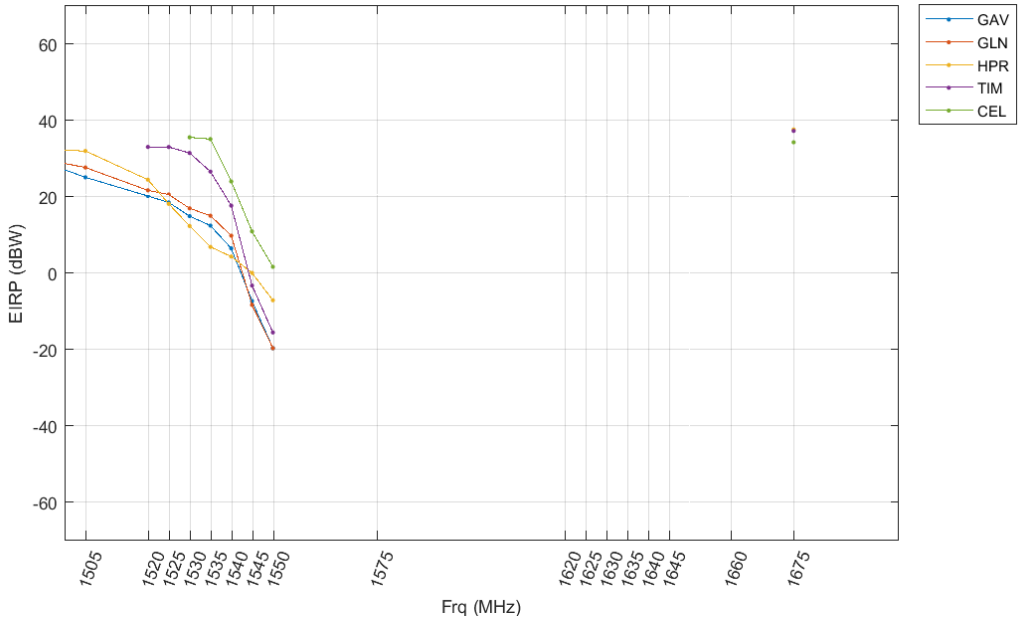

Figure J-32: All GNSS, Micro Urban, Median EIRP Mask: FSPL, $d_{Standoff}$ = 100 m

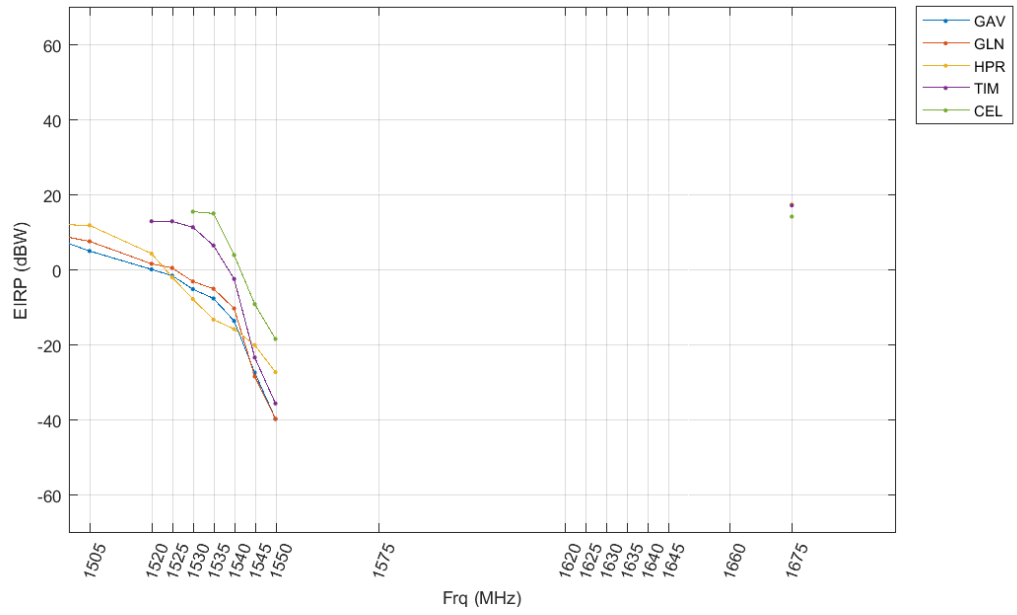

Figure J-33: All GNSS, Micro Urban, Median EIRP Mask: FSPL, $d_{Standoff}$ = 10 m

J.2.1.2.2 2-Ray Path loss model

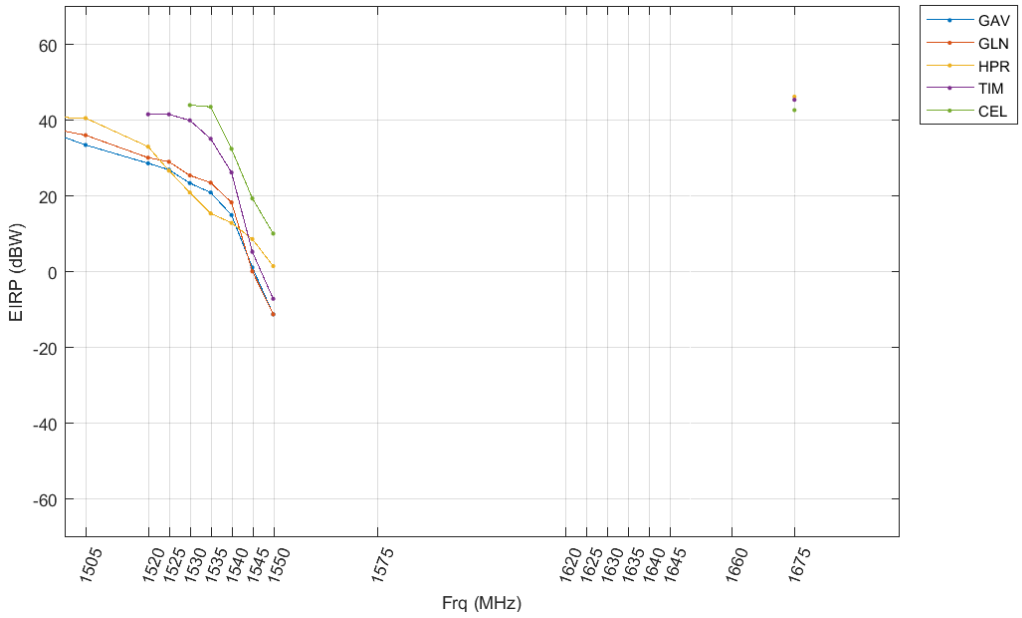

Figure J-34: All GNSS, Micro Urban, Median EIRP Mask: 2-Ray, $d_{Standoff}$ = 500 m

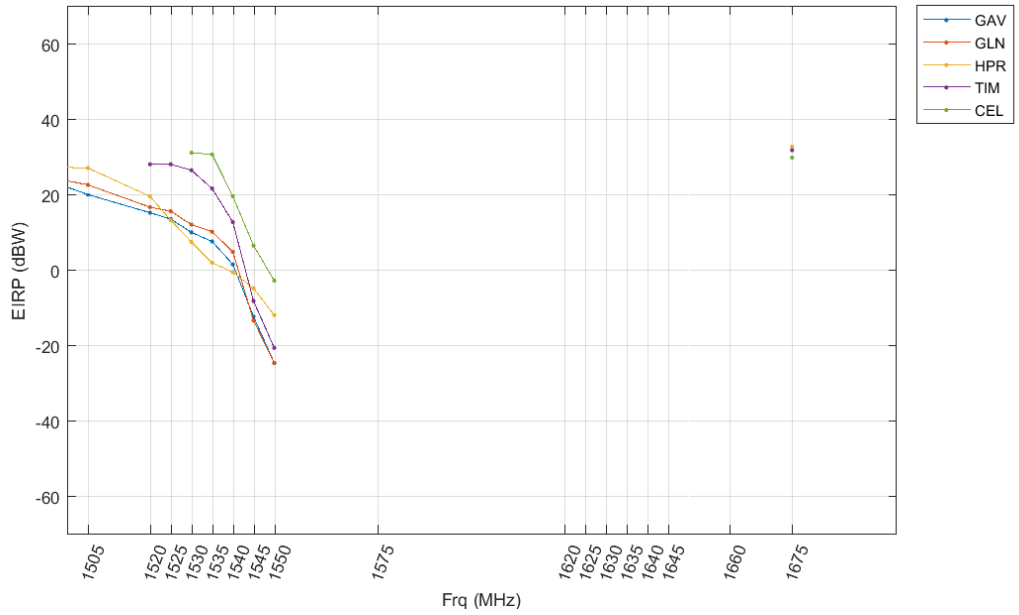

Figure J-35: All GNSS, Micro Urban, Median EIRP Mask: 2-Ray, $d_{Standoff}$ = 100 m

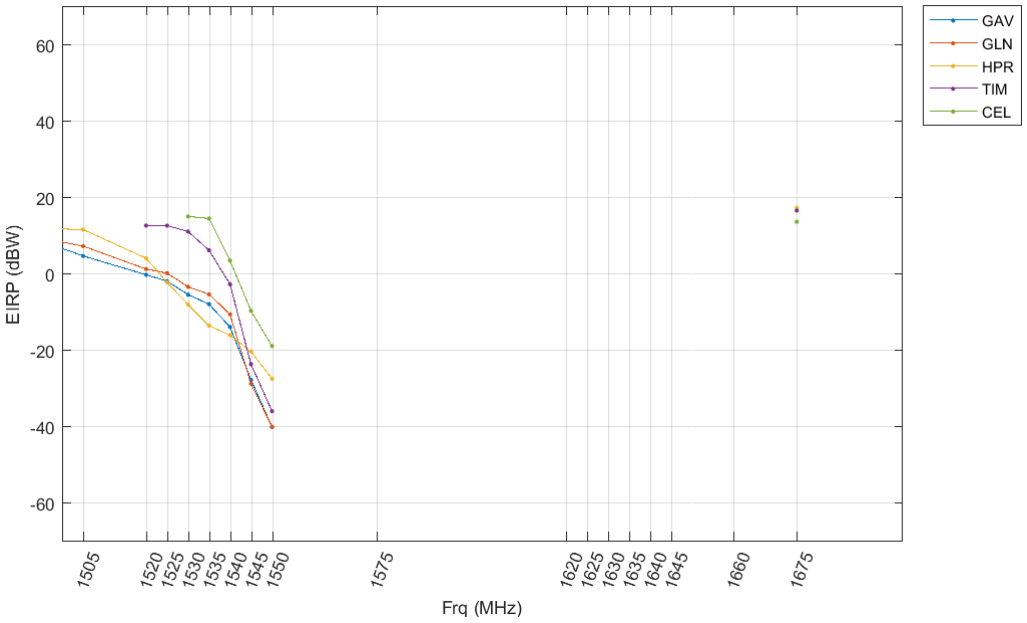

Figure J-36: All GNSS, Micro Urban, Median EIRP Mask: 2-Ray, $d_{Standoff}$ = 10 m

J.2.2 Macro Urban Deployment

J.2.2.1 Bounding ETMs

J.2.2.1.1 FSPL Propagation Model

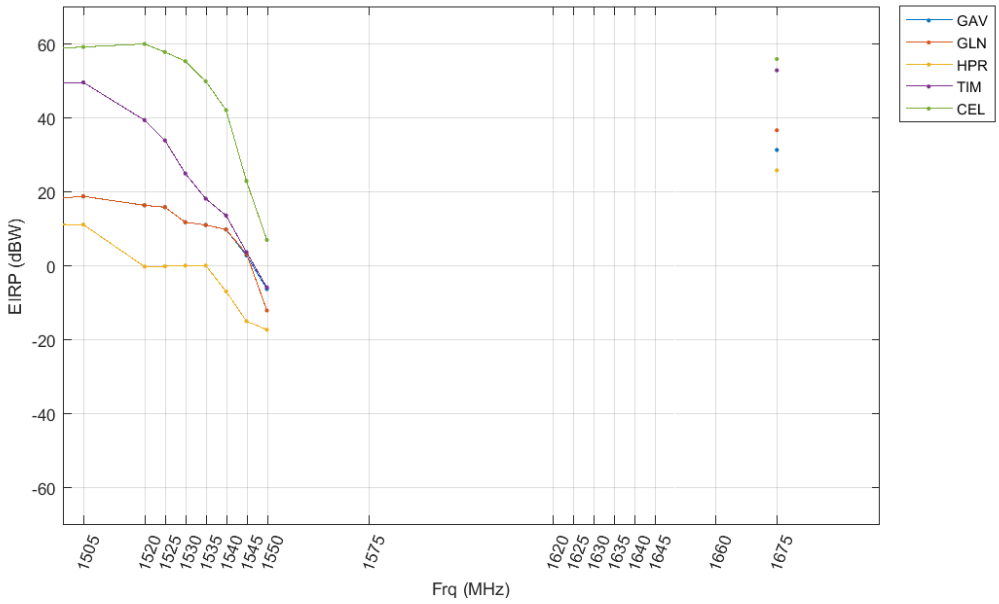

Figure J-37: All GNSS, Macro Urban, Bounding EIRP Mask: FSPL, $d_{Standoff}$ = 1000 m

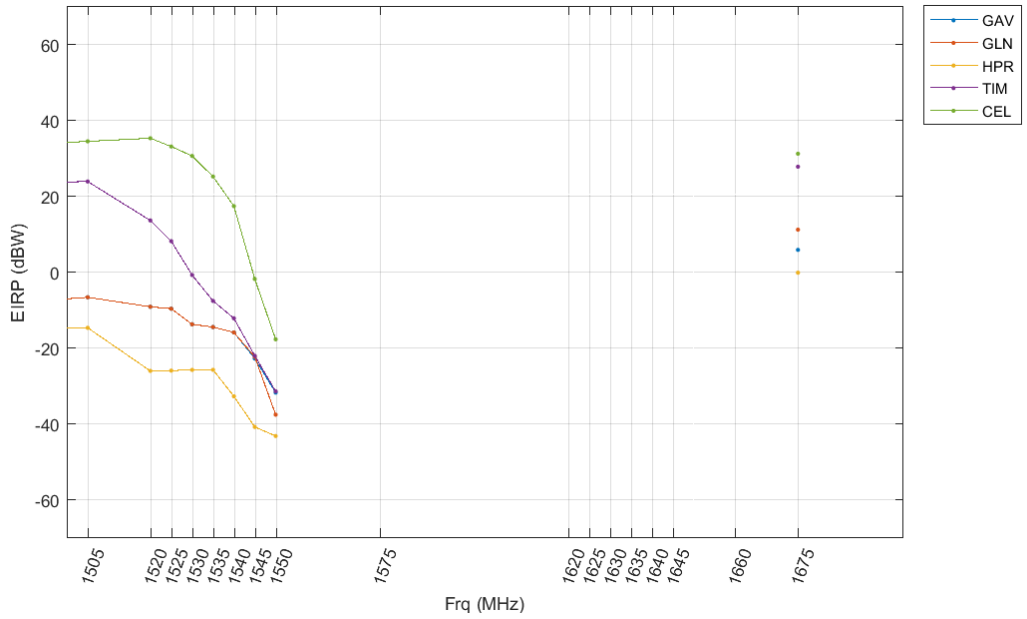

Figure J-38: All GNSS, Macro Urban, Bounding EIRP Mask: FSPL, $d_{Standoff}$ = 100 m

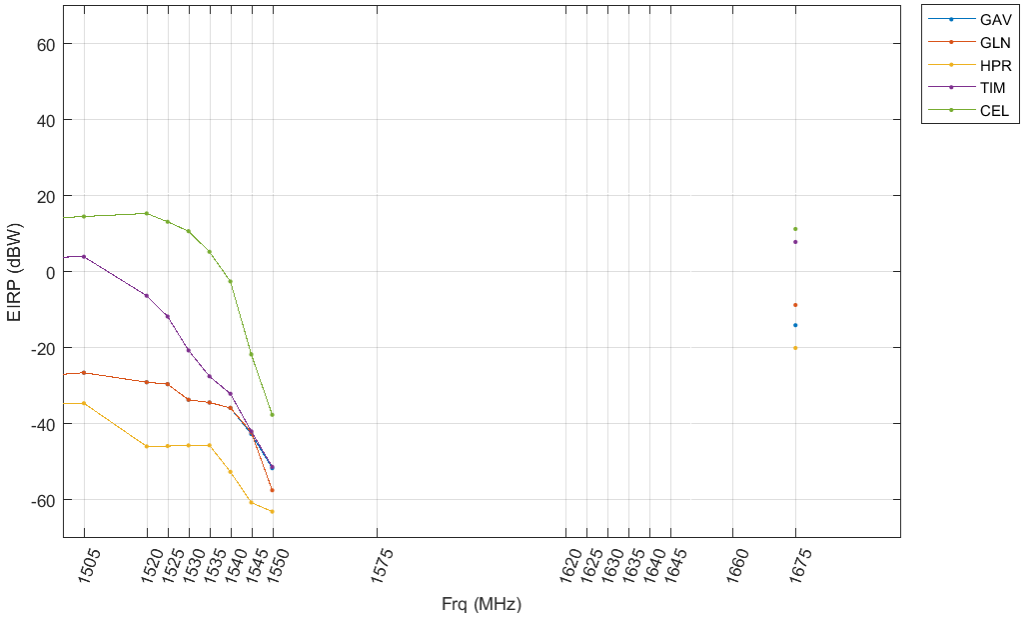

Figure J-39: All GNSS, Macro Urban, Bounding EIRP Mask: FSPL, $d_{Standoff}$ = 10 m

J.2.2.1.2 2-Ray Path loss model

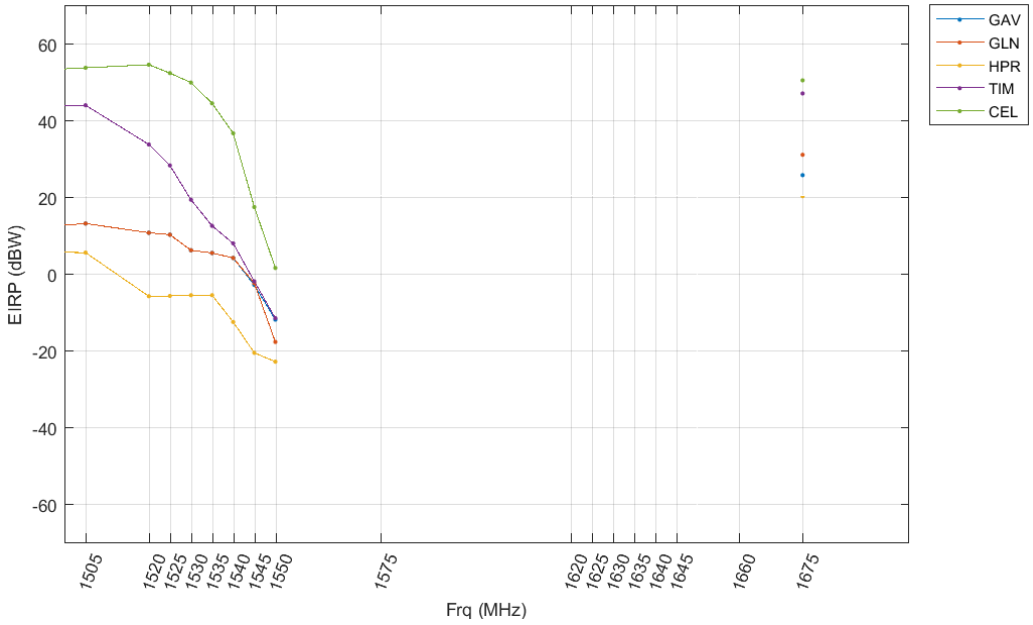

Figure J-40: All GNSS, Macro Urban, Bounding EIRP Mask: 2-Ray, $d_{Standoff}$ = 1000 m

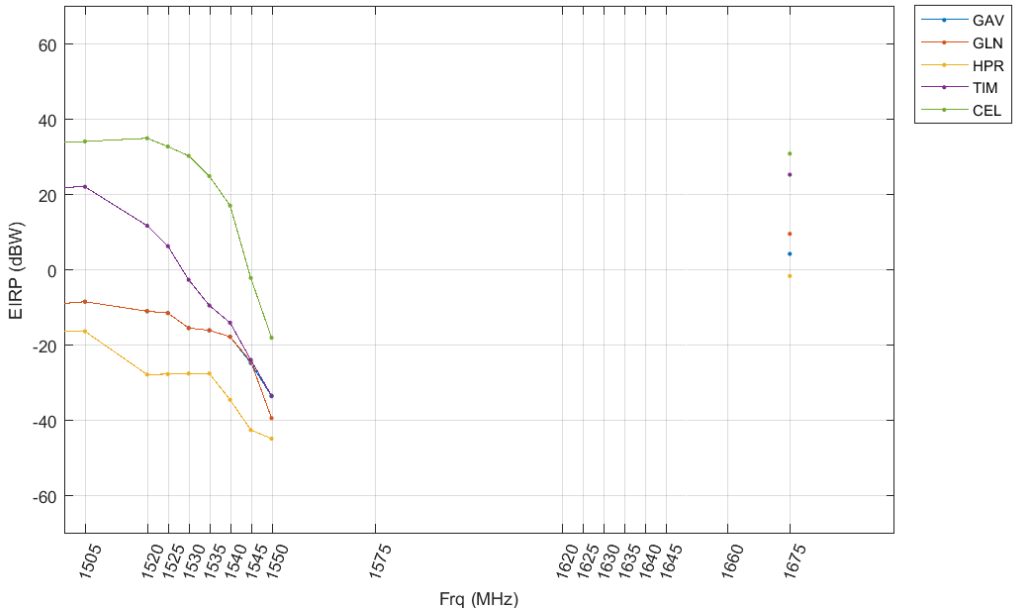

Figure J-41: All GNSS, Macro Urban, Bounding EIRP Mask: 2-Ray, $d_{Standoff}$ = 100 m

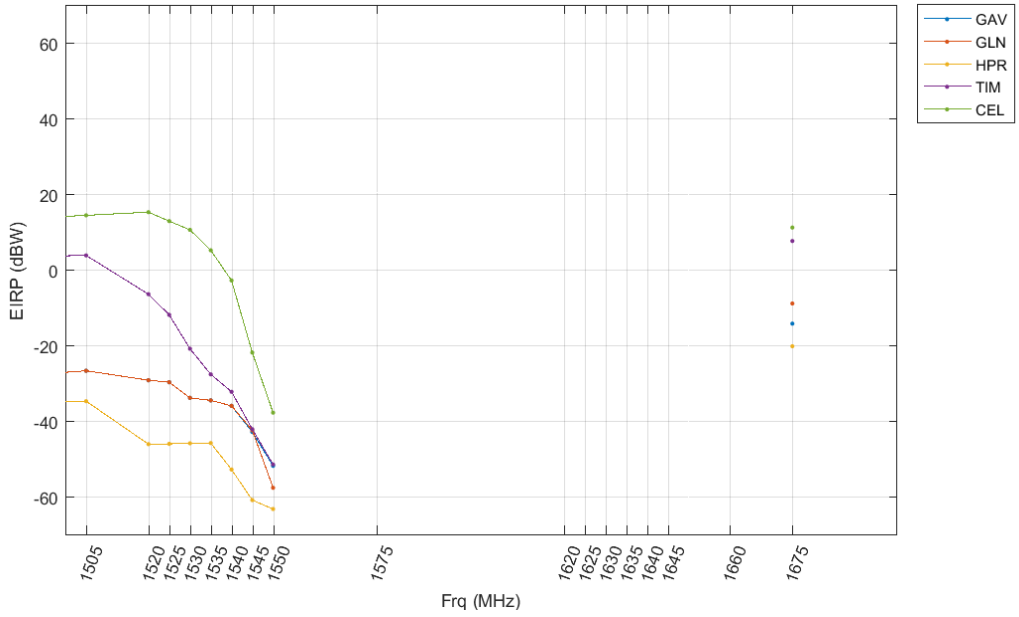

Figure J-42: All GNSS, Macro Urban, Bounding EIRP Mask: 2-Ray, $d_{Standoff}$ = 10 m

J.2.2.2 Median ETMs

J.2.2.2.1 FSPL Propagation Model

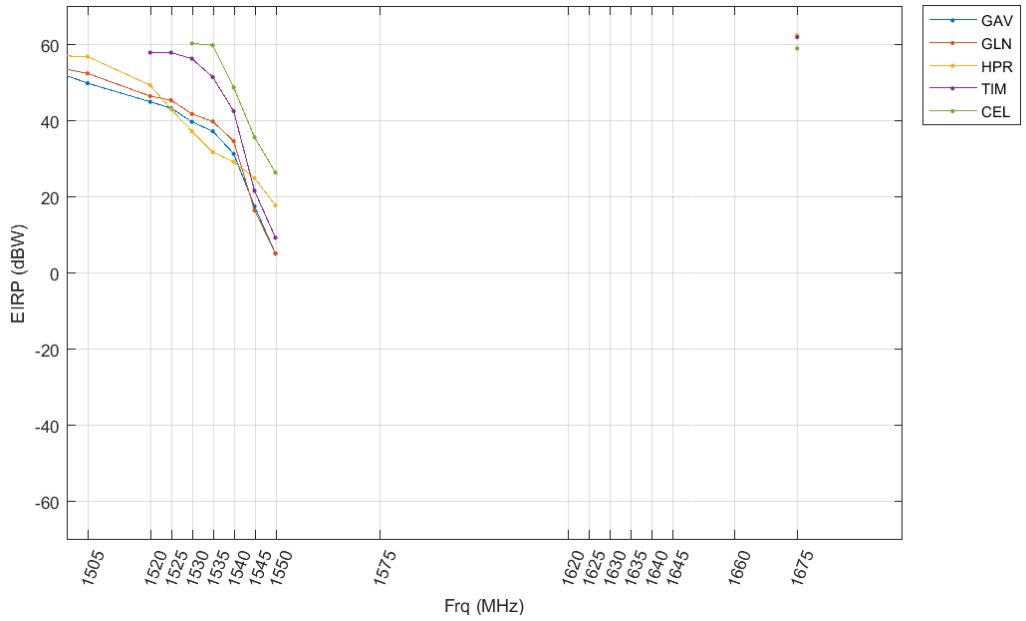

Figure J-43: All GNSS, Macro Urban, Median EIRP Mask: FSPL, $d_{Standoff}$ = 1000 m

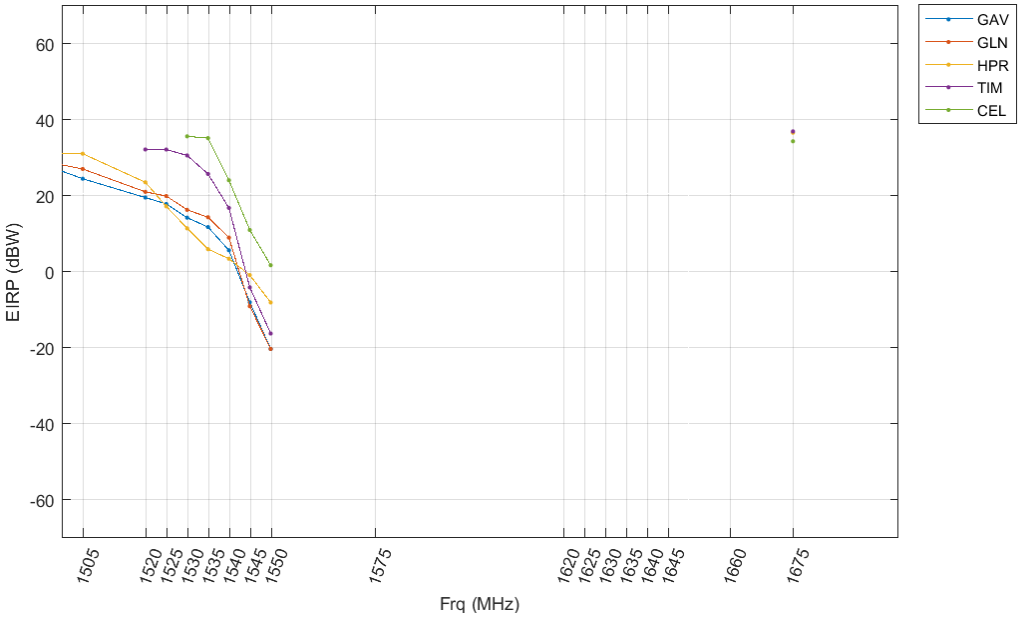

Figure J-44: All GNSS, Macro Urban, Median EIRP Mask: FSPL, $d_{Standoff}$ = 100 m

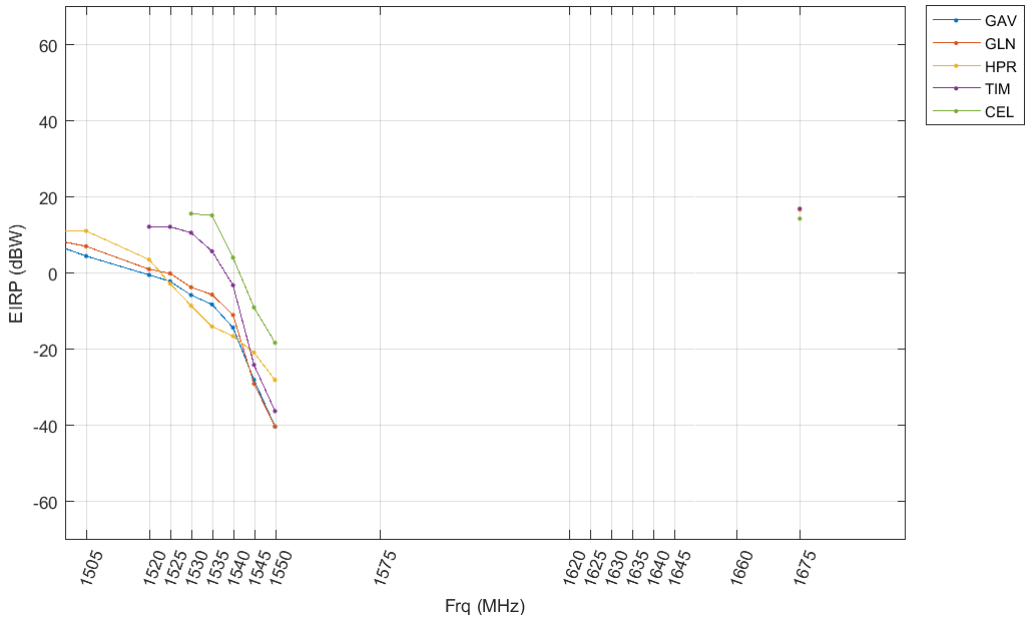

Figure J-45: All GNSS, Macro Urban, Median EIRP Mask: FSPL, $d_{Standoff}$ = 10 m

J.2.2.2.2 2-Ray Path loss model

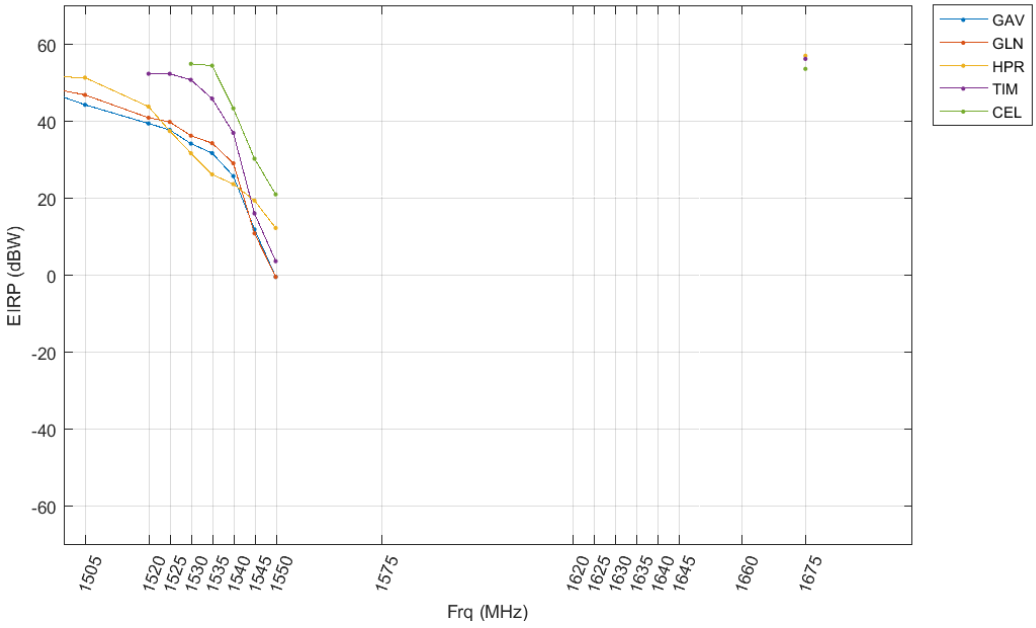

Figure J-46: All GNSS, Macro Urban, Median EIRP Mask: 2-Ray, $d_{Standoff}$ = 1000 m

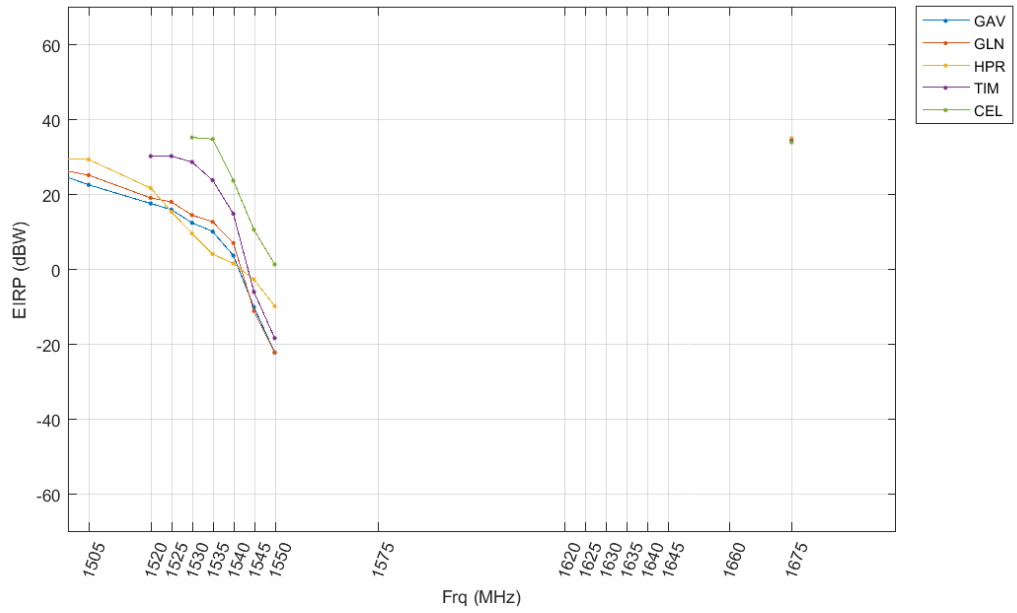

Figure J-47: All GNSS, Macro Urban, Median EIRP Mask: 2-Ray, $d_{Standoff}$ = 100 m

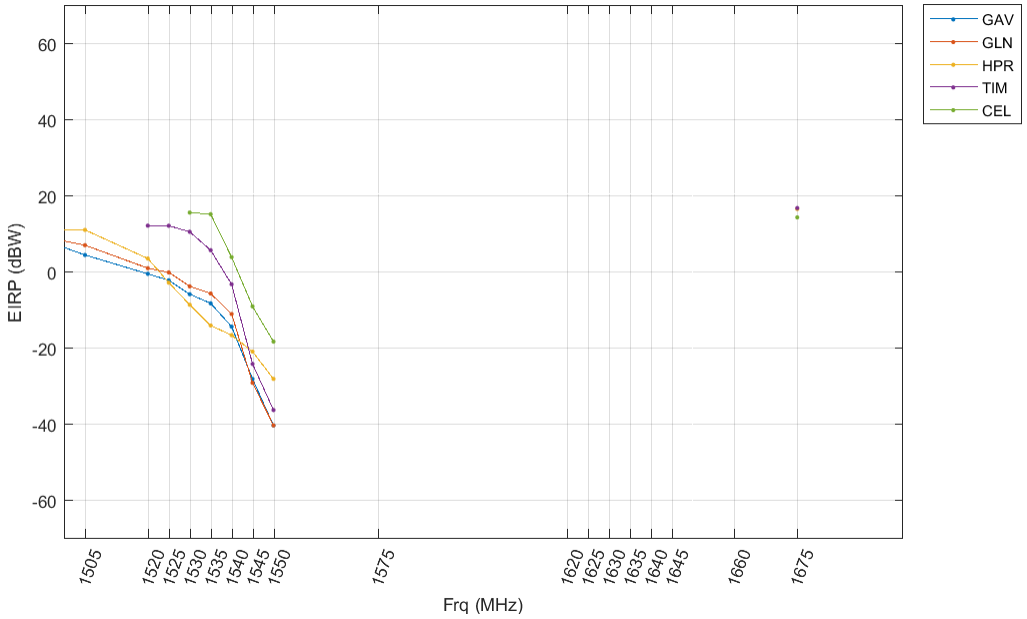

Figure J-48: All GNSS, Macro Urban, Median EIRP Mask: 2-Ray, $d_{Standoff}$ = 10 m

APPENDIX K

SPACEBORNE AND SCIENCE GNSS APPLICATIONS

SPACEBORNE AND SCIENCE-APPLICATIONS

Overview

This section of the report describes the analysis and evaluation of a proposed LTE base station network's interference to space-based receivers. A comprehensive assessment on GNSS receivers, used in various applications, supporting NASA's portfolio of missions is also addressed. However, the emphasis of this section is on the assessment to GNSS receivers used for science applications.

The following evaluation assesses the impact to space-based GNSS receivers performing radio occultation ("RO") measurements (a scientific application of GNSS) of the ionosphere, stratosphere, and the troposphere. RO measurements, coupled with traditional methodologies for weather prediction, provide weather and science data observations from ocean areas, the atmosphere, and other natural phenomena, which have improved accuracy and predictability of weather forecasts by as much as two days.

Specifically, NASA's assessment focuses on the most recent developed RO receiver, called the TriG, developed by the NASA/Jet Propulsion Laboratory (JPL). The TriG is the newest RO receiver of the BlackJack class of GNSS receivers. The increase in performance by these receivers is partially due to the TriG's ability to receive all GNSS signals: GPS, Galileo, GLONASS, Compass, as well as other future navigation signals (QZSS, DORIS, etc.).

Radio Frequency Interference (RFI) is an utmost problem when GNSS signals are being used for science applications. When RFI occurs at low ray heights, the GNSS signal is defocused by tens of dB, and the signal-to-noise ratio (SNR) is already being measured in a marginal zone. In fact, in this already marginal zone, tracking loops cannot be closed and the captured data is running open loop. The spatially correlated noise can bias the captured data and affect the climate record, in addition to reducing weather forecast accuracy over the USA where the LTE base stations would be deployed.

This assessment demonstrates the effect of RFI generated by the ground-based LTE network. Several iterations of the modeling and simulation (M&S) runs were performed to more accurately model the presumed network deployment of the interfering network. The M&S scenarios estimate the receive interference levels to the TriG, utilizing specific mission parameters, and comparing them against interference limits/thresholds obtained through anechoic chamber testing described under Section 3.

Background

Radio Occultation (GNSS-RO)

GNSS-RO is the measurement of GNSS signals as they are refracted by the atmosphere. RO is a relatively new method for the indirect measurement of temperature, pressure and water vapor in the stratosphere and the troposphere, and of charged particles in the ionosphere. These measurements are made from specifically designed GNSS receivers on-board a Low-Earth-Orbit

(LEO) satellite. The techniques utilize the unique radio signals continuously transmitted by the GNSS satellites (GPS, GLONASS, Galileo, etc.) orbiting the Earth at an approximate altitude of 20,000 km above the surface. The GNSS radio signals are influenced both by the electron density in the ionosphere and by the variations of temperature, pressure and water vapor in the atmosphere which are used in meteorology and climate science. RO measurements are also used to derive various ionospheric parameters (Total Electron Content (TEC), Electron Density Profiles (EDP), L-band scintillation, etc.) for understanding earth and space weather dynamics.

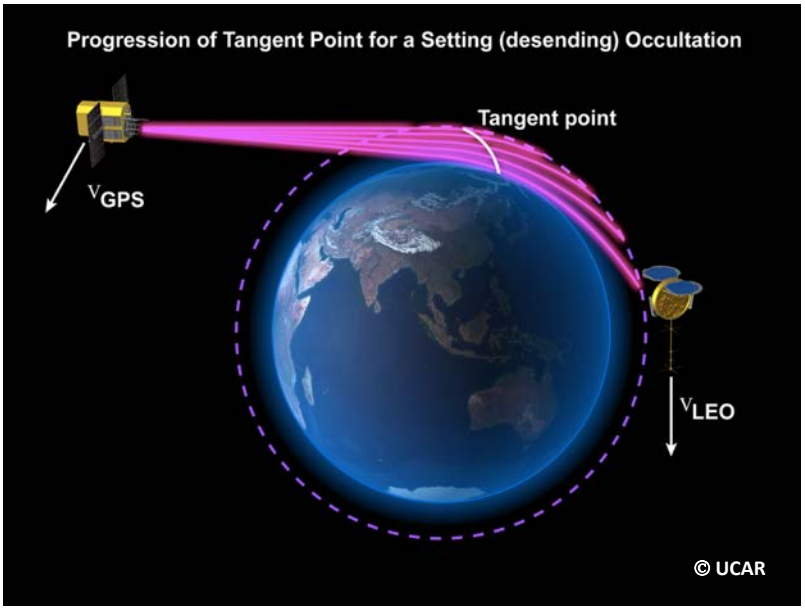

Figure K-1: Progression of Tangent Point for a Setting (Descending) Occultation

From the point of view of a LEO satellite (at an altitude of 700-800 km), the GNSS satellites continually rise above, or set behind, the horizon of the Earth. During these so-called "radio occultations", where the GNSS and the LEO satellite are just able to "see" each other through the atmosphere, the GNSS signals will be slightly delayed and their ray path slightly bent (refracted) on the way through the layers of the atmosphere (see **Figure K-1**). The excess range increases as the ray propagates through denser mediums and water vapor at lower altitudes. This delay is a function of density (n/V), which is related to temperature by the ideal gas law (Equation K-1),

$$P*V = n*R*T$$

Equation K-1: Equation Used to Translate Refractivity to Atmospheric Temperature

A typical occultation sounding will last one (1) to two (2) minutes, and during this time the LEO satellite will receive signals where the ray paths have different minimum distances to the surface of the Earth, from zero up to approximately 100 km. The GNSS satellites transmit on multiple frequencies, and with a receiver rate of 50 Hz this will yield around 6000 rays, making up a profile of excess phases (actual path minus straight-line path) through the lowest 100 km of the atmosphere.

The residual positioning error and determination of time delays (see **Figure K-2**), derived from the measurements taken during a RO event, are key parameters in the obtaining the temperature, pressure, and water vapor characteristics of the atmosphere at different heights. Given sub-mm measurement precision, RO can determine atmospheric temperature profiles to 0.1 – 0.5 Kelvin (K) accuracy from 8 - 25 km height levels. These are unprecedented levels of accuracy for global measurements.

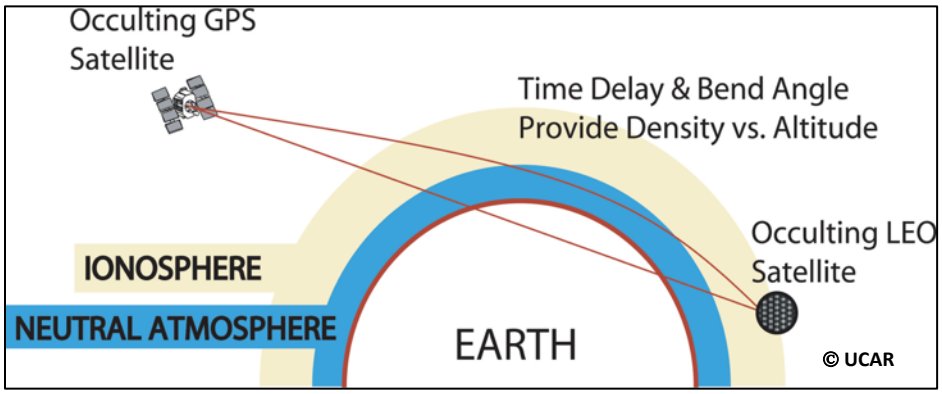

Figure K-2: Straight Line versus Actual Path of GNSS Signal

NASA has several radio occultation receivers in its portfolio, including the Integrated GPS Occultation Receiver (IGOR), the IGOR+, and a more recently developed receiver called the TriG receiver.

NASA/JPL TriG Receiver Overview

The NASA/JPL developed TriG receiver functions as a multi-function GNSS receiver. This single receiver has multiple antenna inputs and can be configured to operate in a navigation capacity, as well as, simultaneously, in a scientific measurement role.

In its traditional function, coupled with choke ring antenna (see Figure K-3), the TriG serves as a device for space vehicle navigation and precise orbit determination (POD). The receiver provides accurate information to space vehicle operators on position, velocity, and time.

Figure K-3: Typical Choke Ring Antenna

Configured in a scientific measurement mode, the TriG, coupled with a series of specially designed antenna arrays, performs RO measurements of GNSS signals. TriG receiver hardware is able to receive all GNSS signals: GPS, Galileo, GLONASS, Compass, as well as other navigation signals (QZSS, DORIS, etc.). This capability increases the number of RO measurements that can be made during any given orbit.

Additional information on TriG can be found in a document titled, "TriG - A GNSS Precise Orbit and Radio Occultation Space Receiver", written by the Jet Propulsion Laboratory and California Institute of Technology[1].

TriG Pre-Select Filter

Much akin to high-precision (HP) GPS receivers, the TriG has been designed with a wide front-end receiver filter. This wider pre-select filter can be derived from the ITMs developed by the DOT (see Section 3). Although the DOT developed ITMs for each of the six (6) categories of GPS receivers using bounding results, NASA specifically tested two (2) spaced-based receivers during the anechoic chamber tests.

The pre-select filter contains two 150 MHz-wide pass bands. The first covers the L5 and L1 bands. The second pass band covers only 1 but was designed with the same bandwidth to equalize filter delay changes with temperature. This is important for the ionospheric measurements, a prime product of the COSMIC-2BB mission. The TriG also has 2nd stage narrow band filters that are centered around the GPS L1 and L2 bands.

Receivers are purposely designed to have a wider bandwidth for both HP and the TriG receivers. The wider bandwidth front-end filter takes advantage of:

- The ability to track all current and future GNSS L-band signals:
  - GPS
  - Galileo (Europe)
  - GLONASS (Russia)
  - Compass/BeiDou (China)
  - QZSS (Japan)
  - NaVIC (formerly, IRNSS) (India)
  - DORIS (France)
  - GPS augmentation systems operating on mobile satellite service (MSS) frequency allocations, and
  - Other future GNSS constellations.

- Avoiding the disadvantages that narrow filters with sharp cutoffs produce, such as:
  - Distorted ranging code transitions
  - Introduction of inter-signal biases which vary with temperature and Doppler
  - Increased insertion loss that degrade SNR, and
  - Phase and delay distortion across signal band.

[1] http://authors.library.caltech.edu/21729/1/Esterhuizen2009p12347Proceedings_Of_The_22Nd_International_Technical_Meeting_Of_The_Satellite_Division_Of_The_Institute_Of_Navigation_(Ion_Gnss_2009).pdf

In addition to the typical advantages afforded to HP receivers that are designed with wider front-end bandwidth filters, the TriG gains additional benefits for employing wide bandwidth filters by:

- Avoiding extensive development cost and time,
- Avoiding the additional cost for pre-flight testing,
- Avoiding the additional costs associated with size and mass restrictions of flight instrument, and
- Leveraging on advanced techniques such as:
  - Oversampling the GNSS signal and use of narrow-lag correlators for better precision, and
  - On-receiver multipath mitigation techniques.

Upcoming TriG Missions

TriG receivers will be flown on the next generation radio occultation capable satellites as part of the COSMIC-2B[2] mission, which is sponsored by several U.S. federal agencies and NASA international partners. The COSMIC-2 mission is broken down into two (2) sub-missions, which will deploy six (6) satellites each. Table K-1 displays the upcoming missions where the TriG receiver will be deployed.

Note: The list of missions in Table K-1 depicts the known missions, as of the writing of this report. As NASA continues to develop partnerships with other International Space Agencies and other U.S. Federal partners, coupled with the success of integrating RO measurements into the weather prediction models, it should be noted that this list may change in the future.

Mission	Launch Date	TriG Function
Deep Space Atomic Clock (DSAC)	Jul-18	Precise clock validation
		Timing
		POD
Constellation Observing System for Meteorology, Ionosphere and Climate (COSMIC)-2 (A) - 6 satellites	Jul-18	RO
		SWO
Gravity Recovery and Climate Experiment (GRACE) Follow-On	Feb-18	Micron ranging
		POD
		RO
COSMIC-2B (B) - 6 satellites		RO

[2] Reference, http://www.cosmic.ucar.edu/cosmic2/

	2020 (pending funding) *	SWO
Sentinel-6A and B (2 launches)	2020 and 2025*	RO
		POD
Surface Water and Ocean Topography (SWOT)	2021*	POD
NASA-ISRO Synthetic Aperture Radar (NISAR)	2021*	POD

Table K-1: TriG Mission List (as of Oct-2017)

Table Legend:
POD – Precision Orbit Determination
RO – Radio Occultation
SWO – Space Weather Observation
* Tentative mission launch year

Other Scientific Applications of GNSS

GNSS technology has become an essential tool to monitor and improve our understanding of earth systems, including weather monitoring and solid earth hazards such as earthquakes and volcanic activity. This knowledge of our environment and its changes is also used for resource management and protection, and environmental impact mitigation. Some examples of the use of GNSS to improve our knowledge of the Earth are determining the atmosphere's water content, improving the accuracy of weather forecasts, enabling ocean topography measurements to determine currents and secular changes in sea height. Ground based GNSS networks are also playing an increasingly prominent role to monitor ground movement to identify potential conditions that may precede Earthquakes and volcanic activity. In addition, some insurance companies use GNSS-based maps of accumulated tectonic strain to predict risk. The same data are used by other government agencies beyond NASA. GNSS technology assists NASA scientists in understanding the physical characteristics of the earth and its atmosphere, and changes over time. NASA scientists use GPS science receivers, in combination with other measurement techniques such as laser ranging and radar altimeters, to monitor the changes in Earth's surface, sea level height, and atmospheric measurements and provide precise knowledge of Earth's shape and rotation.

As the scientific community continues to embrace leveraging on GNSS, additional techniques have been developed to measure and monitor earth and space weather phenomena. These techniques take advantage of:

- Existing development and deployment of satellite constellations, thereby, saving money in developing and deploying a separate constellation for science signals;

- Existing satellite constellations providing signals known and consistent position determinations all around the Earth; and
- GNSS signals transmit precise time and positioning information continuously in all weather conditions.

Ground-based GNSS Receivers Used for Integrated Precipitable Water Measurements

This recently developed technique in performing atmospheric observations utilizes ground-based GNSS receivers that employ zenith (away from earth) pointing antennas to measure GNSS signals. As the GNSS satellite comes into view of the antenna overhead, the amount of measured delay of the signal due to water vapor in the atmosphere can be measured and attributed to specific weather conditions. As a meteorological application, ground-based GNSS receiver data is used to derive the Integrated Precipitable Water which is fed into the Numerical Weather Prediction model. This data is complementary to the space-based data (RO), and together, they provide valuable ionospheric information for space weather specification and forecasting.

In this system, commercially available HP GPS/GNSS receivers are typically utilized and the data is fed into post-processing algorithms to determine the precipitable water vapor content of the atmosphere.

Although NASA utilizes such systems to correlate the water vapor data with RO measurements to more accurately predict weather phenomena, NASA did not perform any specific assessments to these systems under the DOT ABC Assessment. Since NASA leverages on commercial HP GPS/GNSS receivers to perform these measurements, any such protection criteria and separation distances afforded to the HP category of receivers under Section 3 will be applicable to locations where ground-based GPS/GNSS receivers are used for metrology.

Reflectometry (GNSS-R)

In addition to radio occultation and ground-based GNSS measurements, measuring the characteristics of Earth and bodies of water through a technique called “reflectometry” (GNSS-R) is also valuable application for science and weather.

For example, NASA’s Cyclone Global Navigation Satellite System (CYGNSS) mission, consisting of eight (8) small satellite observatories, which was launched in 2016, will make frequent and accurate measurements of ocean surface winds throughout the life cycle of tropical storms and hurricanes. In addition to using GNSS signals for satellite navigation, each satellite observatory can measure four (4) separate GNSS signals at the specular reflection points on the ocean to obtain information about ocean surface roughness. Ocean surface roughness is correlated to surface wind speed. The CYGNSS data will enable scientists to probe key air-sea interaction processes that take place near the core of storms, which are rapidly changing and play a critical role in the genesis and intensification of hurricanes.

Spacecraft equipped with GNSS-R systems receive a direct GNSS signal, as well as a “reflected” GNSS signal from the Earth’s surface. The direct signal is transmitted from a GNSS satellite and received by a zenith pointing antenna onboard the spacecraft, while the reflected signal is received by the two (2) nadir (towards the earth) pointing antennas. If the surface is perfectly

smooth, the specular reflection point is the location on the surface where all of the scattering originates. In comparison, if the surface is roughened (e.g., due to over the surface wind speed), the scattering of the GNSS signal originates from a diffuse region called the glistening zone around the specular point. Figure K-4 demonstrates a pictorial of GNSS-R concept of operations.

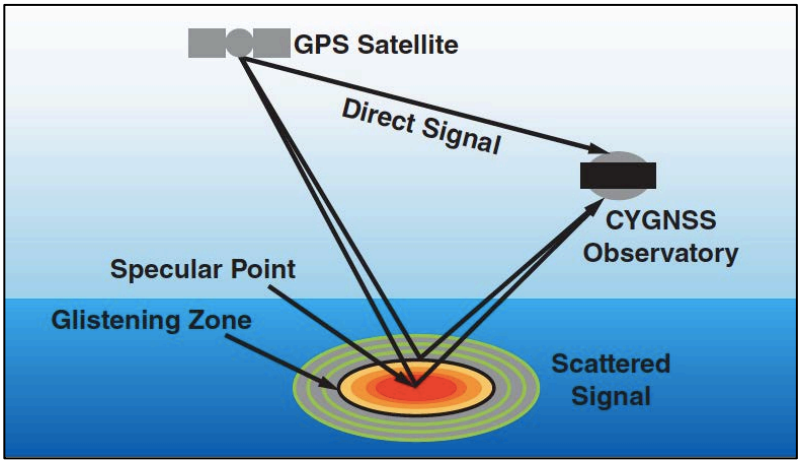

Figure K-4: GNSS-R Concept of Operations (Image Credit – University of Michigan)

Algorithms measure the amplitude of the reflected signal versus delay and Doppler shift. If the surface is smooth, nearly all power originates at the specular reflection point. If the surface is rough, there are reflections from facets separated from the specular points. Those reflections have more delay, and a spread of Doppler shifts. An example of Delay Doppler Maps for 2, 7, and 10 meter per second (m/s) wind speeds [*top to bottom*] is shown in Figure K-5.

[Illustration Note: The images show how progressively stronger wind speeds, and therefore progressively rougher sea surfaces, produce a weaker maximum signal (at the top of the "arch") and a scattered signal along the arch that is closer in strength to the maximum. A perfectly smooth surface would produce a single red spot at the top of the arch.[3] Image credit: University of Michigan.]

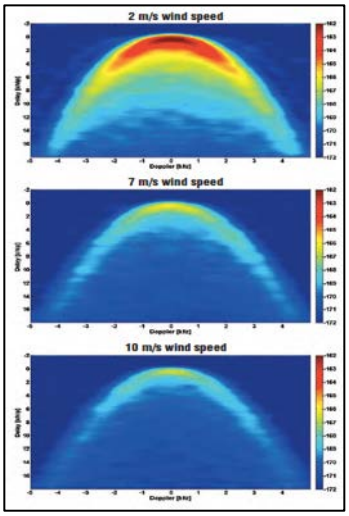

Figure K-5: Example Delay Doppler Maps

In addition to weather forecasting (e.g., cyclonic and hurricane activity), GNSS-R has shown promises to predict other Earth surface phenomena relating to

[3] Additional information on CYGNSS can be found at the following weblink to the NASA CYGNSS Mission site: https://www.nasa.gov/cygnss/overview.

bodies of water. NASA scientists are exploring the capability of GNSS-R receivers to monitor and anticipate:

- Coastal tidal surges,
- River and lake overflows,
- Flood plains,
- Water surges beneath foliage canopies (e.g., swamps and mangroves),
- Potential dyke, reservoir, and dam exceedances, and
- Many more areas that may be impacted due to watershed anomalies.

Since GNSS-R is a relatively new technique used as a scientific application of GNSS, NASA was unable to obtain a GNSS-R receiver to be tested during the testing phases (anechoic chamber or conducted) of the DOT ABC Assessment. Therefore, the effects of adjacent band LTE operations to GNSS-R are currently unknown.

Geodesy/Geodetics

Geodesy or geodetics is the science of accurately measuring and obtaining data to understand the properties of the Earth. In this scientific discipline, observations are performed to obtain information on the Earth's geometric shape, orientation (relative to Earth's axis and the sun), crustal motion, oceanic tides, and Earth's gravitational field. Since these Earth properties are continuously changing, measurements are taken with respect to time. To ensure stability and consistency in these measurements, scientists leverage on a known and constant signal source, like GPS and other GNSS signals, where accurate three-dimensional positioning attributes and timing can be obtained.

In order to accurately measure these Earth properties, commercially available HP GPS/GNSS receivers are typically utilized at fixed locations on the Earth's surface. Scientifically measured data is fed into post-processing algorithms to determine the three-dimensional positioning (in some cases such as for earthquake monitoring, accuracy levels must be down to millimeters). The variations of the receiver positons with time are compared with physical models to determine inter-earthquake strain accumulation, earth orientation parameters, etc.

Since NASA leverages on commercial HP GPS/GNSS receivers to perform these scientific measurements, any such protection criteria and separation distances afforded to the HP category of receivers under Section 3 will be applicable to locations where ground-based GPS/GNSS receivers are used for geodesy/geodetic science.

Real-time Response to Natural Hazards

The U.S. Geological Survey (USGS) mandate includes monitoring and responding to natural hazards due to earthquake faults, volcanoes, landslides, and tsunamis. Many of these applications depend critically upon GNSS data and require the broadest available spectrum of GNSS signals, including side bands, to achieve the highest station position accuracy and precision possible in real-time. In particular, the USGS Earthquake Hazards Program, in collaboration with universities and other governmental and private agencies, is developing an earthquake early warning (EEW) system, called ShakeAlert (USGS OFR # 2014-1097).

ShakeAlert will issue life-critical alerts of impending strong ground motion for public safety and emergency response in the event of a major earthquake.

Seismometers often go off-scale when recording seismic waves during large and great earthquakes, and magnitudes calculated from the earliest portion of a seismogram can be significantly underestimated. In an EEW system this leads, in turn, to underpredicted ground shaking. GNSS data have the unique capability to measure large displacements reliably at the centimeter level without going off-scale, thus augmenting seismic data to enable accurate magnitude estimates for M7+ earthquakes.

In order to do this, the GNSS component of ShakeAlert requires real-time, uninterrupted GNSS signals without interference at all times from a broadly distributed network with stations near the earthquake faults. Even brief outages due to RFI can significantly affect the precision of the GNSS observations and degrade the performance of the system. In addition to data from GNSS stations in the earthquake source region themselves, calculating their absolute positions in real-time also requires the continuous availability of data from GNSS stations outside the affected region in order to generate real-time clock correction streams. It can take up to 15 minutes for a receiver to recover from its own loss of lock and/or loss of the correction streams and resume production of the position streams. During this recovery time, a receiver cannot contribute to EEW because it will not output reliable positions, which are needed for rapid earthquake and ground motion characterization. Since early warnings must be sent within seconds of the onset of an earthquake to be useful, such delays would compromise the EEW system. The growing USGS volcano alert system could be similarly affected by RFI-related outages.

In addition to the use of GNSS-derived positions for earthquake response, the USGS seismic networks rely on the GNSS constellation L1 signal in order to mitigate seismometer clock drift. To implement this, seismic instruments typical of those used by USGS networks include a GPS chipset centered at 1550 MHz. The accuracy of time tags assigned to seismic data recorded in the field is critical for determining accurate earthquake locations, but GPS loss of lock leads to clock drift. This is particularly detrimental for EEW, in which the correct location of an earthquake must be determined within seconds in order to maximize the warning time that can be given to affected populations.

Other NASA Applications of GNSS Receivers

Statistically, nearly 60% of projected worldwide space missions present-2027 will operate in LEO. Additionally, 35% of space missions that will operate at higher altitudes will remain at or below Geostationary-Earth-Orbit (GEO). Therefore, approximately 95% of projected worldwide space missions over the next 20 years will operate within the GNSS service envelope and will rely on GNSS for space activities associated with navigation, POD, science, and other applications.

The following sections describe the uses of GNSS receivers that support various NASA missions.

Note: Although the following applications, coupled with the science applications of GNSS (in above sections) provide for a comprehensive list of NASAs' uses of GNSS, it should be noted that this does not provide a full complement of NASA's uses of GNSS receivers. Other uses for day-to-day operations, NASA security, fire and rescue, etc., typically utilize GLN receivers, which are addressed in Section 3. Therefore, any constraints to LTE operations required to protect GLN devices will be applicable to these NASA functions.

Figure K-6: NASA Security Vehicle

Aviation Systems

NASA's Aeronautical Research Mission Directorate operates NASA owned, maintained, and operated aircraft, which are certified by the FAA to operate in the National Airspace System. If such NASA aircraft are equipped with GPS receivers, they are required to be compliant with FAA Certification Regulations and are equipped with FAA certified GPS receivers.

Figure K-7: Example of NASA Aircraft Fleet

Moreover, NASA also possesses and operates several Unmanned Aerial Systems (UAS) that are equipped with GPS receivers. Some of the UAS are designed and developed by NASA Program Offices, while other UAS are operated under a leasing contract with the UAS developer. UAS are used by NASA in various manners, from developing UAS Traffic Management policies and procedures - to performing airborne science measurements - to performing research and development of new aircraft materials and aircraft designs. Regardless what mission or function the UAS is supporting, if required and necessary for flight in the National Airspace System, UAS will be equipped with certified aviation receivers or with general aviation (GAV) receivers.

Figure K-8: Example of NASA UAS

Spacecraft

Spacecraft, as defined by the International Telecommunication Union (ITU)[4], is a man-made vehicle which is intended to go beyond the major portion of the Earth's atmosphere. NASA's spacecraft portfolio consists of, but not limited to:

- Space vehicles,
- Space stations,
- Space platforms, and
- Satellites.

The orbital mechanics and flight operation of spacecraft, including navigation, POD, metrics tracking, timing, velocity, and attitude, rely on GNSS signals for accuracy. During development, spacecraft are typically fitted with either commercially available HP GPS/GNSS receivers or NASA developed GNSS receivers.

Throughout the years, NASA has developed and continues to develop GNSS receivers that meet specific mission requirements and designed with the robustness to withstand the harsh elements of space. Some of these devices are the:

- TurboRogue,
- BlackJack, IGOR, and IGOR+,
- Navigator, and
- TriG.

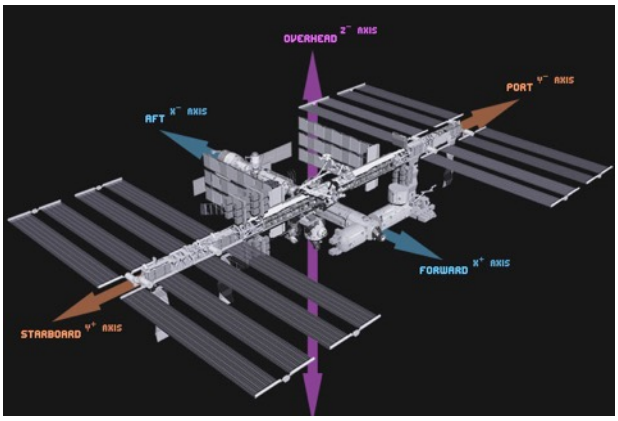

Figure K-9: Orientation Designations of Spacecraft

Employed to perform orbital mechanics and flight operations, GNSS receivers (commercial or NASA-developed) are unlikely to be significantly affected by the ground-based LTE broadband operations in adjacent bands. NASA has previously studied the IGOR, TriG[5], and Navigator[6,7] in this mode of operation. This is due to the configuration and placement of the antenna. Since most spacecraft operate within GNSS constellation orbits, antennas are located in the zenith (away from earth) position of the spacecraft.

Launch Vehicles

Launch vehicles are rockets used to propel a payload from the Earth's surface to outer space. In some cases (e.g., sounding rockets), the rockets are designed to carry a scientific measuring

[4] International Telecommunication Union, Radiocommunication Sector, (ITU-R), Radio Regulations, Edition 2016, Volume 1, Chapter I – Terminology and technical characteristics. (http://www.itu.int/pub/R-REG-RR-2016)
[5] 2011 National Space-Based Positioning, Timing, and Navigation Systems Engineering Forum Report, Subtask 6, NASA Simulations.
[6] GPS Navigator (Nav) Near-band and In-band RFI Susceptibility Report (461-NAV-ANYS-0256), NASA Goddard Space Flight Center.
[7] Limited distribution due to proprietary system information contained within the document.

device into sub-orbital altitudes; while some rockets are designed with enough inertia and thrust to enable its payload to entirely escape Earth orbit.

Through the past two decades, the design and development of launch vehicles include the equipage of GNSS receivers. The use of these receivers facilitates ground control operators by providing key metric tracking of launch vehicles. Integrated metric tracking units provide accurate and stable positioning on high dynamic platforms.

More recently, NASA has implemented an Autonomous Flight Safety System (AFSS)[8], which is a real-time safety system comprised of the ground software used to write mission rules and convert the mission rules into a mission data load. Coupled with the ground system, the AFSS includes on-board hardware and software. Specifically, the launch vehicle is equipped with an Automated Flight Termination Unit (AFTU) used for the Automated Flight Termination System (AFTS) of the AFSS.

Figure K-10: Antares Rocket Launch, Wallops Island, Oct-2016
(Photo Credit: NASA/Joel Kowsky)

The AFTS augments or replaces the functions of the traditional human-in-the-loop (HITL) process and procedures. Redundant AFTS processors evaluate data from onboard AFTUs, which include GNSS receivers and other navigation sensors, and are used to make flight termination decisions. The mission rules are developed by the local Range Safety Authorities using the inventory of rule types taken from current HITL operational flight safety practices[9]. HP GNSS receivers are typically configured in the AFTUs to achieve the high-level of accuracy necessary to track the position of the launch vehicle within the projected launch path safety boundary.

[8] An Autonomous Flight Safety System, James B. Bull and Raymond J. Lanzi, NASA Goddard Space Flight Center and NASA Wallops Flight Facility. https://ntrs.nasa.gov/archive/nasa/casi.ntrs.nasa.gov/20080044860.pdf

[9] Reference: Autonomous Flight Termination System Reference Design Hardware, Lisa Valencia, Robert Morrison, and Roger Zoerner, NASA Kennedy Space Center, FL.
http://www.techbriefs.com/component/content/article/ntb/tech-briefs/machinery-and-automation/24084

NASA employs commercial HP GNSS as a part of the AFTU and any such protection criteria and separation distances afforded to the HP category of receivers under Section 3 will be applicable to locations where these receivers are used on launch vehicles as part of the AFSS.

Spaceborne Receiver Assessment for Science-Based Applications

NASA has performed an assessment of the potential impacts caused by a proposed terrestrial LTE network operating in the adjacent band to GPS L1. Two (2) future science missions, COSMIC-2B and Sentinel-6 (formerly, Jason Continuity of Service (Jason-CS)), were used as the basis for these assessments. NASA's assessment is to the TriG receiver performing a science application using the RO technique.

To determine the impact to the TriG receiver, the aggregate interference power at the output of the TriG receiver antenna was calculated using MATLAB to model the interference scenario, as well as the TriG receiver system, and simulate the interference effects to the satellites in orbit. Satellites operating in LEO gain a much broader view of the earth (dependent upon antenna characterizations and operating parameters), which must be accounted for in performing the analysis.

Unlike the assessments performed in Section 3, in-orbit satellites will see a greater number of potential interference sources (e.g., increased number of terrestrial base stations) and the aggregate of those interference sources will be the major contributing factor in the assessment, see **Figure K-11**.

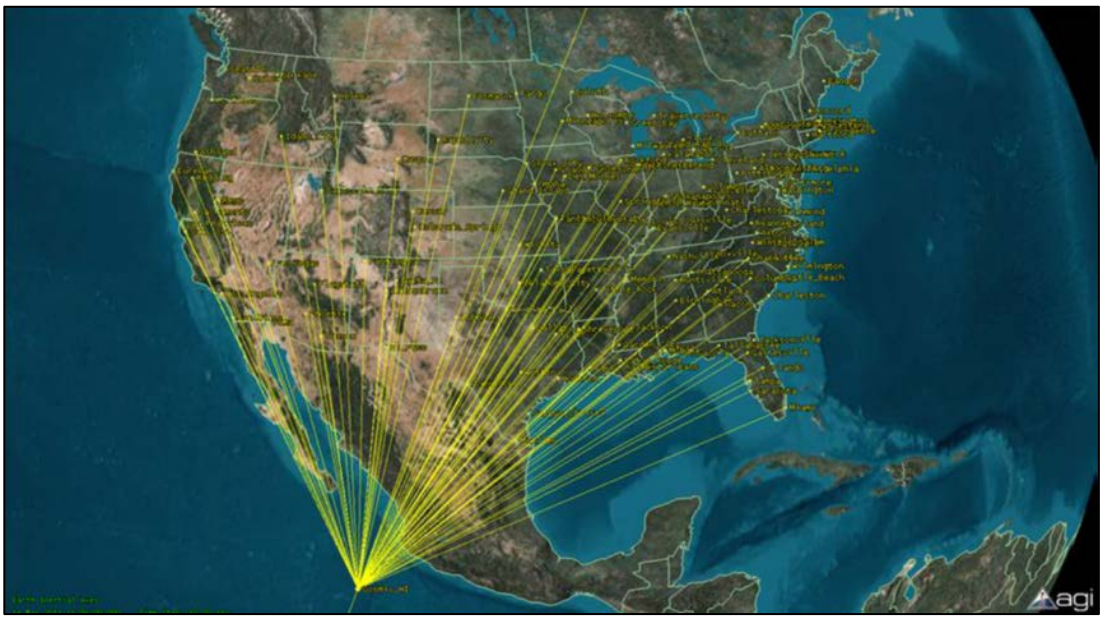

Figure K-11: Example Satellite View of the U.S. Cities

This section describes the modeling and simulation (M&S) for a variety of terrestrial LTE base station deployment scenarios. Further, this section will also describe, where applicable, assumptions made in the M&S, population density of the LTE network, and other dependent parameters or characteristics. Finally, this section will also provide the results and NASA's assessment on impacts/effects on TriG mission performance.

Assumptions

Interference Protection Threshold (TriG)

NASA participated during the DOT ABC Testing of various GPS/GNSS receivers at the ARL facility in WSMR, NM. One (1) of the various systems NASA tested was the TriG receiver (see Section 3). The results of the testing produced an interference protection threshold of -73 dBm. This protection threshold value is based upon the IPC of -1 dB C/N_o for LTE signals being present in 1526 – 1536 MHz.

Furthermore, the testing produced a loss-of-lock threshold down to -59 dBm.

Table K-1: TriG Interference Protection Threshold

Parameter	Threshold	Effect on TriG
-1 dB C/N_o	-73 dBm	Degraded performance, inaccurate measurements
Loss-of-Lock	-59 to -35 dBm	Saturated/jammed (no longer able to receive signals)

Impacted Receiver Satellite Orbit Specifications

The impacted receiver, in the context herein, is referred to at the receiver system that will be impacted by interference from the interfering source (e.g., terrestrial LTE broadband network).

Typical TriG receiver specifications have been previously described in this Appendix. The following provides the satellite-specific parameters for each of the assessed Missions.

Table K-2: Simulation Parameters - Satellite Orbit Parameters

Orbit Characteristic	COSMIC-2B	Sentinel-6
Altitude	800 km	1330 km
Inclination Angle	72°	66°

TriG Receiver Antenna

The TriG receiver system can be configured to use a variety of NASA/JPL developed antennas to meet its mission needs. The following provides a description of the antenna configurations used to support COSMIC-2B and Sentinel-6.

Antenna Configuration for COSMIC-2B Mission

The antenna configuration to support COSMIC-2B utilizes a set of two (2) proprietary beam forming array antennas. Each antenna is a 12-element array comprising 3 subarrays of 4 vertically stacked elements with a peak gain at 1530 MHz of +13.4 dBic. Each array uses a 60 cm tall x 40 cm wide backplane mounted on the spacecraft so that the plate is vertical and the outward normal to the plate is parallel to the spacecraft's velocity vector (assuming circular orbit). The first antenna is mounted in the forward direction of a satellite (to receive rising GNSS satellite signals) and the second antenna is mounted in the aft direction (to receive setting GNSS satellite signals). The TriG receiver has eight (8) independent antenna inputs (three (3) inputs from each of the two (2) subarrays and two (2) inputs from the antennas performing POD and space weather data acquisition functions.) Three (3) subarrays (performing the RO technique) are combined for the fore and aft antennas, increasing the gains by approximately 4.8 dB to a total main beam gain of +18.2 dBic. Note that the gain and beam shape used for the simulation is from the 4-element subarray. Since each subarray has its own filter/LNA chain, the effects of RFI apply at the subarray level.

Based on the satellite altitude (for COSMIC-2B altitude = 800 km), the receiver main-beam is directed towards the earth limb (approximately 26.2° below the satellite velocity vector). **Figure K-12** demonstrates an example of an in-orbit satellite with the forward antenna subarray with its down-tilt. [Note: For graphical simplicity, the aft subarray is not pictured.] Consequently, the potential interfering signals from terrestrial LTE BS will be in view of the receive antenna array main-beams.

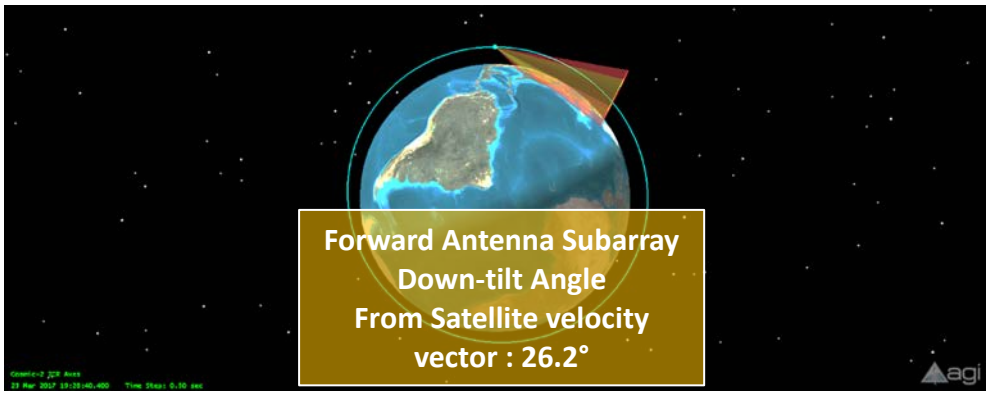

Figure K-12: TriG RO Antenna Array Main-Beam Down-tilt (26.2°)

The antenna subarrays are designed to receive right-hand circular polarized signals from the GNSS satellites. For the analysis, an antenna coupling mismatch (cross-polarization loss) of -3 dB is used (assuming a typical vertically polarized LTE signal).

Figure K-13 and **Figure K-14** show the gain pattern for the forward antenna with the main-beam directed 26.2° below the satellite velocity vector towards earth limb.

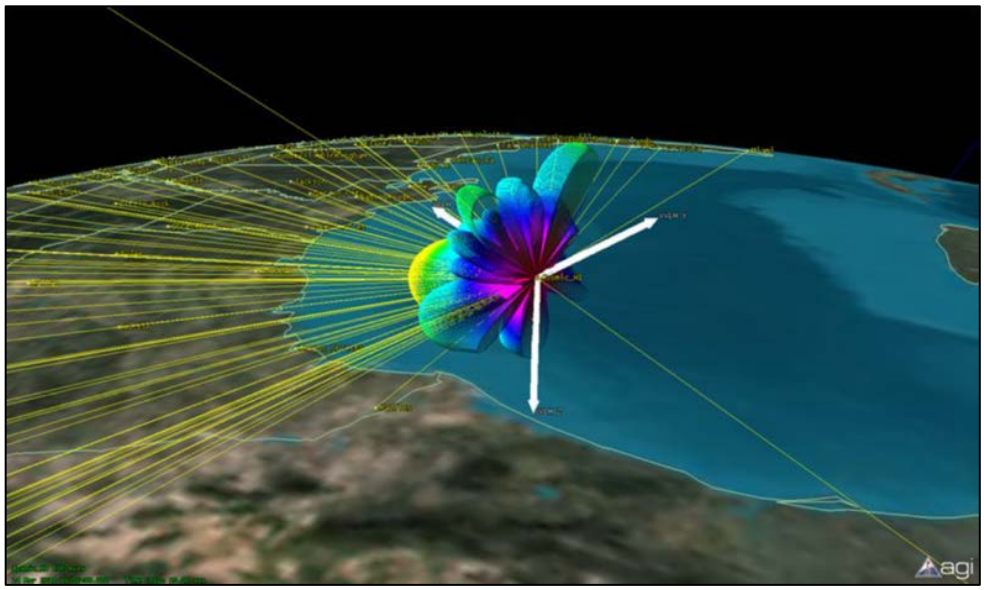

Figure K-13: Forward Direction Antenna Array (12-Element, 13.4 dBic @ 1530 MHz, main-beam pointed towards Earth limb)

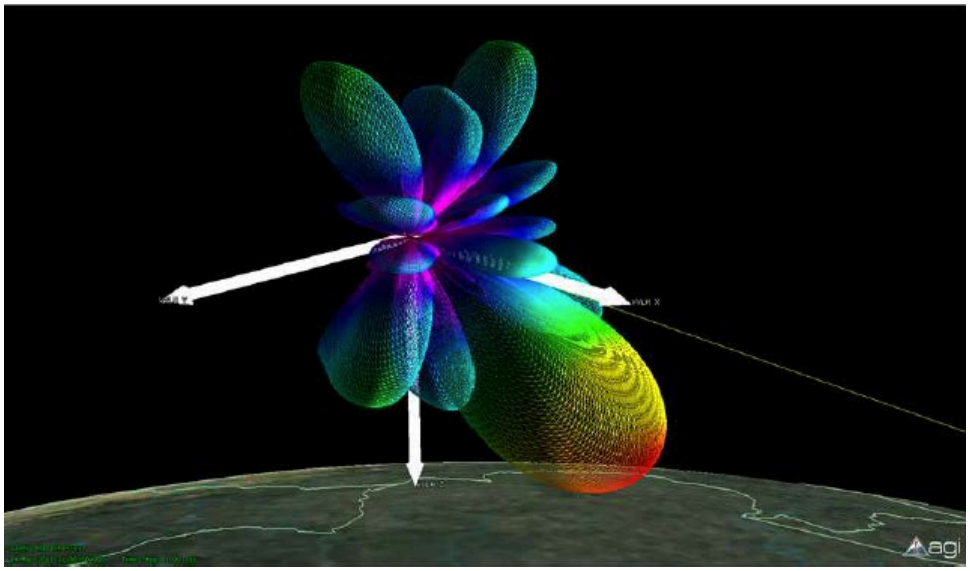

Figure K-14: Aft Direction Antenna Array (12-Element, 13.4 dBic @ 1530 MHz, main-beam pointed towards Earth limb)

Based upon the antenna array specifications and operational parameters, above, the 3 dB antenna beam width coverage footprint from COSMIC-2B is approximately 1.6 million square miles. The yellow shaded area over the U.S. in **Figure K-15** displays the footprint for the forward antenna array. [*Note*: It should be noted that a similar area of coverage (mirror-image in the horizontal plane) would also be succeeding the satellite.]

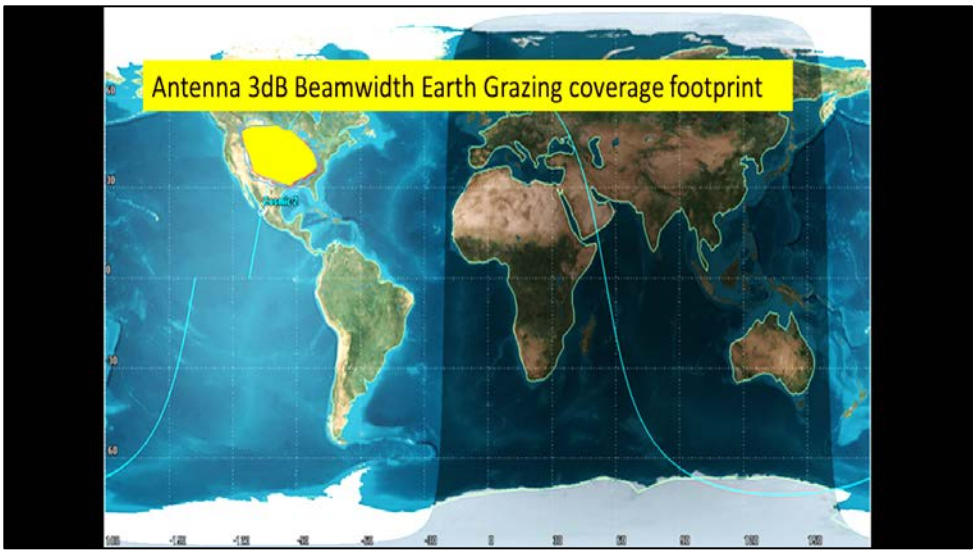

Figure K-15: COSMIC-2B Antenna 3 dB Beam width Coverage Footprint

COSMIC-2B Antenna Configuration Used for M&S Analysis

Although the COSMIC-2B antenna has 2 beamforming arrays the M&S was configured to model only the forward antenna since the aft antenna should show near-identical RFI statistics when averaged over ten days.

The effects of this modification are discussed in the results section for COSMIC-2B.

Antenna Configuration for Sentinel-6 Mission

Similar to the COSMIC-2B antenna configuration, the antenna configuration to support Sentinel-6 utilizes a set of two (2) proprietary beam forming array antennas. However, the mission requirements for Sentinel-6 call for a different array configuration, as well as a difference of subarrays on the forward and aft directions of the spacecraft.

The forward antenna array is comprised of a six (6) element array in a 2 x 3 configuration. This array will nominally produce a main beam gain of approximately +15.5 dBic at 1530 MHz. Based on the orbit altitude of Sentinel-6 (1330 km), the forward antenna is mechanically down-tilted so that the main-beam is 34.2° below the satellite velocity vector towards earth limb.

The aft antenna array is comprised of a 12-element array in a 4 x 3 configuration. This array will nominally produce a main beam gain of approximately +17.5 dBic at 1530 MHz. Based on the orbit altitude of Sentinel-6 (1330 km), the aft antenna is electrically phased down (down-tilted) by 22°, as well as mechanically down-tilted an additional 12.0° below the satellite velocity vector towards earth limb.

Sentinel-6 Antenna Configuration Used for M&S Analysis

The Sentinel-6 antenna will digitally combine the outputs of each of the three subarrays on the fore and aft antennas. Because each RF front end is separate for each subarray, the effect on a single subarray was analyzed for degradation and saturation. For the forward subarray, a 2-element array (2 x 1 configuration) with a peak main beam gain of +10.5 dBic at 1530 MHz was modeled for the simulation. In the aft subarray, a 4-element array (4 x 1 configuration) with a peak main beam gain of +12.5 dBic at 1530 MHz was modeled for the simulation.

The effects of this modification are discussed in the results section for Sentinel-6.

Summary of TriG Receiver System Characteristics Used for Analyses

Table K-3 summarizes the satellite TriG receiver system characteristics for the analyses performed on COSMIC-2B and Sentinel-6. The interference threshold in this table is the RFI power at the output of the flight RO antenna which causes a -1 dB C/No degradation in the TriG receiver as used in the COSMIC2 mission. It was derived from the power density observed by the 0 dBiL standard gain horn used in during the DOT ABC test at a RFI power level causing a 1 dB C/No degradation. Since the TriG choke ring antenna was located at a different spot, it actually received about 3.2 dB more RFI power per meter squared (m^2). In addition, the choke ring antenna had about +3.7 dBi linear gain toward the RFI source, adding 3.7 dB to the threshold power. After these corrections, the LTE power at 1530 MHz that causes a 1 dB C/No degradation is -78.2 dBm + 3.2 dB + 3.7 dB = -71.3 dBm, defined at the output of the receive antenna.

Another adjustment that was made to estimate the effect on the flight receiver is the difference in noise floors due to the extra antenna temperature from black body radiation coming from the ceiling and walls of the WSMR anechoic chamber. During the test, the noise floor is estimated to be 349 Kelvin (K). This is based on preamplifier (Preamp) noise of 51 K, antenna temp of 300 K, and filter loss of 0.8 dB. The noise floor in flight is estimated to be 224 K based on Preamp noise of 51 K, antenna temp of 150 K, and filter loss of 0.8 dB. This difference shows an adjustment to lower the 1 dB threshold by 1.9 dB. Therefore, the normalized in-flight RFI power of is calculated to be approximately -73 dBm (-71.3 dBm – 1.9 dB = -73.2 dBm) from the antenna corresponding to a -1 dB degradation of C/No.

Table K-3: Summary Table of Satellite TriG Receiver Characteristics Used for M&S

Receiver Characteristic	COSMIC-2B	Sentinel-6
Satellite Orbit Altitude	800 km	1330 km
Satellite Orbit Inclination Angle	72°	66°
TriG Forward Receive Antenna Type	12-Element Array	6-Element Array
TriG Forward Receive Antenna Downtilt (relative to satellite velocity vector)	26.2°	34.2°

TriG Forward Receiver Antenna Subarray Gain @ 1530 MHz	+ 13.4 dBic	+ 10.5 dBic
TriG Aft Receive Antenna Type	Not modeled	12-Element Array
TriG Aft Receive Antenna Downtilt (relative to satellite velocity vector)	Not modeled	34.0°
TriG Aft Receiver Antenna Subarray Gain @ 1530 MHz	Not modeled	+ 12.5 dBic
Interference Threshold (-1 db C/N_o)	- 73 dBm	- 73 dBm
Loss-of-Lock (*Note*: The LOL value ranged from a low of -59 dBm for Test 04 at 1525 MHz to a high of -35 dBm for Test 04 at 1530 MHz, all corrected for antenna location and gain.)	- 59 to -35 dBm	- 59 to -35 dBm
Antenna Coupling Mismatch (Cross-Polarization Loss)	- 3 dB	- 3 dB

Terrestrial LTE Deployment Scenarios

The aggregate interference is dependent upon several factors. A few of those factors are the satellite related, to include, orbital parameters and receiver system characteristics. The other determining factor comes from the interference sources. Most importantly, the transmitter characteristics and the total number of sources (e.g., LTE BS). Since TriG receiver systems (performing the RO technique) operate in LEO, they have a direct line-of-sight to a broad area of the U.S., and the aggregate interference is dependent upon the long-term deployment scenario of the LTE operator.

The following describes the LTE parameters and the developed scenarios used during M&S.

Base Stations used for LTE Deployment

To model the terrestrial LTE base station deployment, the analyses used base station (BS) macro and microcell parameters, which are primarily derived from ITU-R M.2292.

For this analysis, the following BS macro and microcell antenna bore-sites with respect to True North were assumed:

- Macrocell Sector-1 bore-site: 0°
- Macrocell Sector-2 bore-site: 120°
- Macrocell Sector-3 bore-site: 240°
- Microcell Sector bore-site: Randomly selected from (0°, 120°, 240°)

NASA used two (2) different methodologies to determine the total number of BS that could be deployed to support the LTE network. The assumptions used for each of the methodologies are described below and resulted in a different number of cell sites.

City Zone Model

The City Zone model was used to determine the physical area around a city center location that the simulated LTE network would be deployed over. The baseline City Zone model was chosen to conform to the only available accepted model given in ITU Report ITU-R SA.2325-0[10] (International Mobile Telecommunication (IMT) sharing at 2GHz) for an BS deployment based on three (3) zones (e.g., urban, suburban, and rural) with given radial distances from a city center latitude/longitude location. Figure K-16 demonstrates an example of the City Zone model with the typical macro cellular hexagonal grid layout deployed about a city center.

Because the LTE services to be provided by the proposed and analyzed network may not be as widespread in terms of city area as the conventional LTE deployment described in SA.2325-0 a second City Zone model with a smaller Suburban and Rural zone size was analyzed. Parameters for both the City Zone models are listed in Table K-4.

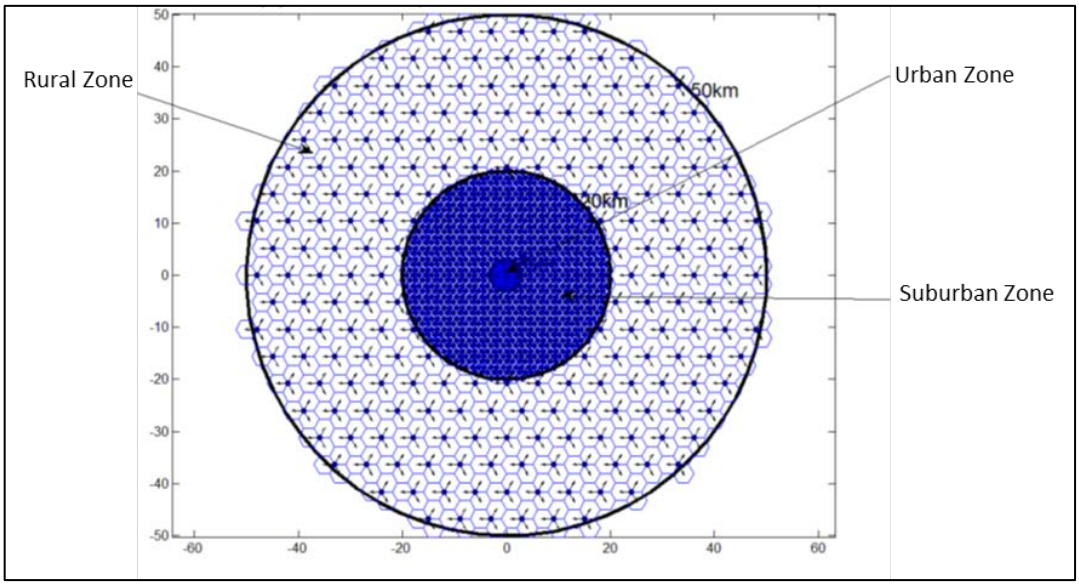

Figure K-16: Base Station Deployment Zone Model (Report ITU-R SA. 2325-0)

[10] Reference, https://www.itu.int/dms_pub/itu-r/opb/rep/R-REP-SA.2325-2014-PDF-E.pdf

Table K-4: Zone Model - BS Zone-specific Radial Distance from City Center

Zone Model	Urban Zone (km)	Suburban Zone (km)	Rural Zone (km)
1	0 – 3	3 – 20	20 – 50
2	0 – 3	3 – 10	10 – 30

City Population Size / Base Station Cell Radius

In addition to a City Zone model it was necessary to define the BS cell radius (CR) parameter in order to determine the BS grid layout within each City Zone. The typical ITU-R M.2292 zone values listed in Table K-6 were used as the baseline cell radius (CR) in the simulation.

Table K-5: Typical Cell Radius (CR) - ITU-R M.2292

Zone type	City Population	CR (km)
Urban	All	0.5
Suburban	All	1.0
Rural	All	5.0

In consideration to the where the proposed LTE network is to be deployed, the size of the city population was an additional parameter that was included in the simulations. If a U.S. city had a population of greater than 125,000, but less than 250,000, it was included in the analyses for half of the simulations. Cities with populations of over 250,000 were included in all simulations. Accordingly, the number of assumed cities included in each simulation was chosen from:

- City Population > 125K: 225 cities or
- City Population > 250K: 82 cities

Additionally, since a smaller population city could have a smaller amount of Base Stations with a larger Cell Radius (CR), then the typical M.2292 CR values where scaled by the city population and included in the set of simulation runs. Table K-7 shows the addition inclusion of the largest M.2292 CR Table values.

Table K-7: Cell Radius Scaled by City Population Density (ITU-R M.2292)

Zone type	City Population (in 1000s)	CR (km)
Urban	> 125 > POP < 250	1.0
	> 250 > POP < 500	0.75
	POP > 500	0.5 (Typical)
Suburban	> 125 > POP < 250	2.0
	> 250 > POP <500	1.5
	POP > 500	1.0 (Typical)
Rural	> 125 > POP < 250	10.0
	> 250 > POP < 500	10.0
	POP > 500	5.0 (Typical)

Total Number of Base Stations in Simulations

Using the set of Zone Model, City Population and Cell Radius parameters, NASA calculated the total number of BS required for deployment for each simulation run. Table K-8 depicts the number of base stations for the set of three parameters for a LTE network deployment consisting of only macrocells. Table K-9 accounts for microcells to be included in the LTE network deployment.

Table K-8: Total # of BS (Macrocell Deployment Only)

Zone Model	City Population (in 1000s)	Cell Radius	Number of BS			
			Urban	Suburban	Rural	Total
1	> 125	Table K.6	11,700	143,100	29,700	184,500
1	> 250	Table K.6	4,264	52,152	10,824	67,240
1	> 125	Table K.7	5,330	58,962	10,320	74,612
1	> 250	Table K.7	3,024	35,796	6030	44,868
2	> 125	Table K.6	11,700	33,750	12,150	57,600
2	> 250	Table K.6	4,264	12,300	4,428	20,992
2	> 125	Table K.7	5,330	13,500	5,310	24,140
2	> 250	Table K.7	3,042	8352	2,736	14,130

Table K-9: Total # of BS (Macro + Microcells)

Zone Model	City Population (in 1000s)	Cell Radius	Number of BS		
			Macrocells	Microcells	Total
1	> 125	Table K.6	184,500	97,686	282,186
1	> 250	Table K.6	67,240	35,601	102,841
1	> 125	Table K.7	74,612	41,014	115,626
1	> 250	Table K.7	44,868	24,609	69,477
2	> 125	Table K.6	57,600	36,450	94,050
2	> 250	Table K.6	20,992	13,284	34,276
2	> 125	Table K.7	24,140	15,555	39,695
2	> 250	Table K.7	14,130	9,240	23,370

Additional LTE Network Deployment Assumptions for Analysis

In addition to the parameters described above, the following simulation parameters were considered and chosen by NASA for the analysis performed.

- Since specific latitude and longitude locations for the BS in each city were not available, BS are placed at respective city center latitude/longitude and BS power aggregated for urban, suburban and rural BS transmitters to get single equivalent urban, suburban, rural and microcell BS.
  Rationale 1: The angular separation between two (2) BS separated by 10 km is only 0.7°, assuming a TriG receiver at 800 km altitude. This angular separation is relatively small with respect to the transmitter and receiver antenna gain patterns.

  Rational 2: The time and resources required to model separate BS locations for each city would be exhaustive. Further, the computational time to run the simulations and amount of processing power would be extensive.

- BS antenna side-lobe pattern:
  - ITU-R F.1336-4 Recommends 3.1. (Macro)
  - ITU-R F.1336-4 Recommends 3.2. (Micro)

- Per M.2292, 30% of the macrocell BS are below rooftop and the simulation considered half of the 30% blocked from contributing interference and have already been excluded in the total BS calculations in Table K-8.

- Per M.2292, microcell BS antennas are below rooftop with 50% of the microcells in the urban zone and 30% of the microcells in the suburban zone considered blocked. These BS have already been excluded in the total BS calculations in Table K-9.

- Elevation Mask:
  Consideration given to blockage from terrain, vegetation, and addition man-made structures. This was simulated by providing a 5° transmitter elevation mask in the vertical plane of the transmitter, 360° around the BS in the horizontal plane.

  Two (2) BS mask angles are utilized for the analysis:

  - A 0° elevation mask on the BS so that all BS which see the satellite above 0° elevation angle are included in the aggregate interference calculation, and
  - A 5° mask angle so that only BS which see the satellite above 5° elevation angle contribute to the aggregate interference.

- One (1) 10 MHz LTE channel per sector.

- Propagation Loss: Free-space

- BS Activity Factor (AF):
  An AF of 3 dB, corresponding to 50% of the base stations transmitting simultaneously, is used throughout the analysis.

  Note: If 100% of the base stations are transmitting simultaneously, the peak interference levels in the results will be 3 dB higher. This will also hold true for other resultant statistics, as well.

- BS Transmitter Power (EIRP):
  Table K-10 depicts the nominal transmit power used for some of the simulations (as per ITU-R M.2292). Considerations were also given to the maximum transmit powers of +10 dBW[11] and +32 dBW[12] EIRP per channel per sector.

[11] Proposed maximum transmit power per channel per sector through negotiations with the FAA.
[12] Maximum transmit power per channel per sector as authorized in the current FCC license.

Table K-10: Assumed Maximum Transmitter Levels per Sector (Typical per ITU-R M.2292)

BS Type	Typical Max. Transmit Power/Channel/Sector (EIRP)
Macrocell - Urban	26 dBW
Macrocell - Suburban	26 dBW
Macrocell - Rural	28 dBW
Microcell (any zone)	7 dBW

TriG Receiver Analysis

Two (2) NASA missions (COSMIC-2B and Sentinel-6) that include the TriG receiver, as a science-based function (e.g., RO technique) were utilized for analysis. A MATLAB simulation program was developed to model the receiver on-board a satellite, using mission-specific parameters, and interference statistics were calculated for an LTE network deployment of BS distributed in U.S. cities.

MATLAB Simulation

For the spaceborne receiver analysis the aggregate interference power at the output of the GPS receiver antenna is calculated at ten (10) second time steps in the satellite orbit from BS distributed among U.S. cities. The MATLAB program was setup to model a 10-day orbit of the satellite. **Figure K-17** provides an example of the COSMIC-2B satellite simulation of a 10-day orbit.

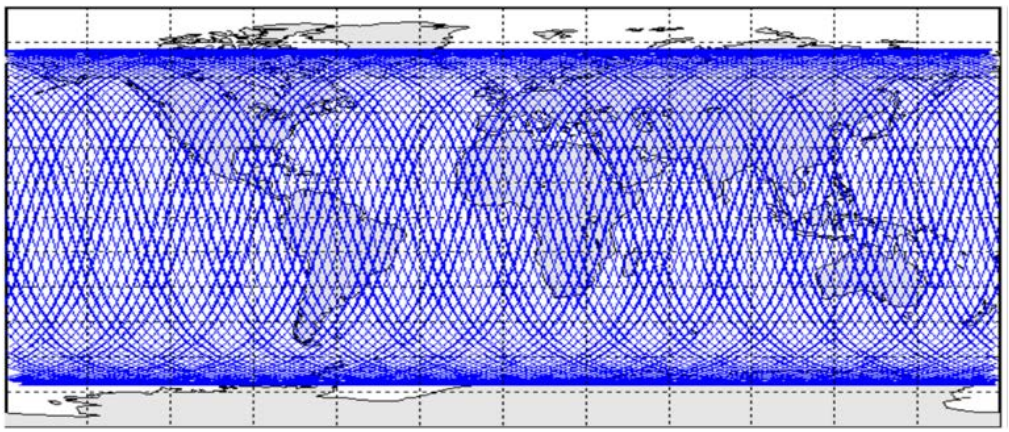

Figure K-17: Ground Track of COSMIC-2B Orbital Path (10-Day Simulation at 10-Second Time Steps)

A similar program written in Python was implemented for the Sentinel-6 simulation.

Aggregate Interference Calculation

The analysis calculates the Io/No value and is not dependent upon the carrier (C) signal. Thresholds for determining the saturation (-1 dB C/No) and jammed (loss-of-lock) values of the TriG are discussed in this report.

The aggregate interference to the receiver antenna output is calculated using a summation of the interference from each source. A simple link budget formula is used to calculate the interference received by a single source, LTE BS. The total aggregate interference is determined through the summation of interference from the individual sources, see Equation K-2.

$$\text{Rx Int Pwr}_{agg} = \sum(\text{Int sources}) \ \text{Tx Pwr (EIRP)}_{\text{off-boresite}} - \text{FSPL} - \text{Pol Loss} + \text{Rx Ant Gain}_{\text{off-boresite}}$$

Equation K-2: Formula in Determining Received Aggregate Interference at the TriG Antenna Output

Where,

Rx Int Pwr_{agg} = Aggregate interference power level (dBm)

$\text{Tx Pwr (EIRP)}_{\text{off-boresite}}$ = Tx power output including antenna off-boresite calculations (dBm) (See below)

FSPL = Free Space Path Loss (dB)

Pol Loss = Loss of dissimilar polarizations (Linear to RCHP Polarization = - 3 dB)

$\text{Rx Ant Gain}_{\text{off-boresite}}$ = Rx antenna gain including antenna off-boresite calculations (dBic)

The BS sector antenna gain towards the satellite is calculated by first determining the appropriate azimuth (AZ) (horizontal plane) and elevation (EL) (vertical plane) angles based on the BS and satellite geometry. The antenna off-boresite gain is calculated by, first, summing the AZ plane discrimination with the EL plane discrimination and, secondly, subtracting this total discrimination from the maximum sector gain[13] to get the net sector gain towards the satellite.

Note: The maximum interference from an BS will occur when it sees the satellite at low elevation angles.

Simulation Runs

A total of 96 simulation runs were performed for COSMIC-2B, while a lesser number, but still representative, number of runs (16 runs) were performed for Sentinel-6. Each of the simulation runs varied one or more LTE BS deployment parameters.

While it is unknown for how the LTE operator will be performing their network deployment, the variations in simulation runs should be demonstrative. Further, the variations in runs may be representative of an LTE network through its various phases of deployment (initial deployment through full deployment). **Table K-6** summarizes the various simulation runs.

[13] As defined in ITU-R M.2292 and ITU.R F.1336-4.

Table K-6: Summary of Simulation Runs

Run	Sim No.	Run Designator	COSMIC-2B	Sentinel-6	BS Tx Power	Zone Model	City Population	Cell Radius	Elevation Mask	Macrocell Only	Macro + Microcell	Total # of Base Stations
1	1	a	X		M.2292 levels	1	> 125K	Typical	0°	X		184,500
2	1	b	X	X	M.2292 levels	1	> 125K	Typical	5°	X		184,500
3	1	c	X		32 dBW	1	> 125K	Typical	0°	X		184,500
4	1	d	X		32 dBW	1	> 125K	Typical	5°	X		184,500
5	1	e	X		10 dBW	1	> 125K	Typical	0°	X		184,500
6	1	f	X	X	10 dBW	1	> 125K	Typical	5°	X		184,500
7	2	a	X		M.2292 levels	1	> 250K	Typical	0°	X		67,240
8	2	b	X	X	M.2292 levels	1	> 250K	Typical	5°	X		67,240
9	2	c	X		32 dBW	1	> 250K	Typical	0°	X		67,240
10	2	d	X		32 dBW	1	> 250K	Typical	5°	X		67,240
11	2	e	X		10 dBW	1	> 250K	Typical	0°	X		67,240
12	2	f	X	X	10 dBW	1	> 250K	Typical	5°	X		67,240
13	3	a	X	X	M.2292 levels	1	> 125K	Scaled	0°	X		74,612
14	3	b	X	X	M.2292 levels	1	> 125K	Scaled	5°	X		74,612
15	3	c	X	X	32 dBW	1	> 125K	Scaled	0°	X		74,612
16	3	d	X	X	32 dBW	1	> 125K	Scaled	5°	X		74,612
17	3	e	X	X	10 dBW	1	> 125K	Scaled	0°	X		74,612
18	3	f	X	X	10 dBW	1	> 125K	Scaled	5°	X		74,612

19	4	a	X	X	M.2292 levels	1	> 250K	Scaled	0°	X		44,850
20	4	b	X	X	M.2292 levels	1	> 250K	Scaled	5°	X		44,850
21	4	c	X	X	32 dBW	1	> 250K	Scaled	0°	X		44,850
22	4	d	X	X	32 dBW	1	> 250K	Scaled	5°	X		44,850
23	4	e	X	X	10 dBW	1	> 250K	Scaled	0°	X		44,850
24	4	f	X	X	10 dBW	1	> 250K	Scaled	5°	X		44,850
25	5	a	X		M.2292 levels	2	> 125K	Typical	0°	X		57,600
26	5	b	X		M.2292 levels	2	> 125K	Typical	5°	X		57,600
27	5	c	X		32 dBW	2	> 125K	Typical	0°	X		57,600
28	5	d	X		32 dBW	2	> 125K	Typical	5°	X		57,600
29	5	e	X		10 dBW	2	> 125K	Typical	0°	X		57,600
30	5	f	X		10 dBW	2	> 125K	Typical	5°	X		57,600
31	6	a	X		M.2292 levels	2	> 250K	Typical	0°	X		20,992
32	6	b	X		M.2292 levels	2	> 250K	Typical	5°	X		20,992
33	6	c	X		32 dBW	2	> 250K	Typical	0°	X		20,992
34	6	d	X		32 dBW	2	> 250K	Typical	5°	X		20,992
35	6	e	X		10 dBW	2	> 250K	Typical	0°	X		20,992
36	6	f	X		10 dBW	2	> 250K	Typical	5°	X		20,992
37	7	a	X		M.2292 levels	2	> 125K	Scaled	0°	X		24,140
38	7	b	X		M.2292 levels	2	> 125K	Scaled	5°	X		24,140

39	7	c	X		32 dBW	2	> 125K	Scaled	0°	X		24,140
40	7	d	X		32 dBW	2	> 125K	Scaled	5°	X		24,140
41	7	e	X		10 dBW	2	> 125K	Scaled	0°	X		24,140
42	7	f	X		10 dBW	2	> 125K	Scaled	5°	X		24,140
43	8	a	X		M.2292 levels	2	> 250K	Scaled	0°	X		14,130
44	8	b	X		M.2292 levels	2	> 250K	Scaled	5°	X		14,130
45	8	c	X		32 dBW	2	> 250K	Scaled	0°	X		14,130
46	8	d	X		32 dBW	2	> 250K	Scaled	5°	X		14,130
47	8	e	X		10 dBW	2	> 250K	Scaled	0°	X		14,130
48	8	f	X		10 dBW	2	> 250K	Scaled	5°	X		14,130
49	9	a	X		M.2292 levels	1	> 125K	Typical	0°		X	282,186
50	9	b	X		M.2292 levels	1	> 125K	Typical	5°		X	282,186
51	9	c	X		32 dBW	1	> 125K	Typical	0°		X	282,186
52	9	d	X		32 dBW	1	> 125K	Typical	5°		X	282,186
53	9	e	X		10 dBW	1	> 125K	Typical	0°		X	282,186
54	9	f	X		10 dBW	1	> 125K	Typical	5°		X	282,186
55	10	a	X		M.2292 levels	1	> 250K	Typical	0°		X	102,841
56	10	b	X		M.2292 levels	1	> 250K	Typical	5°		X	102,841
57	10	c	X		32 dBW	1	> 250K	Typical	0°		X	102,841
58	10	d	X		32 dBW	1	> 250K	Typical	5°		X	102,841

59	10	e	X		10 dBW	1	> 250K	Typical	0°		X	102,841
60	10	f	X		10 dBW	1	> 250K	Typical	5°		X	102,841
61	11	a	X		M.2292 levels	1	> 125K	Scaled	0°		X	115,626
62	11	b	X		M.2292 levels	1	> 125K	Scaled	5°		X	115,626
63	11	c	X		32 dBW	1	> 125K	Scaled	0°		X	115,626
64	11	d	X		32 dBW	1	> 125K	Scaled	5°		X	115,626
65	11	e	X		10 dBW	1	> 125K	Scaled	0°		X	115,626
66	11	f	X		10 dBW	1	> 125K	Scaled	5°		X	115,626
67	12	a	X		M.2292 levels	1	> 250K	Scaled	0°		X	69,477
68	12	b	X		M.2292 levels	1	> 250K	Scaled	5°		X	69,477
69	12	c	X		32 dBW	1	> 250K	Scaled	0°		X	69,477
70	12	d	X		32 dBW	1	> 250K	Scaled	5°		X	69,477
71	12	e	X		10 dBW	1	> 250K	Scaled	0°		X	69,477
72	12	f	X		10 dBW	1	> 250K	Scaled	5°		X	69,477
73	13	a	X		M.2292 levels	2	> 125K	Typical	0°		X	94,050
74	13	b	X		M.2292 levels	2	> 125K	Typical	5°		X	94,050
75	13	c	X		32 dBW	2	> 125K	Typical	0°		X	94,050
76	13	d	X		32 dBW	2	> 125K	Typical	5°		X	94,050
77	13	e	X		10 dBW	2	> 125K	Typical	0°		X	94,050
78	13	f	X		10 dBW	2	> 125K	Typical	5°		X	94,050

79	14	a	X		M.2292 levels	2	> 250K	Typical	0°		X	34,276
80	14	b	X		M.2292 levels	2	> 250K	Typical	5°		X	34,276
81	14	c	X		32 dBW	2	> 250K	Typical	0°		X	34,276
82	14	d	X		32 dBW	2	> 250K	Typical	5°		X	34,276
83	14	e	X		10 dBW	2	> 250K	Typical	0°		X	34,276
84	14	f	X		10 dBW	2	> 250K	Typical	5°		X	34,276
85	15	a	X		M.2292 levels	2	> 125K	Scaled	0°		X	39,695
86	15	b	X		M.2292 levels	2	> 125K	Scaled	5°		X	39,695
87	15	c	X		32 dBW	2	> 125K	Scaled	0°		X	39,695
88	15	d	X		32 dBW	2	> 125K	Scaled	5°		X	39,695
89	15	e	X		10 dBW	2	> 125K	Scaled	0°		X	39,695
90	15	f	X		10 dBW	2	> 125K	Scaled	5°		X	39,695
91	16	a	X		M.2292 levels	2	> 250K	Scaled	0°		X	23,370
92	16	b	X		M.2292 levels	2	> 250K	Scaled	5°		X	23,370
93	16	c	X		32 dBW	2	> 250K	Scaled	0°		X	23,370
94	16	d	X		32 dBW	2	> 250K	Scaled	5°		X	23,370
95	16	e	X		10 dBW	2	> 250K	Scaled	0°		X	23,370
96	16	f	X		10 dBW	2	> 250K	Scaled	5°		X	23,370

Results

The aggregate interference results for the TriG receiver, functioning as a science measurement instrument, are presented in the following sections.

The received aggregate interference levels calculated during the simulations range from -90 dBm to -40 dBm.

The following tables use an aggregate interference threshold of -73 dBm (1526 – 1536 MHz) which corresponds to a -1 dB degradation of receiver C/No.

It should be noted that the loss-of-lock threshold for the TriG receiver occurs between -59 to -35 dBm aggregate interference power in the 1526-1536 MHz band. Loss-of-Lock at -59 dBm was seen in Test 04 with RFI at 1525 MHz and LOL at -35 dBm was seen in Test 04 at 1530 MHz.

The entries in the results tables are interpreted as follows:

- Column 3: Max Int. Level (dBm)

  Indicates the maximum aggregate interference level calculated at the receiver antenna output.

  Note: Any value ≥ -66 dBm in this column indicates that there is sufficient aggregate interference received from the terrestrial LTE network for the TriG receiver to lose lock.

- Column 4: % Time > Threshold

  Indicates the percent time, over the 10-day simulation period, where the aggregate interference at the TriG receiver antenna output exceeds the threshold level (-73 dBm).

  As an example, if the value is about 10% of the time, the TriG receiver will have C/No degraded by at least 1 dB for a cumulative of 24 hours. This is calculated by, as an example:

  10 days (total period of simulation run) = 240 hours

  % Time > Threshold = 10%

  10% of 10 days (240 hours) = 0.10 x 240 = 24 hours

  Note: The value reported represents the % Time > Threshold for the entire 10-days of the simulation, to include the time and instances where the continental U.S. is not within the field-of-view of the satellite. Consideration must be taken based on this. If the master time schedule only included the instances where the continental U.S. (and surrounding bodies of water) were in the field-of-view of the satellite, these values would increase.

- Column 5: # of Int Events

  Indicates that over the 10-day period, the total number of interference events which exceed the -73 dBm threshold.

  Note: The interference time intervals for each interference occurrence may be short or long depending on how many interfering BS the satellite sees on the particular orbit pass over the U.S. The sum duration of all of the interference events (provided in this column) is the reported in column 4 (% Time > Threshold). Furthermore, it should be noted that there can be multiple interference events for a single satellite pass, as different BS pass through the field-of-view of the TriG receiver antenna.

- Column 6: Avg Dur Int Event (min)

  Indicates the mean average duration (in minutes) of an interference event for the entire 10-day period.

  Note: As discussed in Section 5.3.1, the duration of an atmospheric occultation (as the signal path moves from skimming the Earth‘s surface to an altitude of about 100 km) is one to two minutes.

- Column 7: Max Int Event (min)

  Indicates the maximum duration (in minutes) that was recorded for a single interference event over the 10-day period.

- Column 8: Max Allow EIRP Level (dBW)

  Indicates a reverse-engineered maximum BS transmitter power level (in dBW) distributed across a 10 MHz bandwidth per channel per sector. The calculated level is based on the maximum interference level received during the 10-day period.

  Note 1: The reverse-engineered value calculated in this column would bring the interference level below the -73 dBm threshold value. However, it should be also noted that interference to the TriG receiver occurs well before the -73 dBm threshold value occurs, which causes degradation in scientific measurements (e.g., interference occurs at interference levels -90 dBm to -73 dBm (threshold).

  Note 2: Where applicable (i.e., simulations that utilized variable maximum transmitter power levels), the maximum allowable EIRP level is linearly calculated for each zonal category of BS sector.

  As an example, if the maximum interference level (column 3) indicates -70 dBm, the BS transmitter power needs to be reduced by 3.1 dBm in order for the received interference to be below the -73 dBm threshold. The 3.1 dBm reduction in power is linearly attributed to each of the maximum transmitter power for the urban/suburban (+26 dBW), rural (+28

dBW), and microcells (+7 dBW). The resulting maximum allowable transmitter power is calculated for the urban/suburban zone as +22.9 dBW, rural zone as +24.9 dBW, and microcells as +3.9 dBW.

Results Caveats

Caveat 1:

The results are only for the LTE deployment scenarios derived from parameters outlined. Deviation of such LTE system characteristics from ITU-R M.2292 may adversely impact the interference received at the satellite. This is especially true if the typical BS antennas vary in the vertical plane from what was defined in ITU-R F.1336-4, or if the nominal down-tilt angles, as defined in ITU-R M.2292, are deployed at 0 deg or with an up-tilt (e.g., more LTE BS signal energy pointing directly over the horizon or into the atmosphere).

Caveat 2:

The results presented in the following sections are intended to draw no conclusions or make any recommendations as to what level of interference may be tolerated by the other missions employing the TriG receiver for science applications. Aggregate interference received by the TriG receiver system in-orbit is dependent upon the satellite orbit parameters and receive antenna configurations.

Caveat 3:

The results are for the simulated operational use of the TriG receiver while in-orbit. It should be noted that the TriG receivers are currently researched, developed and tested (RD&T) in facilities that are not electromagnetically shielded from the existing RF environment. As such, the TriG receivers may be impacted by LTE BS sites located within close proximity. The effects to the RD&T facilities have not been studied and additional analyses would be required to further understand the impacts to the TriG receivers at the RD&T facilities.

Results for COSMIC-2B

Tables **Table K-7** through

Table K-12 provides a results summary of the analyses performed for the TriG receiver simulated aboard a single COSMIC-2B satellite, and for all simulation parameters shown in **Table K-6**. (The COSMIC-2B mission is comprised of six (6) total satellites.)

[*Note*: Only the forward antenna array was used in the M&S. In reality, COSMIC-2B will utilize a set of 3 subarrays on the forward and aft ends of the satellite. These three (3) subarrays (each having +13.4 dBic gain at 1530 MHz) will be digitally combined in the TriG receiver to achieve a total of +16.7 dBic antenna gain at 1530 MHz in both the fore and aft antennas.]

The results below show results for the fore antenna. The viewing geometries will be similar for the aft antenna, and the calculated values for the tables below would be expected to have similar values from the aft antenna. There will be slight variations due to the fact the individual Base Stations are viewed from azimuths which differ by about 180 degrees (in the BS reference frame).

Table K-7: COSMIC-2B Interference Results
(Macro BS Only, Urban/Suburban: Tx Power +26 dBW,
Rural Tx Power: +28 dBW)

Sim No.	Run Designator	Max int. Level (dBm)	% Time > Thresh	# of Int Events	Avg Dur Int. Event (min)	Max Int Event (min)	Max Allow EIRP Level (dBW)	
							Urban/ Suburban BS	Rural BS
1	a	-57	3.3	83	5.5	11.0	10	12
1	b	-62	2.1	61	4.8	8.8	15	17
2	a	-62	1.8	59	4.1	9.0	15	17
2	b	-67	1.1	43	3.4	6.3	20	22
3	a	-62	1.9	62	4.3	9.0	15	17
3	b	-66	1.2	40	4.0	7.0	19	21
4	a	-64	1.3	44	3.9	7.7	17	19
4	b	-68	0.6	31	2.8	4.8	21	23
5	a	-63	1.6	52	4.2	8.5	16	18
5	b	-67	0.9	32	3.7	6.7	20	22
6	a	-68	0.7	43	2.2	5.5	21	23
6	b	-72	0.1	10	1.9	2.7	25	27
7	a	-67	0.8	32	3.4	6.0	20	22
7	b	-71	0.2	19	1.4	3.0	24	26
8	a	-69	0.4	31	1.6	4.2	22	24

8	b	-74	0.0	0	0.0	0.0	27	29

Table K-8: COSMIC-2B Interference Results
(Macro BS Only, All BS Tx Power +32 dBW)

Sim No.	Run Designator	Max int. Level (dBm)	% Time > Thresh	# of Int Events	Avg Dur Int. Event (min)	Max Int Event (min)	Max Allow EIRP Level (dBW)
1	c	-52	5.4	137	5.5	13.2	11
1	d	-56	3.7	84	6.2	10.7	15
2	c	-57	3.7	115	4.5	10.7	16
2	d	-61	2.3	67	4.9	9.3	20
3	c	-57	3.9	93	5.8	11.5	16
3	d	-61	2.5	70	5.1	9.5	20
4	c	-58	3.1	87	5.0	10.5	17
4	d	-63	2.0	57	4.8	8.0	22
5	c	-57	3.4	83	5.7	11.2	16
5	d	-61	2.2	57	5.4	8.8	20
6	c	-62	1.9	62	4.2	9.2	21
6	d	-66	1.2	47	3.5	6.5	25
7	c	-62	2.1	66	4.4	9.2	21
7	d	-66	1.3	47	3.9	7.3	25
8	c	-64	1.4	44	4.3	7.8	23
8	d	-68	0.7	32	3.2	5.3	27

Table K-9: COSMIC-2B Interference Results
(Macro BS Only, All BS Tx Power +10 dBW)

Sim No.	Run Designator	Max int. Level (dBm)	% Time > Thresh	# of Int Events	Avg Dur Int. Event (min)	Max Int Event (min)	Max Allow EIRP Level (dBW)[14]
1	e	-74	0.0	0	0.0	0.0	10
1	f	-78	0.0	0	0.0	0.0	10
2	e	-79	0.0	0	0.0	0.0	10
2	f	-83	0.0	0	0.0	0.0	10
3	e	-79	0.0	0	0.0	0.0	10

[14] Based on the assumption that the maximum transmitter power level is limited to +10 dBW.

3	f	-83	0.0	0	0.0	0.0	10
4	e	-80	0.0	0	0.0	0.0	10
4	f	-85	0.0	0	0.0	0.0	10
5	e	-79	0.0	0	0.0	0.0	10
5	f	-83	0.0	0	0.0	0.0	10
6	e	-84	0.0	0	0.0	0.0	10
6	f	-88	0.0	0	0.0	0.0	10
7	e	-84	0.0	0	0.0	0.0	10
7	f	-88	0.0	0	0.0	0.0	10
8	e	-86	0.0	0	0.0	0.0	10
8	f	-90	0.0	0	0.0	0.0	10

Table K-10: COSMIC-2B Interference Results
(Macro + Microcells, Urban/Suburban: Tx Power +26 dBW,
Rural Tx Power: +28 dBW, Microcell Tx Power +7 dBW)

Sim No.	Run Designator	Max int. Level (dBm)	% Time > Thresh	# of Int Events	Avg Dur Int. Event (min)	Max Int Event (min)	Max Allow EIRP Level (dBW)		
							Urban/ Suburban BS	Rural BS	Microcell
9	a	-57	3.3	81	5.8	11.2	10	12	-9
9	b	-62	2.1	60	5.0	8.8	15	17	-4
10	a	-62	1.8	59	4.3	9.0	15	17	-4
10	b	-66	1.1	42	3.8	6.3	19	21	0
11	a	-62	2.0	62	4.5	9.0	15	17	-4
11	b	-66	1.2	43	3.9	7.0	19	21	0
12	a	-64	1.3	44	4.1	7.8	17	19	-2
12	b	-68	0.7	30	3.1	5.0	21	23	2
13	a	-63	1.7	52	4.5	8.7	16	18	-3
13	b	-67	1.0	43	3.1	6.8	20	22	1
14	a	-68	0.7	40	2.5	5.5	21	23	2
14	b	-71	0.2	15	1.4	2.8	24	26	5
15	a	-67	0.8	33	3.4	6.2	20	22	1

15	b	-71	0.2	18	1.8	3.0	24	26	5
16	a	-69	0.4	35	1.5	4.3	22	24	3
16	b	-73	0.0	4	0.1	0.2	26	28	7

Table K-11: COSMIC-2B Interference Results
(Macro + Microcells, All S Tx Power +32 dBW/10MHz)

Sim No.	Run Designator	Max int. Level (dBm)	% Time > Thresh	# of Int Events	Avg Dur Int. Event (min)	Max Int Event (min)	Max Allow EIRP Level (dBW)
9	c	-49	8.5	160	7.5	15.5	8
9	d	-50	6.3	136	6.5	13.5	9
10	c	-53	7.0	147	6.7	13.5	12
10	d	-54	5.2	128	5.6	11.5	13
11	c	-53	6.9	137	7.0	14.3	12
11	d	-54	5.1	111	6.5	11.8	13
12	c	-55	6.4	135	6.7	13.2	14
12	d	-56	4.6	132	4.9	11.2	15
13	c	-53	6.5	128	7.2	13.8	12
13	d	-54	4.9	111	6.2	11.7	13
14	c	-58	4.9	119	5.7	11.8	17
14	d	-59	3.5	97	5.0	10.2	18
15	c	-57	4.8	95	7.1	12.3	16
15	d	-58	3.5	86	5.7	10.5	17
16	c	-59	3.8	91	5.9	11.0	18
16	d	-61	2.7	71	5.3	9.5	20

Table K-12: COSMIC-2B Interference Results
(Macro + Microcells, All BS Tx Power +10 dBW)

Sim No.	Run Designator	Max int. Level (dBm)	% Time > Thresh	# of Int Events	Avg Dur Int. Event (min)	Max Int Event (min)	Max Allow EIRP Level (dBW)[15]
9	e	-71	0.5	32	1.9	3.8	7
9	f	-72	0.1	12	1.0	2.2	8
10	e	-75	0.0	0	0.0	0.0	10
10	f	-76	0.0	0	0.0	0.0	10
11	e	-75	0.0	0	0.0	0.0	10
11	f	-76	0.0	0	0.0	0.0	10
12	e	-77	0.0	0	0.0	0.0	10
12	f	-78	0.0	0	0.0	0.0	10
13	e	-75	0.0	0	0.0	0.0	10
13	f	-76	0.0	0	0.0	0.0	10
14	e	-80	0.0	0	0.0	0.0	10
14	f	-81	0.0	0	0.0	0.0	10
15	e	-79	0.0	0	0.0	0.0	10
15	f	-80	0.0	0	0.0	0.0	10
16	e	-81	0.0	0	0.0	0.0	10
16	f	-83	0.0	0	0.0	0.0	10

Results for Sentinel-6

Tables **Table K-13** through **Table K-15** report the results of the analyses performed for the TriG receiver simulated aboard the Sentinel-6 satellite.

[*Note*: A 2-element subarray (2 x 1 configuration) with a gain of +10.5 dBic at 1530 MHz was modeled for the forward subarray, and a 4-element subarray (4 x 1 configuration) with a peak gain of +12.5 dBic at 1530 MHz was modeled for the aft subarray. Results represent the total interference in both antennas. When the full array output is combined, the 6-element forward array consisting of three 2x1 subarrays will have a main beam gain of +15.5 dBic at 1530 MHz, and the 12-element aft array consisting of three 4x1 subarrays will have a main beam gain of +17.5 dBic at 1530 MHz.]

[15] Based on the assumption that the maximum transmitter power level is limited to +10 dBW.

Table K-13: Sentinel-6 Interference Results (Macro BS Only, Urban/Suburban: Tx Power +26 dBW, Rural Tx Power: +28 dBW)

Sim No.	Run Designator	Max int. Level (dBm)	% Time > Thresh	Max Allow EIRP Level (dBW)	
				Urban/ Suburban BS	Rural BS
1	b	-66	3.7	19	21
2	b	-70	1.9	23	25
3	b	-72	0.6	25	27
4	b	-76	0	29	31
3	a	-70	2.1	23	25
4	a	-74	0.2	27	29

Table K-14: Sentinel-6 Interference Results (Macro BS Only, All BS Tx Power +32 dBW)

Sim No.	Run Designator	Max int. Level (dBm)	% Time > Thresh	Max Allow EIRP Level (dBW)
3	c	-64	5.8	23
3	d	-66	3.7	25
4	c	-68	3.4	27
4	d	-70	1.9	29

Table K-15: Sentinel-6 Interference Results
(Macro BS Only, All BS Tx Power +10 dBW)

Sim No.	Run Designator	Max int. Level (dBm)	% Time > Thresh	Max Allow EIRP Level (dBW)[16]
1	f	-76	0	10
2	f	-76	0	10
3	f	-78	0	10
4	f	-82	0	10
3	e	-76	0	10
4	e	-80	0	10

Results Summary

The results tables represent a myriad of LTE BS deployment scenarios and reports the maximum allowable EIRP levels for the terrestrial LTE BS sectors per channel.

In the case of COSMIC-2B, for the simple scenario of macro cell BS at 32 dBW EIRP, as the number of stations decreases from simulation 1 to 2 for the zone-1 model, and from simulation 5 to 6 for the zone-2 model, there is about 5 dB less interference in zone-2 compared to zone-1, which is expected because the zone-2 model uses about 3 times less stations. There is about 4 dB less interference in models using transmitter elevation mask of 5^o (run d) compared to the 0^o mask (run c), indicating that less than half of the available stations affect the satellite in the 5^o mask case.

For the most challenging model (1c), using 184,500 macro cell stations, the tolerable EIRP is 11 dBW(i.e., 12.6 Watts). For a deployment of macro and microcells, utilizing the same transmitter power, the maximum tolerable EIRP is approximately 8 dBW(i.e., 6.3 Watts).

In the case of the Sentinel-6, for the simple scenario of macro cell BS at 32 dBW EIRP, as the number of stations decreases from simulation 3 to 4 for the zone-1 model, there is about 2 dB less interference in models using transmitter elevation mask of 5^o (run d) compared to the 0^o mask (run c). For the most challenging model (3c), using 74,612 macro cell stations, the tolerable EIRP is 23 dBW.

It should be noted that simulations 3 and 4 use the aforementioned variation of the cell model, referred to as ‘scaled’ model, in which the cell radius increases up to double its typical value, as the city population decreases; this results in fewer stations, and less interference, compared to the simulations 1 and 2.

[16] Based on the assumption that the maximum transmitter power level is limited to +10 dBW.

These tolerances only predict the impact to two (2) NASA Missions (COSMIC-2B and Sentinel-6), and the results from these simulations cannot be used to deduce the impacts of other missions where the TriG receiver will be employed for science applications. Specific orbit and antenna configuration for other TriG missions will need to be considered in order to make a holistic determination of the maximum tolerance values (e.g., maximum transmitter power and total number of LTE BS) for the terrestrial LTE network.

As an example of this, while the maximum antenna gain for Sentinel-6 is lower than the antenna configuration used for COSMIC-2B, the percent time above the threshold (-73 dBm) is greater. This is due to the higher orbit altitude of the Sentinel-6 providing a much larger field-of-view of the U.S. resulting in a larger total number of LTE BS in view. This results in a lower peak interference power due to greater space loss, but greater average power.

Also, consideration needs to be given to the reported results on TIME, when assessing the overall impact of the scientific measurements. The typical duration for an atmospheric sounding using RO is only one (1) to two (2) minutes. In certain modeled LTE BS deployment scenarios, the average duration of an interference event may be well above the one (1) or two (2) minutes needed perform an occultation measurement. Loss of any data during a given RO event will generally result in loss of the entire RO profile.

Further, in conjunction with the TIME aspect, the time associated when a satellite in-orbit has the continental U.S. (and adjacent areas in surrounding bodies of water – Atlantic Ocean, Pacific Ocean, and Gulf of Mexico) within its field-of-view needs to be considered. As the reported results under the % Time > Threshold are referenced to a timeframe that is representative of a satellite orbiting the entire Earth, the deduced interference time to occultations performed over the continental U.S. will be significant. The results tables indicate that the TriG receiver will effectively be degraded (> threshold) up to 9.6% of the time during a 10-day orbit. Since the continental U.S. (and surrounding bodies of water) represent approximately 2.5% of the surface of the earth, this represents a significant degradation to the ability for the TriG receiver in providing valuable scientific data.

Finally, it is important to note that the results generated here use a 50% utilization factor. In a time of weather crisis such as a hurricane, the utilization may increase substantially in response to emergency responder and population communication needs. This increase in utilization would increase the interference by 3dB at a time when the occultation measurements would be useful in predicting a storm's intensity and direction.

Impact Plots

It is important to provide a visual representation of the areas affected by the aggregate interference received by the terrestrial LTE BS network. **Figure K-18** through Figure K-20 depict the areas where the TriG receiver will be impacted for COSMIC-2B and Sentinel-6, respectively. These figures are provided as a sample - additional impact plots for all of the simulations run for COSMIC-2B, and for a majority of the simulations for Sentinel-6, are available.

COSMIC-2B Impact Plots

Figure K-18 demonstrates the locations of where the TriG receiver will receiver various levels of interference. In the COSMIC-2B plots, below, the colored levels are defined as:

Table K-16: COSMIC-2B Impact Plot Threshold Levels

Received Interference Level (dBm)	Color	Comment
< -90	None	Below simulation parameters. No interference recorded.
≤ -90 < -73	YELLOW	Interference received, but below -73 dBm (-1 dB C/No) threshold
≤ -73 < -59	ORANGE	Interference received above -73 dBm (-1 dB C/No) threshold, but below -66 dBm (loss-of-lock) threshold
≥ -59	RED	Interference received causes TriG to lose lock

Although the impact plots provide a representation of the areas where degraded performance of the TriG receiver will occur, it must be noted that the position of the degradation signifies the location of the LEO satellite and not where the occultation measurement is taking place, which is about 3,200 km (COSMIC-2BB) or 4,200 km (Sentinel-6) before and behind the satellite.

The plots demonstrate the received interference levels based on the simulation parameters. Therefore, the plots for COSMIC-2B depict simulations with the forward antenna subarray. RO measurements from the forward array will slightly skew the overlaid interference plots toward the equator, while the satellite is traversing in the southwest to northeast direction. In converse, the RO measurements from the forward array while traversing over the U.S. in a northwest to southeast direction will skew the overlaid interference plots toward the north pole.

Additional consideration must be given to the aft antenna array for COSMIC-2B, in combination with these plots.

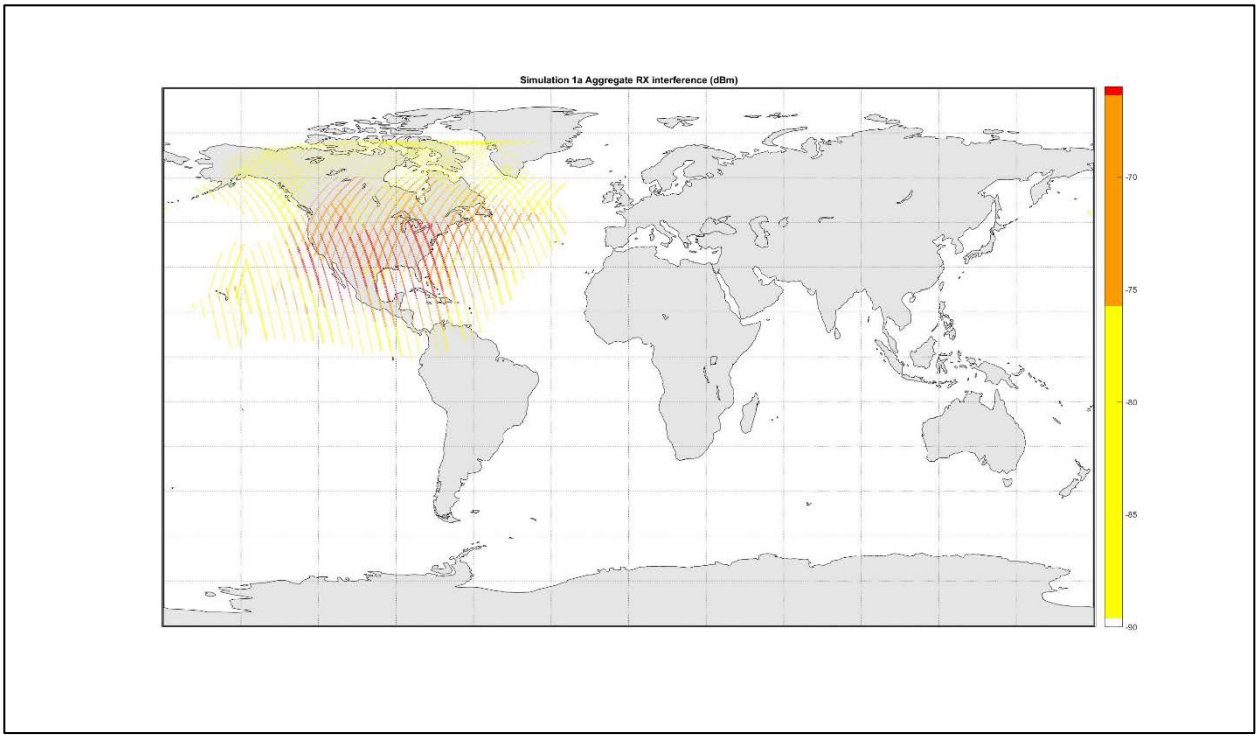

Figure K-18: COSMIC-2B Interference Impact Plot for Simulation 1a (Sample Plot)

Sentinel-6 Impact Plots

Figure K-19 and Figure K-20 demonstrate the interference impacts to Sentinel-6. Figure K-19 depicts the positions where the RO measurements are located when the interference power is greater than 73 dBm. Coupled with Figure K-19, Figure K-20 depicts the level of received interference from the LTE BS network as experienced at the satellite as it passes over the Continental United States. These two (2) plots have been generated for each of the Sentinel-6 simulation runs performed with simulation 3c depicted.

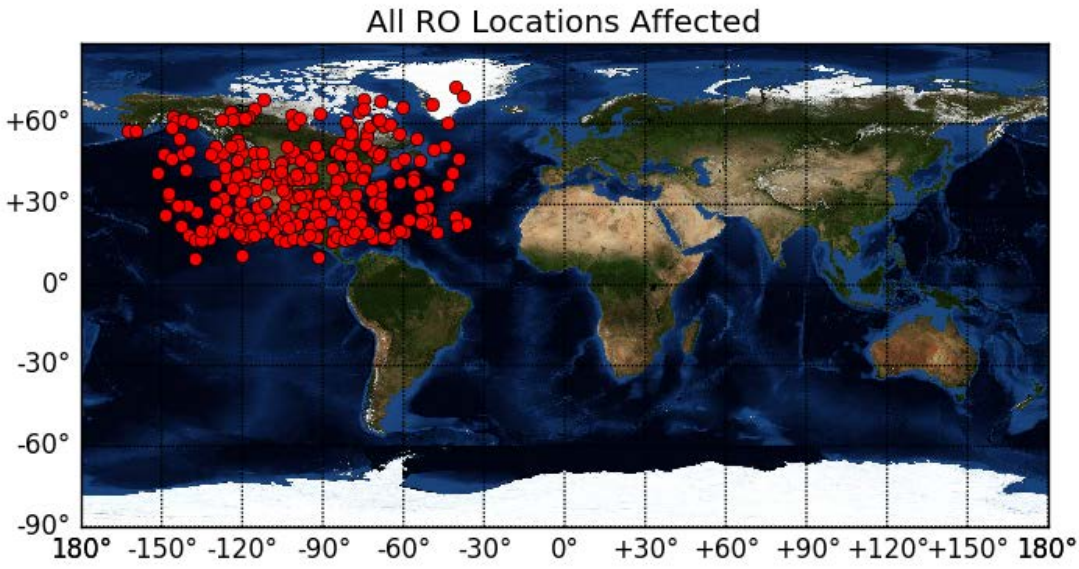

Figure K-19: Sentinel-6 Plot of RO Locations for Simulation 3c (Sample Plot): Occultation measurement locations affected when interference power is greater than 73 dBm

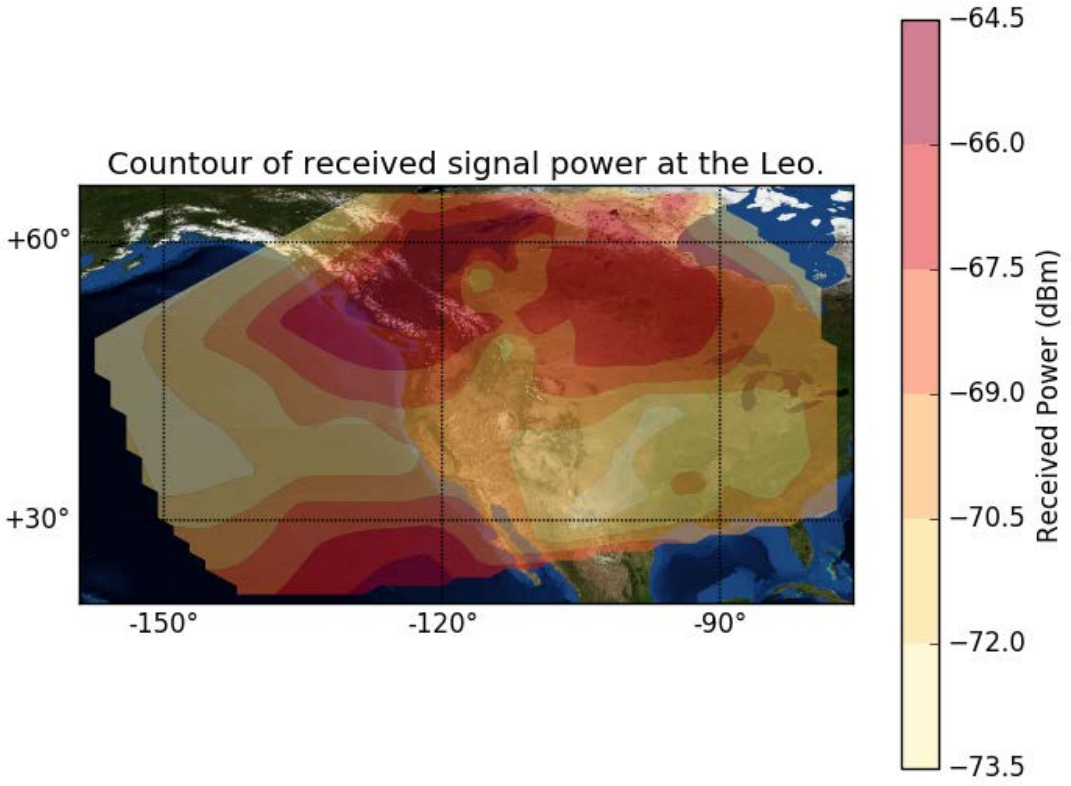

Figure K-20: Sentinel-6 Interference Impact Plot of Simulation 3c (Sample Plot) This plot shows the level of interference in dBm experienced when the satellite passes over the Continental United States.